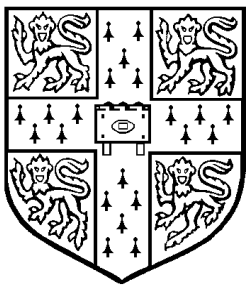

The Scale-Up of Oscillatory Flow Mixing

by
Keith B. Smith

Christ's College
Cambridge
September 1999

A dissertation submitted for the degree of
Doctor of Philosophy
in the University of Cambridge

To my parents

Summary

Oscillatory Flow Mixing is a recent development in mixing technology which has evolved over the past decade. It has a number of similarities to other mixing technologies, particularly pulsed and reciprocating plate columns, but at the laboratory scale has demonstrated a number of advantageous properties. These properties (such as control of residence time distribution, improved heat transfer and predictable mixing times) have been demonstrated at the laboratory scale for a wide range of different potential applications, but until now there has been a lack of firm understanding and research into how the technology could be scaled-up into an industrial scale process.

This thesis addresses the problem of scale-up in Oscillatory Flow Mixing. It reports on a programme of experiments on geometrically scaled apparatus with the measurement of residence time distributions and flow visualisation as the principal methods of investigating the wide range of flow conditions that can be achieved by control of net flow and of oscillatory conditions. Results from these investigations are interpreted as axial dispersion coefficients and also compared with results obtained computationally using a fluid mechanics approach to simulate flow fields and the injection of inert tracers into those flow fields.

Significant clarification is reported concerning the analysis of axial dispersion measurements using the diffusion model for which conflicting solutions were identified in the literature. The development of a flow visualisation technique using fluorescent dye streaklines is also reported. Using the latter technique stable manifolds in Oscillatory Flow Mixing have for the first time been experimentally observed as well as a range of other flow regimes.

The study of scale-up was extended by the successful construction and investigation of an alternative reactor geometry with the potential for use in large-scale plant.

From the work presented in the thesis it is concluded that Oscillatory Flow Mixing is a technology which in general lends itself readily to scaling-up from laboratory to pilot plant scale, and most probably to industrial scale. Experiments performed on small laboratory apparatus (containing less than one litre of fluid) can with confidence be used to predict mixing behaviour in much larger plant (containing hundreds of litres of fluid.)

Preface

The work described in this dissertation was carried out in the University of Cambridge Department of Chemical Engineering between October 1995 and September 1999. It is my original work, unless it is acknowledged to be otherwise in the text, and includes nothing which is the outcome of work done in collaboration. Neither the present dissertation, nor any part thereof, has been previously submitted for a degree at any university.

I am indebted to my supervisor and mentor Dr Malcolm Mackley for his help and enthusiasm throughout the course of this research. I would also like to thank the many departmental staff who have given practical assistance and valuable discussions towards the project, and to thank especially Rob Marshall for his technical support.

I am most grateful to the E.P.S.R.C. for providing funds for the research.

Keith B. Smith

Christ's College

Cambridge

September 1999

1. Introduction

1.1 Motivation for the Study

It has often been the goal of chemical engineers to construct a reactor design which would give perfect plug flow, even under variable throughput conditions. Tubular reactors are a close approximation, yet in general are reliant on turbulent flow, are susceptible to variations in throughput and can for long residence times require very long tubes with resulting high pressure differences along the length of the reactor.

Oscillatory Flow Mixing (O.F.M.) is a recent development in mixing technology which has been researched over the past decade. It has a number of similarities to other tubular mixing technologies, particularly pulsed and reciprocating plate columns, but at the laboratory scale has demonstrated a number of advantageous properties (Mackley 1987 and Mackley 1991). Most notably, control of the oscillatory conditions when operating as a continuous process allows axial dispersion to be minimised (Dickens et al 1989), permitting the control of residence time distributions independently of the throughput rate (Mackley & Ni 1991). In this way the technology can be operated as a near-perfect plug flow device, unaffected by changes in throughput.

O.F.M. generally consists of periodically spaced annular baffles inside a long tube in which either a liquid or a multiphase mixture is oscillated axially (Brunold et al 1989). This flow past the baffles induces vortices which provide both axial and radial mixing in the tube. The intensity of mixing can be varied by tuning the oscillatory conditions (amplitude and frequency of oscillation) and several different mixing regimes have been identified, ranging from creeping laminar to fully turbulent flow (Howes 1988).

The ability to generate radial mixing gives a unique form of control in respect of intensity of mixing, axial dispersion and other transfer processes. These and other properties have been studied on a number of occasions by previous researchers, both by experiment and simulation, but such studies have in general been limited to laboratory scale with at most only a few litres of liquid in the reactor volume. There is therefore a need to understand more fully the effect of scale-up on the performance of Oscillatory Flow Mixing.

1.2 The Problem of Scale-up

Scale-up has traditionally been a problem for technologies such as the Stirred Tank Reactor (S.T.R.) or Continuous Stirred Tank Reactor (C.S.T.R.) where mixing is a very strong function of scale: laboratory scale experiments cannot reliably predict behaviour of large scale plant, where stagnant zones and excessive shear-rates at the impeller tip can limit the effectiveness of the reactor (Perry 1984 Chapter 4). In this case, the expensive and time-consuming construction of pilot scale plant is necessary before design of the full-scale process.

Until now there has been a lack of firm understanding and research into how O.F.M. technology could be scaled-up into an industrial scale process. Individual properties such as control of residence time distribution, improved heat transfer (Mackley & Stonestreet 1995) and particle suspension (Mackley et al 1993) have been demonstrated at the laboratory scale, but the issue of scale-up not addressed.

By the nature and design of O.F.M. it has always been hoped that predictions of large-scale behaviour would be reliable, but problems have existed in that, according to the expected scaling laws, mixing-rate would decrease rapidly (inverse square law) as a function of increasing tube diameter. Different schemes have been proposed to circumvent this problem, including arrangements with many smaller tubes bundled in parallel (Mackley & Ni 1993) or one large diameter tube containing baffles with multiple orifices (this thesis).

1.3 Structure of the Thesis

The thesis studies the effects of scale-up on O.F.M.. In order to characterize the effects, axial dispersion has been chosen as the principal parameter to be measured as a function of tube diameter. Knowledge of axial dispersion allows for the prediction of bulk mixing times (batch systems) or of residence time distributions (continuous systems.) Flow visualisation is also used to compare flow conditions for experiments under different conditions, as well as for experiments under dynamically similar conditions with varying tube diameter. Both experiment and simulation are used to research these properties.

Following this introduction, the thesis commences in Chapter 2 with a survey of the background literature relevant to the scale-up of O.F.M., measurement and quantification of axial dispersion, and flow visualisation. The background to analogous systems such as

pulsed packed beds and reciprocating plate columns is also discussed in so far as it is relevant to O.F.M..

Chapter 3 introduces the sets of experimental apparatus that have been designed and constructed in order to investigate axial dispersion and scale-up. There are three sets of geometrically similar apparatus with tube diameters 24, 54 and 150 mm. The reasons for choice of construction and selection of oscillation device are discussed, as well as the selection and development of an imperfect pulse dye-tracer technique to measure axial dispersion. Brief details of the technique developed for flow visualisation are also discussed.

In Chapter 4 the development of software for the analysis of axial dispersion using the diffusion model is described. During the development of the software it was discovered that solutions to the diffusion equation quoted in the literature were inconsistent, and the correct solution for the given boundary conditions was identified. Using data gathered during a typical experiment, a case study analysis is then presented to show how a value for the axial dispersion coefficient is arrived at for a given set of experimental conditions.

Chapters 5 and 6 present the results of axial dispersion coefficients obtained by experiment and by fluid mechanical simulation respectively. Experiments were performed on the 24, 54 and 150 mm diameter sets of apparatus. The fluid mechanical simulation is derived from a Fortran code written by co-workers in the Department of Chemical Engineering, Cambridge University (detailed in Appendix VI) and run on a Sun Workstation. For the purposes of this thesis it has been adapted to simulate experimental dye tracer experiments.

Flow visualisation of fluid streaklines captured experimentally using video and still photography are compared in Chapter 7 with flow fields obtained by fluid mechanical simulation. Different flow regimes are identified and the effect of tube diameter on the transition between flow regimes is discussed.

In light of the results presented in Chapters 5 to 7, in Chapter 8 a potential design for large-scale O.F.M. is investigated in the 150 mm diameter apparatus, using closely spaced baffles with 37 orifices per baffle in place of the conventional single-orifice baffles with a wide spacing. Estimates of axial and radial dispersion are given, together with flow visualisation. The work highlights the observation (both experimentally and by simulation) of manifolds in the flow field under certain low Reynolds Number oscillatory conditions.

An important aspect of the thesis is the relating of the measured trends in axial dispersion to the appearance of the physical flow, whether laminar, chaotic or turbulent. This is presented in Chapter 9, which then continues to discuss the relationship between the new results presented in this thesis and those already in the literature. Consideration is also given to the likely effect of scale-up on heat transfer and energy dissipation. Finally, brief notes are given concerning likely engineering considerations when designing a large-scale O.F.M. plant.

The main part of the thesis is concluded in Chapter 10 followed by a list of references and nomenclature; appendices on the apparatus design, Optical Dye Tracer Technique, Fluid Mechanical Simulation and Treatment of Errors are given at the end.

2. Background

This chapter surveys the background literature which is relevant to the scale-up of Oscillatory Flow Mixing (O.F.M.), and is divided into three sections:

§2.1 presents a basic description of O.F.M. and a summary of the range of direct research into the various properties of O.F.M. from which industrial interest in the technology has arisen. Then follows a chronology and description of the results and conclusions drawn from the various published O.F.M. experimental and modelling studies most relevant to this thesis (concerning the measurement and quantification of axial dispersion, and flow visualisation).

§2.2 deals in more detail with the measurement and modelling of axial dispersion. It presents the literature available on experimental techniques of axial dispersion measurement and on the models that have been used to quantify axial dispersion. Emphasis is placed upon the diffusion model (the model adopted in this thesis) for which it is shown that the literature presents conflicting conclusions. Reported methods for theoretical measurements of axial dispersion using fluid mechanical simulations are also presented.

In §2.3 the background to analogous systems such as reciprocating plate columns is discussed in so far as it is relevant to O.F.M., particularly in respect of scale-up.

2.1 Background to O.F.M.

This section is divided into four parts:

§2.1.1 gives a generalised description of O.F.M.. §2.1.2 presents the principal dimensionless groups used in the literature to describe the fluid flow in O.F.M.. §2.1.3 presents a tabular summary of the main reported experimental research into O.F.M. and shows also the range of tube size, baffle geometry, oscillation method and oscillatory conditions studied. §2.1.4 gives an overview of the results drawn from experimental studies of O.F.M. with emphasis on axial dispersion and flow visualisation. §2.1.5 discusses numerical simulation studies of O.F.M..

2.1.1 A General Description of O.F.M.

Oscillatory Flow Mixing is generally understood to be a long tube of typically between 12 mm and 150 mm diameter containing periodically spaced baffles and in which a liquid or

multiphase fluid is oscillated axially by means of diaphragms, bellows or pistons at one or both ends of the tube. The resulting flow of fluid past the baffles induces vortex formation and hence radial mixing from which the various useful properties of O.F.M. stem. For small amplitude, low frequency oscillations the flow is viscous and well defined; for large amplitude, high frequency oscillations the flow is chaotic or even turbulent.

A number of different configurations for the baffles have been tested including central and helical geometries (Hewgill et al 1993), but the most commonly adopted is the single orifice (or annular) baffle, spaced at intervals of approximately 1.5 tube diameters apart along the tube. Using these baffles, the flow is axisymmetric for small amplitude, low frequency oscillations.

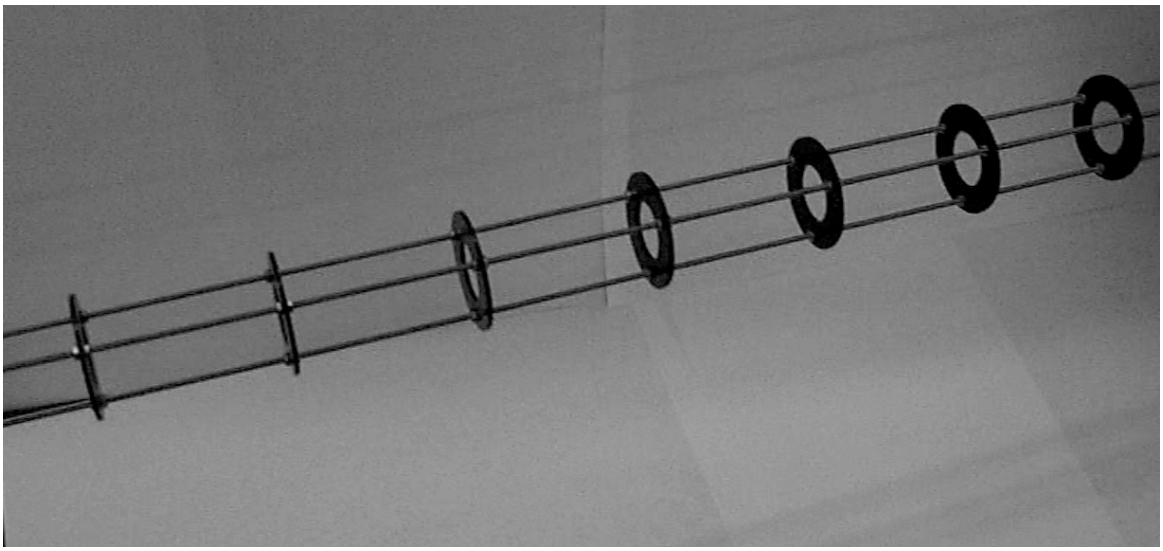

Figure 2.1: Photograph of Periodically-Spaced Single Orifice Baffles Which Can Be Inserted into a 54 mm Internal Diameter Tube. The Baffles Are Supported By Three Stainless-Steel Rods

O.F.M. can be operated either in batch mode (simply a mixing device) or in continuous mode with a net flow of fluid along the tube (Howes 1988).

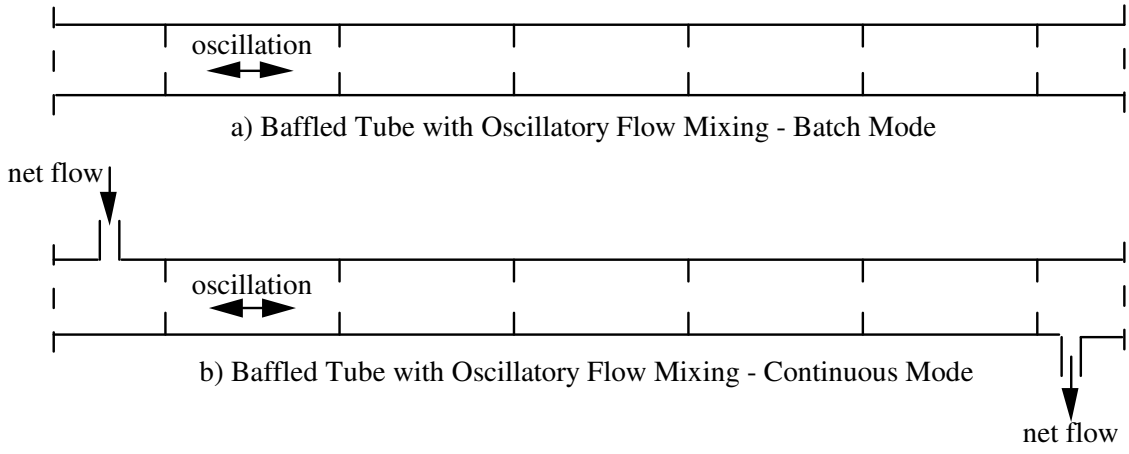

Figure 2.2: Schematic Diagram of O.F.M. either in (a) Batch or (b) Continuous Mode

2.1.2 Dimensionless Groups Used to Describe O.F.M.

Previous studies of O.F.M. have adopted the following dimensionless groups to describe flow conditions in the baffled tube, assuming an approximately sinusoidal driving oscillation:

Net flow Reynolds number $$Re_n = \frac{\rho U d}{\mu}$$ eqn (2.1)

Oscillatory Reynolds number $$Re_o = \frac{\rho \omega x_o d}{\mu}$$ eqn (2.2)

Strouhal number $$Str = \frac{d}{4\pi x_o}$$ eqn (2.3)

In additional, the following dimensionless groups have been adopted to quantify axial dispersion:

Peclet number $$Pe = \frac{UL}{E}$$ eqn (2.4)

Schmidt number $$Sc = \frac{\mu}{\rho E}$$ eqn (2.5)

d	tube internal diameter	E	axial dispersion coefficient
L	length of tube	U	mean net flow velocity through tube
x_o	oscillatory amplitude (centre to peak)	μ	viscosity of fluid
ρ	density of fluid	ω	angular velocity of oscillation

The Strouhal number Str is therefore inversely proportional to the amplitude of oscillation, and together with the Re_o and Re_n are assumed in the literature to define fully the fluid dynamic conditions for a particular geometry. In the case of Re_n the characteristic velocity is the mean net flow velocity U, and in the case of Re_o the characteristic velocity is the peak mean velocity during the oscillatory cycle, i.e.

$$\text{peak mean velocity of oscillation} = \omega x_o = 2\pi f x_o \qquad \text{(eqn 2.6)}$$

where f is the frequency of oscillation. For both Re_o and Re_n the characteristic dimension is conventionally the tube diameter d.

The Peclet Pe and Schmidt Sc numbers are both inversely proportional to the axial dispersion coefficient; the Peclet number is also related to the physical geometry and flow conditions of the experiment and is therefore of use when gauging the likely

magnitude of experimental errors or the effectiveness of a particular reactor, whereas the Schmidt number is related to the fundamental properties of the fluid and therefore is relevant for the consideration of scale-up.

An obvious limitation of the dimensionless groups adopted in the literature (equations 2.1 to 2.6) is that they do not take into account the spacing of the baffles, the baffle thickness nor the orifice diameter. Although all these geometrical parameters have been shown to have an effect on the fluid mechanics in O.F.M. (Brunold et al 1989, Kim & Baird 1976b, Saraiva 1997), this thesis effectively deals only with one geometry for single-orifice baffles and it is therefore not helpful to include the baffle geometry in the dimensionless groups for the presentation of data.

A further subject for debate is the value of the characteristic velocity used to calculate Re_o. It might be supposed that the strong effect of orifice diameter on the generation of vortices (for a given mean oscillatory flow) should be taken into account; again, because only a single orifice diameter was investigated in this thesis it is not helpful to include this geometrical factor in the dimensionless groups, as well as wishing to maintain a consistent nomenclature with other research in the area of O.F.M..

The definition of the Strouhal number as applied to O.F.M. was discussed by Ni & Gough (1997) who concluded that since the Strouhal number was originally conceived to describe the frequency of vortex shedding around objects in a flow (for example vortex shedding behind a cylinder in a flowing fluid) then a more consistent definition of the Strouhal number would be

Modified Strouhal number (Ni & Gough 1997) $$Str = \frac{c}{\pi x_o}$$ eqn (2.7)

where c is the orifice diameter. This modified definition of the Strouhal number takes into account not only that the orifice diameter (rather than tube diameter) is the more appropriate length scale but also that two vortices are shed (one on each side of the baffle) during each full oscillation. The modified definition appears to be well conceived, however the experiments in this thesis do not vary orifice diameter therefore in order to make consistent comparisons with other research, the more widely defined version of the Strouhal number (eqn 2.3) will be used for the presentation of data.

2.1.3 An Overview of Research into O.F.M.

Table 2.1 summarises the major experimental studies of O.F.M. that have been published in the literature and indicates the tube dimensions and baffle constriction.

Worker	Purpose	Tube diameter mm	Tube length m	Baffle spacing ratio*	Baffle constric-tion %
1989 Brunold et al	Flow visualisation	46	3.75	1.5	55
1989 Dickens et al	RTD measurement	23	0.67	1.5	68
1990 Howes & Mackley	Axial Dispersion	51	2.5	1.5	61
1990 Mackley et al	Heat Transfer	12	1	1.5	66
1991 Mackley & Ni	Axial Dispersion	25	1	1.5	34
1991 Mackay et al	Power Dissipation; wall or centre baffles	26	0.75	1.5	61
1993 Mackley & Ni	Axial Dispersion	25	6.3	1.5	34
1993 Mackley et al	Solids Suspension	23	0.5	1.5	91
1993 Ni & Mackley	Batch Chemical Reaction	51	0.3	1.5	76
1994 Ni	Axial Dispersion	25	1	1.5	66
1995 Ni	Axial Dispersion	25	1	1.5	66
1995 Mackley & Stonestreet	Heat Transfer & Energy Dissipation	12	1	1.5	66
1995 Baird & Stonestreet	Energy Dissipation	12	1	1.5	66
1995 Ni et al	Mass Transfer	50	0.5	1.5	Not given
1996 Ni & Gao	Mass Transfer	100	0.7	1.0 – 2.0	66
1998 Mackley et al	Mass Transfer	190	0.9	1.05	various
1998 Ni et al	Geometry & Mixing	50, 90	0.86, 0.5	1.0 - 2.5	49-89

Table 2.1: Summary of Previous Studies of O.F.M.

* ratio of baffle spacing to tube diameter

The Baffle constriction % quoted in Table 2.1 is the percentage reduction of cross-sectional area in the tube provided by the baffle.

From Table 2.1 is it readily seen that there is already a substantial body of literature concerning experimental measurements of axial dispersion in O.F.M. but that each of the studies has concentrated upon a very specific geometry and tube diameter.

Table 2.2 summarises the variety of experimental oscillation methods and the range of flow conditions presented in the literature. Typically Re_n is less than Re_o:

Worker	Oscillator	Wave form	Range of Re_n	Range of Re_o	Range of Str
1989 Brunold et al	Manometer effect	Sinusoidal	-	300 – 100 000	0.01-1
1989 Dickens et al	Cam + piston	Sinusoidal	110	100 - 3300	0.3-9
1990 Howes & Mackley	Cam + diaphragm	Sinusoidal	40, 106	160 - 2500	0.8, 2
1990 Mackley et al*	Cam + diaphragm	Sinusoidal	15 - 800	250 - 1600	0.64
1991 Mackley & Ni	Pneumatic piston	Square	128	40 - 3600	0.35-4
1991 Mackay et al	Moving coil + diaphragm	Sinusoidal	1, 100, 200	40 - 7000	0.3-1.9
1993 Mackley & Ni	Pneumatic piston	Square	106 - 3400	100 - 750	0.4-3
1993 Mackley et al	Moving coil + bellows	Sinusoidal	-	870 – 11 560	0.45-1.2
1993 Ni & Mackley	Cam + diaphragm	Sinusoidal	-	354	1.35
1994 Ni	Pneumatic piston	Square	42, 424	435	2.15
1995 Ni	Pneumatic piston	Square	128	150 - 1600	0.35-4
1995 Mackley & Stonestreet	Cam + pistons	Sinusoidal	50 - 1250	220 - 800	0.15-0.95
1995 Baird & Stonestreet	Cam + pistons	Sinusoidal	-	220 - 6750	0.15-0.95
1995 Ni et al	Cam	Sinusoidal	-	7500 – 26 400	0.28-1
1996 Ni & Gao	Cam + bellows	Sinusoidal	-	5030 – 15 080	2
1998 Mackley et al	Cam	Sinusoidal	-	4000 – 37 600	0.7-1.5
1998 Ni et al	Cam	Sinusoidal	-	800 – 47 500	0.2-1.6

Table 2.2: Summary of Oscillating Methods and Flow Ranges from Previous Studies

* Experimental results of Howes's PhD thesis (1988) are presented in Howes & Mackley (1990)

From Table 2.2 is can be seen that a range of mechanical devices have been employed for the creation of the oscillation and that with one exception a sinusoidal wave form has been adopted. It is also seen that many researchers have observed a quite limited range of oscillatory conditions (Re_o, Re_n & Str) normally constrained by practical limitations of their apparatus.

It is also noted that the range of oscillatory conditions in axial dispersion investigations is approximately limited to $40 < Re_o < 10\,000$ and $0.3 < Str < 4$.

2.1.4 Experimental Studies of Axial Dispersion in O.F.M.

The earliest observation of O.F.M. was as part of a 4th year research project in the early 1980s under the supervision of Dr M.R. Mackley at the Department of Chemical Engineering, Cambridge University and which was later published as Brunold et al (1989). Using a manometer-style 46 mm diameter tube containing annular baffles they observed the flow over a large range of amplitudes created by unforced simple harmonic oscillation of the fluid following an initial height displacement on one side of the U-shaped tube. They estimated viscous and eddy dissipation energy losses in the flow by measuring damping. They used a baffle constriction of 55% and observed flows with a baffle spacing equal to 1, 1.5 and 2 tube diameters; they demonstrated that 1.5 tube diameters was a good compromise between excessive channelling of the flow (1 tube diameter spacing) and insufficient vortex interaction (2 tube diameters spacing). This baffle spacing has been chosen by many subsequent researchers but was not necessarily optimised since subsequent studies have involved smaller amplitude oscillations together with varying baffle constriction. They were able to observe the flow using neutrally buoyant 100 µm polyethylene particles seeded into the flow and illuminated by a slit light source in a cross-section through the flow.

In a subsequent 4th year research project in 1984 Dickens and Williams measured residence time distributions in a 23 mm diameter baffled tube with an oscillatory flow superimposed upon a net flow. Their findings were subsequently published as Dickens et al (1989). They injected a potassium chloride solution (KCl) tracer into the baffled tube inflow and placed a conductivity cell at the outflow. This simple arrangement allowed them to measure residence time distributions for a range of oscillatory amplitudes.

The horizontal tube was closed at both ends by coupled pistons, driven by a motor and cam which gave an approximation to a sinusoidal wave form; the annular baffles had a 45˚ angle at the orifice edge. They used a fixed flow rate and frequency, and observed the effect of varying amplitude of oscillation on the measured dispersion. They quantified dispersion using a diffusion model and assumed a perfect pulse of tracer: the variance of the resulting conductivity trace for each experiment was used to calculate an inverse Peclet *Pe* number using the result derived by Levenspiel and Smith (1957):

$$\sigma^2 = 2\left(\frac{E}{UL}\right) + 8\left(\frac{E}{UL}\right)^2 = 2\left(\frac{1}{Pe}\right) + 8\left(\frac{1}{Pe}\right)^2 \qquad \text{eqn (2.8)}$$

where σ^2 is the calculated variance of the exit concentration profile (see Figure 2.3).

They discovered a minimum value of the inverse Peclet number of about 0.025 which compared closely with the value that would be obtained using a simple tanks-in-series model (Levenspiel 1972) where *N* is the number of perfectly-stirred tanks if it was assumed that each inter-baffle cavity represented one perfectly-stirred tank:

$$\sigma^2 = \frac{1}{N} \qquad \text{eqn (2.9)}$$

and since the value of $\left(\frac{E}{UL}\right)$ was much less than one,

$$\left(\frac{E}{UL}\right) \approx \frac{1}{2N} \qquad \text{eqn (2.10)}$$

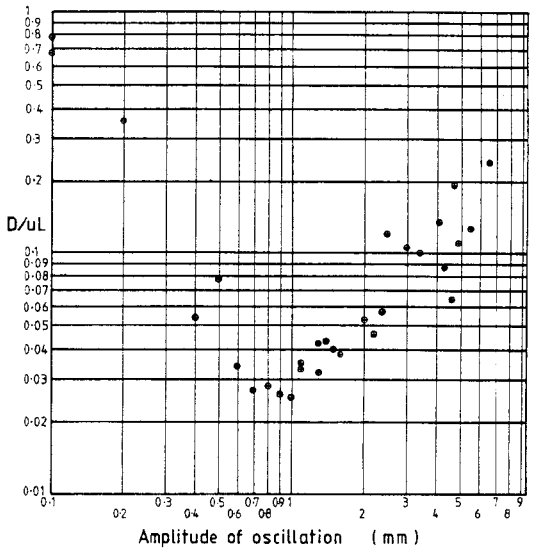

Fig 2.3: Axial Dispersion Measurements by Dickens et al (1989) f = 3.5 Hz

(reproduced with permission)

This important result established that O.F.M. could be used as a method for producing tightly controlled residence time distributions in a tubular reactor, with only weak dependence on the net flowrate through the tube and apparently mimicking the effect of having many continuous stirred tank reactors in series.

Following on from this discovery, a detailed study of axial dispersion was made by Howes (1988) in his PhD thesis which included both experimental results and theoretical modelling. Experimental results from the thesis were summarised in his subsequent joint paper (Howes and Mackley 1990.) They injected potassium chloride solution (KCl) tracer directly into a 51 mm diameter horizontal baffled tube and measured the resulting concentration profiles in the tube using conductivity coils. The assumption was made that the measured conductivity was the average value of the concentration in the inter-baffle cell containing the conductivity probe, but the authors noted that this gave poor results when there were large concentration differences within the cell and that the range of their experiments was limited by the shortness of the tube. They ensured that the KCl solution was neutrally buoyant by addition of methylated spirits. The annular baffles were flat with 90° orifice edges.

Howes analysed the concentration data with a tanks-in-series-with-back-mixing model; the model assumed that each inter-baffle cavity was a perfectly mixed tank with flow to both the upstream and downstream neighbouring tanks. He presented an algorithm for calculating a back mixing coefficient and the model could be fitted to give a reasonable agreement with his experimental dispersion data. Howes performed a series of experiments in which the tracer was injected either upstream of both probes (an imperfect pulse technique) or between the probes in order to determine the degree of back-mixing of the system; he also performed a no-net flow experiment with both probes on one side of the injection point.

Howes varied Re_o, *Str* and Re_n and similarly to Dickens et al (1989) found that imposing the oscillatory flow upon the steady net flow could substantially reduce the axial dispersion which could be minimised for a given net flow rate by adjusting the oscillatory conditions. To explain this phenomenon Howes argued that increasing the oscillatory flow component would simultaneously increase both the radial and axial mixing in the tube from which the effect of increasing radial mixing is to reduce axial dispersion while the effect of increasing axial mixing would serve to increase axial dispersion. Hence there existed a set of oscillatory conditions for which there would be a balance of radial and axial mixing to produce a minimum in overall axial dispersion when there was a net flow present. He also defined a mixing Reynolds number the value of which was determined from the no-net-flow experiments and which allowed him to predict the value of oscillation frequency giving minimum dispersion for a given Re_n and *Str*.

Mackley & Ni (1991) injected NaCl solution as a tracer in a 25 mm diameter baffled tube and measured the changing concentration using point conductivity probes which drew off a small volume of fluid and which had a reported resolution of about $1mm^3$. The spatial resolution of the probes allowed Mackley & Ni to determine differences in the dispersion as a function of radial position and they concluded that O.F.M. greatly enhanced the radial distribution of the tracer. The oscillations used by Mackley & Ni (1991) were driven by a pneumatic cylinder at each end of the closed tube and the authors claimed to have a square displacement wave form; this unfortunately leaves uncertainty as to the peak velocity (which in theory must have been infinite!) and creates uncertainty when making a quantitative comparison with other results.

To quantify the degree of axial dispersion they made use of the diffusion model that is discussed in detail in §2.2. Their experiments produced similar order-of-magnitude results to Howes (1990) although using the diffusion model instead of Howes' tanks-in-series model approach. There was however no satisfactory explanation for the v0ariation in the measured values of the dispersion coefficient within a particular experiment (three probes allowed three separate estimates of the axial diffusion coefficient *E* to be made, from probes $1 \rightarrow 3$, $2 \rightarrow 3$ and $1 \rightarrow 2$.) Moreover, what should have been a single parameter diffusion model was effectively made a two-parameter model since both *E* and

U were adjusted to fit the model to the data; it is not clear to what extent the values of U used for calculation in the model differed from reality. In fact, the reason for the discrepancy between results obtained from the three different sets of probes originated in incorrect analysis used by the researchers - the correct analysis was identified as part of this thesis and is dealt with in Chapter 4.

A similar experiment was performed by Mackley & Ni (1993) on a much longer tube of about 6.3 m with approximately 160 baffles including U-bends. This extra length allowed measurement of the dispersion in the baffled tube as a function of net flow Reynolds number without oscillations; a minimum value in the diffusion coefficient was observed for a net flow Reynolds number of about 400. No evidence was found that the U-bends affected the axial dispersion. They also reported an experiment using a bundle of five parallel 25 mm diameter tubes to demonstrate a potential method for scale-up; a reader of the paper will however observe that there are slight differences in the residence time distributions for the five tubes which may be indicative of uneven flow distribution to the five tubes and so probably the method would need some refinement. Ni (1994) presents similar material.

A rigorous approach to correlating data for axial dispersion in both packed beds and baffled tubes was presented by Crittenden et al (1995). They proposed equation (2.11) for curve-fitting:

$$\frac{E}{UL} = A_1 Re_n^r + A_2 Re_o^m Str^{m-q} + \frac{A_3 Re_n^{2r}}{A_1 Re_n^r + A_2 Re_o^m Str^{m-q}} \qquad \text{eqn (2.11)}$$

where A_1, A_2, A_3, m, q and r are constants. They included the results of Dickens et al (1989) and Howes and Mackley (1990) in their argument to demonstrate the validity of their equation which was originally developed for packed columns but appeared potentially valid for O.F.M. as well. The point was not fully proven since the data sets were incomplete, however their analysis suggested that for a given net flow rate through a baffled tube the minimum dispersion conditions were achieved when

$$(frequency) \times (amplitude)^{0.5} = constant \qquad \text{eqn (2.12)}$$

Using an apparatus similar to that reported in 1991, Ni (1995) made a comparison between the diffusion model and the tanks-in-series-with-backmixing model for the data analysis. For each model, he calculated a value for the Peclet number and found discrepancies in the value depending upon which model was used. This was most likely the result of using an inappropriate solution to the diffusion equation for the particular boundary conditions, as has previously been noted.

Stonestreet (1997) also investigated residence time distributions in a 24 mm diameter baffled tube with oscillations, and concluded that as a rule-of-thumb the axial dispersion

could be minimised for a given net flow if the oscillatory Reynolds number was in the range between two to five times greater in magnitude than the net flow Reynolds number. This applied to net flows in the range $50 \leq Re_n \leq 300$.

2.1.5 Numerical Simulation Studies of O.F.M.

The majority of the numerical simulation work performed on O.F.M. has taken place under the supervision of M.R. Mackley at the Department of Chemical Engineering, Cambridge University, and was initiated by T. Howes during his doctoral research in the form of a finite difference model run on Fortran code. Subsequent researchers at the Department (Roberts and Neves Saraiva) have developed these algorithms further and have generously made them available to other researchers, including the author of this thesis in which the code has been used to simulate streaklines, velocity maps and dispersion.

Two-dimensional axisymmetric numerical flow simulations for steady and oscillatory flow patterns in a baffled tube were made by Howes (1988) who compared the results to experimentally obtained flow visualisation photographs. These flow visualisations were obtained via the method adopted by Brunold et al (1989) using timed-exposure photographs of the flow containing neutrally-buoyant 100 micron polyethylene particles with slit-illumination to produce streaklines through a cross-section of the flow. Howes developed a finite-difference model based on Fortran code to simulate the dispersion of fluid marker particles within the simulation, the results of which he could then compare with experimental data. The flow was experimentally found to be axisymmetric for Re_o less than about 300 in the geometry studied and simulations matched experimental observations well for $Re_o \leq 200$.

The nature of the flow at low Re_o is that vortices are formed behind the baffles, grow, and then are ejected towards the centre of the tube when the flow direction reverses, eventually dissipating. At higher Re_o (above 300) the vortices interact, breaking the axisymmetry and forming chaotic flow patterns. Howes' calculated flow patterns were unable to predict such complex flow and were therefore limited to flows with $Re_o \leq 200$.

Numerically generated two-dimensional flow visualisations of flow without oscillations in a two-dimensional baffled channel using a particle mapping technique were reported by Howes, Mackley & Roberts (1991) which predicted a critical Re_n between 100 and 200 at which the flow becomes unsteady and the symmetry of the flow pattern is broken. A similar critical value for Re_o was also discovered and the model was thought valid up to $Re_o = 700$. They noted that so long as $Re_n \leq Re_o$ then the oscillations would have a useful effect in increasing chaotic mixing.

Wang et al (1994) examined numerical simulations for either wall or central baffles and they observed that the vortex strength was stronger for wall baffles; there was a maximum of vortex strength at a Strouhal number (inversely proportional to oscillatory amplitude) of approximately unity.

Kinematic mixing rates in a baffled tube were calculated by Mackley & Roberts (1995) who observed that for oscillatory flow the mixing rate was well distributed over the flow field for $Re_o \geq 80$. They used both a particle separation approach and a stretch rate approach to describe the mixing. Under oscillatory conditions $Str = 1$ and $Re_o = 60$ or 80 they predicted optimum stretch rates at baffle spacings of 0.6 and 0.9 channel diameters respectively. It seems therefore that for optimum mixing conditions, the baffle geometry should ideally be tailored to the particular oscillatory conditions.

The work of Howes, Roberts and Mackley was further developed by Saraiva (1997) who in his PhD thesis presents mainly theoretical results related to mixing in O.F.M. at low Reynolds numbers for axisymmetric flows, both for mixing in the region between baffles (intra-cell mixing rates) and for the mixing between regions separated by baffles (inter-cell mixing rates.) He examined two different methods for quantifying the intra-cell mixing rate (firstly a fluid element deformation method and secondly a concentration-time evolution tracer injection method) and concluded that there was a direct correlation between the two methods. He studied the effect of baffle spacing on mixing performance and concluded that for the conditions $Re_n = 0$, $Re_o = 100$ and $Str = 1$ the mixing rate was only a weak function of baffle spacing: there was a weak maximum at a baffle spacing of around 2 tube diameters but remained substantially unchanged between 1.25 and 2.75 diameters spacing. In collaboration with the work carried out in this thesis, he also carried out modelling on manifolds in O.F.M. and used experimental results from this thesis to substantiate his values for axial dispersion obtained by fluid-mechanical modelling. Saraiva also showed that molecular diffusion (of a salt tracer in water) only made a significant contribution to the overall measured axial dispersion for oscillatory Reynolds numbers of less than approximately 100.

2.2 Measurement and Modelling of Axial Dispersion

Axial dispersion is a measure of the rate at which an inert tracer spreads axially along a tube such as is found in O.F.M.. It can be a measure of macro-mixing (e.g. mechanical mixing of the bulk fluid) or of micro-mixing (e.g. molecular diffusion) or most commonly a combination of both types of mixing. Quantification of axial dispersion is of particular interest for tubular-style reactors since the results can then be used to predict residence time distributions for either larger or smaller reactors.

Several different models for axial dispersion are presented in the literature; in this thesis the "diffusion equation" is the primary model chosen for the quantification of axial dispersion from experimental data.

This section is divided into three parts. The first (§2.2.1) discusses the various models available to quantify axial dispersion and their suitability to the problem of O.F.M.. In §2.2.2 the solutions to the diffusion equation presented in the literature are treated in more detail, and conflicting results are highlighted. Finally, §2.2.3 deals with methods used by researchers to estimate axial dispersion using fluid mechanical simulations, particularly in flow regimes where regular experimental techniques have proved inadequate.

2.2.1 Models Available for Quantification of Axial Dispersion

The two principal models adopted in the literature to describe dispersion in O.F.M. are

i) The diffusion model, and

ii) The tanks-in-series model, with or without backmixing.

The diffusion model uses the analogy of molecular diffusion to describe macro-mixing and was first used as a model for axial dispersion in O.F.M. by Mackley & Ni (1991). So as (hopefully) to avoid confusion this thesis will use the symbol E for axial diffusion and the symbol D for molecular diffusion. The mathematics of the diffusion model are dealt with in detail in §2.2.2.

The diffusion model is inherently appropriate for describing a physical situation where homogenous mixing exists (Levenspiel 1972). It may therefore be supposed that it is a good model for O.F.M. when substantial mixing occurs (i.e. under chaotic mixing conditions) but that it may fail if there are large segregated volumes of fluid in the flow (for example at low Reynolds number flows). The model has the advantages that it is in common usage (and therefore familiar to most chemical engineers) and has been well-studied for a variety of boundary conditions. A potential disadvantage of the diffusion

model with respect to O.F.M. is that it takes no account of the geometry of O.F.M. (i.e. the presence of periodically-spaced baffles which compartmentalise the flow.)

The concept of representing O.F.M. as a series of stirred tanks dates back to Dickens et al (1989). This model gives a good physical representation of O.F.M. and is appealing to most chemical engineers because of its simplicity. The simplest form of the model ("tanks-in-series") has only limited success in describing axial dispersion in O.F.M.:

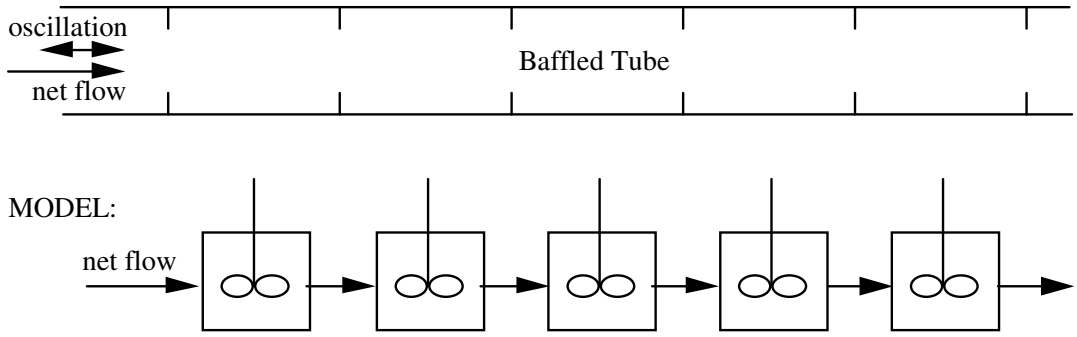

Figure 2.4: The "Tanks-in-Series" Model

The problem here is that the model cannot account for upstream mixing of the fluid due to oscillations; in particular it cannot model oscillation only (with no net flow) situations.

There are many more sophisticated forms of the tanks-in-series model described in the literature (for example Levenspiel 1972). One such model was utilised by Howes & Mackley (1990):

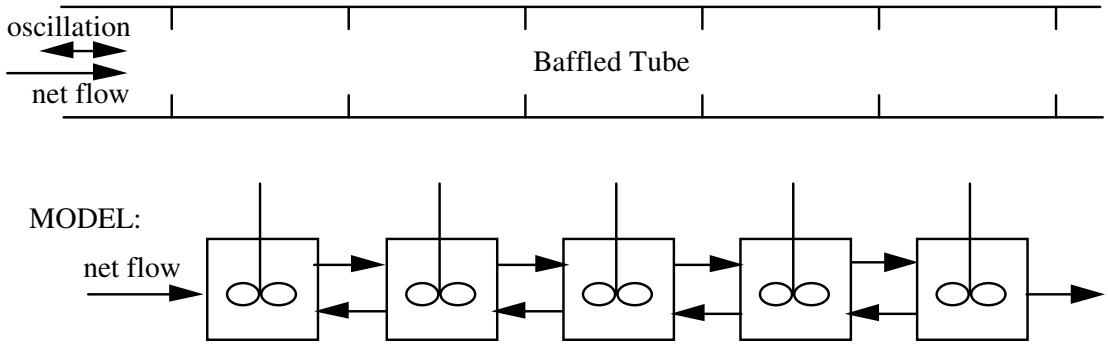

Figure 2.5: The "Tanks-in-Series-with-Backmixing" Model

This model is more satisfactory in that upstream mixing is permitted; using an imperfect pulse technique, the model's single-parameter is the equivalent backmixing coefficient *F*. Referring back to Howes' thesis (1988) a reasonable model fit can be achieved between experimental and model concentration-time profiles although the results only cover a modest range of oscillatory conditions. A disadvantage of the model is that the equivalent backmixing coefficient *F* is not a true measure of the actual physical backmixing since a degree of short-circuiting also occurs and contributes to the value of *F*.

Mecklenburg & Hartland (1975) stated that only a small difference exists between the tanks-in-series-with-backmixing and axial diffusion models: the equivalent Peclet number of each inter-baffle cell Pe_{cell} can be directly related to the equivalent backmixing coefficient:

$$\frac{1}{Pe_{cell}} \approx F + 0.5 \qquad \text{eqn (2.13)}$$

Neither the diffusion model nor the tanks-in-series-with-backmixing model therefore gives a perfect physical representation of O.F.M., and since they are equivalent it is perhaps largely a matter of taste as to which model is preferred. What is so far lacking in the literature is an assessment of the range of flow conditions under which either model adequately describes axial dispersion in O.F.M..

2.2.2 Solutions to the Diffusion Equation for the Imperfect Pulse Technique

Using the analogy of molecular diffusion, the measured concentration C of a dye tracer injected into the tube is predicted to change according to equation 2.14 where x is the distance along the tube and t is time.

$$\frac{\partial C}{\partial t} = E\frac{\partial^2 C}{\partial x^2} - U\frac{\partial C}{\partial x} \qquad \text{eqn (2.14)}$$

A number of workers have discussed analytical solutions to this problem for different situations (for example Danckwerts 1953, Taylor 1953, Taylor 1954, Aris 1956, Levenspiel & Smith 1957, van der Laan 1958, Aris 1959b, Bischoff 1960, Aris 1960 and Nauman & Mallikarjun 1983). If a perfect input pulse of tracer were injected into an infinitely long tube then typical boundary conditions are:

$$C(x,0) = \frac{n}{A}\delta(x) \qquad \text{eqn (2.15)}$$

and $$lim\Big|_{x=^{+}_{-}\infty} C(x,t) = 0 \qquad \text{eqn (2.16)}$$

where n is the volume of unit concentration tracer injected, A is the cross-sectional area of the vessel and $\delta(x)$ is a Dirac delta function (i.e. a perfect pulse.) This yields an analytical solution for concentration as a function of time and distance along the tube, with fixed values of U and E and with a unit impulse at $t = 0$ and $x = 0$ gives rise to

$$C(x,t) = \left[\frac{1}{\sqrt{4\pi Et}}\right] \exp\left\{-\frac{(x-Ut)^2}{4Et}\right\} \qquad \text{eqn (2.17)}$$

A limitation of this solution is that it assumes a perfect input pulse of tracer which is in practice unachievable and unmeasurable experimentally. This theoretical impossibility of

achieving perfect pulse injection can be avoided by the use of the imperfect pulse method (Aris 1959a) where the form of the input tracer pulse does not matter so long as the tracer concentration can be measured at two or more points in the tube both downstream of the injection point and separated by a certain distance *L*.

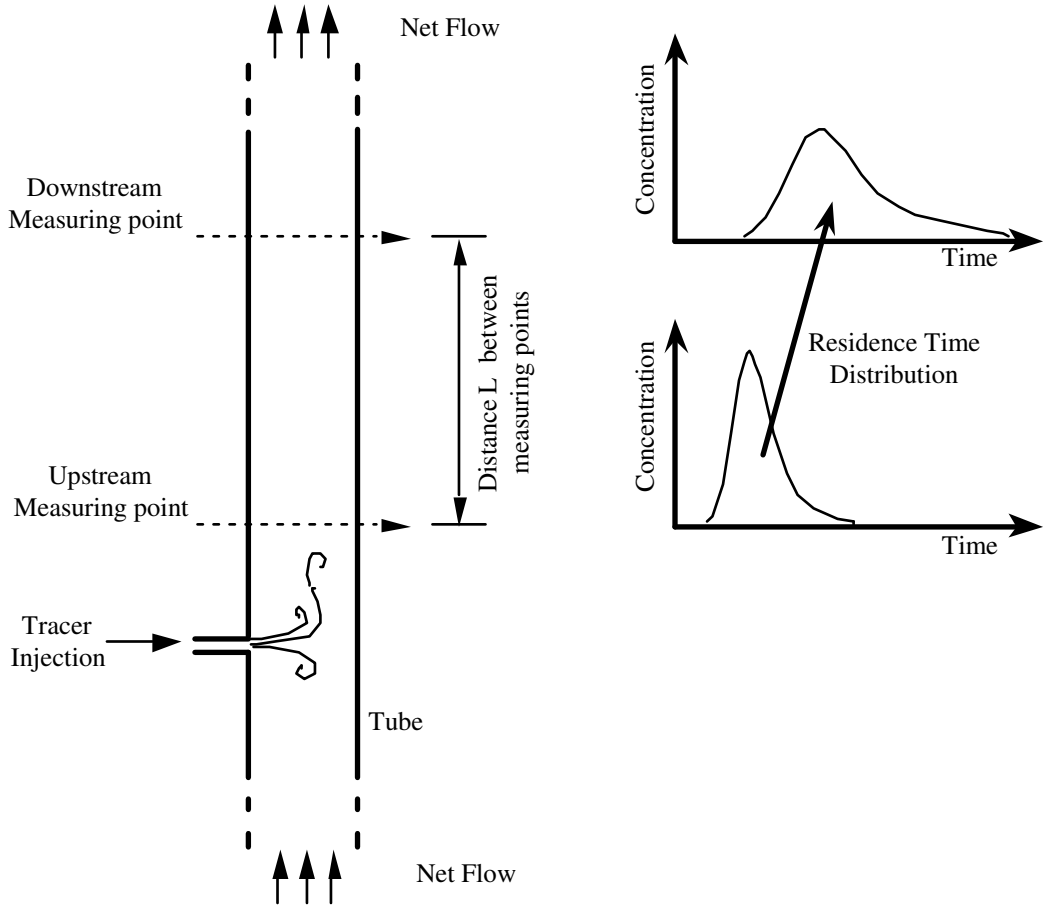

Figure 2.6: The Imperfect Pulse Technique for Axial Dispersion Measurement

The method of analysis of the results is typically to use the upstream data to predict the downstream response with the help of a suitable residence time distribution model and by trial and error to obtain a best-fit value for E , the quoted axial dispersion coefficient, such that the experimental and predicted downstream profiles are as similar as possible.

This approach was adopted for O.F.M. by Mackley & Ni (1991) who used a solution taken from Goebel et al (1986): they argued that the normalised concentration $C'_1(t)$ of tracer measured at the upstream point over a short time interval Δt could be thought of as being equivalent to injecting a perfect pulse of tracer with volume $C'(t')\Delta t$ at time $t = t'$. Taking the limit as Δt tends to zero and integrating over all possible injection times t' would enable one to predict the concentration at the downstream measuring point $C'conv(t)$ as shown:

$$C'_{conv}(t) = C'(L,\ t) = \int_0^t C'_1(t') \left[\frac{U}{\sqrt{4\pi E(t-t')}}\right] \exp\left\{-\frac{(x-U(t-t'))^2}{4E(t-t')}\right\} dt' \quad \text{eqn (2.18)}$$

which is a convolution integral and must be integrated numerically. The value of the diffusion coefficient E was adjusted iteratively to give the best fit between C'_{conv} and the measured concentration C'_2 using either a least squares algorithm or by visual inspection. [The latter method is anyway a wise precaution since it can quickly be seen if there is a large discrepancy between the shape of the profiles].

From equation 2.18 can be extracted the transfer function between measuring points one and two (effectively the residence time distribution between the two measuring points with open-open boundaries):

$$TransferFunction(t) = \left[\frac{U}{\sqrt{4\pi Et}}\right] \exp\left\{-\frac{(x-Ut)^2}{4Et}\right\} \qquad \text{eqn (2.19)}$$

This is however in disagreement with the transfer function proposed by Scott (1997):

$$TransferFunction(t) = \left[\frac{1}{\sqrt{4\pi E\frac{t^3}{x^2}}}\right] \exp\left\{-\frac{(x-Ut)^2}{4Et}\right\} \qquad \text{eqn (2.20)}$$

which is equivalent to the solution given for the same boundary conditions by Westerterp et al (1984) who gave the same transfer function in terms of dimensionless time θ and the Peclet number:

$$TransferFunction(\theta) = \sqrt{\frac{Pe}{4\pi\theta^3}} \exp\left\{-\frac{Pe(1-\theta)^2}{4\theta}\right\} \qquad \text{eqn (2.21)}$$

$$\text{where } \theta = \frac{tU}{L} \qquad \text{eqn (2.22)}$$

Equations 2.19 (after Goebel et al 1986) and 2.20 (after Westerterp et al 1984) both purport to describe the same situation and are of similar mathematical form, but there is a subtle difference in the pre-exponential term which renders them different. This apparent conflict is examined in Chapter 4.

2.2.3 Estimates of Axial Dispersion from Fluid Mechanical Simulations

A large body of literature exists for the experimental quantification of axial dispersion as has been demonstrated in the preceding sections of this chapter. It was found during the course of this thesis that because of the nature of the flow observed in O.F.M. at very low Reynolds numbers (especially channelling of the flow), the axial diffusion model was inadequate under some circumstances. Nevertheless a method was still sought to quantify axial dispersion under these conditions.

In recent years advances in computing power have made it possible to perform numerical fluid mechanical simulations of entire flow fields. Sobey (1985) used a fluid mechanical simulation to estimate axial dispersion in wavy-walled channels. In conjunction with his fluid mechanical simulation he advected a large number of fluid marker particles within one cell and monitored the variance of the particles' axial position from which the dispersion coefficient could be directly calculated.

Sobey's method was adopted by Howes (1988) who advected fluid marker particles within his fluid mechanical simulation to determine axial dispersion in O.F.M.. Howes's simulation was based upon a fluid mechanical simulation of the velocity field in O.F.M. together with the superposition at the end of each oscillatory cycle of a random-walk concept to model molecular diffusion (without which the marker particles would be trapped in certain domains). The model gave satisfactory results for axial dispersion using the method of moments (Aris 1956). The method relies however on the assumption that the rate of increase of variance of the particle cloud is constant. At very low values of Re_n with some net component to the flow, he found that it took many oscillatory cycles before the rate of increase of variance was constant. In order to speed up the calculations he therefore used a transfer function method (based upon a method for determining dispersion in tidal estuaries) which only required knowledge of the position of the particles at a single point in time for an oscillatory cycle. The transfer function was therefore used to compute the change in position over one oscillatory cycle of any particle in a single inter-baffle cell.

Howes's fluid mechanical simulation was further developed by Saraiva (1997) who utilised the advection of inert fluid marker particles to measure both axial dispersion and mixing in O.F.M.. He quantified axial dispersion using equation 2.23 for the case of oscillatory flow only, for which the rate of change of variance was constant soon after the simulated injection of the particles.

$$E = \lim_{t\to\infty} \frac{1}{2} \frac{d < (x(t) - < x(t) >)^2 >}{dt} \qquad \text{eqn (2.23)}$$

where $x(t)$ is the axial position of each marker particle as a function of time (averaged over one oscillatory cycle) and the angular brackets represent an average over all the marker particles. In dimensionless form the relationship between axial dispersion and particle variance becomes:

$$\frac{1}{Sc} = \frac{\rho E}{\mu} = \lim_{t\to\infty} \frac{Re_o Str}{4} \frac{d < (x(t) - < x(t) >)^2 >}{dt} \qquad \text{eqn (2.24)}$$

This method is not applicable to practical experiments since knowledge of the complete tracer distribution at an instant in time is required. A variant of the method can be used

for experimental purposes (see for example Dickens et al 1989) but is prone to large errors resulting from small inaccuracies in the measurement of tracer concentration.

In conjunction with the work in this thesis Saraiva also adapted the simulation to be capable of mapping inert tracer particles so as to mimic the effect of inert dye injection in a practical experiment. Moreover, the mean cross-sectional concentration of these marker particles could be determined in a manner analogous to the optical concentration sensors used in this thesis (Hwu et al 1996). This allowed direct substitution of simulated residence time distributions into the analysis programme developed for the interpretation of experimental residence time distribution measurements as part of this thesis (Chapter 4).

2.3 Studies Of Systems Analogous To O.F.M.

This section is not intended as a comprehensive review of pulsed packed beds and reciprocating plate columns, but aims to high-light similarities with O.F.M. in respect of axial dispersion measurements, modelling and scale-up. It is divided into two sections, dealing respectively with the relevant literature on pulsed packed beds (§2.3.1) and reciprocating plate columns (§2.3.2).

2.3.1 Pulsed Packed Beds

Pulsed packed beds typically consist of a tube filled with small to medium sized particles or beads, through which a continuous flow of liquid is pumped with superimposed oscillations. There are a number of similarities between the behaviour of pulsed packed beds and O.F.M. and some of the observations from pulsed packed beds can probably be applied to the latter. The diffusion model is particularly relevant since the packed bed can be thought of as homogeneous rather than having discrete regions.

In 1958 Carberry & Bretton reported experiments on axial dispersion in steady flow through packed beds in a 38 mm diameter column using a range of packings and a dye-tracer technique. They discovered that axial dispersion increased linearly with Reynolds number (based upon the diameter of the packing and the fluid properties) up to a Reynolds number of about 100, i.e. $E \propto Re_n$. At higher net flows, the dependence reduced until $E \propto Re_n^{0.25}$ at a critical Reynolds number of around 400. This makes an interesting comparison with the findings of Mackley & Ni (1993) for oscillatory flow where they observed a minimum in axial dispersion for steady net flows of Reynolds number approximately 400. Carberry & Bretton also reported larger axial dispersion than

predicted by diffusion theory and concluded that this was due to bed-capacitance. Their experiments also showed higher dispersion in shorter beds.

Axial dispersion in a 50 mm diameter by 4 m long pulsed packed column was measured by Goebel et al (1986) using potassium chloride salt solution tracer and an imperfect pulse technique. They plotted their data as a graph of $\frac{E}{u' d_p}$ against $\frac{4\pi\omega x_0}{u'}$ where u' is the mean interstitial velocity and d_p is the packing diameter. The first group is therefore similar to an inverse Peclet number and the latter group is a ratio of the oscillatory and net flow velocities. The data showed a characteristic minimum value for $\frac{E}{u' d_p}$ as a function of $\frac{4\pi\omega x_0}{u'}$. This concept of relative importance of oscillatory and net flows may be a useful method for describing flows in O.F.M., although very low net flows are of primary interest for the design of long residence time reactors.

Pulsed packed columns ranging from 50 mm to 2400 mm diameter were examined by Simons et al (1986). They used both KCl solution and a radioactive indium tracer to measure axial dispersion. Importantly, they determined that axial dispersion E was a function of ωx_0 and geometry only, and not a function of column diameter as had been suggested by previous workers.

Axial dispersion data from a 50 mm packed column was correlated by Mak et al (1991) who found that for $0 < Re_n < 180$ and $0 < Re_o < 600$ the dependence of E was given by:

$$\frac{E\rho}{\mu} = A_1 Re_n^n + A_2 Re_o + \frac{A_3 Re_n^{2n}}{A_1 Re_n^n + A_2 Re_o} \qquad \text{eqn (2.25)}$$

which is very similar in form to eqn (2:11) from Crittenden et al (1995) although the latter is slightly more refined in its approach in that it separates the dependence of E with respect to amplitude and frequency of oscillation.

2.3.2 Reciprocating Plate Columns

Reciprocating plate columns are most often used for contacting immiscible liquids for separation processes and as such are well described by Long (1967). Some axial dispersion work has nevertheless been carried out in a liquid single phase system and this is of interest because of the stage-wise partitioning of the column which is comparable to the geometry of O.F.M.. Reciprocating plate columns contain stacks of multi-orifice plates that are oscillated at around 1Hz and with an amplitude of a few mm. The orifices are of the order of 12 mm diameter and the total area constriction of the plate is typically 50%. [Note that *pulsed* plate columns are generally considered to have smaller orifices of

around 2 mm diameter and operate on a mixer-settler principle for immiscible liquid contacting; these are not discussed.]

A reciprocating plate column of 150 mm diameter was examined by Baird (1974) who used the colour change acid-base reaction to indicate axial dispersion. Interestingly, for coarsely perforated plates the dispersion was proportional to $amplitude^2 \times frequency$ but semicircular unperforated plates showed a dependence on $amplitude \times frequency$ and the author comments upon the excellent radial mixing with this kind of baffle. The latter could be considered to be closest in nature to single orifice baffles in O.F.M..

A 50 mm diameter reciprocating plate column was studied by Kim & Baird (1976a). They surprisingly discovered that the Teflon baffles (3.4 mm thick) produced significantly lower axial dispersion than with stainless steel baffles (1.5 mm thick) for which E was more than 30% larger; they repeated the experiments with double-thickness steel baffles (to give approximately the same total baffle thickness as for the Teflon) for which the axial dispersion was then the same as for Teflon, from which they reasonably concluded that the baffle thickness was a parameter affecting axial dispersion.

They also observed that increasing the viscosity of the fluid (by a factor of 4 using glucose syrup in water) had negligible effect upon the value of the dispersion coefficient from which they concluded that viscous effects were unimportant in the essentially turbulent nature of the flow. Orifice diameter was 14 mm and the oscillatory conditions were 0.5 to 6 Hz and 6 to 22 mm centre-to-peak amplitude. Column diameter also had little effect on axial dispersion. These results may not hold as well for O.F.M. operating at low Reynolds flow in which case viscous effects may become important. Kim & Baird also varied plate spacing H as a parameter and correlated their results for a wide range of oscillatory conditions. They plotted the data on a single graph with the correlation $E \propto \frac{x_o^{1.74}\omega^{0.96}}{H^{0.69}}$. The notation has been adjusted to be consistent with this dissertation; the dependence of E almost proportional to frequency but with a power-relationship to amplitude is interesting.

In a subsequent paper (Kim & Baird 1976b) they examined further the effect of orifice diameter c, plate thickness T and separation H and concluded that $E \propto \frac{x_o^{1.8}\omega^{1.0}c^{1.8}}{H^{1.3}T^{0.3}}$. They found that halving c with plate free area kept constant reduced the amount of axial dispersion by about 75%. The dependance upon H appeared to be strongly related to the precise baffle geometry.

A model for axial dispersion suggested by Stevens & Baird (1990) considered that the region swept out by the plates was very well mixed but with relatively poor mixing between the plates; the model could in principle be applied to O.F.M..

A review paper (Lo et al 1992) noted from the literature a power-law dependence of the form $E \propto d^n$ where d is the column diameter and n is between 0.3 and 0.67 depending upon plate geometry.

Baird (1996) reported axial dispersion measurements in a 150 mm diameter reciprocating plate column employing single orifice baffles with a constriction of approximately 75% for which E was found to be proportional to Re_O. Although measurements were only made at high Reynolds numbers (8000 and above), the results can be directly compared with experiments carried out as part of this thesis (but with oscillating fluid rather than oscillating baffles as the only substantial difference.)

Lounes & Thibault (1996) investigated axial dispersion using KCl tracer in a 0.1 m diameter batch reciprocating plate column with multi-orifice baffles with orifice diameter 6.25 mm and a total baffle constriction of 72%. From their experiments they concluded that axial dispersion $E \propto x_o^{0.756} \omega^{1.066}$.

It is concluded that nearly all the correlations for reciprocating plate columns available in the literature predict axial dispersion to be approximately proportional to frequency but for amplitude of oscillation the correlations vary from $E \propto x_o^{0.756}$ to $E \propto x_o^2$.

3. Apparatus and Experimental Method

In order to study the effect of scale-up on Oscillatory Flow, three sets of geometrically similar apparatus were designed and constructed. The smallest apparatus was a 1 m tall tube of 24 mm internal diameter and the largest was a 4.5 m tall tube of 150 mm internal diameter. In conjunction with the design and construction of the apparatus, experimental methods were developed for flow visualisation (using fluorescent dye streaklines) and measurement of residence time distributions (using dye tracer and optical sensors) which could be applied to all three sets of apparatus in order to give directly comparable results between different scales.

The design and construction of the sets of apparatus as well as the selection and development of experimental techniques formed a significant part of the work presented in this thesis and are therefore described in detail: §3.1 discusses the design criteria and construction of the experimental apparatus; §3.2 describes the selection and implementation of the experimental methods used.

3.1 Design Criteria and Construction of Apparatus

In setting out to design apparatus to test scaling laws for a particular reactor geometry, consideration was given to the likely requirements of oscillation and physical size as one moves to a larger or smaller scale; these requirements placed potential restrictions upon the maximum scale of apparatus that could reasonably be constructed. This discussion is set out in §3.1.1, followed by a description of the actual construction of the apparatus in §3.1.2. For clarity, some of the construction detail is presented more fully in the Appendices.

3.1.1 The Required Range of Operating Conditions for the Apparatus

Most experimental investigations of O.F.M. to date have concentrated upon tubes of approximately 24 mm or 51 mm internal diameter (see Table 2.1). In order that comparisons could be made with other studies of O.F.M. (for example investigations into axial dispersion or suspension of particles) it was decided to construct geometrically similar sets of apparatus of 24 mm and 54 mm internal diameter (using standard clear acrylic tubing). For industrial applications it is likely that larger tube diameters would have to be considered in order to accommodate large throughputs and it was therefore decided to construct a third larger apparatus which would be comparable in size to industrial or pilot-scale apparatus.

In order to estimate the likely oscillation requirements for the largest apparatus, the predicted effect of the dynamic scaling laws was considered: taking an oscillation of 1 Hz and 1 mm centre-to-peak (c.t.p.) amplitude and a net flowrate of 120 ml/min as a reference point for a typical experiment in the 24 mm diameter apparatus, a case study was considered for maintaining dynamic similarity for the flow while increasing the tube diameter six-fold (a theoretical increase of tube diameter up to 144 mm).

In order to keep the Strouhal number $Str = \frac{d}{4\pi x_o}$ constant, a six-fold increase in tube diameter implies a six-fold increase in c.t.p. amplitude i.e. from 1 mm to 6 mm. In order to keep the Oscillatory Reynolds number $Re_o = \frac{\rho \omega x_o d}{\mu}$ constant, a six-fold increase in tube diameter and six-fold increase in c.t.p. amplitude implies a thirty-six-fold (i.e. six-squared) *decrease* in oscillatory frequency i.e. from 1 Hz to 0.0278 Hz. In order to keep the Net Flow Reynolds number $Re_n = \frac{\rho U d}{\mu}$ constant, a six-fold increase in tube diameter implies a six-fold decrease of mean net flow velocity of fluid in the tube, but since the area of the tube has increased thirty-six-fold, the net flowrate through the tube (in absolute units) will increase by a factor of six i.e. from 120 ml/min to 720 ml/min (see Figure 3.1).

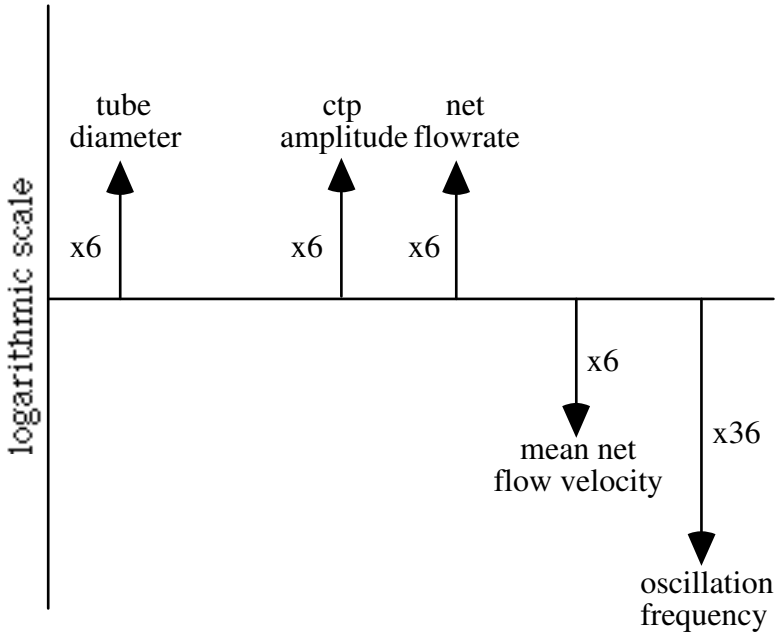

Figure 3.1: The Effect of Increasing Tube Diameter while Maintaining Dynamic Similarity

The decrease in oscillation frequency operates as an inverse-square law with respect to tube diameter, and this was considered to be a limiting factor governing the maximum tube diameter which could sensibly be investigated in the laboratory since very low frequency, low amplitude oscillations are notoriously difficult to achieve and are anyway likely to be dominated by unwanted thermal convection or vibration in the apparatus.

In contrast to net flow, amplitude and frequency, it was predicted from the Schmidt number $Sc = \frac{\mu}{\rho E}$ that the absolute value of the axial dispersion coefficient E would be independent of scale since μ and ρ are properties of the fluid only. This was also consistent with the Peclet number $Pe = \frac{UL}{E}$ where the relative changes in U and L (with respect to tube diameter) are inversely proportional to one another and therefore the value of E should be independent of scale assuming that the dynamic flow conditions were similar. This was a surprising prediction, since it might otherwise have been assumed intuitively that the axial dispersion would be greater in magnitude for larger diameter tubes.

In order that the sets of apparatus should be geometrically similar to one another, the aspect ratio of the tube (height to diameter) was designed to be approximately constant. In addition, in order to avoid the possibility of end-effects substantially altering the results (since the analysis to be used would assume an infinitely long tube, see §3.2) a minimum number of baffles were required in the tube. In practice, the tallest lab-space available was 5 m, which allowed for 18 baffles spaced at 1.5 times the tube diameter for a vertical 150 mm internal diameter tube (making allowance for the oscillator at the base of the tube.) Horizontal tubes or tubes with multiple bends were also considered in order to achieve a greater tube length, but it was determined from small-scale trials that these would not only lead to significant problems of degassing of trapped air but also, as discussed in §3.2, offered negligible benefit to the accuracy of residence time distribution experiments when using an imperfect pulse technique.

Practical height considerations therefore limited the largest tube diameter which could be investigated to 150 mm, and as already discussed the necessarily low oscillation frequencies (down to less than one cycle per minute for 150 mm tubes) in order to achieve dynamic similarity for the same fluid as in a 24 mm tube, also prohibited the investigation of any larger diameter tubes. The use of a more viscous fluid (such as sugar solution, Saraiva 1997) to avoid these low frequency oscillations was considered but rejected because of the very large amounts of fluid involved: requiring up to approximately 300 litres of fluid per experiment, the only practical fluid for the 150 mm diameter apparatus was ordinary mains-water. Table 3.1 shows the apparatus dimensions.

Tube Diameter mm	Tube Height m	Tube Volume litres
24	1	0.45
54	2	4.6
150	4.5	79.5

Table 3.1: Apparatus Dimensions

3.1.2 Construction of the Apparatus

All of the apparatus was self-designed and constructed in-house from a combination of off-the-shelf and self-engineered components (with the exception of the perspex viewing-boxes which were manufactured by the Department of Chemical Engineering Workshop.)

As has been discussed in §3.1.1, one of the major potential difficulties of performing dynamically similar experiments at different scales was the very low oscillation frequencies (of the order 0.01 Hz) required for the larger diameter apparatus. At the same time, the apparatus needed also to be capable of higher frequency oscillations (of the order 10 Hz) in order to explore the full effect of different conditions. With such a wide range of frequencies required, any motor-driven system would have required very substantial changeable gearing to be able to drive a smooth sinusoidal oscillation. (The mass of fluid to be oscillated in the 150 mm apparatus was approximately 80 kg, so inertial effects were important as well as any pressure drop across the baffles.) Motor or stepper-motor with cam-follower oscillators were therefore discounted because of the likely gearing and vibration problems and consequent expense.

Electromagnetic moving-coil oscillations were also considered for the 150 mm apparatus but rejected because of their limited power (and considerable expense) and because of their very limited stroke-length. For smaller apparatus however they are an ideal oscillator and a moving-coil oscillator was used to drive oscillations in the smallest (24 mm diameter) apparatus, having sufficient power and stroke-length to drive a wide range of oscillation frequencies.

Pneumatic pistons were considered for the larger rigs but were rejected because of the severe control problems inherent with oscillating large masses by means of a compressible gas. Another possibility for an industrial system would be direct pressurised air pulsing in a manometer-style tube as described by Baird (1966); such a system would be cheap to install but is limited in performance unless operating close to the resonant frequency of the system, as well as having safety concerns in the laboratory due to being effectively a large volume pressure vessel.

Finally, servo-hydraulics were selected as the most appropriate and cost-effective method of providing oscillations for the 54 mm and 150 mm diameter experimental apparatus; this was the first time that servo-hydraulics had been employed in O.F.M. but were nevertheless successfully implemented and proved to be highly reliable. The hydraulics were constructed from off-the-shelf components which could easily be interchanged or replaced and moreover the hydraulic power unit (supplying high pressure hydraulic oil to a piston) and control electronics could be shared between the 54 mm and 150 mm apparatus since only one or other apparatus was operated at any one time. The only duplication of equipment was therefore the individual hydraulic cylinders and displacement transducers assigned to each apparatus, tailored to the individual

requirements of force and stroke-length (i.e. amplitude of oscillation) for each rig. Servo-hydraulics also offered the potential advantage of being able to provide wave forms other than sinusoidal (for example triangular or trapezoidal wave forms) and of effectively isolating any motor vibration from the experiment.

Tube Diameter mm	Range of ctp Amplitude mm	Range of Frequency Hz	Range of Net Flow ml/min	Oscillation Method
24	0-8	0.1-20	0-2000	Moving Coil Oscillator & Bellows
54	0-25	0.05-10	0-5000	Servo Hydraulics & Piston
150	0-60	0.01-10	0-21,000	Servo Hydraulics & Piston

Table 3.2: Oscillation and Flow Ranges for Apparatus

Previous workers have used a number of different methods to transmit the oscillation from the oscillator to the fluid such as diaphragms and bellows. The apparatus in this dissertation used bellows for the 24 mm apparatus and piston/cylinder arrangements for the 54 mm and 150 mm apparatus (see Table 3.2).

Stainless steel bellows are a convenient solution to the problem of transmitting the oscillation while maintaining a seal for the fluid, but for larger apparatus they are expensive and prone to distortion at high loads. Their durability is also unknown for high frequency oscillations. (Diaphragms are also prone to distortion at high loads and have limited displacement and were therefore discounted for experimental purposes.) Bellows were selected for the 24 mm apparatus based upon previous successful experience (Mackley, Smith & Wise 1993) whereas the 54 mm and 150 mm apparatus used a piston/cylinder arrangement with its advantages of high rigidity and unlimited potential stroke-length: care was taken in the design and manufacture of the cylinder to give low friction movement but nonetheless an adequate seal at the pressures used.

The water-cylinder of the 54 mm apparatus was turned from a 316 stainless steel tube and hand-polished to accommodate a standard piston-seal size of 48 mm. The 150 mm apparatus used an off-the-shelf 160 mm internal diameter hydraulic cylinder adapted for water usage (chromed mild steel) as the water-cylinder, though because of mild corrosion adjacent to the wear seal during periods of disuse this was eventually replaced with a polished stainless steel cylinder.

Both the 54 mm and 150 mm rigs used off-the shelf piston seals (Busak & Shamban Glydring™ S-55044-1600-10 & 48-10) made from low-friction graphite-filled teflon and which were pressurised against the water-cylinder wall by a nitrile rubber O-ring. The 150 mm apparatus used an additional wear seal (Busak & Shamban Slydring™ GP6901600-T51) because of the larger forces involved and to assist piston alignment.

The seals were specified to seal at pressures up to 200 bar, far in excess of what was required for the O.F.M. application: the specified clearances for the pressurised O-rings were therefore relaxed a small amount during piston manufacture in order to reduce water-cylinder/piston friction at the expense of sealing capability.

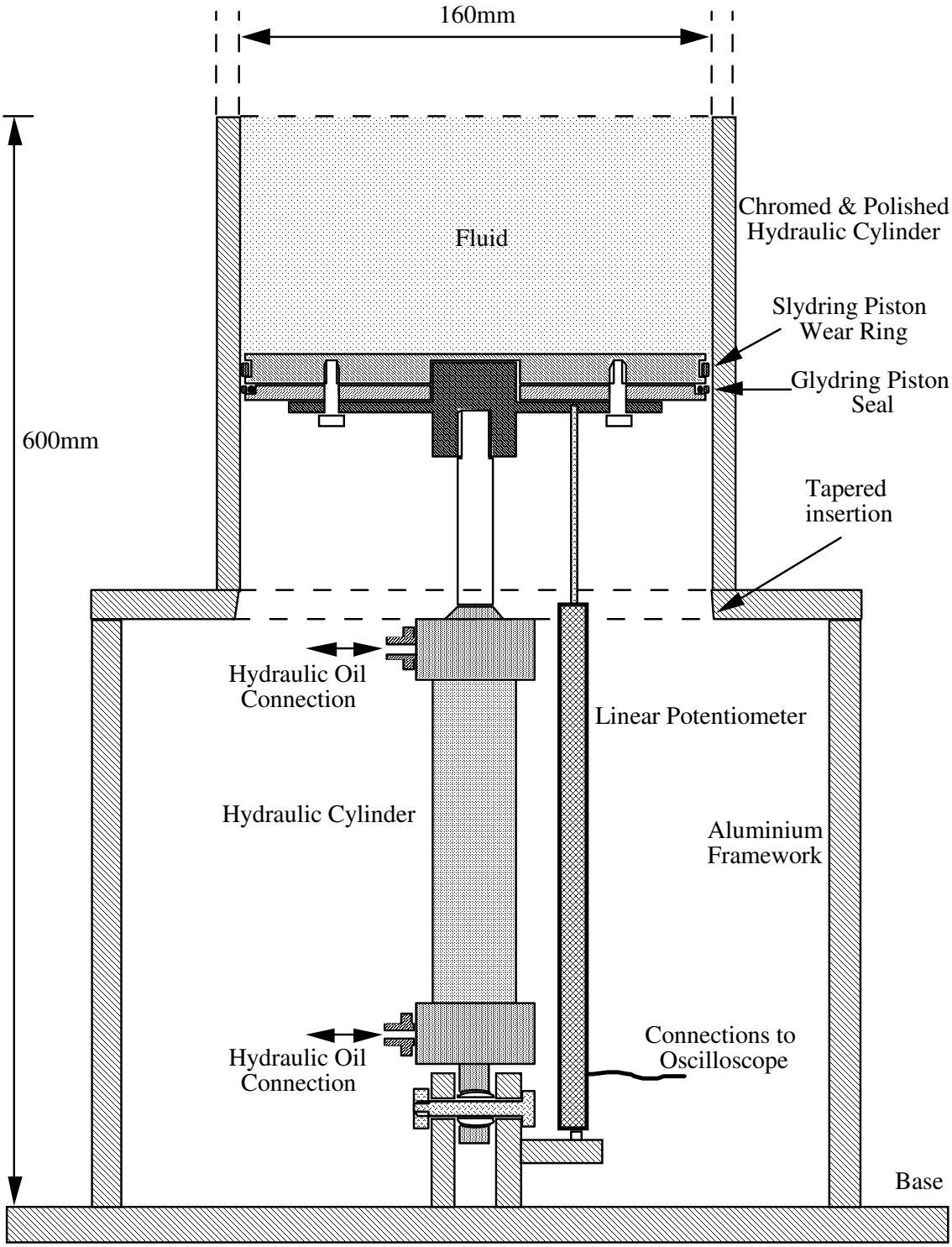

Figure 3.2: Schematic Diagram of the 150 mm Apparatus Oscillator and Base

The water-cylinder/piston arrangements (see Figure 3.2) were connected to a double-acting hydraulic cylinder, the movement of which was driven by an hydraulic servo-valve and whose displacement was measured by a linear transducer attached to the piston. The double-acting hydraulic cylinder for the 150 mm apparatus (Parker-Hannifin PHW 40-

SBD-HMI-RPF-19-M-12b-M-11-00) employed low-friction seals; freedom of alignment for the piston/ water-cylinder arrangement was ensured by the use of a spherical bearing-mounting. Experience of using this hydraulic cylinder suggested that stick-slip would not be a problem for smaller diameter water-cylinder/piston arrangements (where there was a surfeit of available power attainable from the hydraulics) and so a cheaper and less sophisticated hydraulic cylinder (Webtec DA 50-60-Y) was successfully employed for the 54 mm apparatus which was subsequently built. (Increasing the hydraulic cylinder internal diameter from 40 mm to 50 mm also reduced the potential for stick/slip to occur.)

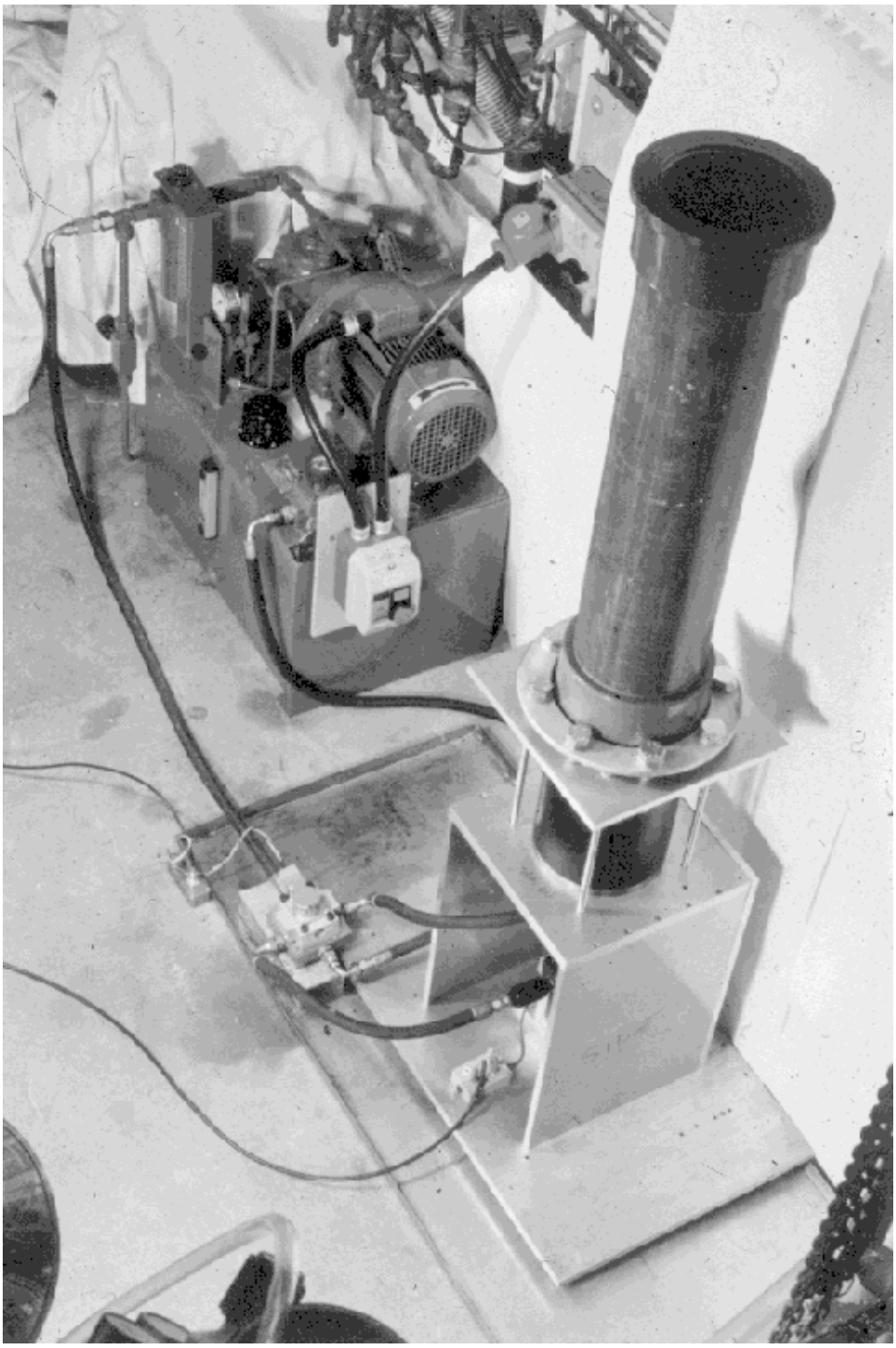

Figure 3.3 Photograph of the 150 mm Apparatus Hydraulics, Oscillator & Base

Sizing calculations for the hydraulic power unit are presented in Appendix I as well as a diagram of the hydraulic flow circuit. Details of the electronic servo-control circuits are given in Appendix II. The power requirements even for the 150 mm apparatus were found to be very modest by hydraulic standards, so in specifying the hydraulic pump and reservoir, special consideration was given to compactness (60 litre reservoir) and maintaining low noise levels with the use of a load-following pressure-compensating vane-pump (Mannesman Rexroth IPV2V7-1X/10-14 REOIMCO-14A1.) The reservoir was sufficiently large that convective cooling alone was sufficient to maintain the oil temperature below 50 ˚C. Sizing calculations presented in Appendix I also applied to the selection of the hydraulic servo-valve (Ultra Hydraulics 4661-114-000.)

The apparatus was required for flow visualisation and for residence time distribution measurements using a dye tracer technique (discussed further in §3.2); in order for these to be possible the tube walls were constructed of extruded transparent acrylic (perspex) for the 24 mm and 54 mm rigs. Smaller lengths of tube were joined together using standard domestic plumbing straight compression connectors (with nitrile O-ring seals.) In this way the tubes were easily constructed and modified. Where injection ports or outlet ports were required they were tapped either into a joint or directly through the wall of the perspex tubing.

Because of the cost and fragility of large diameter perspex tubing, only a 2 metre length of the 150 mm diameter tube was constructed of cast perspex and the rest of stronger, cheaper PVC tube whose main use is in underground water supplies. With readily available flanged joints the apparatus could easily be extended in the future. For flow visualisation purposes the perspex tubes were surrounded by square water-filled viewing boxes (to reduce the amount of optical distortion due to the different refractive indices of perspex and air.)

Since the baffles and other tube internals were to spend much time in-and-out of water, a non-corroding and non-swelling material was required. Punched, nibbled, and laser drilled stainless steel sheeting was considered but was rejected on the grounds of expense and the problems of obtaining a push-fit seal against the tube walls in tubes of slightly varying diameter. An additional problem with punched orifices was that the edges would be significantly rounded on one side due to the punching action; for flow separation a sharp edged orifice is desirable (Keulegan & Carpenter 1958, Knott & Mackley 1980.)

In preference the much cheaper solution of baffles machined from PVC sheeting and coupled using stainless steel studding was adopted. By machining many baffles sandwiched together, a very clean orifice edge could be obtained and also the precise outer diameter could be custom-made to push-fit against the particular tube wall (to an accuracy of order 0.1 mm.) Consideration was given that it might in fact be desirable to leave a small gap between the orifice and the tube wall in order to reduce the significance

of any stagnant corners but since all previous experimentation and flow modelling of O.F.M. has assumed a flush-fit of the baffles with no leakage, it was decided to maintain a seal between the baffles and the tube wall.

Kim & Baird (1976) as already discussed in Chapter 2 discovered that for reciprocating plate columns the plate thickness had a weak yet significant effect on the measured axial dispersion: baffles made from 1 mm, 2 mm and 6 mm PVC sheeting were manufactured proportionately for the 24 mm, 54 mm and 150 mm rigs respectively.

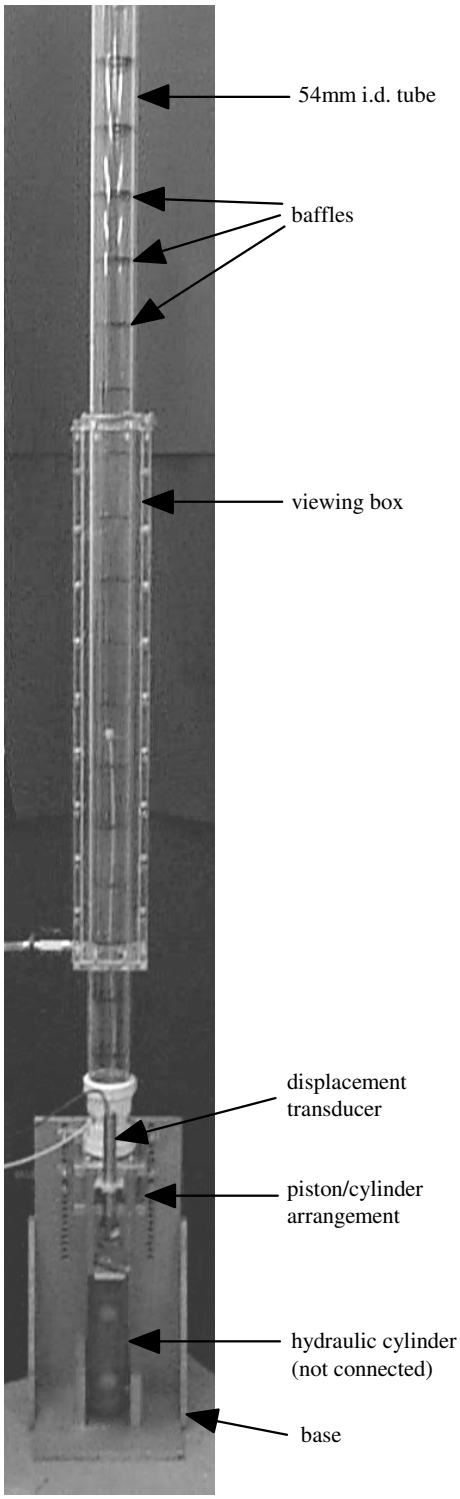

Figure 3.4: Photograph of the 54 mm Apparatus with its Viewing Box

Previous workers have used a variety of tube diameters, tube lengths, tube orientations (including bends), and baffle geometries as discussed in Chapter 2. The baffles constructed for the three sets of apparatus in this dissertation have a spacing equivalent to three tube radii (see Figure 3.4) and a relatively high constriction ratio of 75% by area (see Figures 3.5 & 3.6). This constriction is probably greater than the optimum but was chosen to match other apparatus in the Department for which comparative studies were being made in residence time distribution and heat transfer (Stonestreet 1997) as well as to match reciprocating plate studies performed by Baird (1996.)

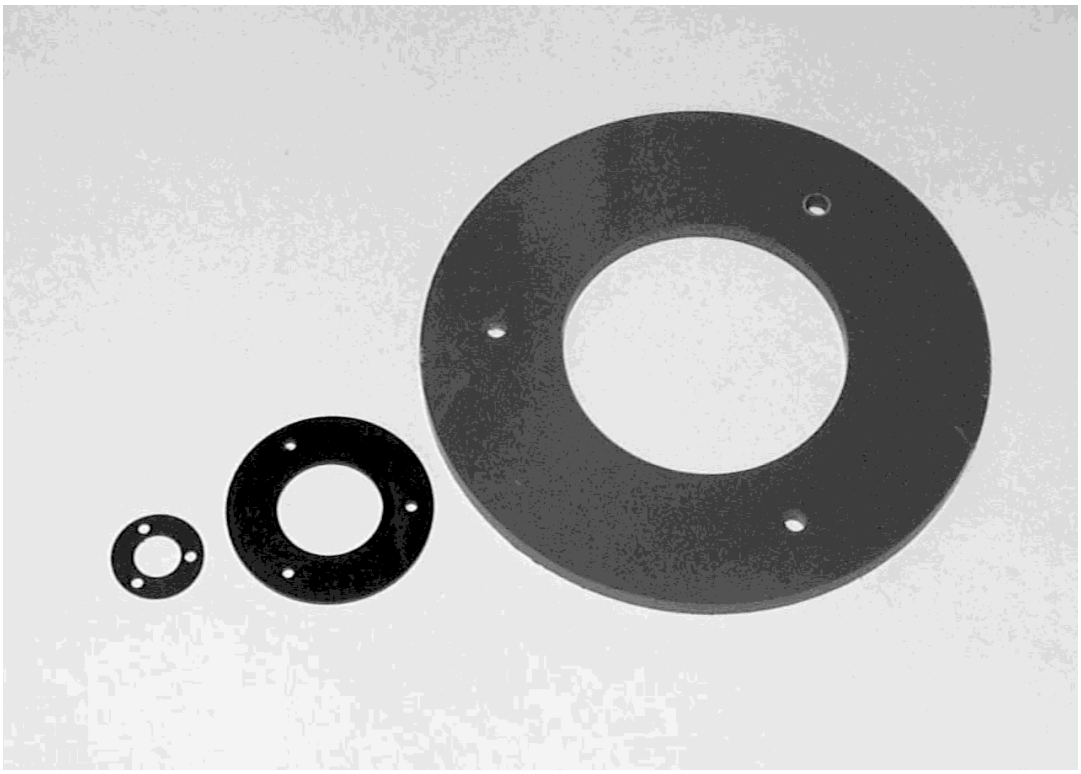

Figure 3.5: Photograph Showing Individual Baffles for the 24 mm, 54 mm and 150 mm Apparatus

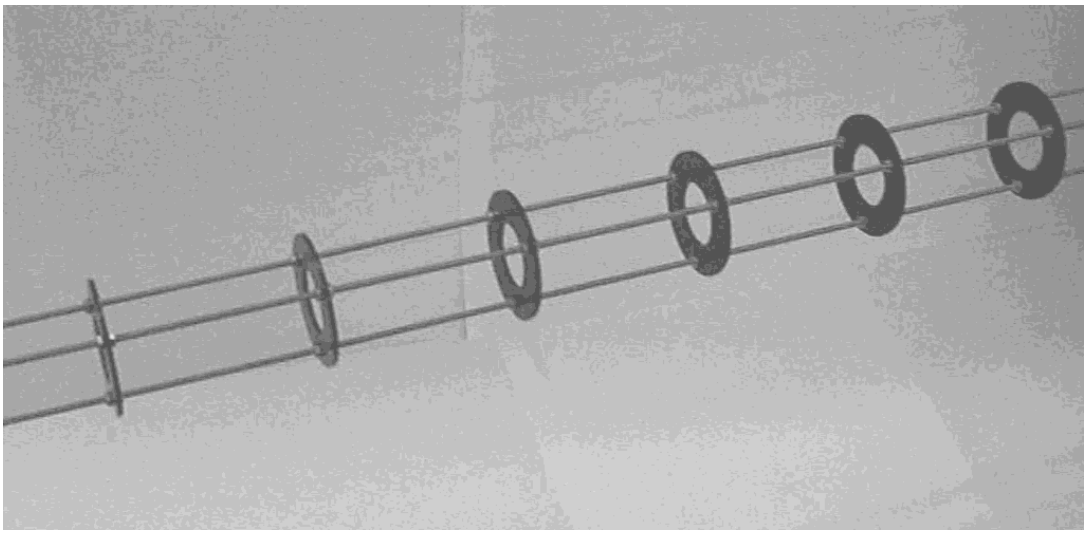

Figure 3.6: Photograph Showing a Baffle Insert for the 54 mm apparatus

3.2 Experimental Methods

The two primary experimental methods reported in this thesis are imperfect pulse dye tracer experiments (§3.2.1) and flow visualisation using fluorescent dye streaklines (§3.2.2). Both methods have been taken from other areas of research and developed as part of this thesis for use with Oscillatory Flow Mixing. Both sections begin with an explanation of the choice of the experimental technique.

3.2.1 Imperfect Pulse Dye Tracer Experiments

All techniques for the measurement of axial dispersion involve some form of tracer injection, whether a dye, salt solution, smoke or radioactive particles; the injection can be a pulse or a continuous stream of tracer. A number of problems have been identified by workers using salt-solutions and conductivity probes to measure axial dispersion and these include inaccuracies due to density differences (Mackley & Ni 1993) and poor averaging across the tube cross-section (Howes & Mackley 1990). The probes may also affect the flow. Smoke is clearly inappropriate for a fluid system and the use of radioactive particles is generally to be avoided where other methods exist, especially when large quantities of (contaminated) liquid must be disposed of after each experiment.

An optical method of detecting a neutrally buoyant dye tracer was therefore selected. A similar technique had already been used successfully for measuring concentrations of suspended particles in O.F.M. (Mackley et al 1993) but not previously for measuring axial dispersion. The optical technique has the advantages of not affecting the flow within the tube and of being very cheap to construct compared to the purchase of commercial conductivity probes, and can easily be located externally anywhere along the length of the tube.

High power Light Emitting Diodes (up to 15,000 mcd power) were used to propagate a beam of red light through the tube (wavelength approximately 660 nm). The intensity of the transmitted light was measured by a photo diode that is sensitive to the same wavelength. The photo diode allowed a current signal to pass proportional to the incident light and this could be amplified and converted to a voltage signal (0-5 Volts) for data recording. A blue dye tracer passing through the tube between the emitter and receiver attenuated the light and hence the average concentration of dye could be calculated as being proportional to the measured optical density. Details of the sensor calibration and signal treatment are given in Appendix III.

The aim of the tracer experiments was firstly to ascertain the effectiveness of a chosen model to describe the axial dispersion in the tube (due to net flow and oscillations) and

secondly to obtain quantitative data for the magnitude of axial dispersion as a function of flow conditions (using the chosen model). Previous researchers (for example Mackley & Ni 1993) have sought to improve the accuracy of their axial dispersion measurements by constructing a tube as long as possible, however with a tube diameter of 150 mm this would entail considerable expense and use of lab-space. The solution found to overcome this issue was to use an imperfect pulse technique on a relatively short section of tube, overcoming the need for a perfect pulse of tracer.

The principle of the imperfect pulse technique is that a pulse of tracer is injected into the tube and then the concentration of that tracer is measured at two points downstream. A model (such as the diffusion equation or the tanks-in-series-with-backmixing model) is then used to calculate a residence time distribution between the two measuring points (based upon their distance apart, the mean net flow velocity of the fluid in the tube and one or more other parameters). This model residence time distribution is then convolved with the concentration-time profile measured at the first measuring point in order to predict a concentration-time profile at the second measuring point as described in detail in Chapter 2; the experimental and model concentration-time profiles are then compared.

The minimum number of measuring points is therefore two, but in practice it is desirable to have at least three measuring points, from which three separate estimates of axial dispersion within the same experiment can be made. This serves as a useful check that conditions are consistent along the tube. In experiments described in this thesis therefore, three optical sensors were placed along the tube downstream of the injection point, as well as an additional sensor upstream of the injection point whose purpose was to obtain a measure of the backmixing in the system (i.e. the degree to which the oscillations forced dye tracer upstream against the direction of mean net flow).

Data from the optical sensors was continuously logged onto a PC via a National Instruments PCM-16 A/D converter. Using the board's proprietary software, the rate of data collection could be set and data saved to a particular file name, as well as visually monitoring the output of each channel on screen in real time. The rate of data collection was adjusted appropriately to the experiment, but as a general rule at least 15 data points were recorded per sensor during each mechanical oscillation and stored as 12-bit binary numbers. This produced data files of between 10 kilobytes and 1200 kilobytes in size depending upon the net flowrate through the tube. Four sensor channels were therefore recorded, plus a further two channels: one channel continuously logged the displacement of the oscillating piston/bellows; the other channel was coupled simultaneously to a PT100-style temperature recorder (monitoring the temperature of the tube during the course of the experiment) plus a push-switch which could be operated to give a step-change marker (a step of +1 Volt) in the data channel to indicate the time at which dye was injected into the tube.

The measurement of the temperature was a precaution since the optical sensors were proven to be sufficiently sensitive to changes in temperature that it was estimated a temperature change of more than 1 ˚C during the course of an experiment could produce significant errors in the final results (due the changing base-line values of the optical sensors). In practice it was found that for the short duration of experiments in the 24 mm and 54 mm apparatus the temperature change was rarely more than 0.2 ˚C and for the 150 mm apparatus where experiments could last for up to 4 hours the temperature changes were limited to 1˚C by protection of the apparatus from direct sunlight and insulation of the tube using bubble-wrap. Results from experiments where temperature changes were unexpectedly large were disregarded.

In the 24 mm and 54 mm tubes the dye was injected directly through the side wall of the tube (see Figure 3.7). Direct injection could not be used on the 150 mm tube since it was already surrounded by a viewing box. The dye solution was therefore delivered along a 3mm diameter PVC hose to a specially manufactured distribution nozzle with six holes which squirted dye radially out from the centre of the tube towards the wall.

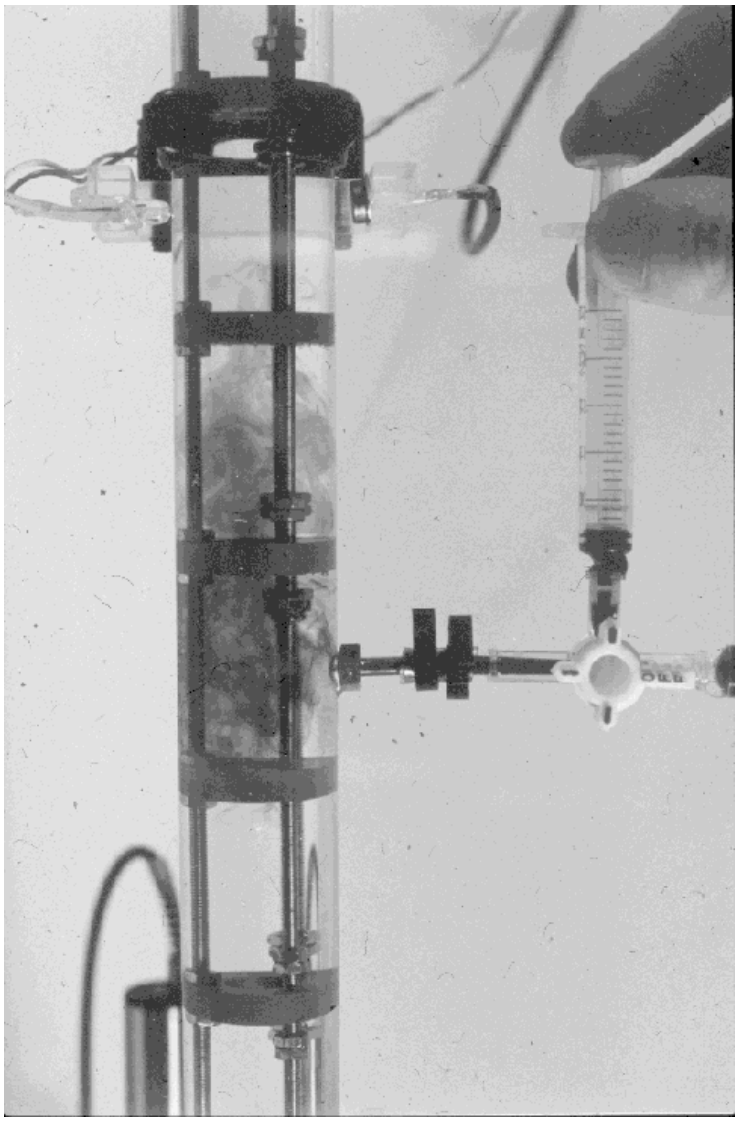

Figure 3.7: Photograph Showing Dye Injection in the 24 mm Apparatus

A technique using two syringes and a three-way valve was developed whereby the dye was injected and then followed by an injection of ordinary water in order to flush any dye remaining in the side-port. This was necessary because of the relatively small volumes of dye solution being injected compared to the volume of the side-port (the distance of tube between the syringe and the tube wall.) Figure 3.8 shows a series of photographs of a typical dye injection experiment with net flow and oscillation. The dye is injected close to the base of the tube (Fig 3.8a) and moves up the tube in the direction of the net flow (Fig 3.8b-f), dispersing as the experiment progresses. The apparatus is shown without the optical sensors used to detect dye concentration.

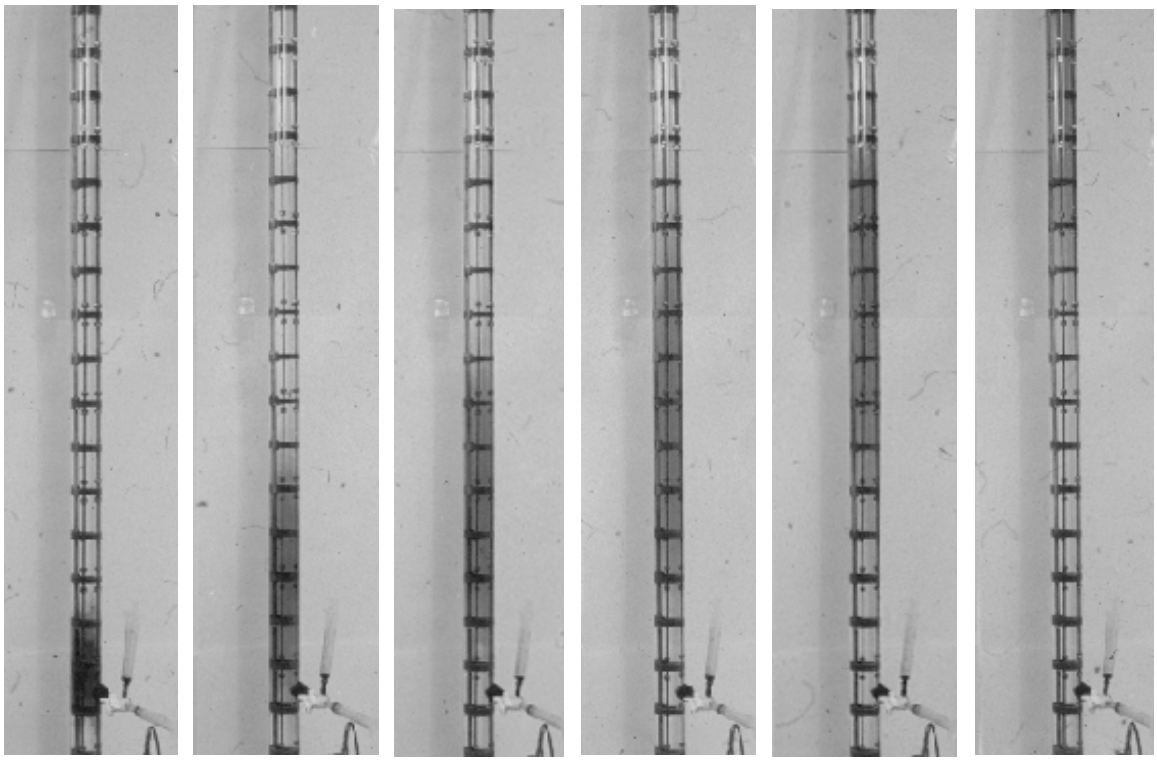

(a) (b) (c) (d) (e) (f)

Figure 3.8: Photograph Showing a Typical Experiment in the 24 mm Apparatus

The dye selected was methylene blue because of its high optical density at low concentrations: this allowed very dilute solutions to be used for which the very small density difference between the dye solution and the bulk fluid in the tube was insignificant over the time scale of most experiments. (The sensitivity of the optical sensor technique also allowed very dilute concentrations of the dye to be measured, even where not detectable by the human eye.)

The volume and quantity of dye injected did not scale proportionally to the volume of fluid in the tube: this was due to the decreasing intensity of the L.E.D. beam of light shining through the tube meaning that more dilute solutions had to be used for the larger apparatus in order to maintain resolution (see Table 3.3). It was found that the results of experiments were insensitive to the rate of dye injection; typically the dye was injected over the course of approximately one oscillation.

Apparatus	Volume of Dye Injected	Concentration of Dye Injected
24 mm Apparatus	0.7 ml	0.0001 g/ml
54 mm Apparatus	2.5 ml	0.0001 g/ml
150 mm Apparatus	20 ml	0.0001 g/ml

Table 3.3: Typical Quantity of Dye Injected for Axial Dispersion Measurements

Particularly for the 150 mm apparatus, the technique was somewhat sensitive to the presence of background light: all the apparatus were therefore shrouded in opaque black paper surrounded with black plastic sheeting (bin-liners!) which effectively eliminated all background light. The method could perhaps have been improved by using a stronger beam light source such as a laser-pen, but the additional expense and potential safety implications outweighed any possible advantage.

A typical experimental was conducted thus:

1. Net flowrate and oscillatory conditions were set and left for several minutes to ensure that quasi-steady-state had been reached
2. The recording of data from the optical sensors (4 channels), oscillation displacement (1 channel) and start/stop/temperature channel (1 channel) was started and the base-levels for each channel recorded for at least 300 data points per channel
4. The dye tracer was injected into the tube while the start/stop push switch was pressed simultaneously to mark the start of the experiment
5. The experiment was allowed to run until the output from the optical sensors readings had substantially returned to their base levels
6. Data recording was ceased and the collected data stored to a particular file name
7. The tube was thoroughly flushed to remove any residual dye before commencing the next experiment

A critical aspect of the experiments was to maintain a constant net flowrate during the course of the experiment: flowrates varied from 30 ml/min up to approximately 20 000 ml/min and had to be a smooth flow (otherwise any pulsation could have caused increased flow separation in the tube). Peristaltic pumps were found to give an unsatisfactory pulsating flow as well as having a limited range of operation. Instead, the flow was regulated by a needle valve and monitored by a range of rotameters (selected according the flowrate). This worked very successfully to give a steady flow, with the water supply being delivered from header-tanks maintained at constant pressure. In each apparatus, the

net flow was delivered as close as possible to the base of the tube for continuous operation, with a simple overflow arrangement at the top of the tube.

3.2.2 Flow Visualisation Using Fluorescent Dye Streaklines

A method of flow visualisation was required in order to understand better the types of flow found in O.F.M., to examine the effect of tube diameter on the observed fluid mechanics and to help interpret the trends in axial dispersion measurements. This was particularly relevant to understanding of the behaviour of multi-orifice baffles described in Chapter 8. Existing techniques such as seeding the flow with particles were inadequate for flow visualisation in tubes of greatly differing diameter, so a novel technique was sought. The required properties for the technique were that it would not affect the flow, would faithfully follow the flow, and that it could be used on tubes of any diameter.

In previous studies of O.F.M. the principal method of flow visualisation used was the slit-illumination of neutrally-buoyant 100 micron polyethylene particles suspended in the flow and photographed using timed-exposures to create streaklines of the particle trajectories (Brunold et al 1989). This method has a number of disadvantages: it does not show the degree of mixing in the tube; it is best used in batch mode since for continuous flow the particles will be washed out of the tube; the particles are difficult to handle and suspend and may affect the flow itself; the particles may not faithfully follow the direction of flow if they are not neutrally buoyant, and the particles are too small to be resolved in photographs of larger tube diameters. The latter problem could in principle be overcome by the use of larger diameter particles, but as their size increases to the order of mm then it becomes more problematic to obtain neutrally buoyant particles and to minimise the inertia of the particles.

Another method for observing flow patterns in O.F.M. is the simple injection of dye (such as is already used in this thesis for the measurement of axial dispersion, also adopted by Saraiva 1997). This technique was used in initial investigations of the flows examined in this thesis but has very limited effectiveness since after only a few oscillations the dye is well-distributed across the tube and no fine detail of the flow can be distinguished.

Particle Image Velocimetry (P.I.V.) and Laser Doppler Velocimetry (L.D.V.) are powerful techniques which yield much information about the flow (Hayden 1997), but both are very costly and time consuming to set up and were therefore impractical for use on three separate rigs.

Flow visualisation using a fluorescent dye has previously been used by researchers in different areas (for example static mixers, Reeder et al 1997). The technique typically used a fanned laser-beam of about 1 mm width to illuminate a longitudinal-section through the tube. Fluorescent dye was then injected into the flow and was illuminated only when it passed through the fanned laser-beam, allowing a section through the flow to be examined, photographed or videoed in detail. The resulting streakline flow

visualisations required substantial subsequent processing to correct for the effects of diminishing light intensity from one side of the tube to the other due to both the fanning of the laser beam and to the absorption of light by the dye itself.

In this thesis the fluorescent streakline technique has been adopted and modified to create a novel method for determining streak-lines in Oscillatory Flow Mixing: a focused mercury-vapour lamp was used as the light source which, when placed a sufficient distance (typically 1 to 2 metres) from the O.F.M. tube gave a nearly parallel-beam light source. There still remained the problem of absorption of light by the dye itself, but this effect was minimised by the light beam having sufficient intensity under most circumstances to pass through the tube with only modest attenuation due to the presence of the dye. The result was to show streaklines within the flow in great detail in a tube of any diameter without affecting the flow, and to give an indication of the degree of mixing taking place. Only limited velocity information can be deduced.

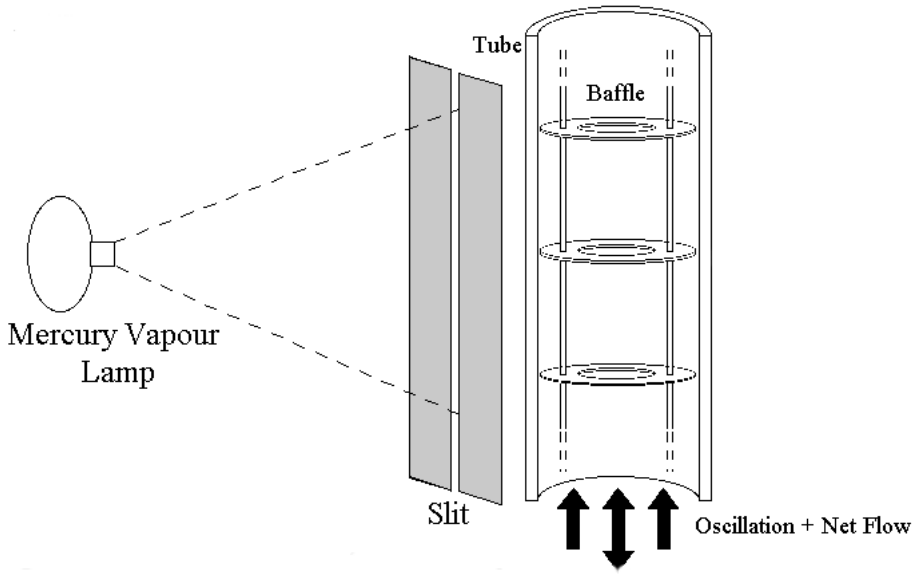

Figure 3.9: Schematic Diagram of Flow Visualisation Using Fluorescent Dye

The dye used was fluoroscein sodium dissolved in water; the concentration and volume of dye solution used was adjusted depending upon the apparatus and the oscillatory conditions. The concentration was typically of order 0.001 g/ml and the injected volume of order 0.7 ml, 2.5 ml and 20 ml for the 24 mm, 54 mm and 150 mm rigs respectively. The dye solution was made neutrally buoyant by the addition (trial and error) of approximately 0.5% ethanol. In order to maximise contrast, the apparatus was completely shielded from background light by black paper and black plastic sheeting. Figure 3.9 shows a schematic diagram of the apparatus.

The light levels emitted by the fluorescent dye are very low, so whilst they are impressively visible to the human eye, their capture on photograph or video is close to the limit of those technologies. Images were captured both with still photography using black

& white high speed film up to ASA 6400 and a Super-VHS video camera with a fully-open aperture.

4. Analysis of Results for Axial Dispersion

This chapter describes the treatment of the experimental raw data acquired for axial dispersion measurements. In order to analyse the data an analysis programme was written using Matlab code. Details of the programme code are given in Appendix IV, while §4.1 describes the algorithms used by the analysis programme to extract axial dispersion measurements from the data. §4.2 gives an explanation of the correct form of the imperfect pulse solution to the diffusion equation (for which conflicting solutions arise in the literature, see Chapter 2). §4.3 is a case study analysis (Case Study 1) of a typical imperfect pulse tracer experiment in the 24 mm apparatus. §4.4 is a case study analysis (Case Study 2) of a typical tracer experiment with no net flow in the 150 mm apparatus.

4.1 Development of Axial Dispersion Analysis Programme in Matlab

Having recorded data from the four optical sensors and from the displacement transducer monitoring the wave form of the oscillation as described in the preceding chapter, the raw data was stored on a standard PC hard disc. In order to extract useful information, an analysis programme was created in Matlab (a Windows-based commercial software package) and used to manipulate the data. This section describes the algorithms used in the analysis programme; at all stages of the development of the code it was rigorously tested for reliability and self-consistency.

Matlab was chosen because of its efficiency at handling very large matrices of data (for some experiments in excess of 600 000 data points). While this number of data points may at first seem excessive, it must be remembered that in order to measure variations in optical sensor output during one oscillation cycle, a substantial sampling-rate was required; during the analysis, the data could be greatly compressed.

Programming in Matlab is quite similar to many other programming languages, except that compiling is not necessary. Many smaller subroutines can be combined together to form a larger programme, and this was the sequential structure chosen for the analysis programme. The most up to date version of the analysis programme happened to be version 7, and this consisted of two separate programmes named `net7` and `nonet7`, both of which shared mostly the same subroutines: `net7` was used to analyse experiments with a net flow (with or without oscillations - see Case Study 1), whilst `nonet7` was used to analyse experiments without a net flow (oscillation only - see Case Study 2). It was necessary to make this distinction because while in experiments with a net flow the dye is eventually washed out of the tube and the concentrations measured by the optical sensors return to zero, in experiments with no net flow the dye remains in the tube and the

concentrations measured only approach zero asymptotically if an infinitely long tube is used; in the latter case the concentration-time profiles cannot be normalised.

The programme `net7` calls a series of subroutines to process the raw data. The first of these simply reads in the raw data plus data from a subroutine which contains supplementary information about the particular experiment (such as the file name under which the raw data is stored, the tube diameter, the net flow, the sampling rate, the density and viscosity of the bulk fluid). The data is rearranged into matrix form and when plotted appears thus:

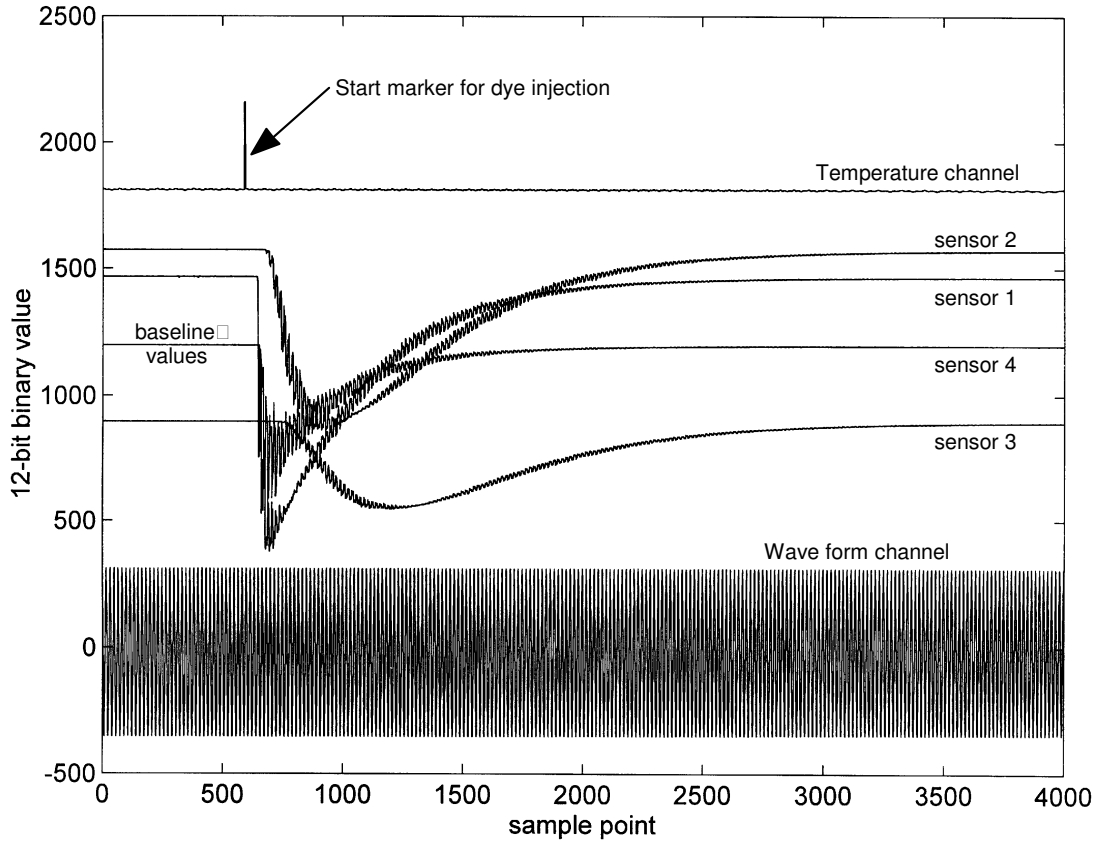

Figure 4.1: Plot of Raw Data from a Typical Axial Dispersion Experiment

The wave form channel shows the displacement of the mechanical oscillator (showing many oscillations – the individual oscillations can only just be distinguished in Figure 4.1). The frequency, amplitude and number of mechanical oscillations was determined by a subroutine which firstly zeroed the average displacement of the oscillation (for an integer number of oscillation cycles) before calculating the cycle frequency:

$$f = \frac{number\_of\_cycles \times samplerate}{number\_of\_samplepoints} \qquad \text{eqn (4.1)}$$

and the oscillation centre-to-peak amplitude :

$$x_o = (root\_mean\_squared\_displacement) \times \sqrt{2} \qquad \text{eqn (4.2)}$$

The points at which the oscillation crossed the zero-axis were also computed and used in the reduction of the size of the data set (by averaging the sensor values over each oscillation). A Fourier analysis of the oscillation wave form was used to display a frequency spectrum for the oscillation: this was a useful check for an irregular wave form. In general, the wave form was consistently very close to a pure sinusoidal wave form. The wave form displayed is that of the experiment shown in Figure 4.1.

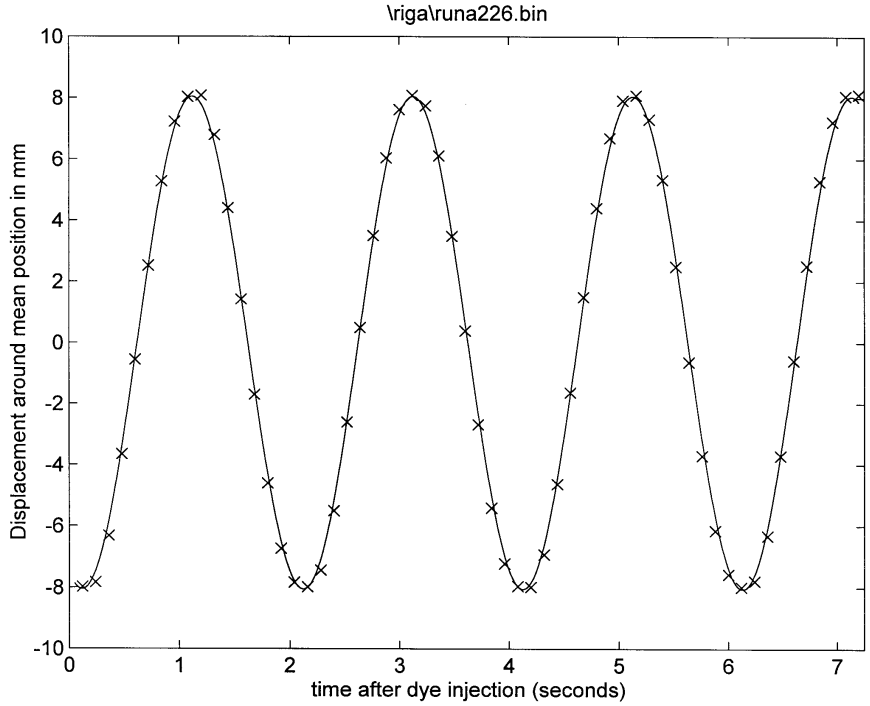

Figure 4.2: The Measured Wave Form of a Typical Oscillation in the 24 mm Apparatus:
x experimentally measured points; --- theoretical sine wave

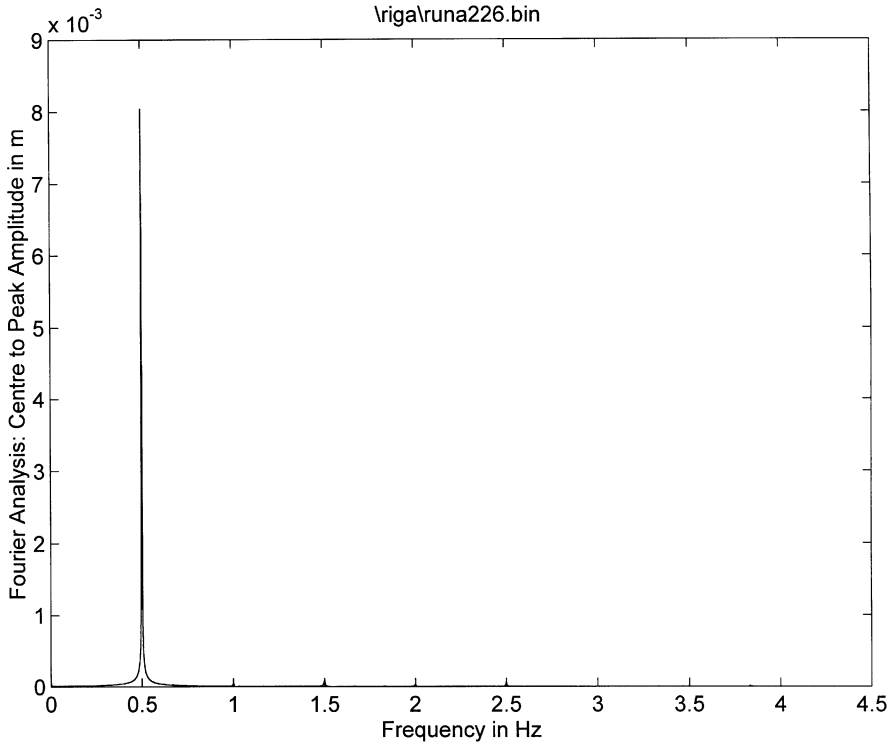

Figure 4.3: Frequency Spectrum of a Typical Oscillation in the 24 mm Apparatus

The start marker of the experiment (the moment of dye injection) is clearly visible in Figure 4.1 as a pulse in the temperature/timing channel; the experiment was stopped sometime after all the dye had exited the baffled tube. Several subroutines in the analysis programme are dedicated to detecting the start marker recorded on the timing/temperature channel and to removing all data points from before the start of the dye injection. An additional subroutine also records the baseline levels of the optical sensors before the start of the dye injection.

Those baseline values are then used to convert the optical sensor output voltages into optical density measurements: since $\log\frac{I_o}{I} \propto concentration$ where I_o is the baseline intensity and I is the experimental intensity, the optical sensor output voltages can be converted into absolute concentrations (see Appendix III). These values, after correction by a previously determined sensor calibration, represent the average concentration of dye along the path of the transmitted light for each optical sensor.

For simplicity, these concentrations are then normalised so that for example C_2' and C_1' are the normalised experimental concentrations at optical sensors 2 and 1 respectively:

$$C_2'(t) = \frac{C_2(t)}{\int_0^\infty C_2(t)dt} \quad \text{and} \quad C_1'(t) = \frac{C_1(t)}{\int_0^\infty C_1(t)dt} \qquad \text{eqns (4.3 \& 4.4)}$$

This is not applicable to the single optical sensor located upstream of the dye injection point, to which a conversion factor is applied which is the average of that of the other optical sensors'. This introduces a small error (<5%) into the values for the upstream sensor. The normalisation is not strictly necessary, but allows the results to be conveniently scaled onto a single axes for comparisons to be made. In the case of experiments without net flow, the normalisation procedure cannot be applied and therefore the data is retained as a concentration in mg/l.

The value of the mean net flow velocity U is calculable directly from the net volumetric flow rate Q, the distance between the probes L and the volume of fluid between probes V:

$$U = \frac{QL}{V} \qquad \text{eqn (4.5)}$$

A second method for calculating U is to calculate the difference in time between the first moments of area of the concentration profiles and which should be in good agreement with that given by the previous equation.

$$U = \frac{L}{\int_0^\infty tC_2'(t)dt - \int_0^\infty tC_1'(t)dt} \qquad \text{eqn (4.6)}$$

In preference equation 4.5 was used to calculate U since it could then distinguish potentially occurring effects such as dead-zones (volumes of fluid between sensors which do not contribute to the reactor volume) and would also be insensitive to errors caused by the premature termination of some experiments before the dye was fully flushed out of the tube (leading to cropping of the concentration-time profiles).

Some researchers (e.g. Goebel et al 1986) have relied upon a third method for determining U, by varying both U and E to achieve a best-fit between model and experiment using the convolution technique, and then taking the best-fit value of U as the true value. This method was inaccurate as discussed in the next section.

Computation of optical densities, concentrations, graphs and convolutions became very intensive and time-consuming when using large numbers of data points. In practice therefore, the majority of optical sensor experimental data sets were initially reduced in size by subroutine `reduce7` such that each data point was the average value measured over one whole period of the mechanical oscillation. For experiments without any oscillations, a different subroutine (`reduce7b`) was used with an arbitrary scaling factor depending upon the size of the file. In this way the total processing time required to analyse a complete experiment on a modest 75 MHz P.C. was only a matter of seconds.

Having been suitably prepared, the concentration-time profiles were used in an iterative subroutine `optim123` to determine the value of the axial dispersion coefficient E which caused the model prediction to most closely match the experimental measurements. Since there were three optical sensors downstream of the dye injection point, three separate estimates of E could be made. Initially a pair of sensors was chosen and the value of the E guessed at 0.0001 m^2/s. A subroutine was called to generate a vector of the appropriate transfer function (depending upon the mean net velocity, the distance between the sensors and the guessed value of E). This transfer function was then convoluted with the more upstream of the pair of experimental concentration-time profiles to produce a predicted profile at the more downstream sensor. The results were displayed on the screen and the process repeated with further guessed values of E until a best fit value was found. Although subroutines were developed to optimise E automatically, these were found to be slow as well as insensitive to anomalous data; with a little experience, a process of visual inspection and guessed values of E was found to be the quickest and most informative method of analysing the data to obtain an estimate of E +/-10%.

This process was repeated for each pair of sensors, giving three separate estimates of E. Once the analysis was completed, the results and compressed data were saved to a new file name for easy recall.

4.2 Debugging of the Imperfect Pulse Solution to the Diffusion Equation

As discussed in Chapter 2, two different transfer functions appeared in the literature as the solution to the diffusion equation for what were apparently the same boundary conditions. The solution after Goebel et al (1986) (equation 2.19) was therefore compared against that published by Westerterp et al (1984) (equation 2.20) using the algorithms developed for `net7` but with the two alternative transfer functions. For test purposes, an artificial perfect pulse input function was used; the first check on the two transfer functions was to test whether they would give the same prediction as the transfer function given in the literature for a perfect pulse experiment.

For a "model" perfect pulse of tracer injected at time $t = 0$, in a tube with a net flow of 0.01 m/s and sensors at $x = 1$ m, $x = 2$ m and $x = 3$ m distance downstream from the injection point and a theoretical axial dispersion coefficient of 0.001 m^2/s, the following artificially-generated "experimental" responses were calculated using equation 2.17 (and taken to be correct):

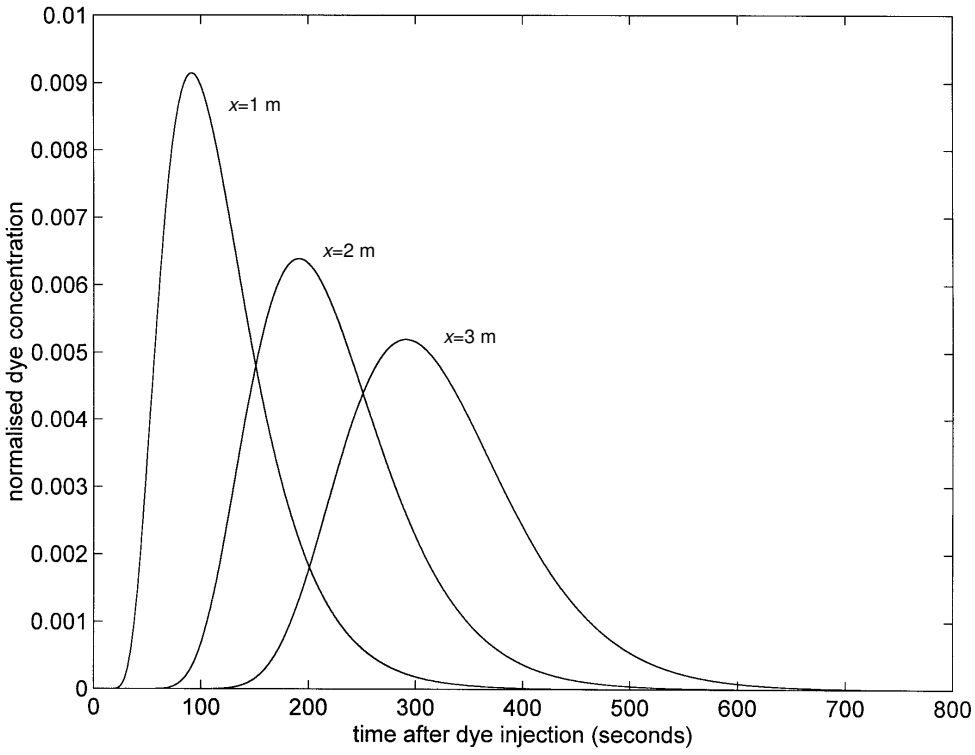

Figure 4.4: Theoretical Responses to a Perfect Pulse of Tracer at Time t=0

The theoretical concentration-time profile for sensor one (at $x = 1$ m) was then convoluted with transfer functions generated using equation 2.20 (after Westerterp et al 1984) to give predicted responses at $x = 2$ m and $x = 3$ m and using the same values of net flow velocity and axial dispersion coefficient. These "model" results were compared with the artificially-generated "experimental" responses and are shown on the following graph:

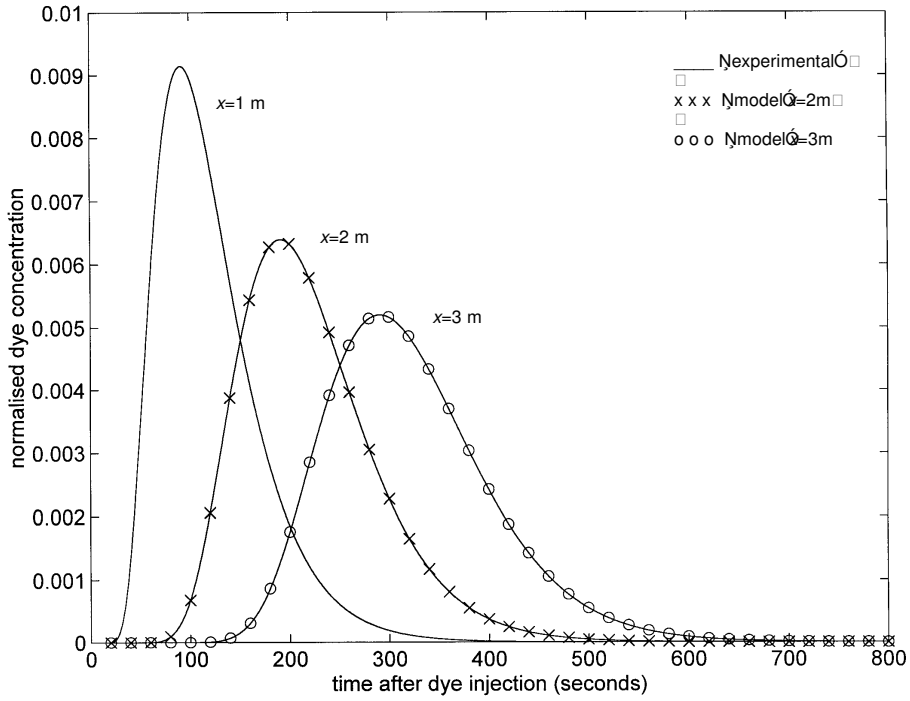

Figure 4.5: Comparing Artificially Generated "Experimental" with "Model" Results Using a Transfer Function after Westerterp et al (1984)

Clearly, there was an excellent agreement between the "experimental" and predicted "model" results. However, if instead the transfer function after Goebel et al (1986) was used (equation 2.19) then there was a clear discrepancy between the "experiment" and "model" profiles:

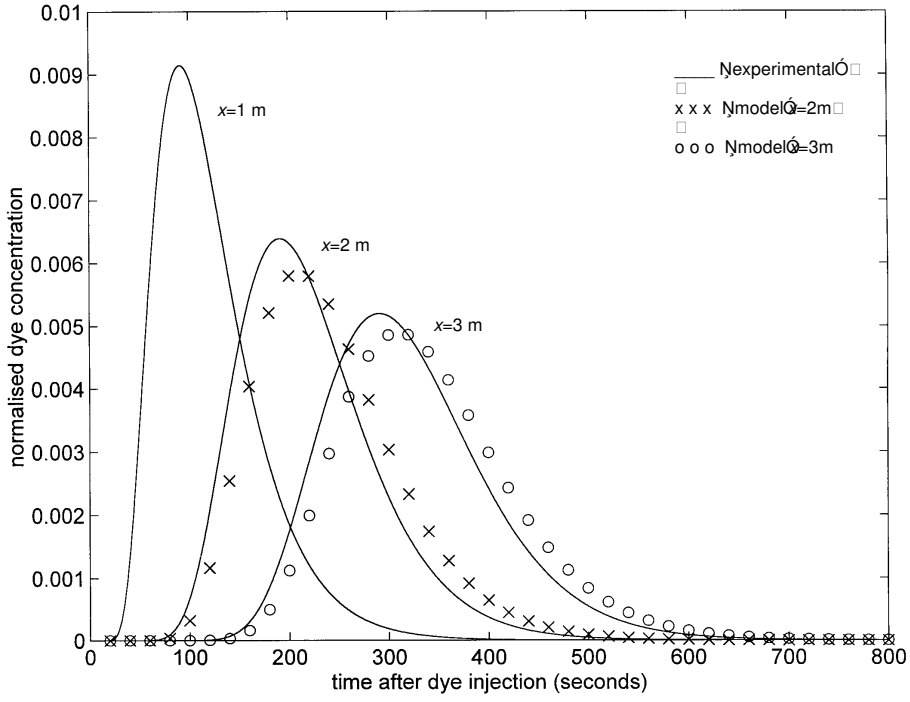

Figure 4.6: Comparing Artificially Generated "Experimental" with "Model" Results Using a Transfer Function after Goebel et al (1986)

Not only was the shape of the profile different but importantly, the effective "centres-of-gravity") of the "model" concentration-time profiles results were later in time than those of the "experimental" results. This gave a clue as to the origin of the error contained in the transfer function used by Goebel et al: they argued that the concentration-time profile measured experimentally at x = 1 m could be modelled as a series of perfect-pulse injections and therefore the sum of the responses to each of those perfect pulses (using equation 2.17) would yield the net concentration-time profile at x = 2 m and x = 3 m. This argument is flawed, since the experimentally determined concentration-time profile in fact represents a volume of tracer entering the reactor volume between two sensors whereas if a perfect pulse of tracer were to be injected then instantaneously half of the tracer would in practice travel upstream of the injection point (due to an infinitely-large concentration gradient) before eventually being washed downstream past the original injection point at a later time. This subtlety was examined by Gilibaro (1978).

This explains why for the "model" predictions using the transfer function used by Goebel et al the mean residence time (the difference between the effective “centres of gravity”) between sensors is larger than in practice (for the "experimental" results): for both the "experimental" and Westerterp "Model" results the mean residence time between sensor 1 and sensor 2 (and also between sensor 2 and sensor 3) is 100 seconds (as expected for a mean net flow velocity of 0.01 m/s over a distance of 1 m). For the Goebel "Model" the mean residence time between sensor 1 and sensor 2 is larger at 120 seconds which is nonsensical: the extra 20 seconds is accounted for by the fraction of the tracer which firstly travels upstream of the injection point before passing sensor 1 at some later time if indeed the measured concentration-time profile at sensor 1 were to be modelled as a series of perfect pulses. The model proposed by Goebel et al (1986) and later adopted by Mackley & Ni (1991) is therefore shown to be erroneous.

	Sensor 1	Sensor 2	Sensor 3
"Experimental"	121 s	221 s	321 s
"Model" - Westerterp et al	-	221 s	321 s
"Model" - Goebel et al	-	241 s	341 s

Table 4.1: Predicted Mean Residence Times for Artificially Generated "Experimental" & "Model" Results

It was discovered that if the magnitude of the axial dispersion coefficient is small compared to the product of the mean net flow velocity and the distance between sensors then the error produced by the Goebel et al (1986) model is small, i.e. if the Peclet number $Pe = \frac{UL}{E}$ is small (< 20) then the error in the predicted mean residence time is large.

$$\text{error} = \frac{\int_0^\infty tC'_{conv}(t)dt - \int_0^\infty tC'_2(t)dt}{\int_0^\infty tC'_2(t)dt} \qquad \text{eqn (4.7)}$$

In the above example Pe = 10 which corresponds to an error in the predicted mean residence time of 9.5%. Another way of looking at the problem is that since tracer moves upstream, the effective bulk volume of fluid is increased hence increasing the residence time between sensors by a factor determined by the Peclet number.

$Pe = \frac{UL}{E}$	1000	100	20	10	5	2	1
error in calculated residence time	<0.1%	0.9%	4.7%	9.5%	16%	33%	50%

Table 4.2: Errors in the Predicted Mean Residence Time Using the Goebel et al (1986) Model

Both Goebel et al (1986) and Mackley & Ni (1991) adjusted the values of both U and E in order to obtain a best fit between their experimental data and model prediction. Their method will therefore have lead to unpredictable errors in their values of E due to variations in the Peclet number for different experiments. Not only was their model transfer function incorrect, but what should have been a single-parameter model (with E as the variable parameter) was changed to a two-parameter model (with U and E). This largely explains why Mackley & Ni (1991) obtained a different value for the axial dispersion coefficient when they altered the distance L between sensors. It also explains discrepancies in the calculated axial dispersion coefficient recorded by Ni (1995) who compared the axial diffusion model with the tanks-in-series model.

4.3 Case Study 1 - Analysis of a Typical Imperfect Pulse Tracer Experiment

The data shown in Figure 4.1 is typical of an experiment in the 24 mm baffled tube. The mean net flow velocity was 116 ml/min with an oscillation frequency of 0.5 Hz and a centre-to-peak amplitude of approximately 8.2 mm. The sample rate per channel was 50/6 Hz. The temperature of the apparatus at the start and finish of the experiment varied only by 0.1 ˚C, so errors due to changing temperature during the experiment were treated as negligible.

After processing of the raw data, the concentration-time profiles of the four optical sensors (three downstream and one upstream of the injection point) were found to be:

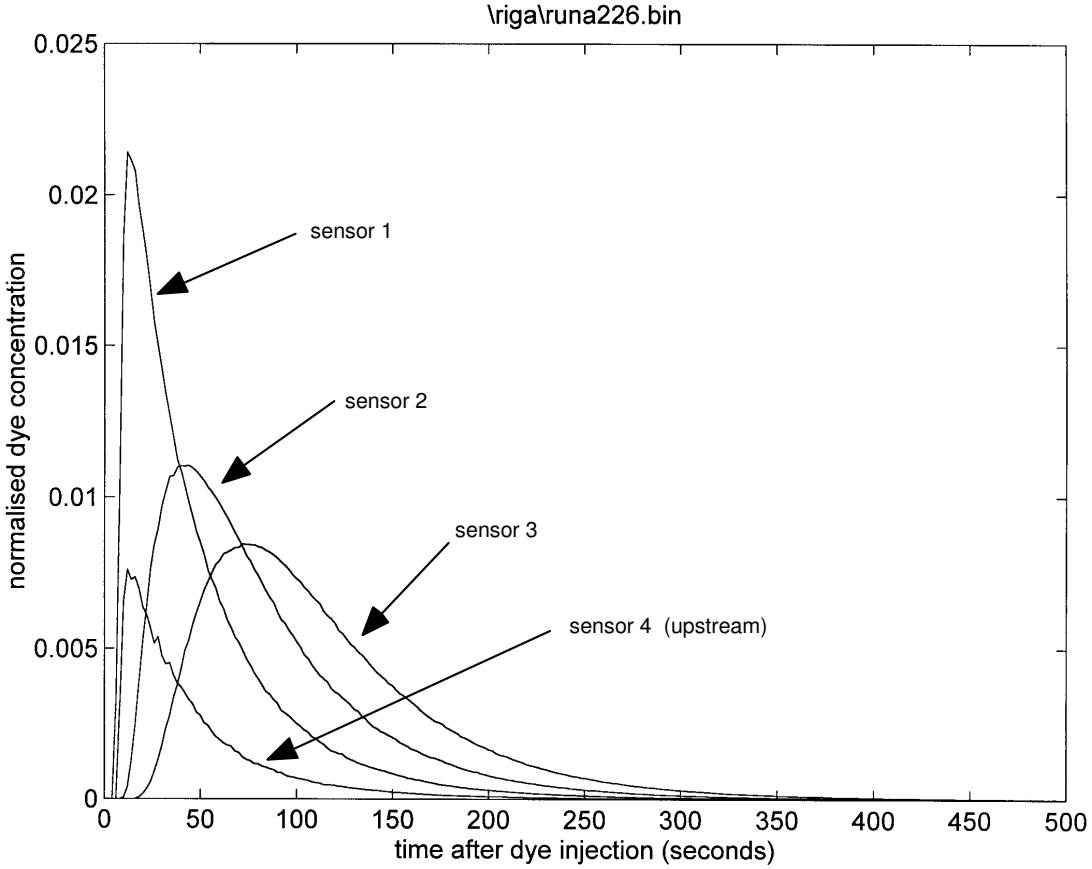

Figure 4.7: Case Study 1 : Concentration-Time Profiles for the Optical Sensors

Note that the area under the concentration-time profile for the upstream sensor was measured to be about 34% of that for the other sensors, a measure of the degree of backmixing (axial dispersion of the dye against the direction of net flow) and which is discussed further in Chapter 5. Note also that the profiles are significantly smoother than in the original raw data: this is because the data points were averaged over one whole oscillatory cycle (§4.1). The discrepancy in the total area under the concentration-time profiles for sensors 2 and 3 compared to sensor 1 was 2.1% and 2.8% before normalisation. This is a relatively small discrepancy within the expected experimental error for the optical sensors; it supports the observation that effectively all the dye had been successfully flushed through the tube.

Firstly sensors 2 and 3 were selected and a model transfer function calculated using equation 2.20 with x the distance between the sensors, U the mean net flow velocity and an estimated value of the axial dispersion coefficient E. The transfer function was then convoluted with the experimental concentration-time profile at sensor 2; the value of E was then adjusted and the process repeated until a best-fit of the model with the experimental profile at sensor 3 was obtained. The model prediction is shown as a smooth line and coincides very well with the experimental profile for a value of E = 0.0003 m^2/s:

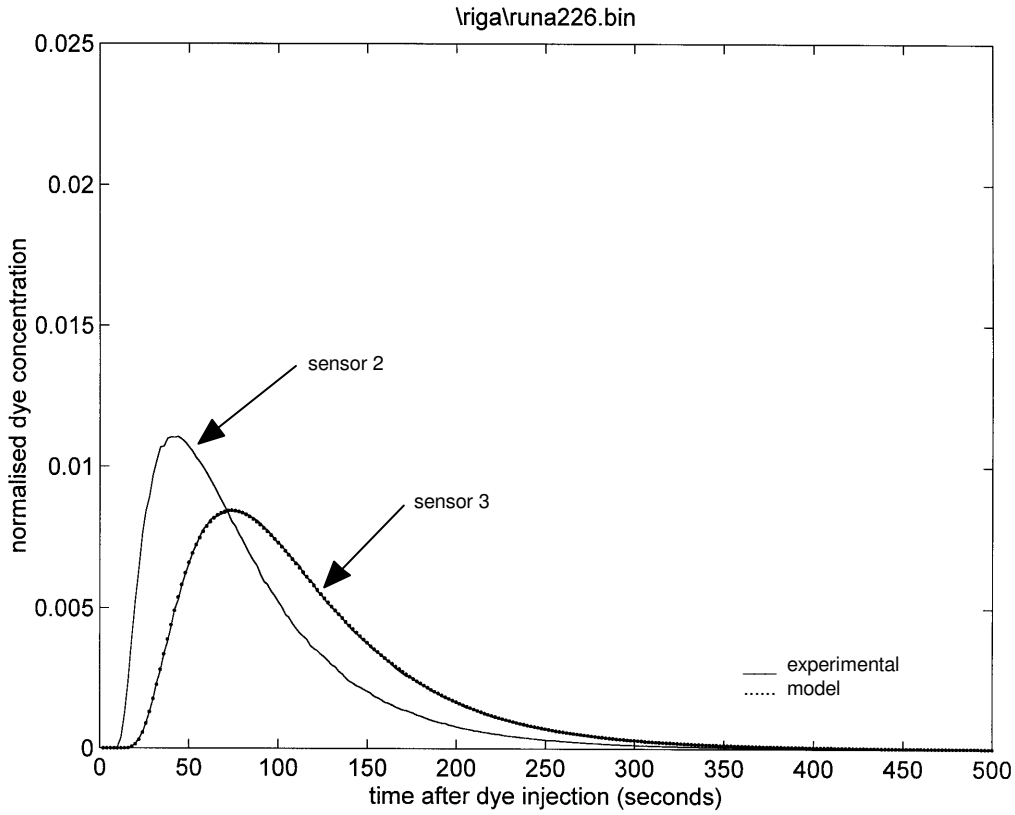

Figure 4.8: Case Study 1: Experimental and Model Results for Sensors 2→3

The process was repeated for sensors $1 \rightarrow 2$ and sensors $1 \rightarrow 3$ for which similarly good agreement between experimental data and the model prediction was obtained for the same value of the axial dispersion coefficient: (see Figures 4.9 & 4.10).

The diffusion model was therefore found to be an excellent and self-consistent model for describing and quantifying axial dispersion in O.F.M. under these dynamic flow conditions.

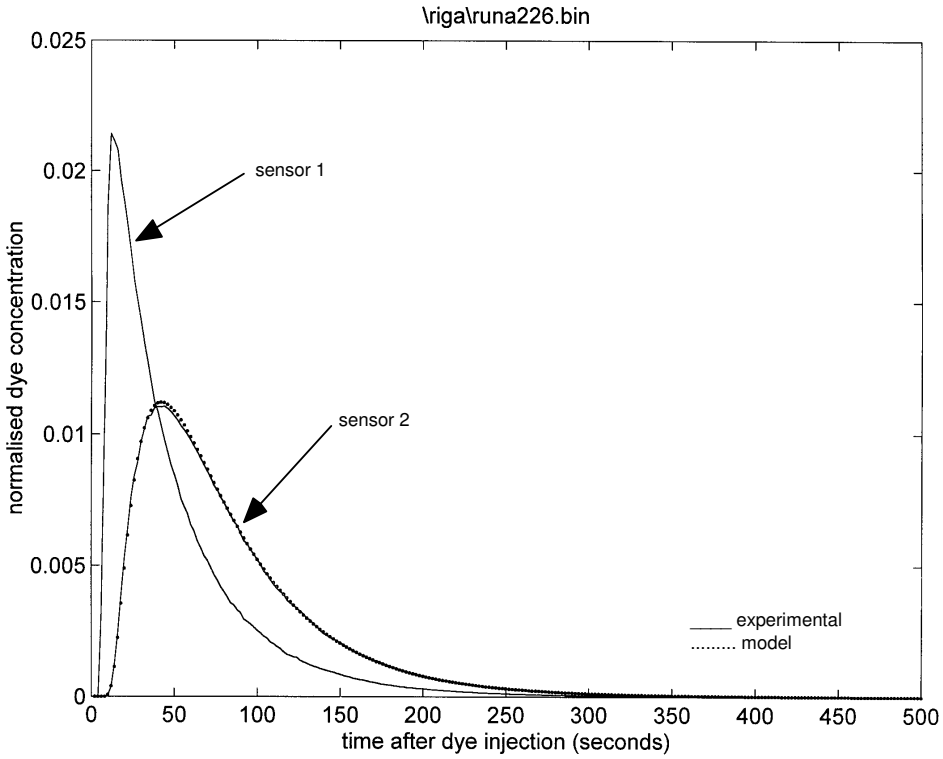

Figure 4.9: Case Study 1: Experimental and Model Results for Sensors $1 \rightarrow 2$

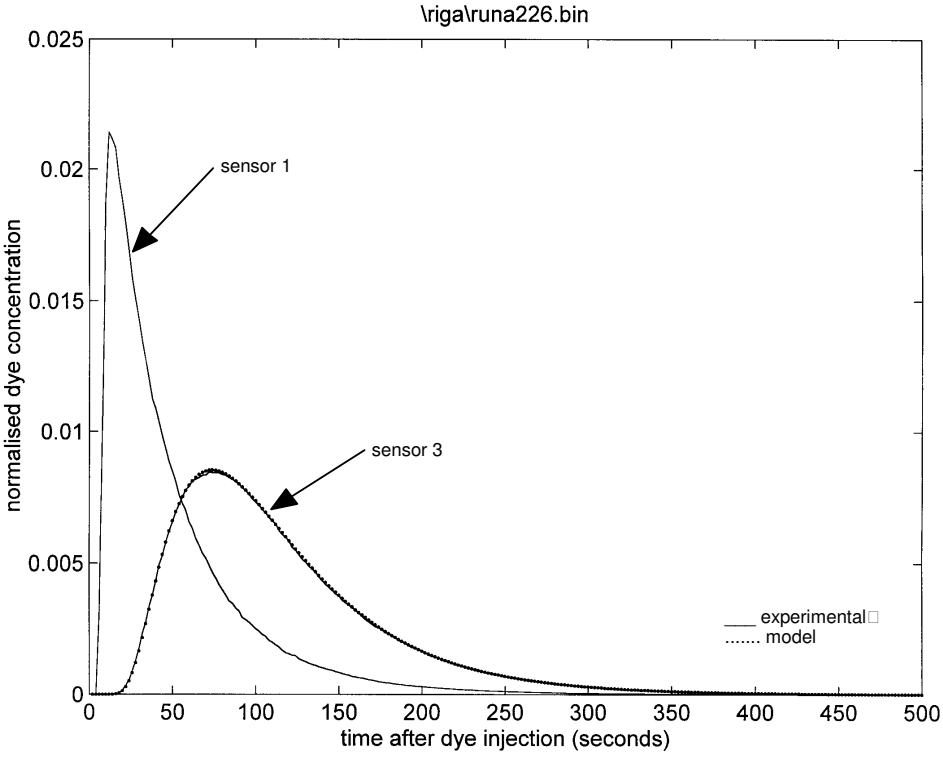

Figure 4.10: Case Study 1: Experimental and Model Results for Sensors $1 \rightarrow 3$

4.4 Case Study 2 - Analysis of a Typical Tracer Experiment with No Net Flow

The analysis required for an experiment with no net flow differed slightly because the dye simply spreads out in near-Gaussian fashion from the injection point and remains in the tube. However, the analysis used for the imperfect pulse experiments still held true for the initial changes in concentration following dye injection: only when the dye reached the ends of the baffled tube did the model (which assumed an infinitely long tube) start to differ from the experimental reality. Therefore the initial concentration transients measured immediately after dye injection were of primary interest in order to determine axial dispersion. The concentration-time profiles for a typical no net flow experiment in the 150 mm apparatus with frequency 0.203 Hz and amplitude 27.8 mm (Re_o = 5300 and Re_n = 0) appeared thus:

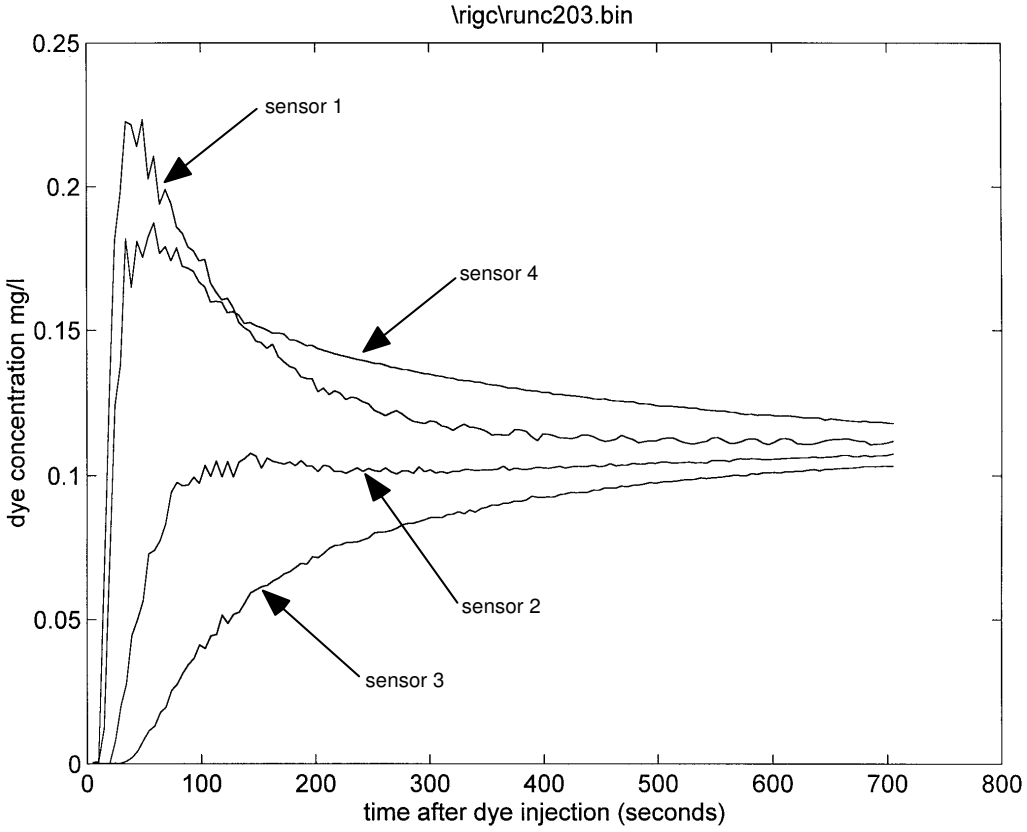

Figure 4.11: Case Study 2 : Typical Concentration-Time Profiles with No Net Flow

The analysis routine for iteratively determining E was carried-out in the same manner as for a net-flow experiment, except that the primary concern was to match the initial transient behaviour of the concentration-time profile; it was expected that at later times the model (dotted line) would not match the experimental profile (continuous line).

A best-fit was obtained for E = 0.0028 m^2/s for which the model closely matched the experimental data for the first 140 seconds after dye injection; thereafter the results no

longer corresponded to the model (which assumed an infinitely-long tube, whereas in practice the dye had reached one end of the tube which would start to affect the results).

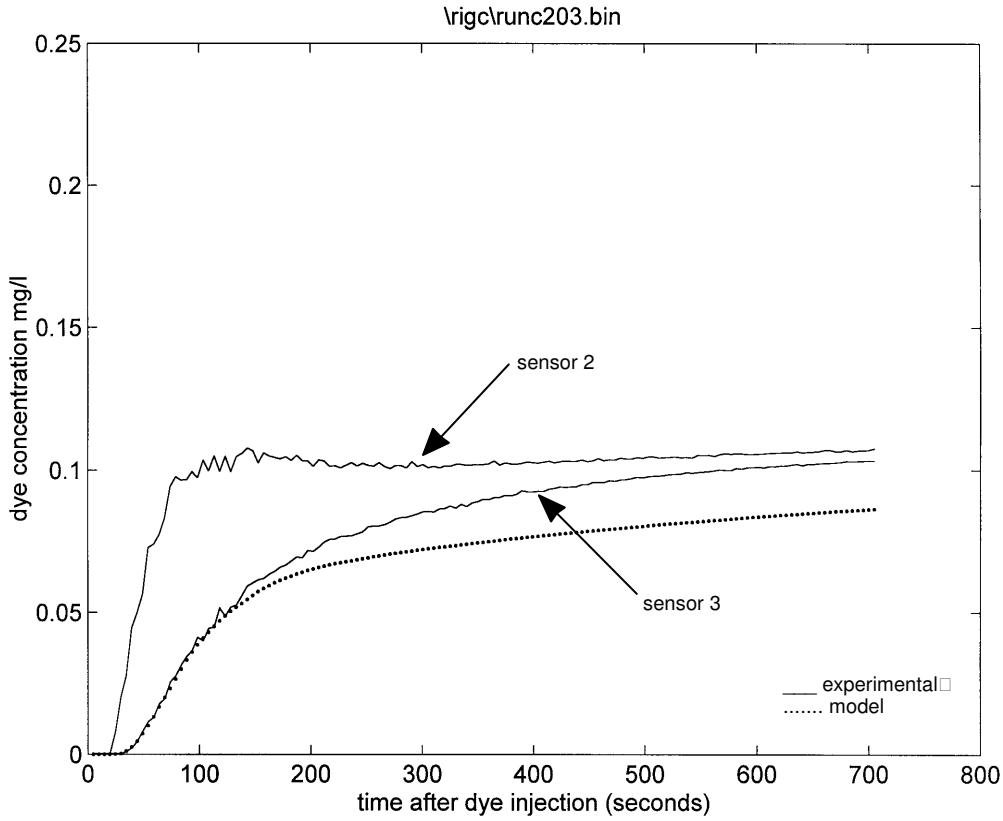

Figure 4.12: Case Study 2 : Experimental and Model Results for Sensors $2 \rightarrow 3$

The same value of the axial dispersion coefficient also gave a good model fit over the initial 140 seconds of the experiment for $1 \rightarrow 2$ and sensors $1 \rightarrow 3$, showing again that the axial diffusion model is self-consistent and a good model for O.F.M. under these flow conditions (see Figures 4.13 and 4.14).

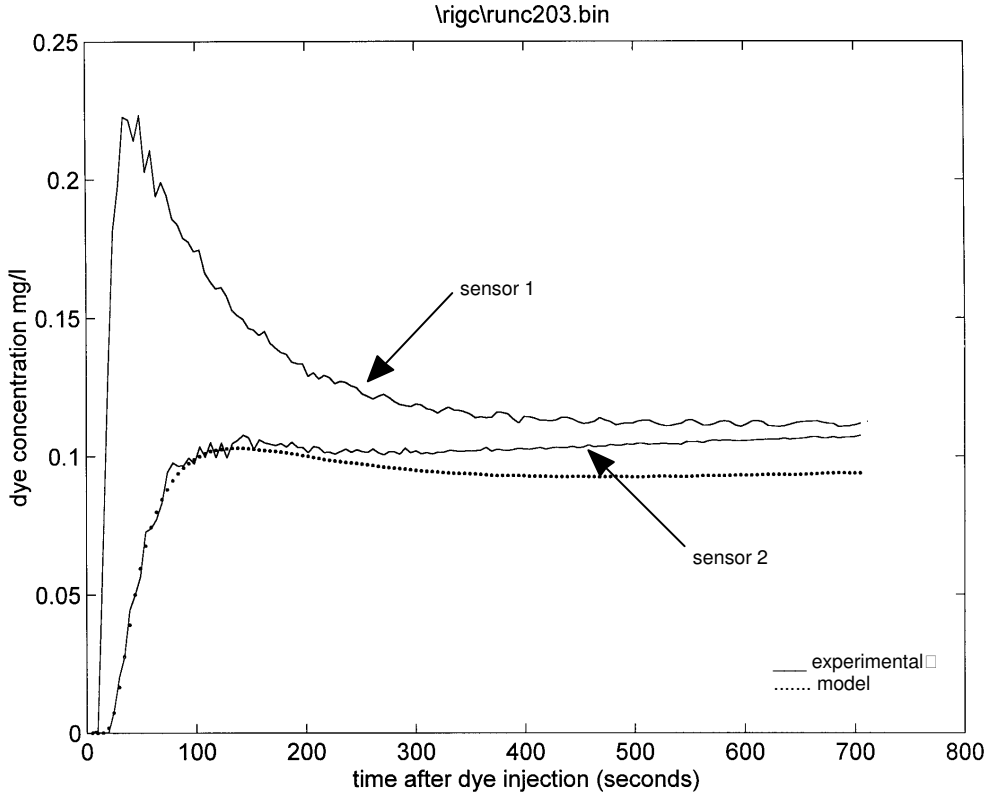

Figure 4.13: Case Study 2 : Experimental and Model Results for Sensors $1 \rightarrow 2$

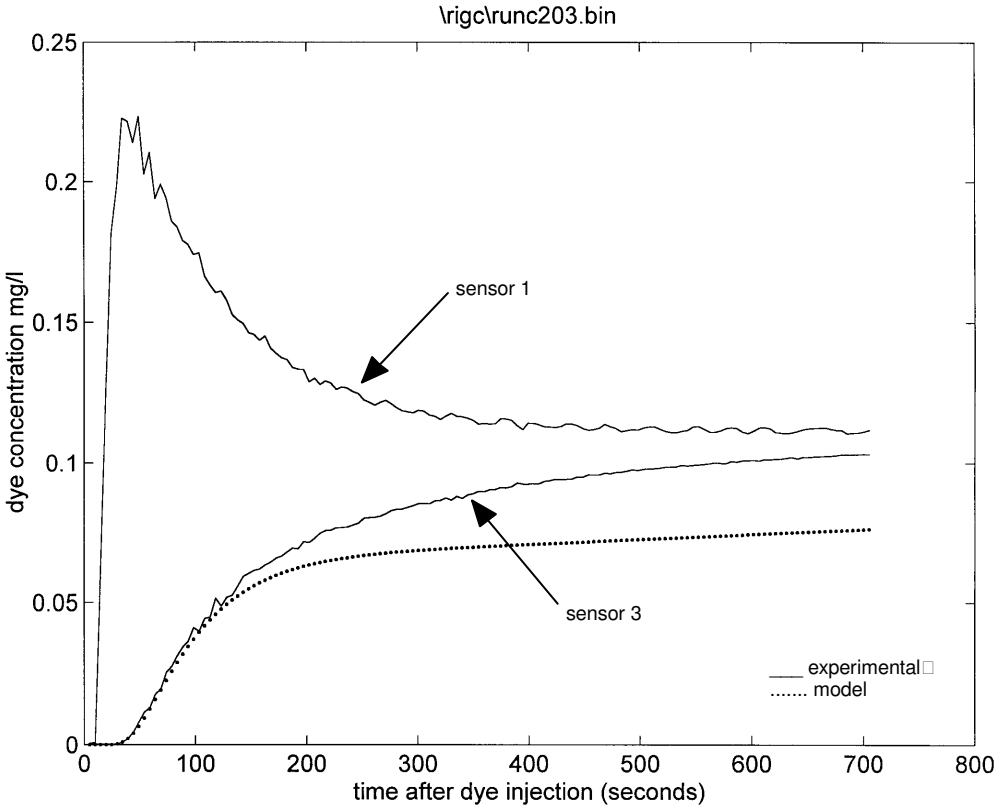

Figure 4.14: Case Study 2 : Experimental and Model Results for Sensors $1 \rightarrow 3$

5. Results of Experimental Axial Dispersion Measurements

This chapter presents data and analysis of axial dispersion measurements in O.F.M. for a large range of flow conditions. Using the experimental methods described in Chapter 3 and the analysis described in Chapter 4, axial dispersion measurements were made in each of the three sets of apparatus (24 mm, 54 mm and 150 mm diameter baffled tubes) under conditions of varying net flow and amplitude and frequency of oscillation. The main objective of these experiments was to compare the experimentally-measured axial dispersion under dynamically similar flow conditions as a function of tube diameter, a task not previously attempted and of direct importance in terms of scale-up considerations.

The first three sections of this chapter present the results from the three sets of apparatus for various flow conditions (oscillation with net flow, oscillation with no net flow, and net flow with no oscillation respectively). These are key results of the thesis, and demonstrate that for the tube diameters investigated, the measured axial dispersion is not a function of tube diameter. §5.4 presents results obtained for the "percentage backmixing" as a function of the flow conditions (a term used in this thesis as a measure of the proportion of dye tracer mixed a certain distance upstream of the tracer injection point); examination of these results shows the range of conditions for which the diffusion model accurately describes the axial dispersion mechanism in O.F.M.. §5.5 presents a correlation for axial dispersion as a function of the flow conditions.

5.1 Oscillation with Net Flow – 24 mm, 54 mm and 150 mm Apparatus

This section describes results of experimental axial dispersion measurements analysed using the method shown in Case Study 1 (§4.3) for experiments with both oscillation and net flow. These results therefore correspond to the situation of a continuously-operated plug flow reactor, for which it may be industrially desirable to minimise the axial dispersion in order to have a well-defined residence-time distribution.

Figure 5.1 shows measured axial dispersion as a function of Re_o for the 54 mm apparatus with oscillations of varying amplitude (0.6 mm $\leq x_o \leq$ 18 mm) and frequency (0.1 Hz $\leq f \leq$ 3.2Hz) and with Re_n = 107 (corresponding to a constant net flow rate of 0.27 l/min). Each data point marked on the graph is an average of 3 separate estimates of the axial dispersion determined from the same experiment (from paired combinations of sensors 1, 2 and 3). The overall error for each data point can only be estimated (see Appendix V) but is thought to be of order +/- 25% for axial dispersion and +/- 5% for Re_o ; for clarity, error bars are not included on these graphs. Also, in order for easy comparisons to be made between the various graphs of results presented in this chapter, the scales of the axes have been kept constant (axial dispersion ranging from 10^{-5} to 10^{-1} m^2/s and Reynolds number ranging from 1 to 100 000).

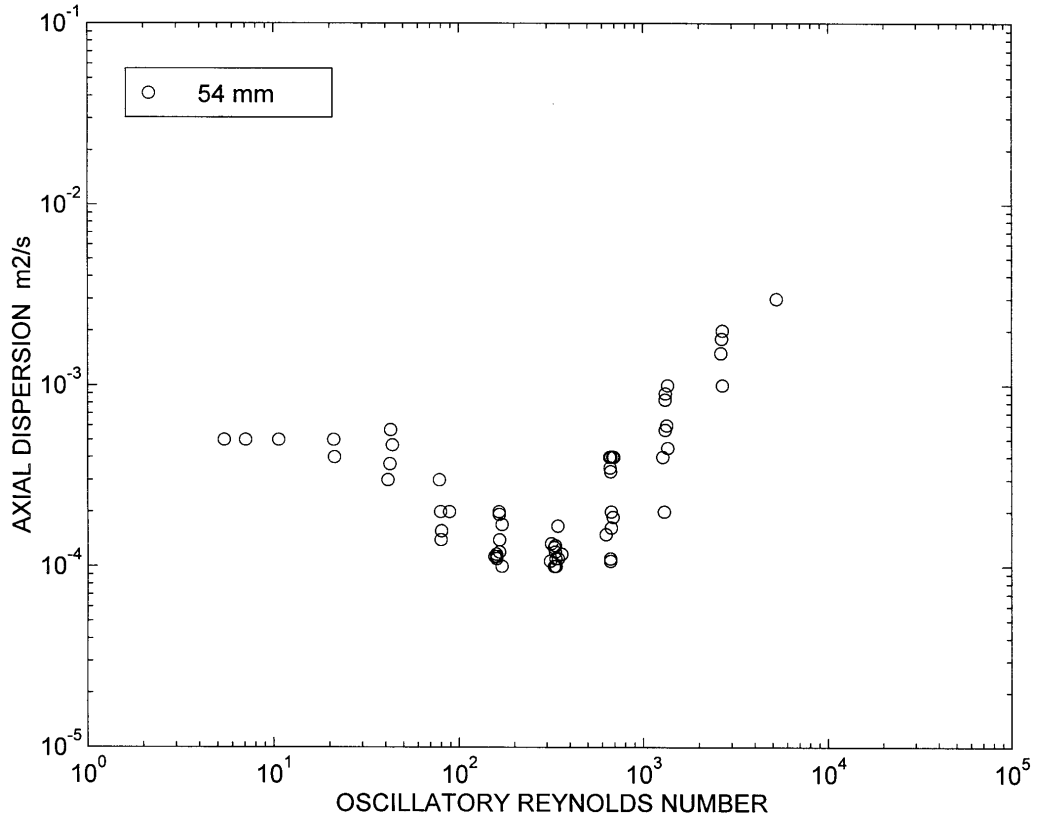

Figure 5.1: E *vs* Re_o in the 54 mm Apparatus; $Re_n = 107$

Three distinct regimes can be identified in Figure 5.1: firstly for $Re_o \leq 80$ the axial dispersion appears to tend to a constant value of approximately 5 x 10^{-4} m^2/s. Secondly there is a characteristic minimum in axial dispersion for $80 < Re_o < 800$ similar in form to that observed by Dickens et al (1989) (see Figure 2.3) and with values as low as 10^{-4} m^2/s. Thirdly, for $Re_o \geq 800$ the axial dispersion increases approximately linearly with increasing Re_o .

In dimensionless terms, the Strouhal number Str (inversely proportional to amplitude of oscillation) was varied between $0.25 \leq Str \leq 8$. The range of Strouhal number investigated was limited for very large amplitude oscillations ($Str < 0.25$) since they exceeded the stroke-length of the apparatus.

The range of Re_o which could be investigated was restricted for large Re_o (up to $Re_o \approx 5000$) by the apparatus itself (limitations of oscillator power meant that the sinusoidal wave form could not be maintained) and for low Re_o by the validity of the model fit obtained using the diffusion model: in cases where the predicted concentration-time profile did not match the shape of the experimental profile for any value of the axial dispersion parameter, the model was taken to be invalid. An example of a failure of the diffusion model is shown in Figure 5.2: there is a marked discrepancy between the best-fit model prediction (for E = 3 x 10^{-4} m^2/s) and the experimental concentration-time profile. In this case the model was not successful because the amplitude of oscillation was very small (x_o = 0.3 mm in the 54 mm apparatus or alternatively Str = 16) and it was

found in general that for Str > 8 in all sets of apparatus the diffusion model was inadequate.

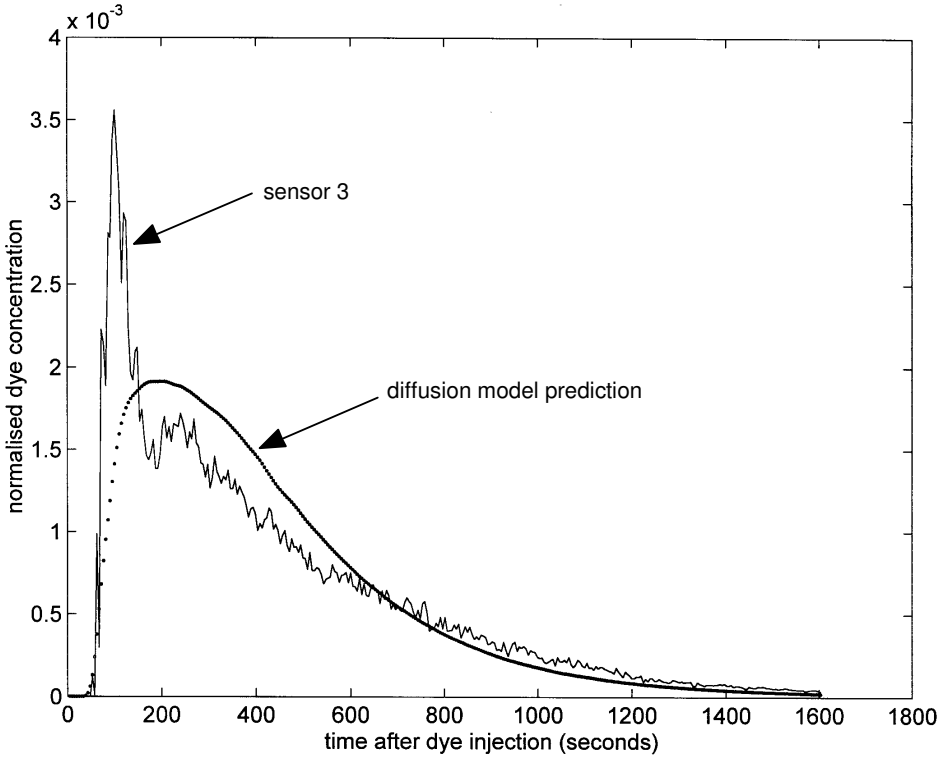

Figure 5.2: Failure of the Diffusion Model in the 54 mm Apparatus under Certain Conditions: Re_n = 107, Re_O = 22, Str = 16 (or alternatively: 0.27 l/min, f = 0.2 Hz & x_O = 0.3 mm)

It was found that there was a clear distinction between results for which the diffusion model was successful in predicting downstream concentration-time profiles and results such as shown in Figure 5.2, i.e. there was very little "grey area" of uncertainty as to whether or not the diffusion model was adequate. It was therefore not considered necessary to develop a quantitative criterion for a successful model fit; the model was either successful or clearly inadequate.

Figure 5.3 shows a key result of this thesis: the data already shown in Figure 5.1 is superimposed on the corresponding results for the 24 mm and 150 mm sets of apparatus. The form and magnitude of these results broadly matches that of the 54 mm apparatus. This is perhaps a surprising result: for O.F.M. in baffled tubes under dynamically similar flow conditions the absolute value (in m^2/s) of the experimentally measured axial dispersion appears to be independent of tube diameter. For this reason, no attempt has been made to present the axial dispersion coefficient in a dimensionless form; although it would have been easy to do so (for example in the form of a Schmidt number), this would have obscured the fact that the measured axial dispersion is independent of scale.

In the data presented in Figure 5.3 there is a significant variation in the magnitude of the axial dispersion for a given Re_o (for a given Re_o , the measured axial dispersion varies by up to an order of magnitude). This was thought to be due to the independent effects of

both amplitude and frequency of oscillation on the axial dispersion, an observation consistent with the results of other researchers (e.g. Howes 1988).

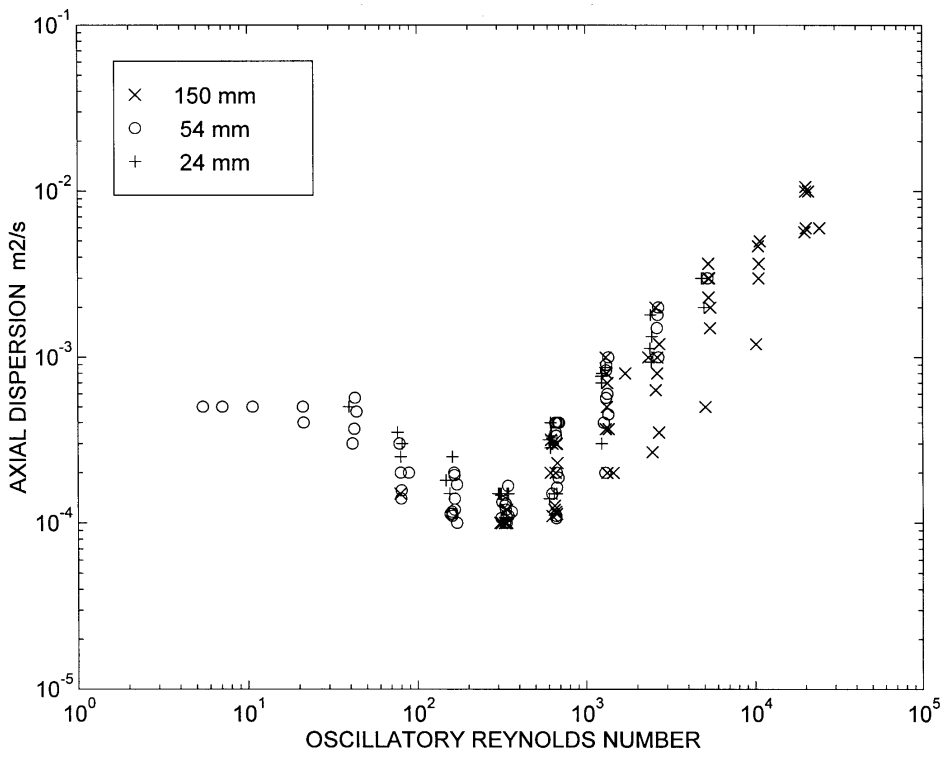

Figure 5.3: E *vs* Re_O in the 24 mm, 54 mm and 150 mm Apparatus; Re_n = 107

In order to examine the effect of Strouhal number, Figure 5.4 plots data taken from Figure 5.3 but shows only those results which correspond to Str = 0.5. There is a remarkably good match in experimental axial dispersion values for the three sets of apparatus for a given Re_O. For low Strouhal number (i.e. high amplitude) oscillations the oscillatory Reynolds number is high even when their frequency is low, so in Figure 5.4 the results are for $Re_O > 320$ only. In this regime, axial dispersion is observed to increase linearly as a function of oscillation frequency; it appears that the oscillation is the dominant mechanism for axial dispersion at high oscillatory Reynolds numbers.

Similar data is plotted in Figures 5.5 to 5.7 for Str = 1, 2 and 4 respectively. Again, there is excellent agreement of axial dispersion values for the three sets of apparatus. As the Strouhal number increases (and amplitude of oscillation decreases) the range of oscillatory Reynolds numbers decrease until in Figure 5.7 results for $Re_O > 40$ are observable: this flow regime exhibits a characteristic minimum in axial dispersion at approximately Re_O = 500. The minimum is a result of the interaction between the net flow and oscillatory flow components: at the minimum, the vortices created by the net flow and oscillations are optimised to redistribute the tracer radially across the baffled tube with each oscillatory cycle and hence minimise the axial dispersion; if the oscillations are increased then they serve to increase the axial as well as the radial dispersion and hence the oscillations become the dominant mechanism for axial

dispersion; if the oscillations are reduced then the efficacy of radial mixing is reduced and eventually the net flow becomes the dominant mechanism for axial dispersion.

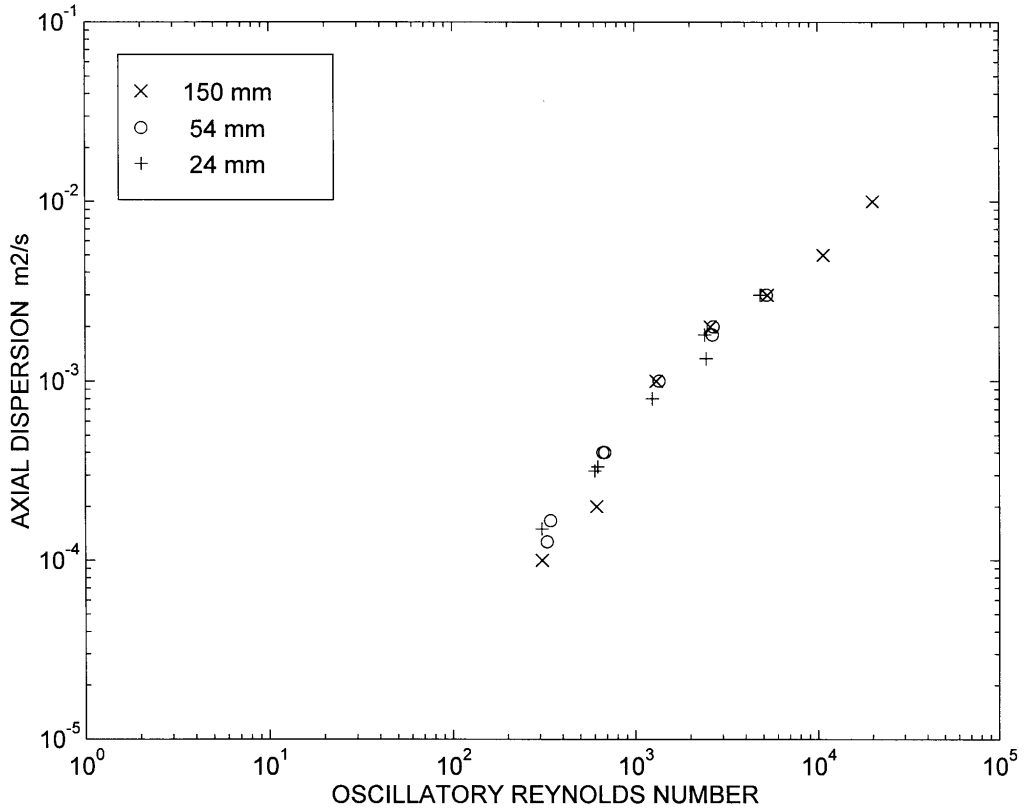

Figure 5.4: E *vs* Re_O in the 24 mm, 54 mm and 150 mm Apparatus; $Re_n = 107$ & $Str = 0.5$

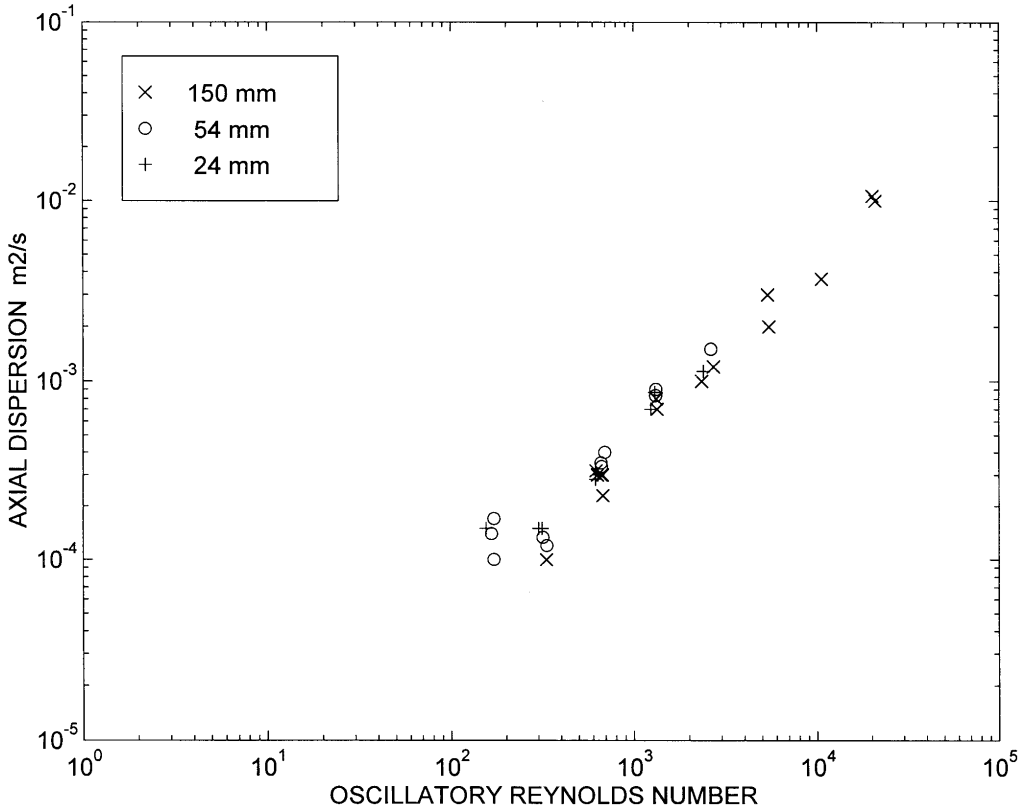

Figure 5.5: E *vs* Re_O in the 24 mm, 54 mm and 150 mm Apparatus; $Re_n = 107$ & $Str = 1$

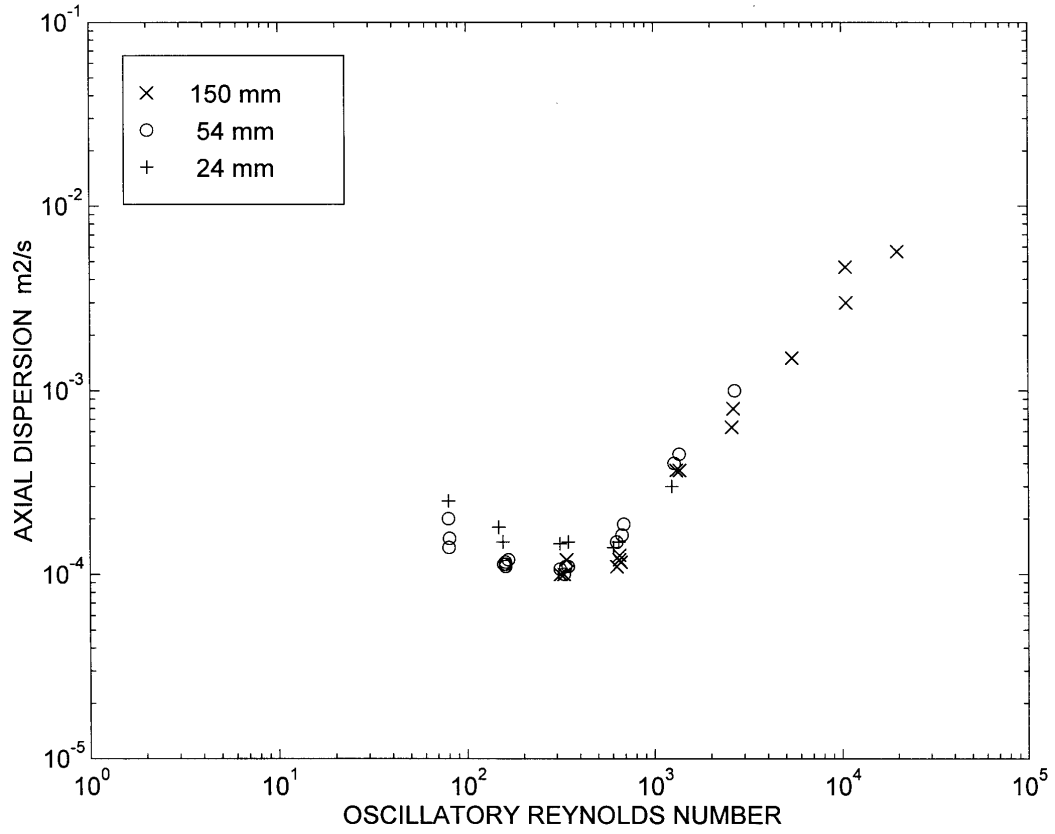

Figure 5.6: E *vs* Re_O in the 24 mm, 54 mm and 150 mm Apparatus; $Re_n = 107$ & $Str = 2$

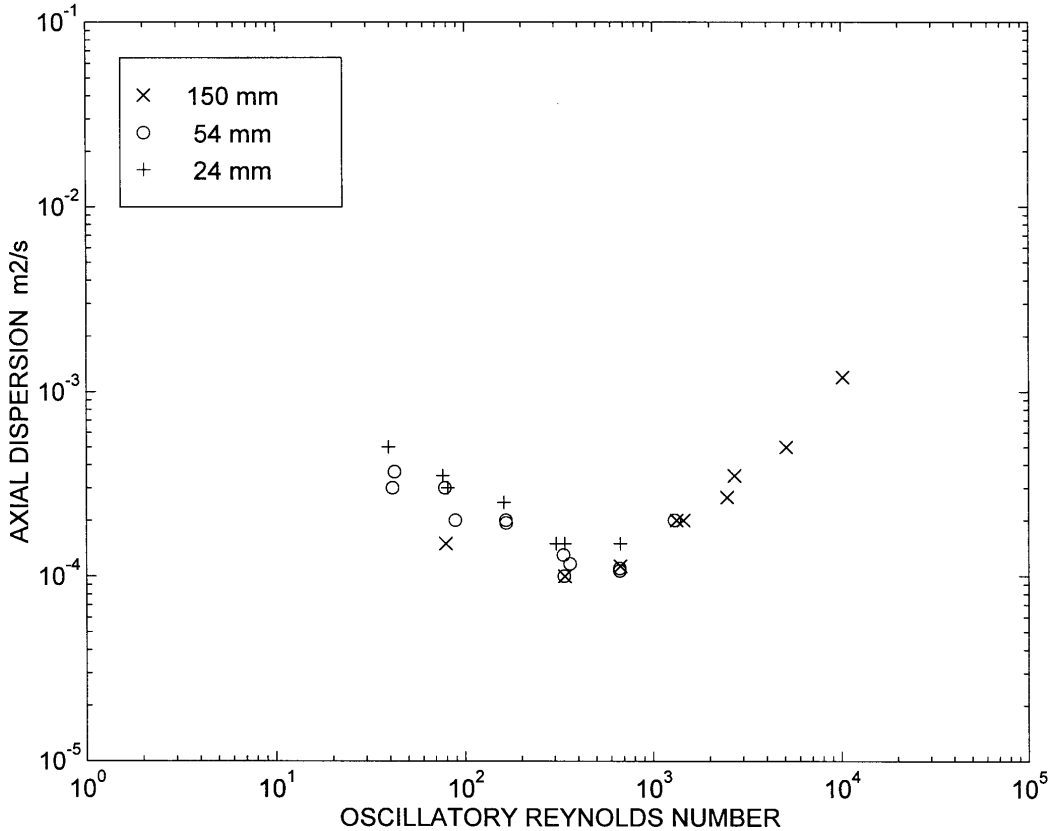

Figure 5.7: E *vs* Re_O in the 24 mm, 54 mm and 150 mm Apparatus; $Re_n = 107$ & $Str = 4$

The largest discrepancies in axial dispersion as a function of tube diameter in Figures 5.4 to 5.7 are observed for oscillatory Reynolds numbers less than the minimum ($Re_o < 500$): in this flow regime the axial dispersion appears particularly sensitive to small variations in experimental conditions (notably the amplitude of oscillation). The variation in results from a particular apparatus is greater than variation between different apparatus at the same Re_o.

5.2 Oscillation with No Net Flow – 24 mm, 54 mm and 150 mm Apparatus

This section describes results of experimental axial dispersion measurements made using the method shown in Case Study 2 (§4.4) for experiments with oscillation but with no net flow. The results therefore correspond to batch mode operation of O.F.M..

Figure 5.8 shows the measured axial dispersion as a function of Re_o . In order to assist comparisons with subsequent sets of data, the lines $y = Re_o \times 10^{-6}$ and $y = Re_o \times 10^{-7}$ have also been plotted between Re_o = 500 and Re_o = 50 000. These lines have no physical significance and are purely a visual aid.

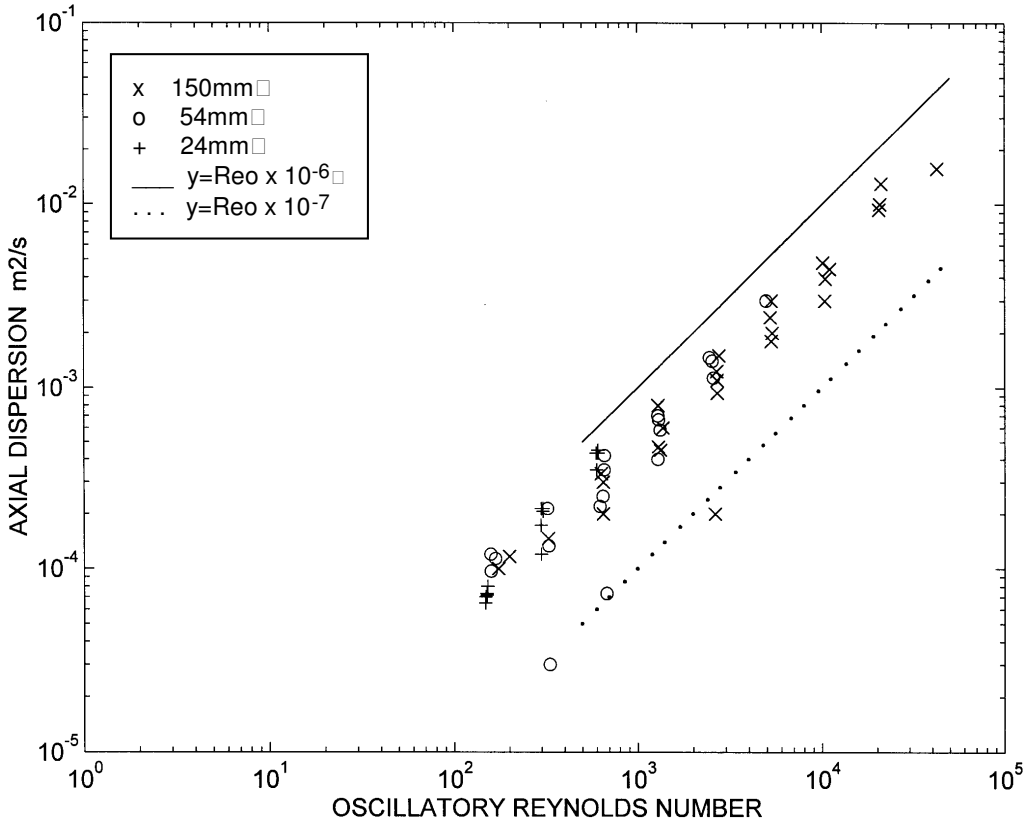

Figure 5.8: *E vs* Re_O in the 24 mm, 54 mm and 150 mm Apparatus; $Re_n = 0$

Similar to the data presented in §5.1, the results show a range of values for a given Re_o . Figures 5.9 to 5.12 show the same results but plotted for a specific Strouhal number (*Str* = 0.5, 1, 2 and 4 respectively). These results again show that the absolute value of experimentally measured axial dispersion in batch O.F.M. is independent of tube

diameter. It is the *absolute* value of the axial dispersion that is unaffected by tube diameter rather than a dimensionless form of the axial dispersion. In order to emphasise this fact the axial dispersion data continues to be presented in units of m^2/s and not in one of the possible dimensionless groups available (*Pe* or *Sc*).

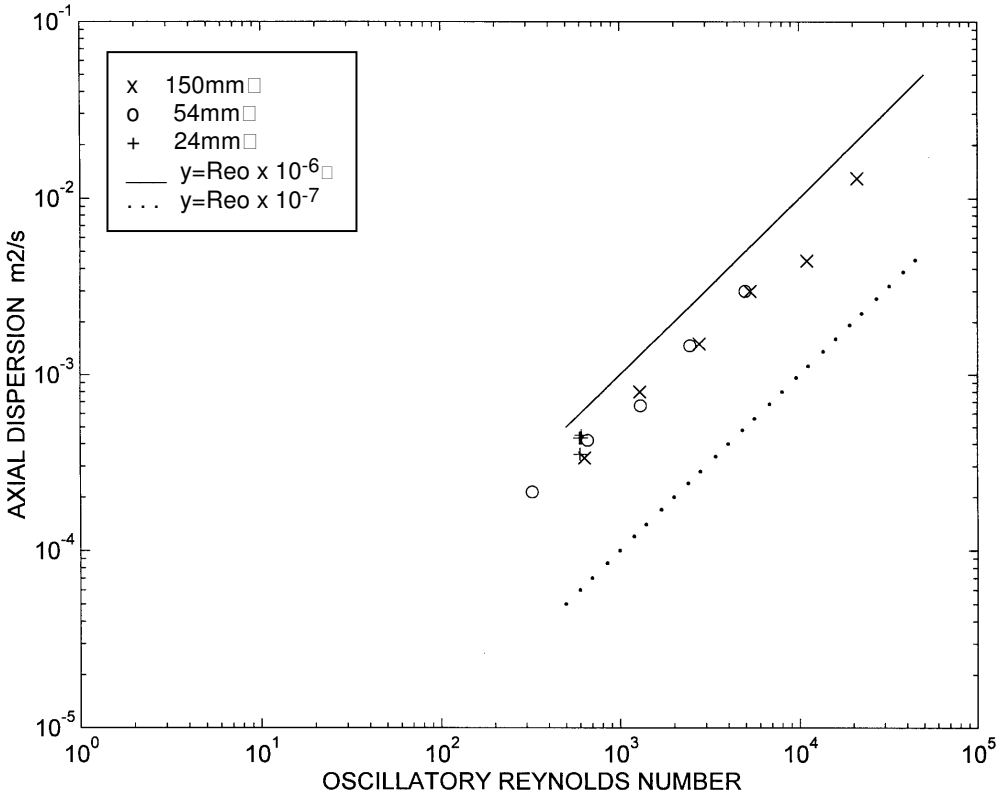

Figure 5.9: *E vs* Re_O in the 24 mm, 54 mm and 150 mm Apparatus; $Re_n = 0$; $Str = 0.5$

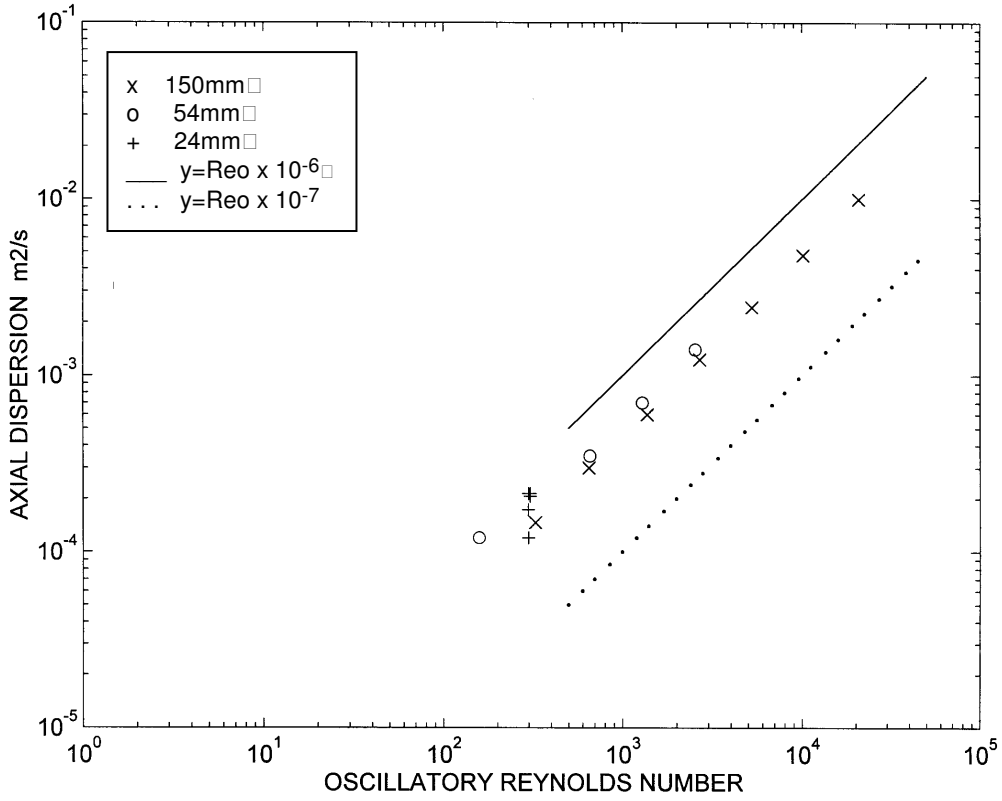

Figure 5.10: *E vs* Re_O in the 24 mm, 54 mm and 150 mm Apparatus; $Re_n = 0$; $Str = 1$

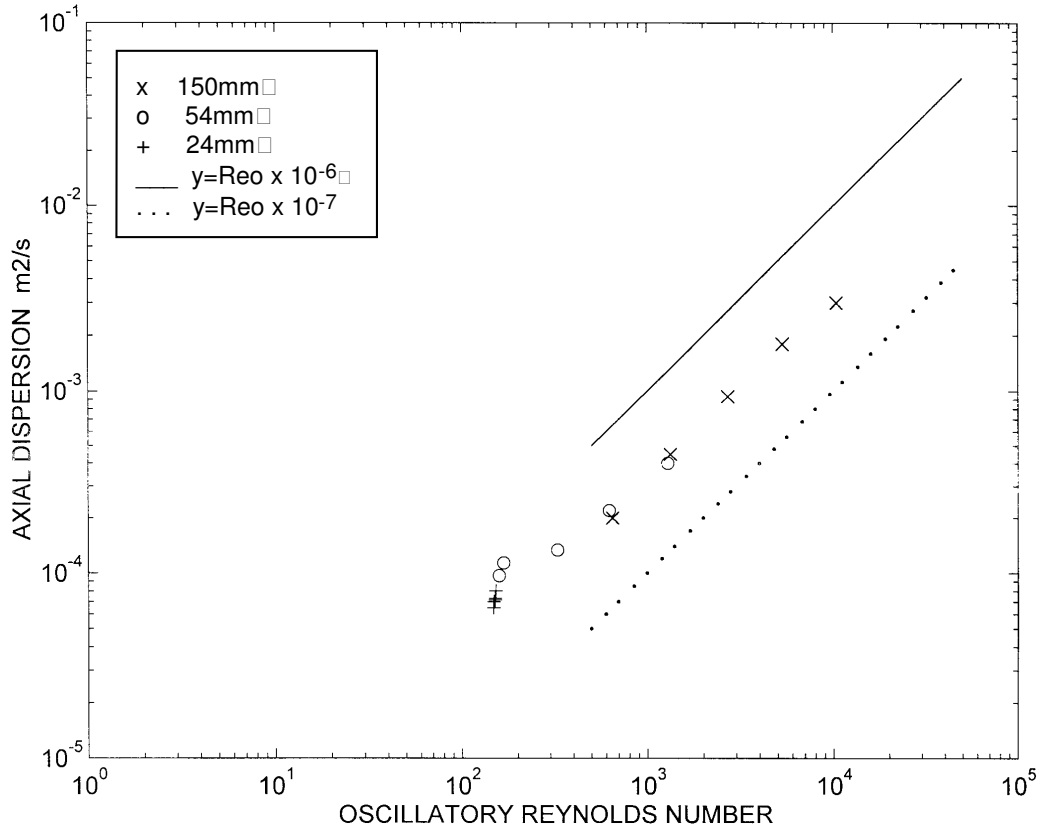

Figure 5.11: E *vs* Re_O in the 24 mm, 54 mm and 150 mm Apparatus; $Re_n = 0$; $Str = 2$

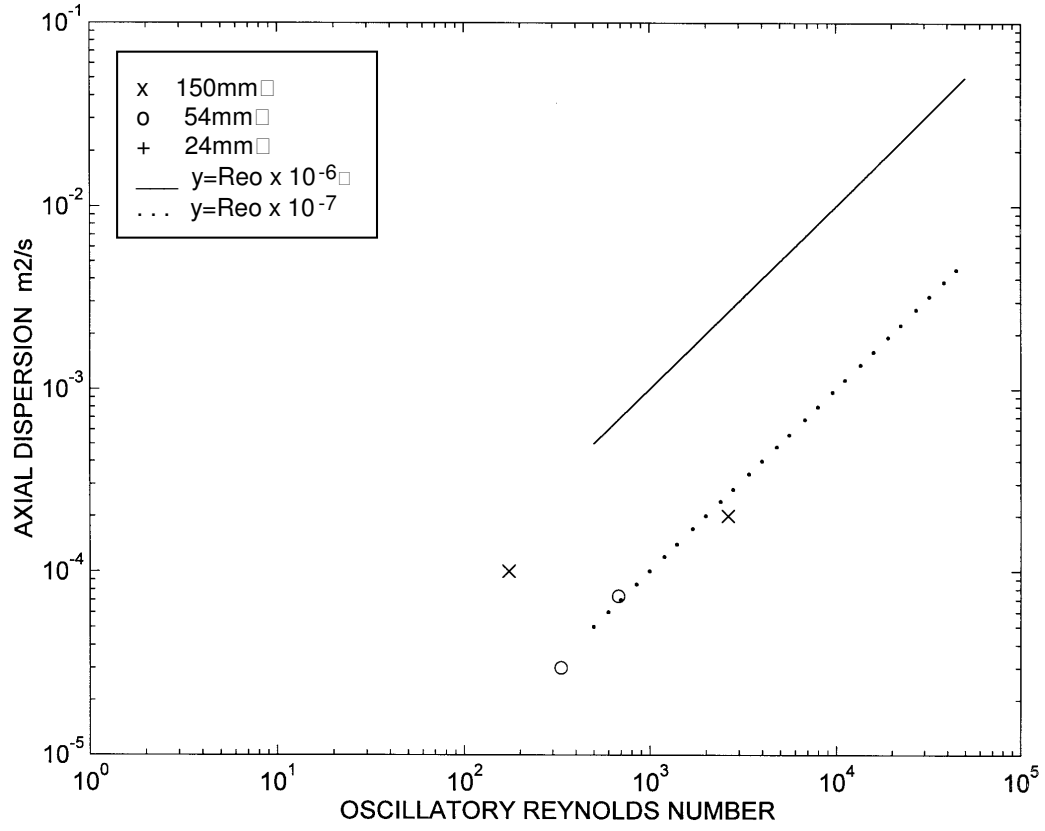

Figure 5.12: E *vs* Re_O in the 24 mm, 54 mm and 150 mm Apparatus; $Re_n = 0$; $Str = 4$

For $Str \leq 2$ and $Re_o > 100$, for a given Str the axial dispersion increases proportionally with oscillation frequency. Decreasing the Strouhal number for a given Re_o increases the magnitude of the axial dispersion. For $Str > 2$ there are few results (mostly, the diffusion model gave a very poor fit and therefore the axial dispersion could not be quantified using the imperfect pulse technique). For those results which did fit the diffusion model at high Strouhal numbers, exceptionally low values of axial dispersion were measured: the lowest recorded value was 2.5 $\times 10^{-5}$ m^2/s. However, such a result is exceptional and more typically the minimum value of the axial dispersion measured by experiment was of order 10^{-4} m^2/s.

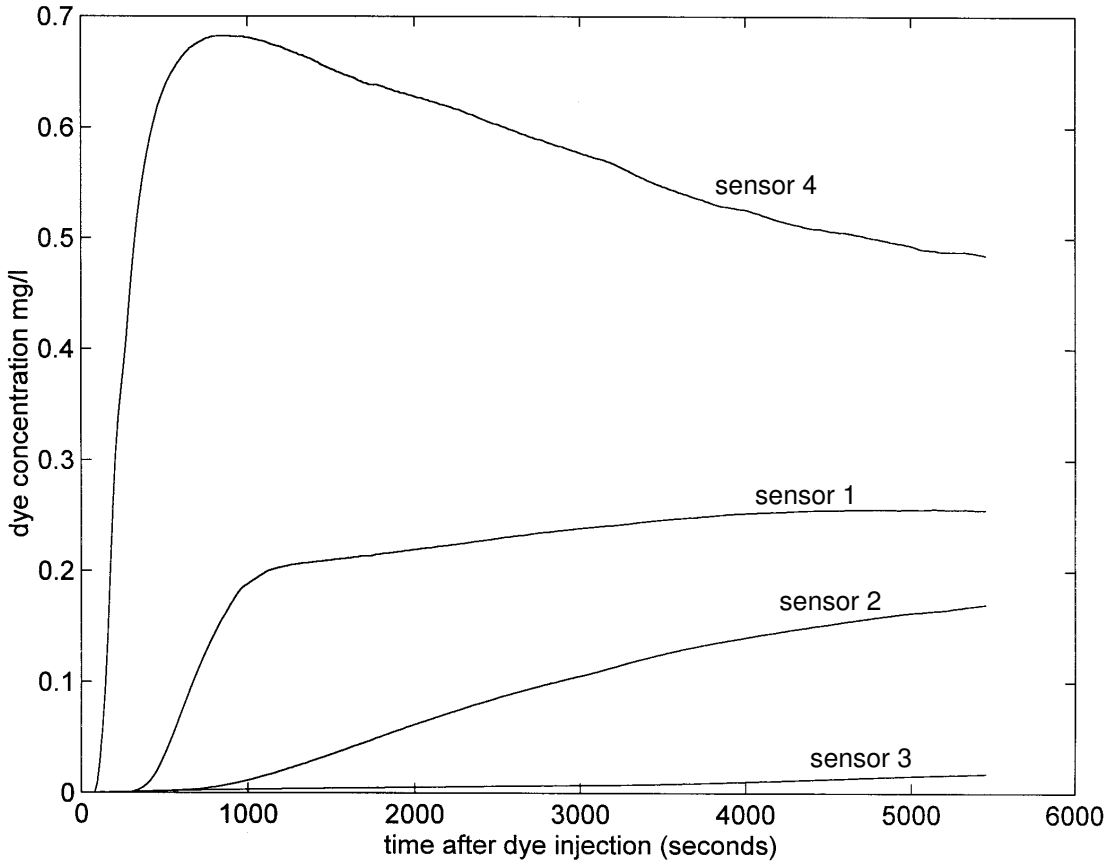

Figure 5.13: Concentration-Time Profiles in the 24 mm Apparatus with Manifolds Present $Re_n = 0$; $Str = 4.0$; $Re_O = 76$

Results from experiments where $Re_o < 100$ were typified by the sample concentration-time profiles shown in Figure 5.13: contrary to expectation, the concentration-time profiles for sensors 1 and 4 (arranged symmetrically on either side of the tracer injection point) were very dissimilar. This was not an indication of any buoyancy effect, but was explained by the creation of "manifolds" by the fluid mechanics resulting from low frequency, low amplitude oscillations: these manifolds were observed experimentally for the first time as part of the flow visualisation work carried out in this thesis - they are formed by the interaction of axisymmetric vortices travelling in opposite directions and which meet midway between two baffles. The vortices have the same sense of rotation which sweeps elements of fluid from the centre of the tube towards the wall and this

creates a separation between the two halves of the inter-baffle cell: because the velocity is primarily radial where the opposing vortices meet, negligible tracer crosses the manifold by advection. Sharp concentration differences therefore develop across the middle of each inter-baffle cell. They are described more fully in Chapter 7.

Since the injection point was equidistant between two baffles, the tracer was effectively injected close to a manifold and would tend to favour either one or other side of the injection point, depending upon the exact timing and rate of tracer injection. This explains the apparent asymmetry observed for sensors 1 & 4 in Figure 5.13.

Figure 5.14 shows an unsuccessful attempt to fit a diffusion model prediction to the measured concentration-time profile when manifolds were present ($Re_n = 0$, $Re_o = 76$, $Str = 4$). Clearly, the diffusion model does not adequately describe axial dispersion when manifolds are present.

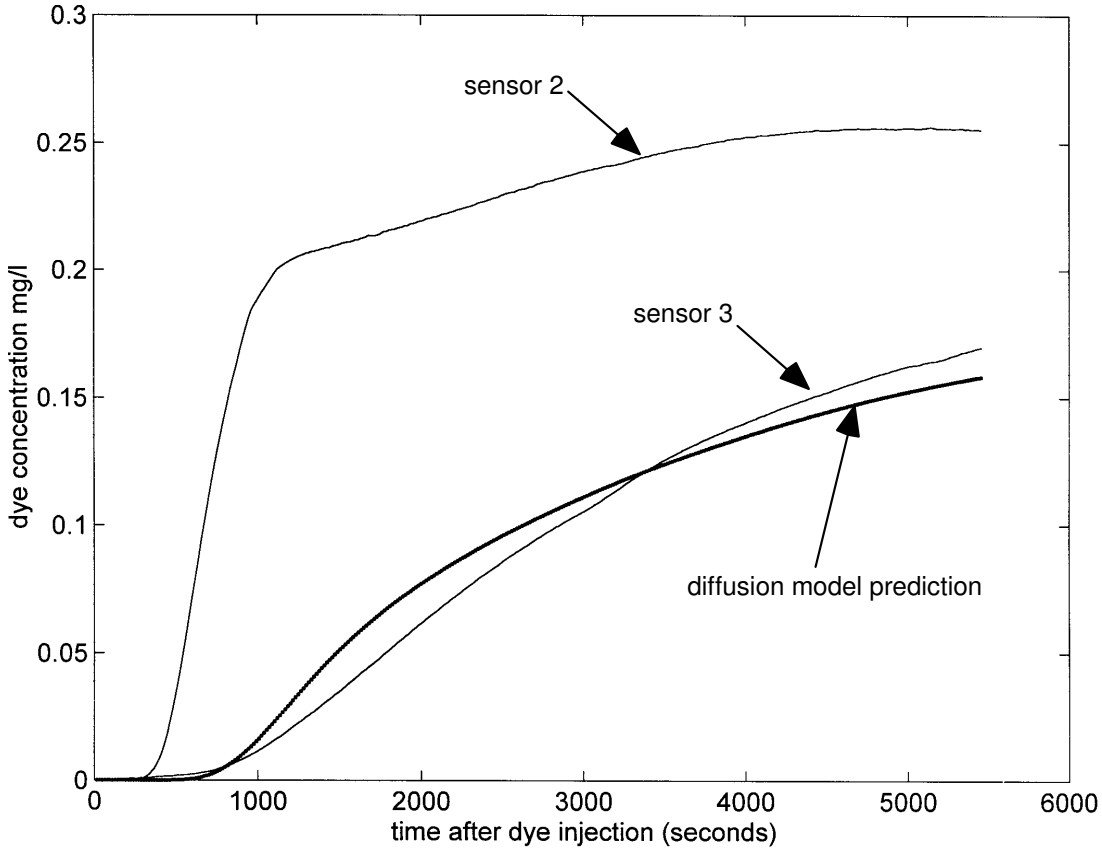

Figure 5.14: Concentration-Time Profiles *vs* Diffusion Model Prediction with Manifolds $Re_n = 0$; $Str = 4.0$; $Re_o = 76$; Model $E = 1 \times 10^{-4}$ m^2/s

5.3 Net Flow with No Oscillation – 24 mm, 54 mm and 150 mm Apparatus

Figure 5.15 shows the results of experimental axial dispersion measurements made using the method shown in Case Study 1 (§4.3) for experiments with net flow but no oscillation. This corresponds to regular pipe flow with a series of flow restrictions (the baffles).

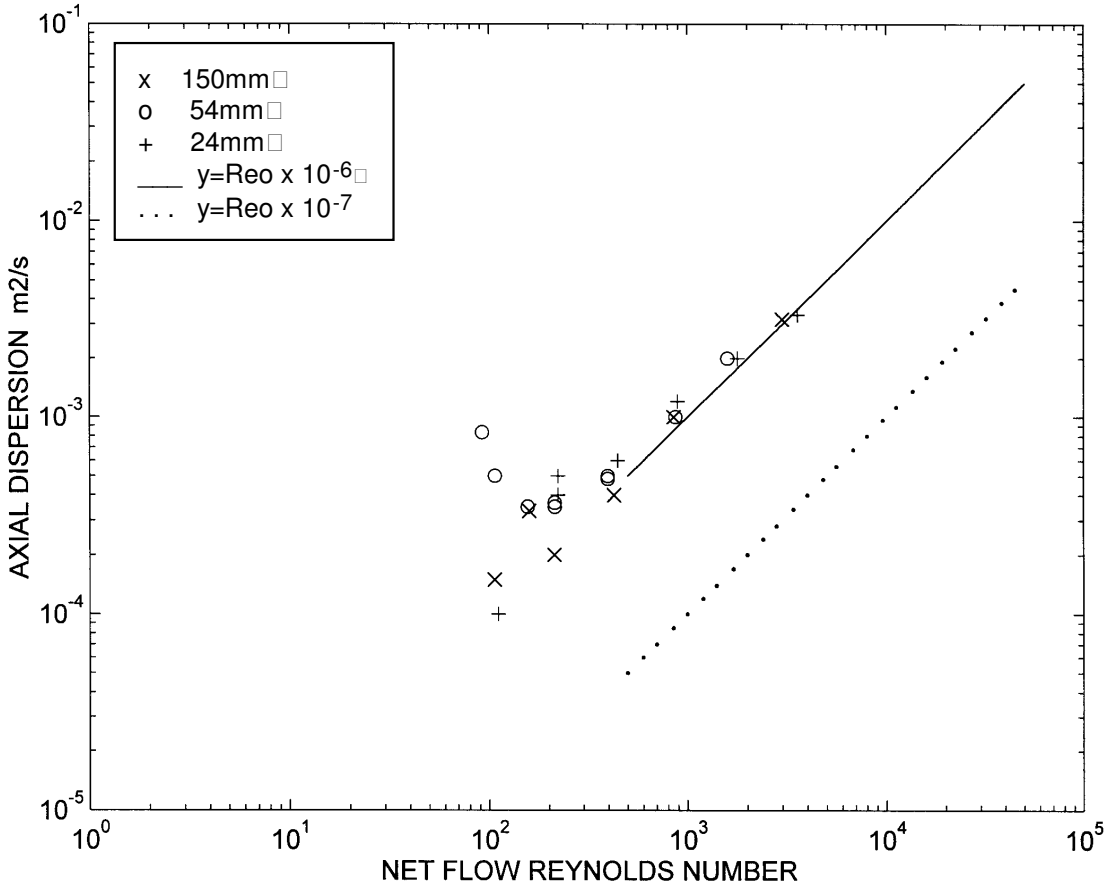

Figure 5.15: *E vs* Re_n in the 24 mm, 54 mm and 150 mm Apparatus; $Re_O = 0$

For $Re_n \geq 400$ the measured axial dispersion increases proportionally with Re_n . For $Re_n < 400$ there are large discrepancies in the results for the three sets of apparatus. This is thought to be a reflection of the unreliability of vortex-formation at these low Reynolds number flows for a non-reversing flow (without oscillation). Under these conditions, non-oscillatory flow mixing appears to be susceptible to very small changes in net flowrate, baffle orifice construction and possibly vibration from the lab surroundings all of which can affect vortex formation at the baffle orifice.

For $Re_n < 100$ there is little or no vortex formation and the diffusion equation does not adequately model over short distances what is essentially a Poiseuille-type flow (see Chapter 7). Under these conditions the axial dispersion cannot be quantified using the imperfect pulse technique.

Interestingly, the measured axial dispersion for a particular Reynolds number (net flow or oscillatory) is greater for a pure net flow than for a pure oscillation (comparing Figures 5.15 and 5.8). This illustrates the effectiveness of O.F.M. at minimising axial dispersion.

5.4 Study of Backmixing for O.F.M. with Net Flow

For the experiments described in §5.1 the optical sensor located upstream of the tracer injection point was used to record a measure of the proportion of dye tracer which travelled a distance of two baffle-spacings upstream of the injection point. In this thesis the ratio of the area under the concentration-time profile at the upstream sensor to the average area under the downstream concentration-time profiles is expressed as a percentage and called "*% backmixing*".

In Figure 5.16 *% backmixing* is plotted against the experimentally-determined axial dispersion for the 54mm apparatus for Re_n = 107 and a range of different oscillatory conditions. There is a clear, if slightly surprising, correlation between *% backmixing* and axial dispersion: there are two possible values of *% backmixing* for a given axial dispersion. These correspond to flow conditions on each side of the observed minimum plotted in Figure 5.1. For oscillatory Reynolds number greater than the minimum in axial dispersion ($Re_o \geq 300$ for these net flow conditions), the increasing intensity of oscillation causes an increasing proportion of the tracer to disperse upstream of the injection point, consequently increasing *% backmixing*. However, for oscillatory Reynolds numbers lower than the minimum in axial dispersion, the dispersion in the baffled tube is enlarged by the net flow component which serves to spread the tracer uni-directionally along the tube rather than providing an equal dispersion in both directions along the tube. Under these conditions there is insufficient driving force to cause tracer to move upstream of the injection point, and the *% backmixing* is zero.

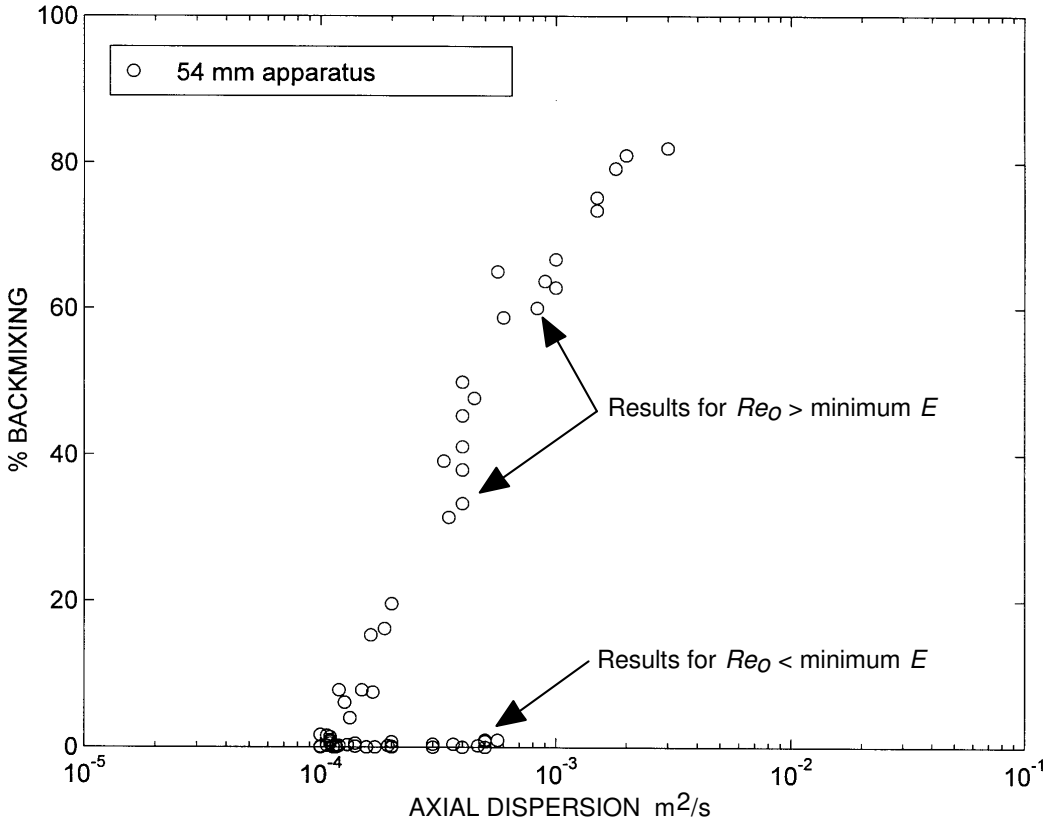

Figure 5.16: *% Backmixing vs E* in the 54 mm Apparatus; Re_n = 107

Similar trends in *% backmixing* were recorded for the 24 mm and 150 mm sets of apparatus. Figure 5.17 shows the results for all three sets of apparatus, together with the theoretical *% backmixing* calculated using the diffusion model. There is broad agreement between model and experiment for non-zero values of *% backmixing*, with no adjustable parameters.

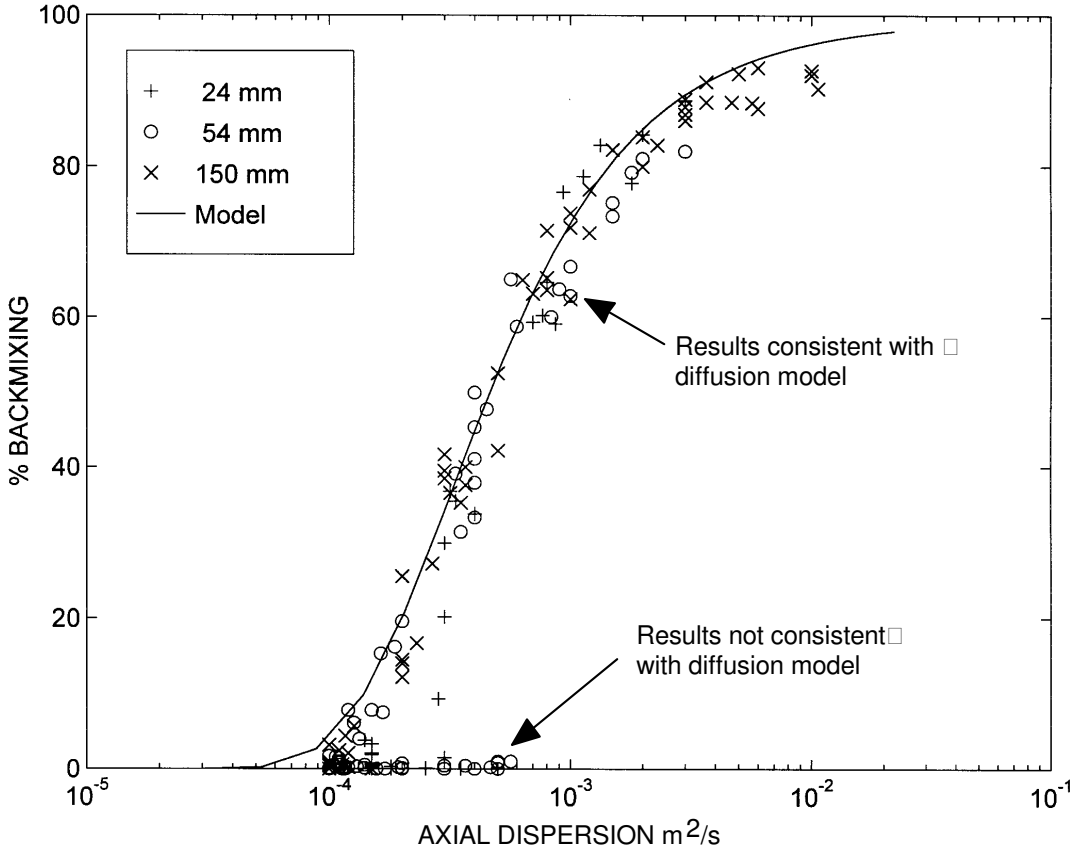

Figure 5.17: *% Backmixing vs E* in the 24 mm, 54 mm and 150 mm Apparatus; Re_n = 107

However, the diffusion model theory does not predict the increasing axial dispersion when *% backmixing* = 0. This is an interesting and important result as the diffusion model is only truly valid when Re_o is greater than the value which corresponds to the minimum in axial dispersion; when Re_o is less than that value then the model can be used to quantify the axial dispersion downstream of the injection point, but cannot predict the upstream movement of the tracer.

In this way, a potentially useful method for determining the optimum oscillatory conditions necessary to minimize axial dispersion for a given net flow has been discovered: if the intensity of oscillations are increased until a small amount of tracer is mixed upstream after injection, (i.e. 0 < *% backmixing* < 10%) then the axial dispersion will be at or very close to its minimum value.

5.5 Correlation for Axial Dispersion at High Reynolds Numbers

An empirical correlation was sought to describe axial dispersion as a function of the experimental flow conditions. Such a correlation would be useful for the estimation of residence time distributions for proposed baffled tube reactors and to help predict the likely effect on residence time distributions of modifying the net flow or oscillatory conditions. This section examines the usefulness of a general form of correlation proposed by Crittenden et al (1995) and uses new data together with the data already presented in this chapter to determine appropriate constants for the correlation. The correlation covers the cases of net flow only, oscillations only, and net flow with oscillations; the three cases will be examined in that order.

The form of correlation proposed by Crittenden et al (1995) was presented in Chapter 2 (equation 2.11). A_1, A_2, A_3, m, q and r are constants.

$$\frac{E}{UL} = A_1 Re_n^r + A_2 Re_o^m Str^{m-q} + \frac{A_3 Re_n^{2r}}{A_1 Re_n^r + A_2 Re_o^m Str^{m-q}} \qquad \text{eqn (2.11)}$$

Examining firstly the case of no oscillations (Re_o = 0), Figure 5.18 shows the data given in Figure 5.15 together with a best fit straight line correlation for axial dispersion as a function of net flow Reynolds number. Using also the results obtained from simulations (see Chapter 6) the best-fit correlation for net flow only was determined to be:

$$E = 5 \times 10^{-6} Re_n^{0.8} \qquad (m^2/s) \qquad \text{eqn (5.1)}$$

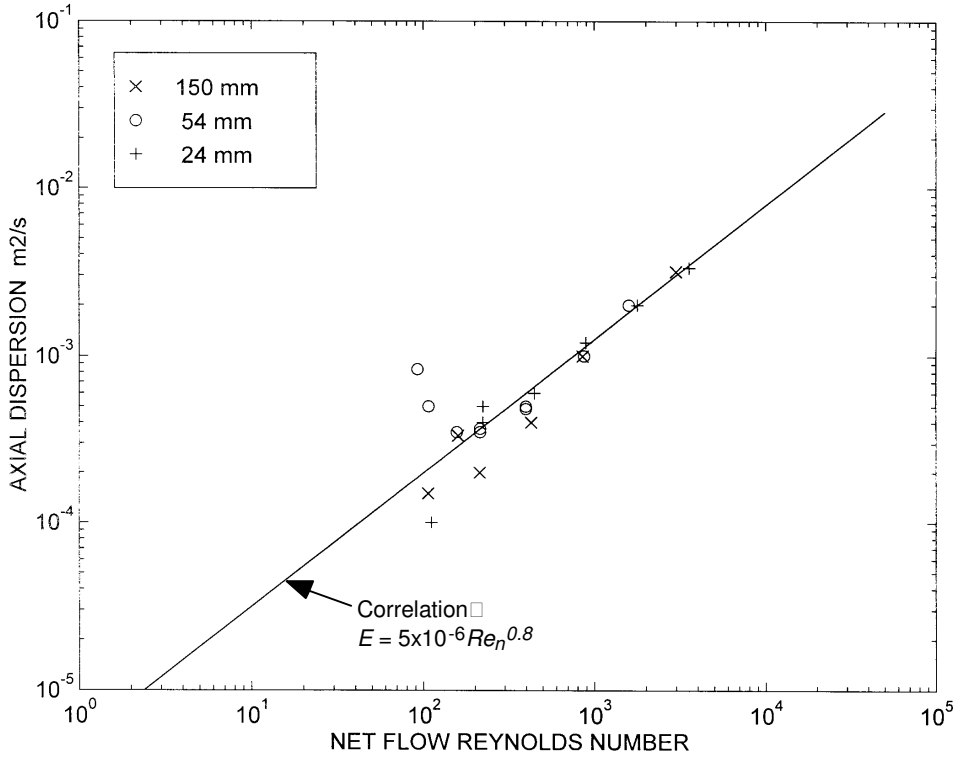

Figure 5.18: Graph Showing a Best-Fit Correlation for Axial Dispersion in the Case of Net Flow Only

Next, the case of oscillations only was considered ($Re_n = 0$). It was found that the power-law dependence of axial dispersion on Strouhal number proposed by Crittenden et al (1995) was inadequate to describe the variation in experimental measurements. Instead, this thesis proposes an exponential dependence of axial dispersion on Strouhal number and this more closely fits the experimental data. The best-fit correlation for axial dispersion as a function of the oscillations only is given in equation 5.2 and is plotted in Figures 5.19 to 5.22 for Strouhal numbers of 0.5, 1, 2 and 4 respectively. (This experimental data was previously shown without the correlation in Figures 5.9 to 5.12).

$$E = 7.5 \times 10^{-7} \, Re_o \, e^{(-0.4 Str)} \qquad (m^2/s) \text{ eqn (5.2)}$$

Equation 5.2 appears to match the experimental results well except for at very low amplitudes of oscillation (Str = 4) where there are anyway few experimental results available due to the frequent failure of the axial diffusion model to match experimental concentration-time profiles under these conditions. It is not immediately clear why the axial dispersion should appear to have an exponential dependence upon the amplitude of oscillation; a first-order model might have assumed that the dispersion would be proportional to both amplitude and frequency of oscillation i.e. proportional to the periodic volumetric flow rate of fluid in the baffled tube. It is speculated that the exponential dependence is a result of strong local interaction between vortices created by small amplitude oscillations whereas at large amplitudes of oscillation, the vortices are ejected away from the baffle orifice and therefore interact much less with one another.

Using equations 5.1 and 5.2, the form of the correlation presented in equation 2.11 was modified to appear as in equation 5.3.

$$E = A_1 \, Re_n^{0.8} + A_2 \, Re_o \, e^{(-0.4 Str)} + \frac{A_3 \, Re_n^{1.6}}{A_1 \, Re_n^{0.8} + A_2 \, Re_o \, e^{(-0.4 Str)}} \qquad (m^2/s) \text{ eqn (5.3)}$$

The constant A_2 for oscillatory flow has already been determined to be 7.5 x 10^{-7} (equation 5.2) and it can also be seen that for net flow in the absence of oscillations

$$A_1 + \frac{A_3}{A_1} = 5 \times 10^{-6} \qquad (m^2/s) \text{ eqn (5.4)}$$

must hold true for equation 5.1 to be satisfied. Whatever the value of A_1, the value of A_3 is therefore determined according to equation 5.5:

$$A_3 = 5 \times 10^{-6} A_1 - A_1^2 \qquad (m^4/s^2) \text{ eqn (5.5)}$$

In order to optimise the correlation for the case of net flow and oscillation, only the constant A_1 need therefore be adjusted in order to obtain a best-fit with the experimental data available.

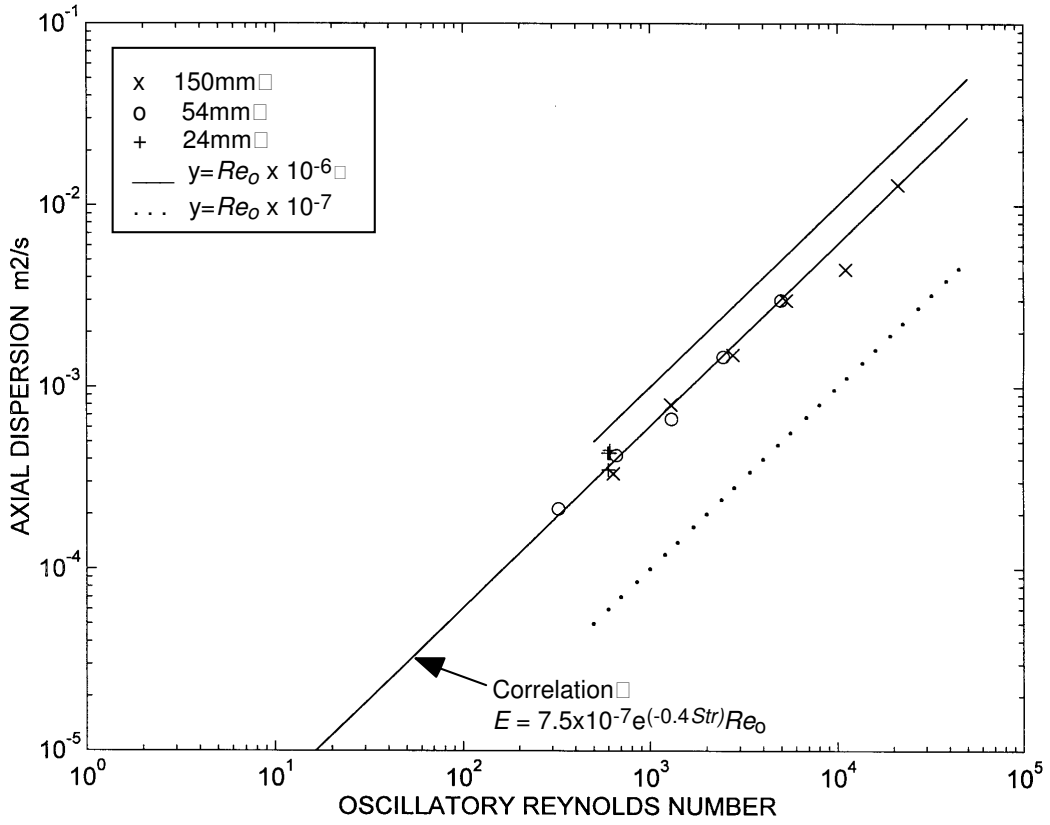

Figure 5.19: Graph Showing a Best-Fit Correlation for Axial Dispersion in the Case of Oscillation Only

$Str = 0.5$

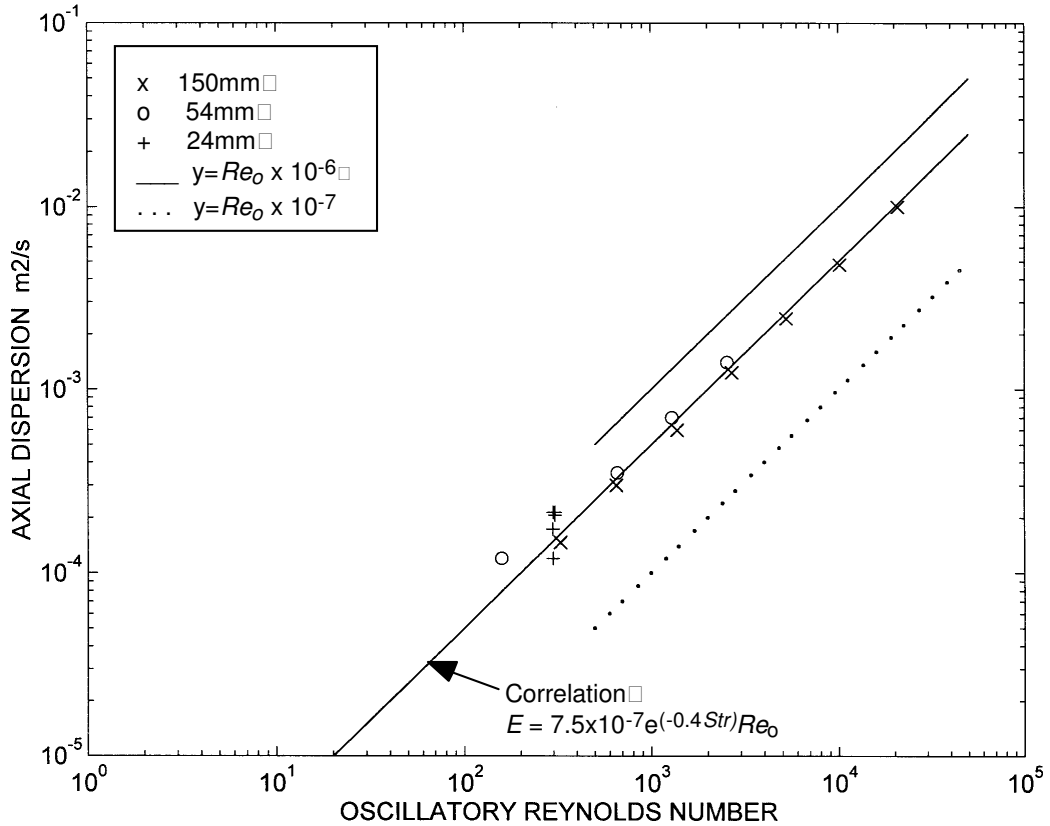

Figure 5.20: Graph Showing a Best-Fit Correlation for Axial Dispersion in the Case of Oscillation Only

$Str = 1$

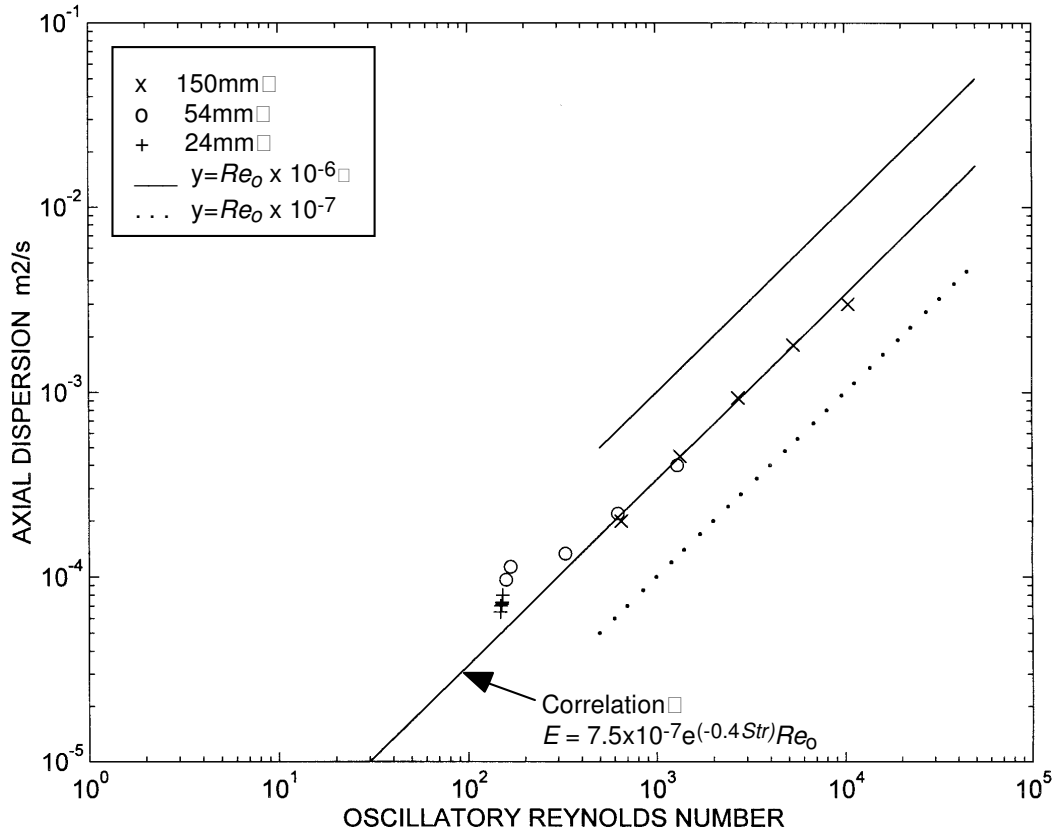

Figure 5.21: Graph Showing a Best-Fit Correlation for Axial Dispersion in the Case of Oscillation Only

$Str = 2$

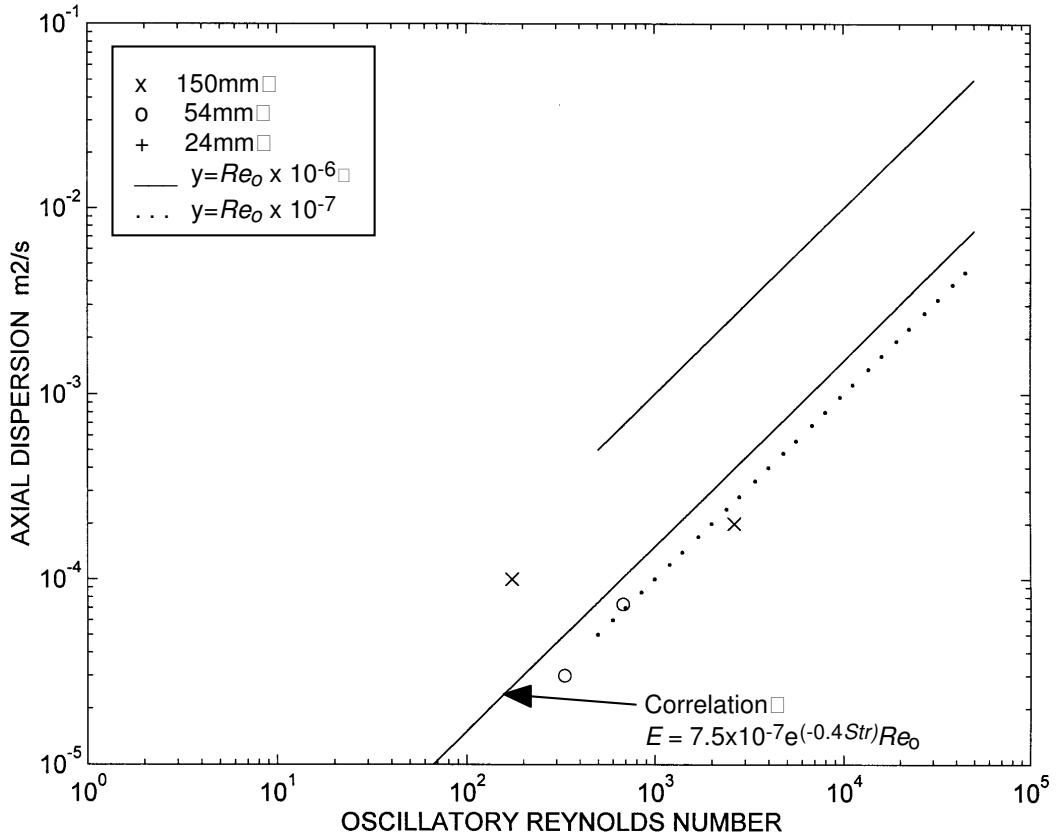

Figure 5.22: Graph Showing a Best-Fit Correlation for Axial Dispersion in the Case of Oscillation Only

$Str = 4$

Having established from the results in §5.1, §5.2 and §5.3 that axial dispersion is not a function of tube diameter, it was not considered worthwhile to perform a large series of additional oscillatory flow experiments on all three apparatus for different net flow rates. Instead, a limited number of experiments were carried out using the 24 mm apparatus only (because the mean residence time in the 24 mm apparatus was typically of order 5 minutes, compared to 20 minutes in the 54 mm apparatus or 3 hours in the 150 mm apparatus). The experiments explored the effect of oscillatory conditions on the measured axial dispersion for net flows of Re_n = 56, 107, 215 and 430.

The results of these experiments in the 24 mm apparatus are presented in Figures 5.23 to 5.26 respectively for Strouhal numbers of 0.5, 1, 2 and 4 respectively. The best-fit correlation was optimised by inspection and is superimposed on the graphs for the values A_1 = 7.0 x 10^{-7} m^2/s, A_2 = 7.5 x 10^{-7} m^2/s and A_3 = 3.0 x 10^{-12} m^4/s^2. The final form of the correlation with water as the fluid is therefore:

$$E = 7.0\times10^{-7}\,Re_n^{0.8} + 7.5\times10^{-7}\,Re_o\,e^{(-0.4Str)} + \frac{3.0\times10^{-12}\,Re_n^{1.6}}{7.0\times10^{-7}\,Re_n^{0.8} + 7.5\times10^{-7}\,Re_o\,e^{(-0.4Str)}} \quad (m^2/s) \quad \text{eqn (5.6)}$$

or if the dimensionless form is required then

$$\frac{\rho E}{\mu} = 0.7\times Re_n^{0.8} + 0.75\times Re_o e^{(-0.4Str)} + \frac{3.0\times Re_n^{1.6}}{0.7\times Re_n^{0.8} + 0.75\times Re_o e^{(-0.4Str)}} \qquad \text{eqn (5.7)}$$

although the dependence on μ and ρ has not been explicitly tested in this study.

Figures 5.23 to 5.26 show good agreement between the correlation (equation 5.6) and the experimental data for large oscillatory Reynolds numbers (approximately $Re_o > 1000$) and a tolerable order-of-magnitude agreement at lower oscillatory Reynolds numbers, although the correlation is clearly not perfect. One very interesting feature of the data is that in several cases, the measured axial dispersion for a given Re_o and Str is actually reduced by the presence of a small net flow. This is most unexpected since it would have been anticipated in practice that a net flow would if anything have served to increase the magnitude of the axial dispersion. The correlation is incapable of modelling such a reduction since by the form of equation 5.6 the introduction of a net flow can only serve to increase the predicted axial dispersion. The reduction is explained in the light of flow visualisations shown in Chapter 7 for which it appears that the introduction of a net flow can increase the degree of axisymmetry of the flow for oscillatory conditions that would otherwise give rise to asymmetric flow. By reducing the asymmetry in the flow the axial dispersion is also decreased since the flow is more ordered.

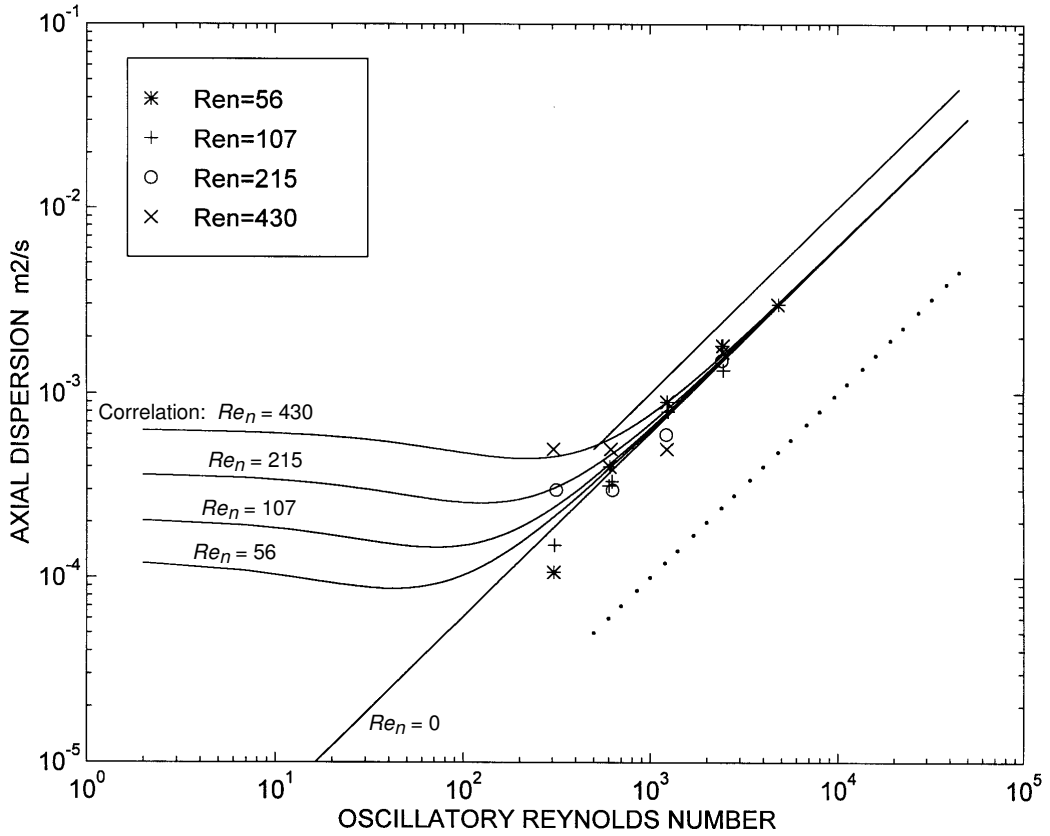

Figure 5.23: Graph Showing a Best-Fit Correlation for Axial Dispersion in the 24 mm Apparatus in the Case of Net Flow & Oscillation *Str* = 0.5

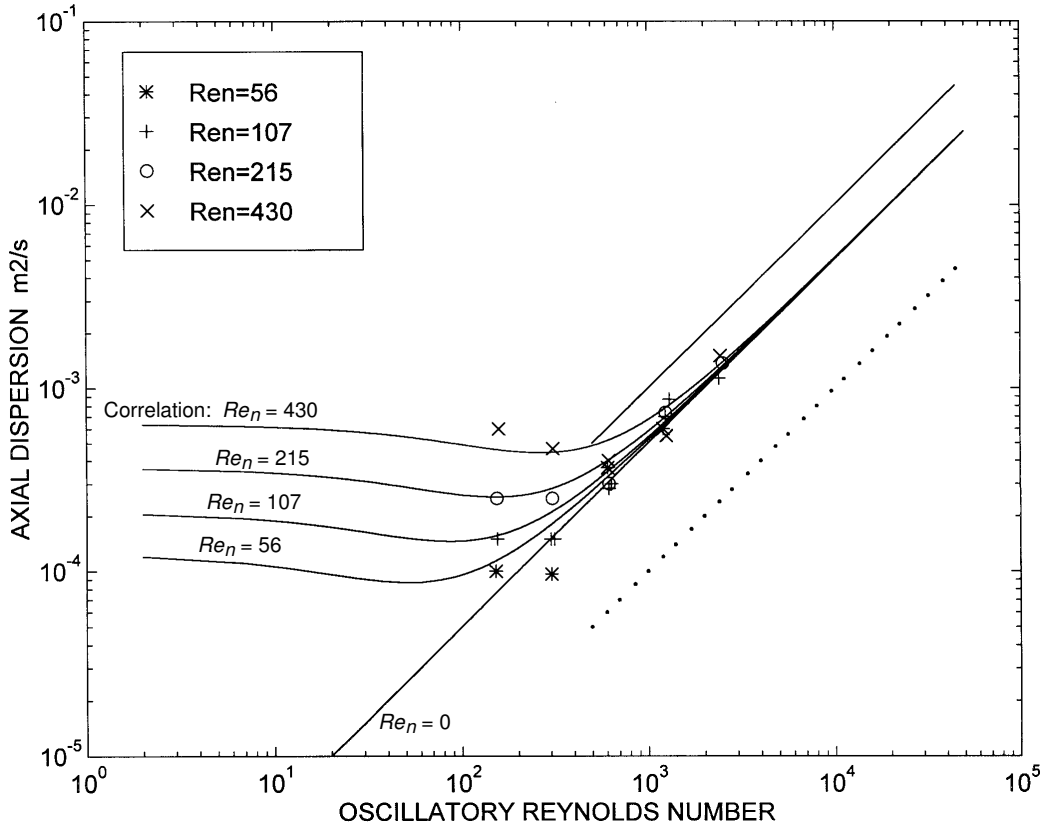

Figure 5.24: Graph Showing a Best-Fit Correlation for Axial Dispersion in the 24 mm Apparatus in the Case of Net Flow & Oscillation *Str* = 1

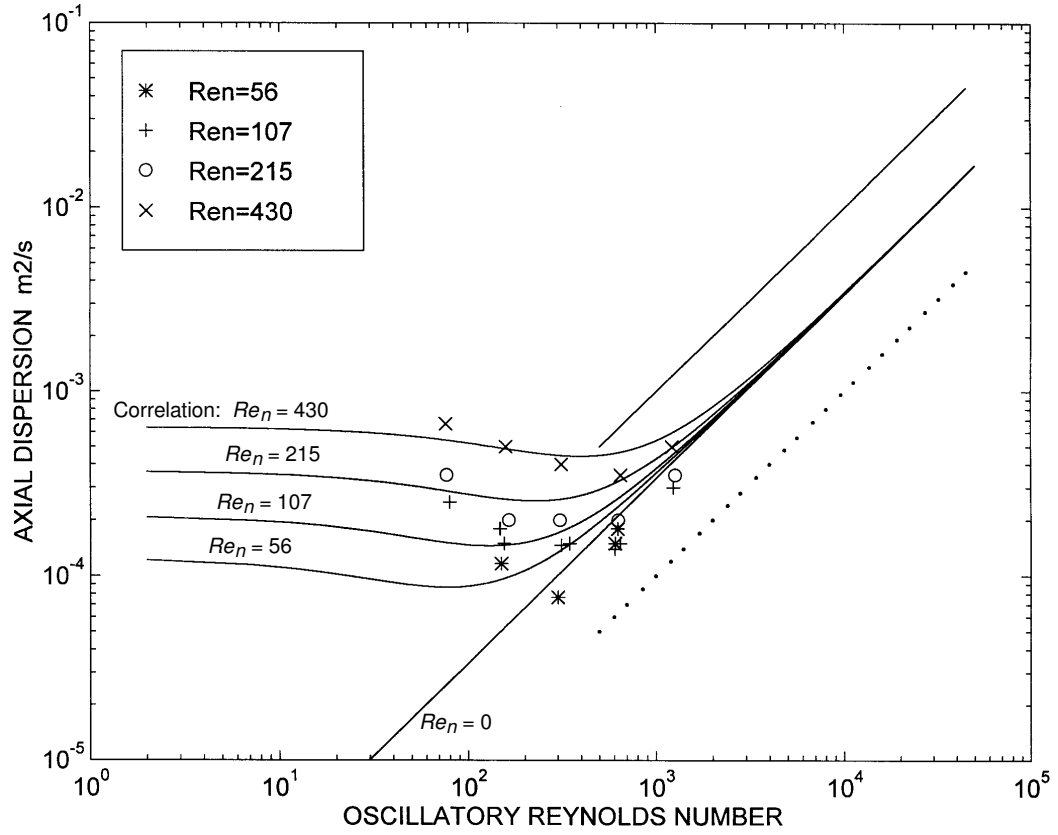

Figure 5.25: Graph Showing a Best-Fit Correlation for Axial Dispersion in the 24 mm Apparatus in the Case of Net Flow & Oscillation $Str = 2$

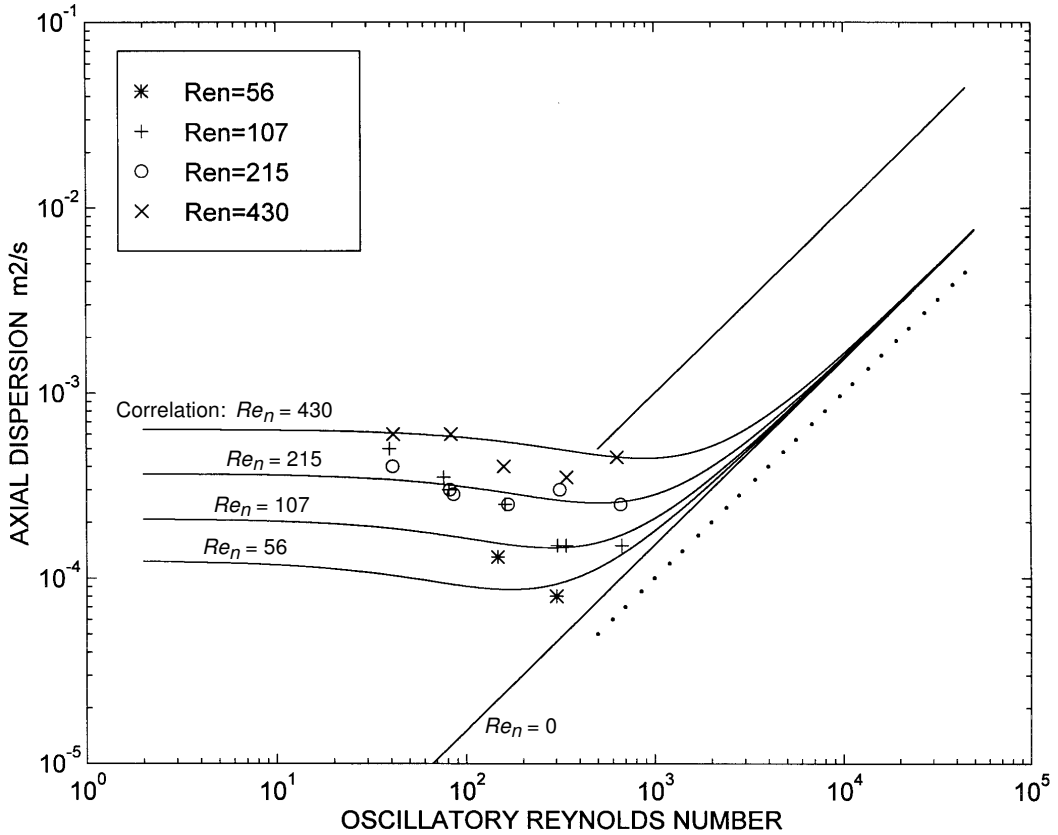

Figure 5.26: Graph Showing a Best-Fit Correlation for Axial Dispersion in the 24 mm Apparatus in the Case of Net Flow & Oscillation $Str = 4$

Using equation 5.6 and the arguments put forward by Crittenden et al (1995) the oscillatory conditions for which the minimum axial dispersion occurs are when:

$$Re_o\, e^{(-0.4Str)} = \frac{\left(\sqrt{A_3} - A_1\right)}{A_2} Re_n^{0.8} = 1.37\, Re_n^{0.8} \qquad \text{eqn (5.8)}$$

for which the predicted minimum axial dispersion is:

$$E = 2\sqrt{A_3}\, Re_n^{0.8} = 3.5 \times 10^{-6}\, Re_n^{0.8} \qquad (m^2/s) \quad \text{eqn (5.9)}$$

For example, in the case of Re_n = 100 and Str = 1 then the minimum value of axial dispersion is 1.4 x 10^{-4} m^2/s and this occurs at an oscillatory Reynolds number of Re_o = 82. This prediction of the oscillatory Reynolds number which will give the minimum axial dispersion is slightly lower than would be expected from experimental experience: a more typical rule of thumb is that the oscillatory Reynolds number should be between two and five times the magnitude of the net flow Reynolds number in order to achieve minimum axial dispersion (Stonestreet 1997).

SUMMARY

The presentation of axial dispersion data measured in each of the 24 mm, 54 mm and 150 mm sets of apparatus has shown that the approximate absolute magnitude of axial dispersion is not a function of tube diameter (§5.1, §5.2 and §5.3). An approximate correlation has been fitted to the experimental data (§5.5).

It has been discovered through the examination of the degree of backmixing of the injected dye tracer upstream of the injection point (§5.4) that the axial diffusion model is only truly applicable when the oscillatory Reynolds number is greater than that which gives the minimum measured axial dispersion. The diffusion model is therefore limited in the range of flow conditions for which it can be used to quantify experimental axial dispersion measured over short tube lengths.

The next chapter (Chapter 6) examines the computer simulation of O.F.M. to enable axial dispersion to be predicted from a fluid mechanics approach; these predictions can then be matched to experimental results and also used to extend the range of flow conditions for which axial dispersion can be quantified.

6. Axial Dispersion Measurements from Fluid Mechanical Simulation

The chapters so far in this thesis have dealt with the experimental measurement and quantification of axial dispersion in O.F.M.. The range of experimental conditions studied was restricted for low Reynolds number flows by the limits of the diffusion model which could not always successfully model experimental concentration profiles. It would therefore be advantageous to be able to predict the axial dispersion of tracer in O.F.M. at low Reynolds numbers (< 300) from fundamental principles: this chapter investigates the prediction of axial dispersion in single-phase O.F.M. using a numerical fluid mechanical simulation. Values of axial dispersion predicted by the fluid mechanical simulation are compared with those measured experimentally and the simulation is used to extend the range of results for flow conditions where the diffusion model did not match the experimental results. The range of overlap between experiment and simulation also improves confidence in both the experimental and simulated results.

The chapter is divided into two sections: §6.1 presents the method by which axial dispersion was modelled using the injection of fluid marker particles into the numerically simulated flow field. Two different approaches were used to try to quantify axial dispersion using the results of the simulation:

i) the imperfect pulse technique, and

ii) the rate of change of particle variance.

Results obtained using the second (preferred) method are presented in §6.2 and are compared with experimental results.

6.1 Simulation of Axial Dispersion in OFM Using Fluid Marker Particles

The finite difference fluid mechanical simulation developed by Dr R. Saraiva (1997) was generously made available for use in this thesis. The simulation is written in Fortran code and was run on an Ultra 170MHz Sun workstation; details of the programme are given in Appendix VI. The simulation is based entirely upon the dimensionless groups Re_o, Re_n and Str in order to define the fluid dynamic conditions and it therefore pre-supposes that there is no dependence upon tube diameter as has been experimentally confirmed in the previous chapter. Experimental results in the previous chapter covered a large range of dynamic conditions, with $10 < Re_o < 30\ 000$. In comparison, the simulation is restricted to axisymmetric flow and is therefore thought to be limited to $Re_o \leq 300$.

Numerical simulations were carried out for the cases of net flow only, oscillations only and net flow with oscillations. In order to model experimental axial dispersion, a cloud

of 10 000 inert fluid marker particles was injected into the simulated flow in a defined region across the centre of an inter-baffle cavity (Figure 6.1) using the same baffle geometry as for the experimental apparatus. The distribution of particles was radially weighted to take into account the diminishing volume of elements closer to the tube centre, such that the concentration of particles per unit volume was constant.

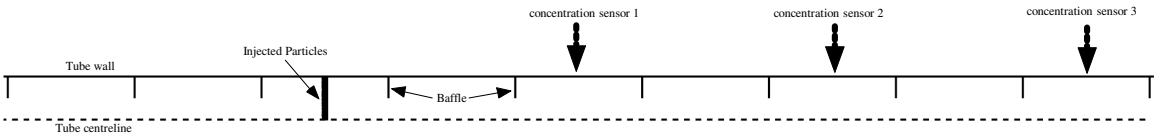

Figure 6.1: Diagram Showing the Initial Position of Fluid Marker Particles in the Simulation; Because the Simulation is Axisymmetric, Only Half the Tube is Shown

The particles were injected instantaneously after the flow field had reached quasi steady state and this was normally after 20 oscillatory cycles. The simulation then advected the particles over a given number of cycles and the position of each particle was recorded twenty-times per oscillatory cycle. An example of this advection is shown in Figure 6.2; the initial location of the injected particles at the position indicated in Figure 6.1 is shown by an unfilled rectangle. (The conditions are equivalent to a net flow of 0.12 l/min and a 1 Hz, 2 mm amplitude oscillation in the 24 mm apparatus). As well as the fluid mechanics of the simulation, a Brownian motion was also applied to the motion of the particles to simulate molecular diffusion equivalent to a Schmidt number of 1000. This corresponds to a molecular diffusion coefficient of approximately 10^{-9} m^2/s if the fluid is water. The presence of molecular diffusion at the tube wall is essential for problems involving net flow otherwise the axial dispersion would tend towards infinity (Taylor 1953) and the effect of the magnitude of molecular diffusion on axial dispersion in O.F.M. has been studied by both Howes (1988) and Saraiva (1997).

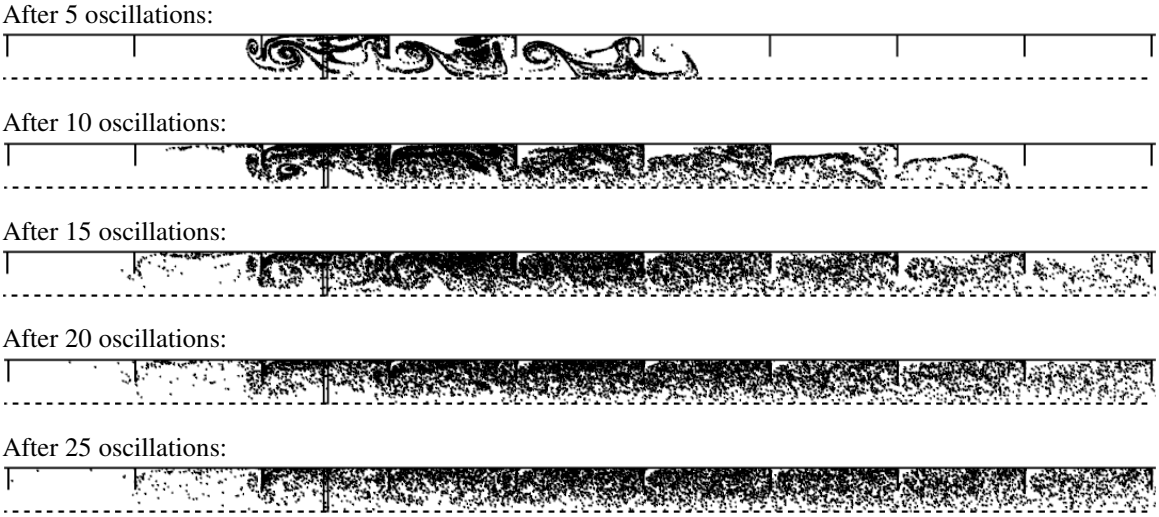

Figure 6.2: Diagram Showing the Simulated Advection of Fluid Marker Particles in O.F.M.
$Re_n = 107$, $Re_o = 300$, $Str = 1$ the Direction of Net Flow is Left to Right

Two different methods were applied to the results in order to quantify axial dispersion in the simulations:

METHOD 1: Imperfect Pulse Technique

Axial dispersion was quantified using the same assumptions used for the experimental measurements of axial dispersion: the programme was modified (courtesy Dr R. Saraiva) to measure the concentration of particles across a line of fluid elements situated a distance of two, four and six baffle-spacings respectively downstream of the initial injection point (see Figure 6.1). These "virtual sensors" at positions one, two and three respectively therefore mimicked the behaviour of the L.E.D. sensors used experimentally; the measuring width of the equivalent optical path was 0.1 tube diameters in the axial direction. The data from these virtual sensors could be analysed directly using the method of analysis already validated in Chapter 4 in order to give a value for the axial dispersion.

METHOD 2: Method of Rate of Change of Variance

Using the simulation, the position and distribution of the cloud of particles could be measured at any instant in time. The method of change of particle variance after Sobey (1985) and also validated for O.F.M. by Saraiva (1997) was therefore used to quantify axial dispersion. The variance of the cloud of particles around its mean axial position is recorded during a simulation and so long as the rate of increase of particle variance $\frac{\partial \sigma^2}{\partial t}$ over each oscillatory cycle is constant then the axial dispersion can be quantified using equation 2.23 which in its simplified form is:

$$E = \frac{1}{2}\frac{\partial \sigma^2}{\partial t} \qquad (m^2/s) \qquad \text{eqn (6.1)}$$

Note that the variance in equation 6.1 has units of m^2. Since both methods derive their results from the same simulation, their values should be close in magnitude. A simple case study to verify this assumption used both methods to evaluate the axial dispersion coefficient for the same simulated experimental conditions. Figure 6.3 shows the outputs from the virtual sensors at two and six baffle-spacings downstream of the initial position of the particles for oscillatory conditions Re_o = 150 and Str = 1 (Re_n = 0) together with the best-fit model line using the imperfect pulse diffusion model analysis. The best fit line is a good match for the simulated concentration-time profile and corresponds to an axial dispersion coefficient using method one of 1.1 x 10^{-5} m^2/s.

Figure 6.4 shows the change in the variance of the cloud of particles between the start of the twentieth oscillation (when the particles are injected) and the start of the one-hundredth cycle. The variance has been made dimensionless through multiplication by $\frac{4}{diameter^2}$ where *diameter* is the tube diameter. After the initial perturbations following the injection of the particles, the rate of increase of variance is approximately constant after a further twenty oscillations. Using equation 6.1 the calculated axial dispersion using method two is 1.2 x 10^{-5} m^2/s.

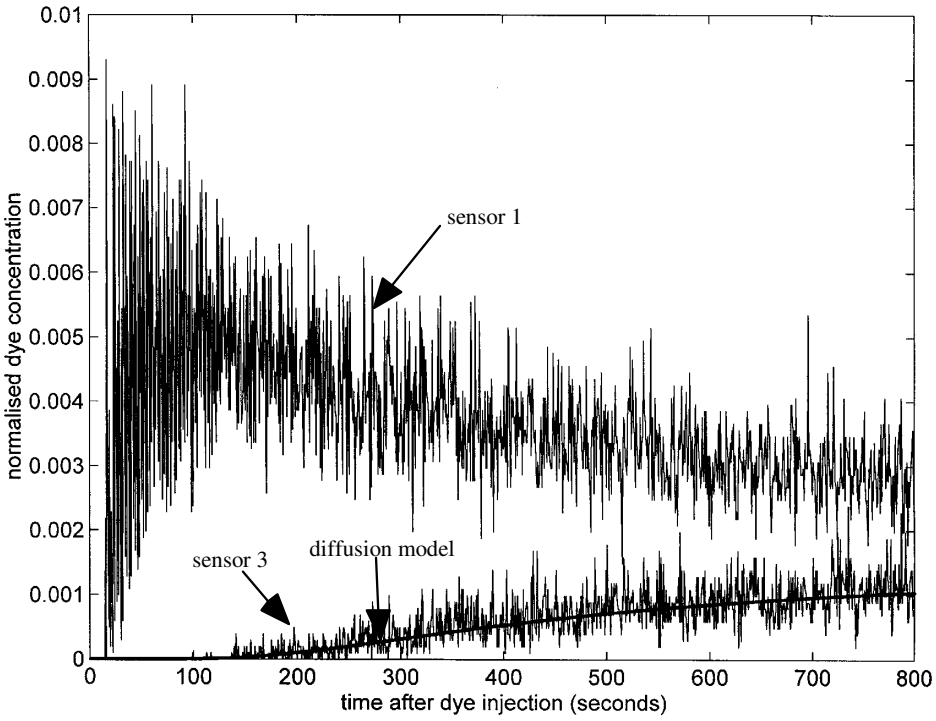

Figure 6.3: Simulated Concentration - Time Profiles for Fluid Marker Particles in O.F.M.
$Re_n = 0,\ Re_o = 150,\ Str = 1$

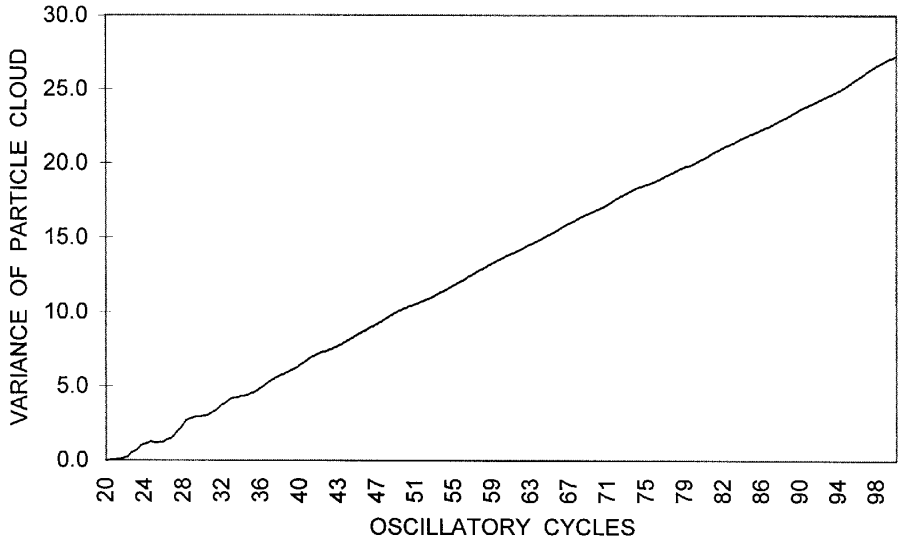

Figure 6.4: Graph Showing the Simulated Change of Particle Variance
$Re_n = 0,\ Re_o = 150,\ Str = 1$

The results obtained using either method one or two are therefore quite similar (1.1 x 10^{-5} m^2/s compared to 1.2 x 10^{-5} m^2/s for the same conditions). This was found to hold true for a range of conditions. Table 6.1 shows both methods predicting similar values (the maximum difference between the methods being of order 15%), however the limitation of the imperfect-pulse method becomes apparent in that under some high *Str* conditions the imperfect pulse technique fails. This is because under certain oscillatory conditions the diffusion model does not match the concentration-time profile of the particle cloud measured by the virtual sensors for any value of the axial dispersion coefficient.

Method two (change of variance) is therefore a much more practical tool for quantifying axial dispersion in the case of a simulation where the instantaneous position of all particles is known. Axial dispersion can be quantified for any conditions so long as the rate of increase of variance is constant, whereas the imperfect pulse method cannot quantify axial dispersion in cases where the diffusion model does not adequately describe the spread of particles. For this reason the rest of the results presented in this chapter are obtained using method two.

Oscillatory Conditions		Axial Dispersion in m^2/s Method One (Imperfect Pulse)	Axial Dispersion in m^2/s Method Two (Change of Variance)
$Re_O = 37$	$Str = 0.5$	1.6 x 10^{-7}	1.7 x 10^{-7}
$Re_O = 75$	$Str = 0.5$	9.0 x 10^{-7}	9.8 x 10^{-7}
$Re_O = 150$	$Str = 0.25$	1.3 x 10^{-5}	1.5 x 10^{-5}
$Re_O = 150$	$Str = 0.5$	1.5 x 10^{-5}	1.7 x 10^{-5}
$Re_O = 150$	$Str = 1$	1.1 x 10^{-5}	1.2 x 10^{-5}
$Re_O = 150$	$Str = 2$	1.5 x 10^{-5}	1.6 x 10^{-6}
$Re_O = 150$	$Str = 4$	(model fails)	1.9 x 10^{-7}
$Re_O = 150$	$Str = 8$	(model fails)	2.2 x 10^{-7}

Table 6.1: Comparison of the Two Methods Used for Estimating Axial Dispersion from Simulation

6.2 Results for Simulation of Axial Dispersion in O.F.M.

This section compares simulation results with experimental results for the cases of net flow only, oscillatory flow only, and net flow with oscillatory flow.

NET FLOW ONLY

Figure 6.5 shows both simulation and experimental results (from the 24 mm apparatus) for net flow only. (Note that the scale of the axial dispersion axis is different to previous graphs in order to accommodate the extended range of the simulation results). The simulation results show axial dispersion increasing approximately linearly with increasing Re_n for either $Re_n < 55$ or $Re_n > 107$ but a markedly non-linear increase in axial dispersion in the range $55 \leq Re_n \leq 107$ which would appear to indicate a change in the simulated fluid mechanics. It appears from flow visualisations in the next chapter (Figures 7.2 and 7.3) that the simulation predicts an increasing size of recirculating vortex on the downstream side of each baffle with increasing Re_n and it is observed that for $Re_n > 55$ the recirculating vortex has a much stronger effect in trapping tracer within the recirculating region thus increasing axial dispersion.

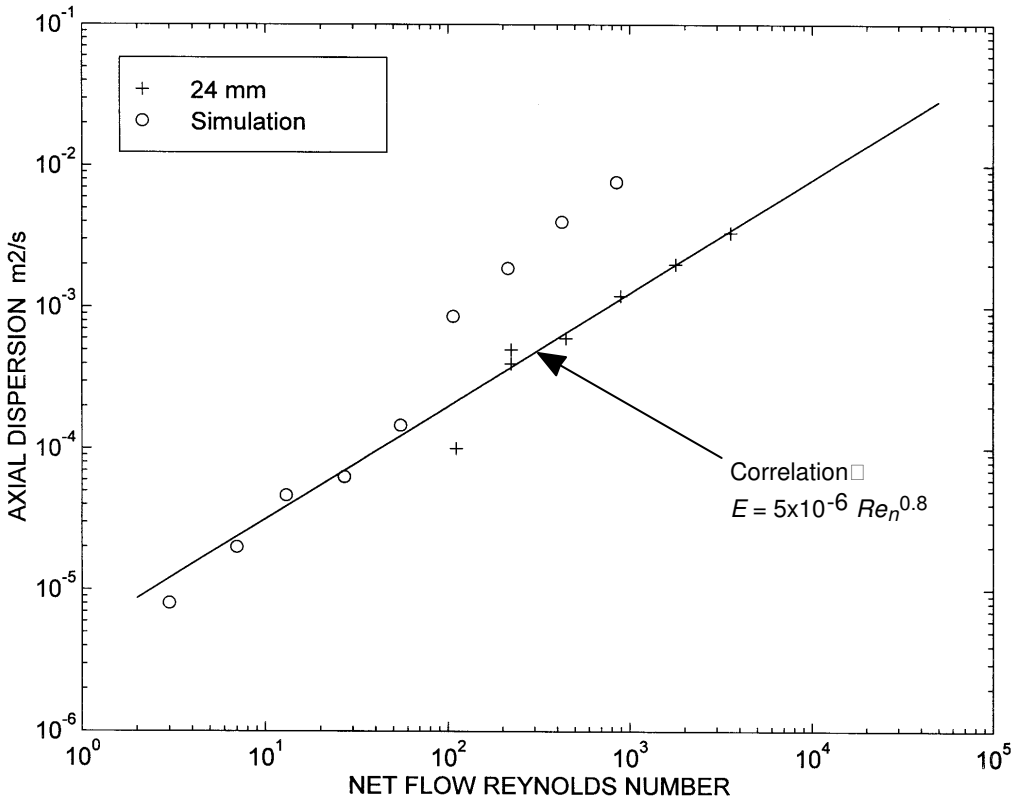

Figure 6.5: Graph Comparing Experimental and Simulated Results for Axial Dispersion for Net Flow Only

For $Re_n > 55$ the simulation significantly over predicts the experimentally measured axial dispersion. It is concluded from flow visualisations in the next chapter (Chapter 7) that this difference is largely due to the axisymmetric limitation of the simulation: in reality,

at around Re_n = 100 the flow becomes asymmetric and this leads to enhanced radial mixing which in turn reduces the axial dispersion. Figure 6.5 also shows the empirical correlation developed in §5.5 for axial dispersion as a function of net flow only: the simulation results for $Re_n \leq 55$ appear to extend linearly the trend of experimental results.

Although axial dispersion has been quantified for low net flow Reynolds numbers using the simulation, it is recognised that the fluid mechanics under these creeping laminar flow conditions do not provide an even radial distribution of tracer which is an assumption of the diffusion model. The simulated values of axial dispersion must therefore be treated with caution if they are to be used to predict residence time distributions over short lengths of baffled tube.

OSCILLATIONS ONLY

Figure 6.6 shows simulated and experimental results (from the 150 mm apparatus) for oscillations in the absence of net flow. The simulation results show a rapid fall in axial dispersion for $Re_o < 150$ (note that the scale of the axial dispersion axis is different from previous graphs in order to accommodate the low values obtained from simulation). This deviation from the expected axial dispersion as a function proportional to Re_o is explained by flow visualisations in the next chapter (Chapter 7) that show the formation of fluid "manifolds" for $Re_o < 150$. These manifolds act as a barrier to dispersion midway between two baffles and are a result of axisymmetric vortices travelling in opposing directions and meeting midway between baffles: they can be likened to an imaginary flexible membrane that allows axial dispersion through it only in the form of molecular diffusion. Sharp concentration differences across the middle of the inter-baffle cell can therefore be maintained and although mixing close to the orifice is good, at low Re_o the only mechanism for axial dispersion over distances greater than one baffle spacing is that of molecular diffusion across the manifold. The axial dispersion measured by simulation therefore decreases rapidly below approximately Re_o = 150 and approaches the magnitude of molecular diffusion ($\approx 10^{-9}$ m^2/s) at lower oscillatory Reynolds numbers.

For $Re_o > 150$ the simulation underpredicts the experimental axial dispersion by around 50%. This is interpreted as being a consequence of the increase in axial dispersion due to loss of axisymmetry in reality for $Re_o > 150$ or less (see Chapter 7 Flow Visualisation) whereas under these conditions the simulation is constrained to be axisymmetric and therefore under predicts the rate of axial dispersion.

Figure 6.7 shows an investigation using the simulation into the effect of Strouhal number on axial dispersion. It is seen that high amplitude oscillations (low *Str*) give much higher axial dispersion than low amplitude oscillations (high *Str*) at the same Re_o .

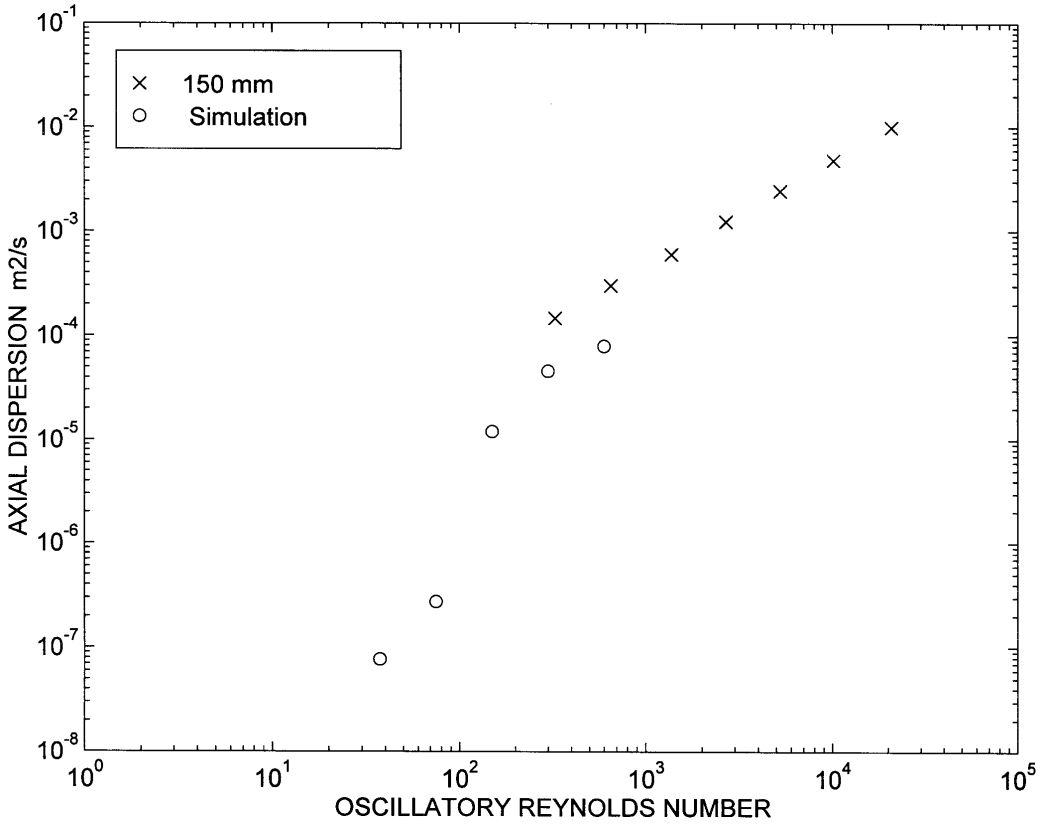

Figure 6.6: Graph Comparing Experimental and Simulated Axial Dispersion Results for Oscillation Only $Re_n = 0,\ Str = 1$

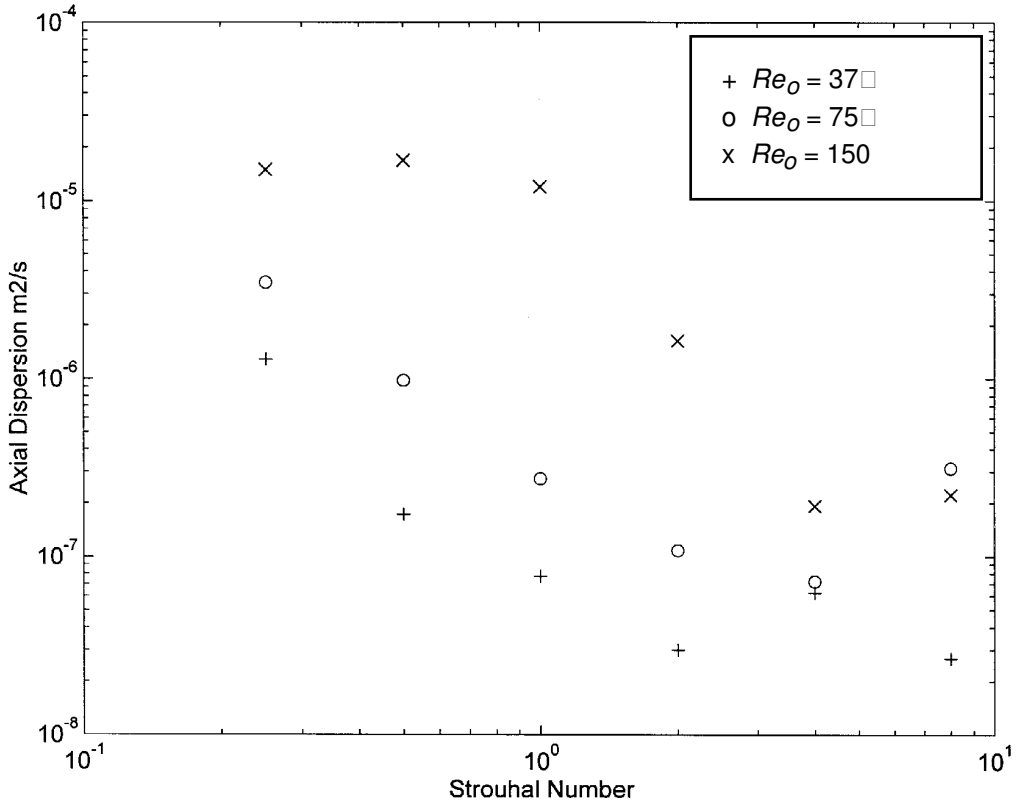

Figure 6.7: Graph Showing Simulated Axial Dispersion for Oscillation Only as a Function of Strouhal Number

There is not a simple trend equating the effect of *Str* to measured axial dispersion although for a particular Re_o the axial dispersion generally decreases with increasing *Str*. For a given *Str* the axial dispersion increases with increasing Re_o. The change in axial dispersion for oscillation only (Figure 6.7) is most apparent across the range $75 < Re_o < 150$ for which halving the oscillatory Reynolds number for $Str = 1$ decreases the axial dispersion by a factor of approximately 50. This indicates the change in the mechanism which dominates the axial dispersion, from diffusional behaviour across manifolds for $Re_o < 80$ to bulk fluid mixing by the interaction of vortices for $Re_o > 150$. In the intermediate range $75 < Re_o < 150$ there is a combination of dispersion mechanisms: manifolds are created but they distort by the formation of lobes close to the tube wall and or by the loss of axisymmetry. The effect is not only to create a larger manifold surface area over which molecular diffusion can take place but also to increase axial dispersion by the physical extension of the manifold lobes into adjacent inter-baffle cells.

It appears that the correlation developed in the previous chapter (equation 5.2) is oversimplified for axial dispersion at low oscillatory Reynolds numbers: there is a complex dependence of axial dispersion upon the oscillatory conditions. It is expected that the dispersion would be a non-linear function of oscillation amplitude for a given Re_o: in the limit, a rapid but small amplitude oscillation (large *Str*) would provide very little bulk displacement of the fluid in the baffled tube hence the axial dispersion would be small, in contrast with low frequency large amplitude oscillations (small *Str*) for which a single oscillation can project a vortex a large distance axially along the tube (possibly even more than a baffle spacing), promoting large axial dispersion.

NET FLOW AND OSCILLATIONS

For the typical experiments reported in Chapter 5 with net flow and oscillation, Figures 6.8 to 6.11 show results from the simulation which extend the range of oscillatory Reynolds number which could be investigated as well as providing a small overlap with experimental results.

For increasing Re_o the results show a striking trend of decreasing axial dispersion for the simulation compared with increasing axial dispersion for the experimental results. The two sets of results meet at a minimum at around $Re_o = 300$ at which point there is an order of magnitude agreement in the value of axial dispersion determined by experiment or by simulation. This match in values lends confidence to the validity of both the experiments and the simulation.

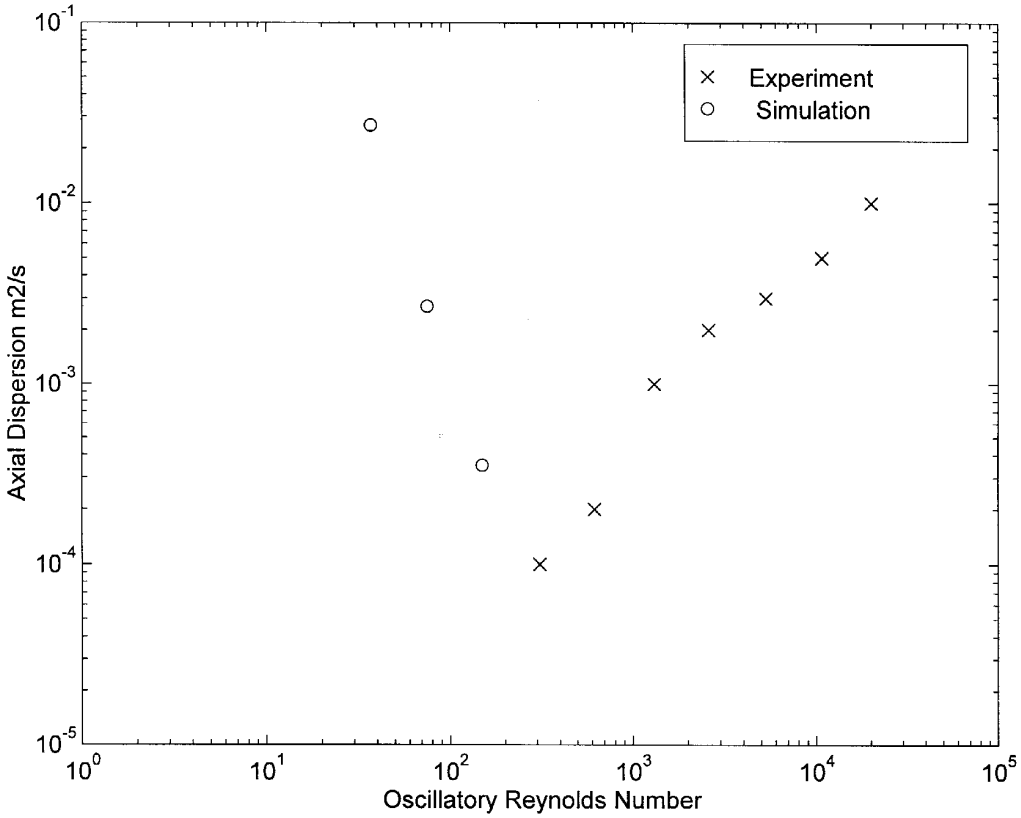

Figure 6.8: Graph Showing Simulated and Experimental Axial Dispersion Results for O.F.M. $Re_n = 107,\ Str = 0.5$

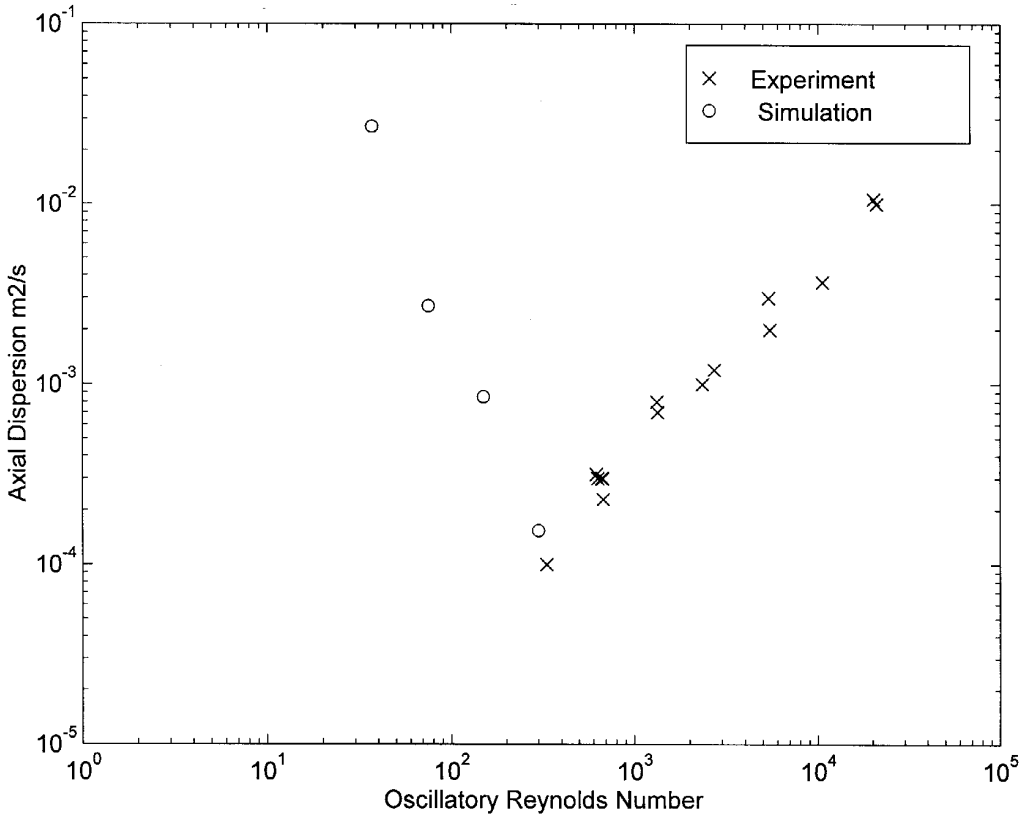

Figure 6.9: Graph Showing Simulated and Experimental Axial Dispersion Results for O.F.M. $Re_n = 107,\ Str = 1$

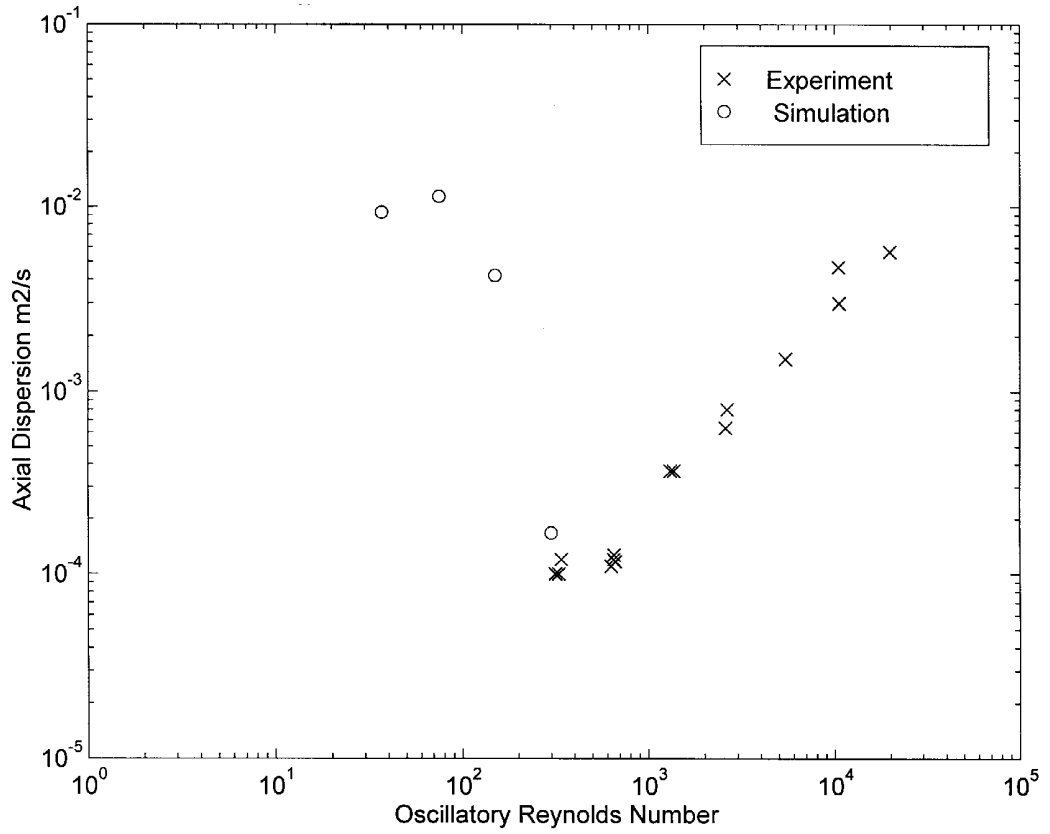

Figure 6.10: Graph Showing Simulated and Experimental Axial Dispersion Results for O.F.M. $Re_n = 107,\ Str = 2$

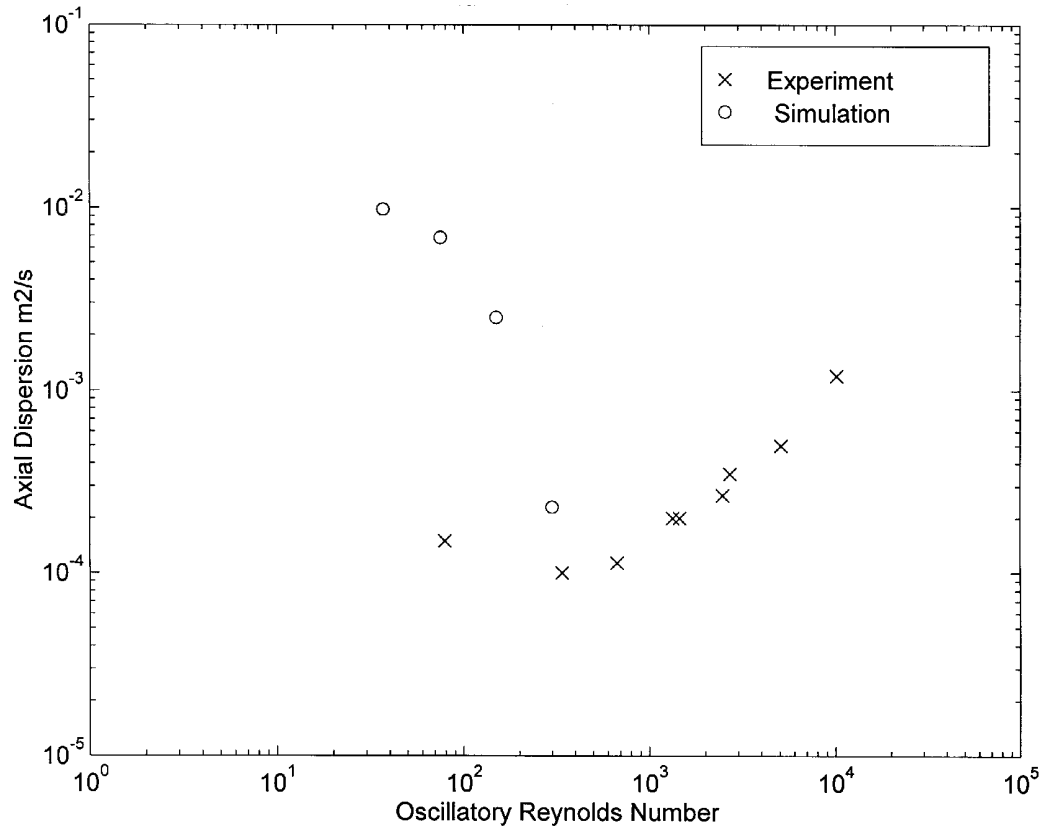

Figure 6.11: Graph Showing Simulated and Experimental Axial Dispersion Results for O.F.M. $Re_n = 107,\ Str = 4$

Inspection of the results shows that in general the addition of oscillations for $Re_o \leq Re_n$ serves to increase significantly the degree of axial dispersion. This is bearing in mind that from Figure 6.5 the axial dispersion due to a net flow of Re_n = 107 in the absence of oscillations is approximately 8.5 x 10^{-4} m^2/s. For an additional oscillation of Re_o = 37 the axial dispersion typically increases to the order of 10^{-2} m^2/s, a more than tenfold increase. However as the oscillations are increased to $Re_o \approx Re_n$ the axial dispersion decreases down to the order of 10^{-4} m^2/s, an almost tenfold decrease compared to the net flow without oscillations.

Such results can best be explained in conjunction with flow visualisations of the fluid mechanics. The results are therefore re-examined and discussed in more detail in Chapter 9 (Discussion) after the flow visualisation results (from both experiment and simulation) have been presented in the next chapter (Chapter 7).

SUMMARY

This chapter has demonstrated the use of a fluid mechanical model together with the simulated injection of passive fluid marker particles to predict axial dispersion in baffled tubes with oscillatory flow mixing. The simulation can be used to investigate axial dispersion and is thought to be valid for axisymmetric flows in the approximate range Re_o < 300 and $Re_n \leq 100$. A small overlap with experimental results shows a reasonable match in measured and predicted axial dispersion and this consistency where it exists gives confidence that both the experiments and simulations are valid. Above the limits Re_o = 300 and Re_n = 100 the simulation appears to either over or under predict the axial dispersion (for net flow and oscillatory flow respectively) and this is thought to be because in experimental reality the flow in the baffled tube becomes asymmetric.

For the cases of net flow only or oscillation only the simulation shows a similar trend to experimental data in that axial dispersion increases with Reynolds number. For combined net flow and oscillation the simulation and experiment show strikingly different trends with increasing oscillatory Reynolds number although they are in agreement at the minimum in axial dispersion when $Re_o \approx Re_n$. It is this reduction in axial dispersion that makes the O.F.M. attractive as a method of controlling residence time distributions. The axial dispersion results for combined net flow and oscillations will be discussed further in Chapter 9 in the light of flow visualisations (Chapter 7).

Comparison between the fluid mechanical simulation and experiment is further developed in the next chapter (Chapter 7) which uses the same fluid marker particle injection simulation technique to model experimental flow visualisations obtained using a fluorescent dye streakline technique.

7. Flow Visualisations Obtained by Experiment and by Simulation

A novel fluorescent dye streakline technique was used to obtain experimental visualisations of Oscillatory Flow Mixing. The development of the technique for use in O.F.M. and the reasons for its selection were discussed in §3.2.2. These flow visualisations have been used to examine fluid mechanics as a function of the fluid dynamic conditions.

The technique comprises the injection into the baffled tube of a fluorescent dye and then the taking of either photographs or video records of the observed flow. The illumination is from a slit light source oriented to give a longitudinal cross-section through the centre of the tube and this allows the detailed structure of the flow to be observed in the form of streaklines. Photographs and video images are normally taken either one or two baffle spacings downstream of the injection point so that concentration differences are large and the streaklines are therefore discernible under the conditions of very low light intensity.

The reason for studying these flow visualisations was two-fold: firstly, and most importantly in the context of thesis, it allowed comparisons to be drawn between the flow behaviour in tubes of different diameter under similar dynamic conditions; secondly, it also aided the understanding of axial dispersion in O.F.M., for example to explain why under certain flow conditions the axial diffusion model does not adequately describe dispersion in the baffled tube.

In addition to experimental flow visualisations, the numerical fluid mechanical simulation code used in the previous chapter to predict axial dispersion in O.F.M. has been used in this chapter in two different ways to produce flow visualisations which could then be compared to experimental results:

i) method one used the simulation to predict velocity profiles and streamlines for specific dynamic conditions;

ii) method two used the method of inert marker particle injection into the simulated flow field to mimic the streaklines observed experimentally using the fluorescent dye technique.

Both of these methods served as a check on the validity of the fluid mechanical simulation compared to the experimentally-observed reality.

This chapter is divided into three sections, each of which contain both experimental and simulated flow visualisations: §7.1 presents results for net flow only; §7.2 presents results for oscillatory flow only, and §7.3 presents results for the case of net flow and oscillation together.

7.1 Flow Visualisation - Net Flow with No Oscillation

A range of net flows were investigated experimentally in the 24 mm, 54 mm and 150 mm sets of apparatus in the range $55 \leq Re_n \leq 3000$. The resulting streaklines captured by video are shown in Figure 7.1 (not all conditions are shown for each apparatus). Each image in Figure 7.1 corresponds to a representative flow pattern at a particular Re_n taken a time after the fluorescent dye injection as soon as the streaklines had developed sufficiently to show clearly the structure of the flow. (At later times the dye had longer to mix and to diffuse therefore the images were less sharp).

Examining first of all the images for the 54 mm apparatus, there is a marked change in the flow above $Re_n = 107$: for $Re_n \leq 107$ the dye is swept axially down the centre of the baffled tube but some remains trapped in slowly recirculating vortices against the walls of the tube in the region behind the baffles (the recirculation is evident from visual and video observations). For $Re_n \geq 214$ the flow becomes non-axisymmetric with vortex-shedding behind the baffles and is increasingly chaotic in nature with increasing Re_n. In addition, there is evidence of toroidal motion in the flow which manifests itself as the sudden disappearance and emergence of streaklines from and into the illuminated cross-section of the tube (the streaklines can therefore appear discontinuous). By the time the net flow rate has increased to $Re_n = 848$, the flow is very complex with very rapid axial and radial mixing in which the individual vortices are no longer discernible.

A similar transition is observed for the 24 mm apparatus (the image is blurred due to reduced video resolution) and also for the 150 mm apparatus, although the transition is less clear for the latter since already at $Re_n = 107$ there is a hint of vortex-generation behind the baffles. It should nevertheless be remembered that the mean net flow velocity is much slower for similar dynamic conditions in the 150 mm apparatus compared to the 24 mm apparatus (for the same Re_n the mean net flow velocity is inversely proportional to tube diameter). It is therefore possible that the effect of any thermal convection, mechanical vibration from the surroundings or density differences between the fluid and the dye will influence the flow much more for the larger tube diameter, where a typical mean net flow velocity would be 0.5 mm/s.

In light of this it was concluded from the experimental flow visualisations that the fluid mechanics for each apparatus with net flow only are largely unaffected by the tube diameter, although flow in the larger tube diameters is more prone to external disturbances.

Figure 7.2 shows velocity-contour profiles generated by fluid mechanical simulation (method one) for $55 \leq Re_n \leq 848$. Each diagram shows the flow field in a single baffled cell (the region between two baffles); the upper half of each diagram shows arrows representing velocity vectors of the flow in the tube, while the lower half (separated by a centre-line) shows streamlines. These streamlines would be expected to be similar in

form, whilst not identical, to the streaklines observed experimentally. The small arrow beneath each diagram shows the direction of the net flow and also the magnitude of the mean net flow velocity (on the same scale as the other arrows on the diagram). The streamlines separate regions of equal volumetric flowrate using an arbitrary scale that is consistent for all the diagrams shown in this thesis.

The simulation has been thought by others (Saraiva 1997) to be valid only for Reynolds numbers of up to 300, and the limitations of the simulation are seen here: although at low net flow rates ($Re_n \leq 107$) the simulation matches adequately well the experimental observations in Figure 7.1, the simulation is by definition axisymmetric and cannot therefore predict the complexity of flow for $Re_n \geq 214$. It is possible that the transition to a non-axisymmetric chaotic flow is triggered at lower-than-expected Reynolds numbers by vibration from the surroundings or by minor inconsistencies in the construction of the baffled tube; it is clear that the fluid mechanical simulation under predicts the complexity of the flow observed in reality for $Re_n > 107$.

Figure 7.3 shows the results of the same fluid mechanical simulations but now used to predict the motion of 10 000 inert fluid marker particles (method two). Only half the baffled tube is shown since the simulation is constrained to be axisymmetric. The simulated baffled tube was considered to be infinitely long, but only seven inter-baffle cells are shown in this case. In order to assist comparison between the flows at different Re_n the results are presented for three different dimensionless times after the initial instantaneous particle injection (the initial position of the particles immediately after injection was evenly distributed radially between two baffles and is shown as an unfilled rectangle). One time period is equivalent to the tube radius divided by the mean net flow velocity.

After five time periods the particles have been swept downstream in an essentially Poiseuille-type flow albeit hindered by the baffles. At higher Re_n the centreline velocity is marginally greater and therefore the particles penetrate further along the tube in an equivalent time; this was observed in practical experiments up to approximately Re_n = 107, but at higher net flows the trend reversed due to vortex-shedding and the associated increase in radial mixing which slowed the axial spread of dye tracer.

After 25 and 45 time periods respectively the particles become trapped in large recirculating regions behind the baffles. This is consistent with the experimental observations for $Re_n \leq 107$, but not true for $Re_n \geq 214$ for which the formation of vortices disrupts the recirculation region.

An interesting feature of the simulation is the increasing degree of predicted recirculation in the inter-baffle cell in which the particles were initially injected: for Re_n = 55, all particles are swept downstream of the injection point but for $Re_n \geq 107$ there is a steadily increasing recirculation of particles upstream of the injection location. The particles do

not however move past the first upstream baffle nearest the injection point. This flow phenomenon could not have been detected experimentally because of the impossibility of injecting the fluorescent dye radially across the tube without disturbing the flow.

Using the fluid mechanical simulation pre-supposes that the fluid mechanics are independent of tube diameter, and this appears to be true for a net flow only in a baffled tube. The simulation appears to be limited to flows where $Re_n < 214$. It can be seen why it was not possible to model axial dispersion using the diffusion model for $Re_n < 107$ in the absence of oscillations since the recirculation behind baffles creates large inhomogeneous regions with large radial concentration differences. In comparison, for $Re_n \geq 214$ the formation of vortices serves to homogenise the flow and to provide radial mixing; under these conditions the diffusion model describes well the axial spread of tracer.

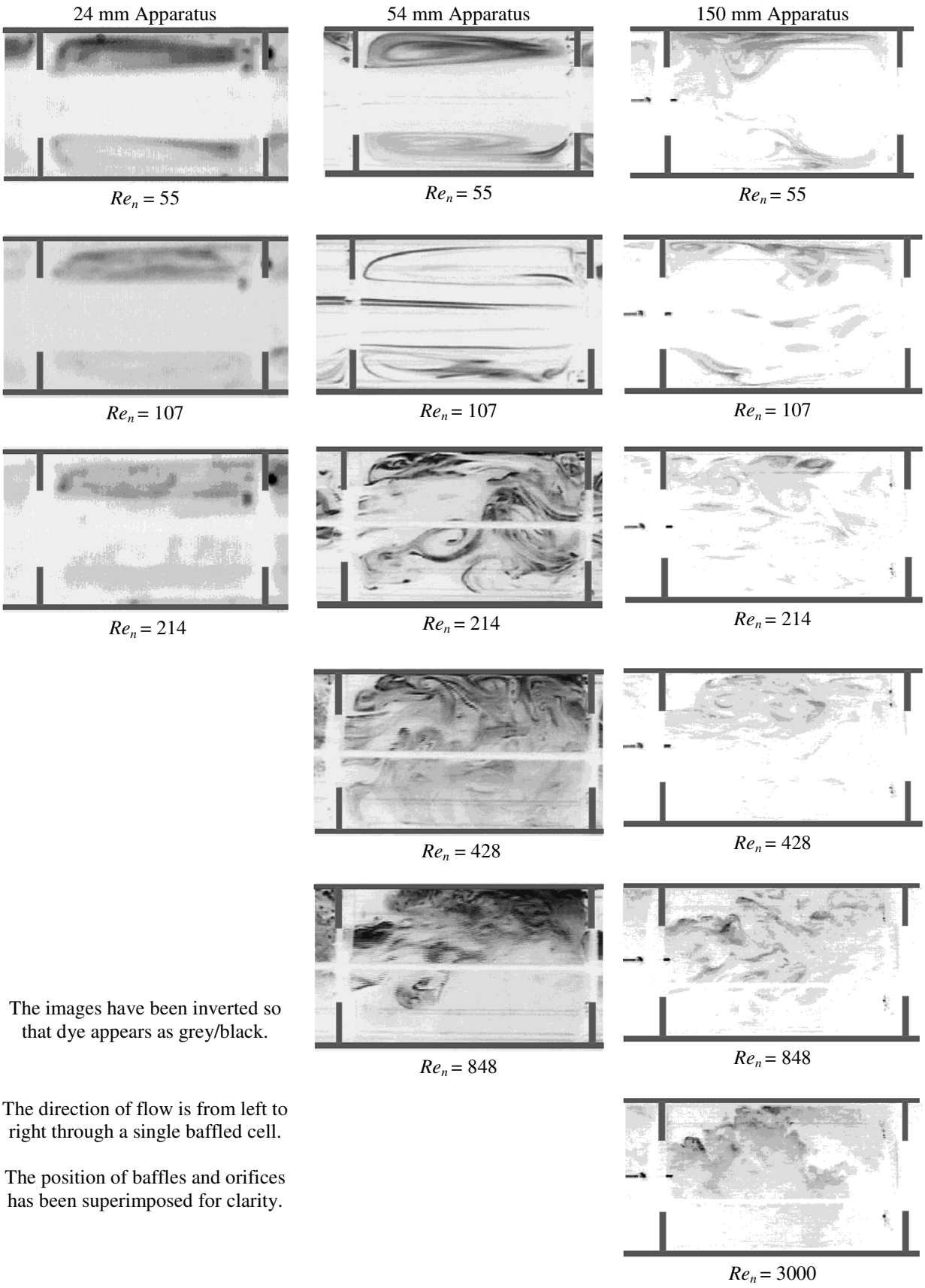

The images have been inverted so that dye appears as grey/black.

The direction of flow is from left to right through a single baffled cell.

The position of baffles and orifices has been superimposed for clarity.

Figure 7.1: Representative Flow Visualisation for Net Flow in a Baffled Tube

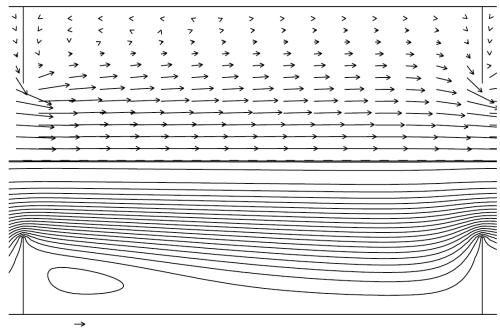

$Re_n = 55$

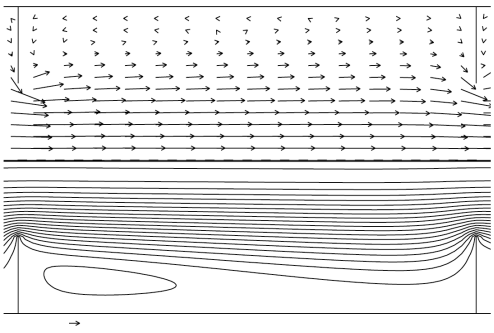

$Re_n = 107$

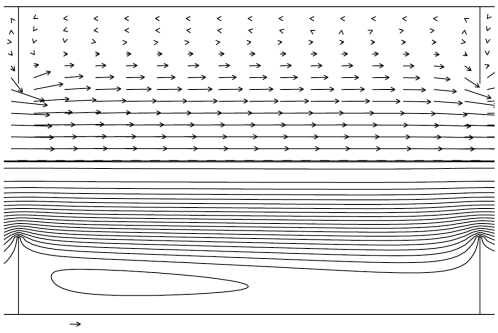

$Re_n = 214$

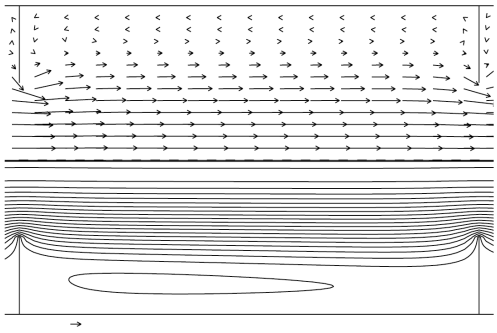

$Re_n = 428$

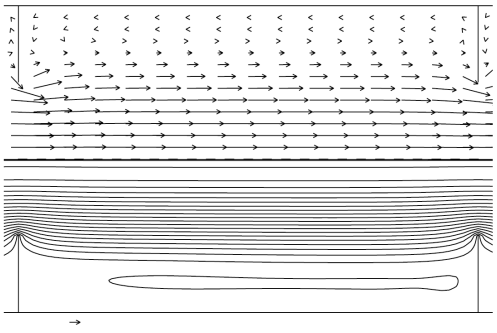

$Re_n = 848$

Figure 7.2: Velocity Profiles and Streamlines Predicted by Fluid Mechanical Simulation – Net Flow Only

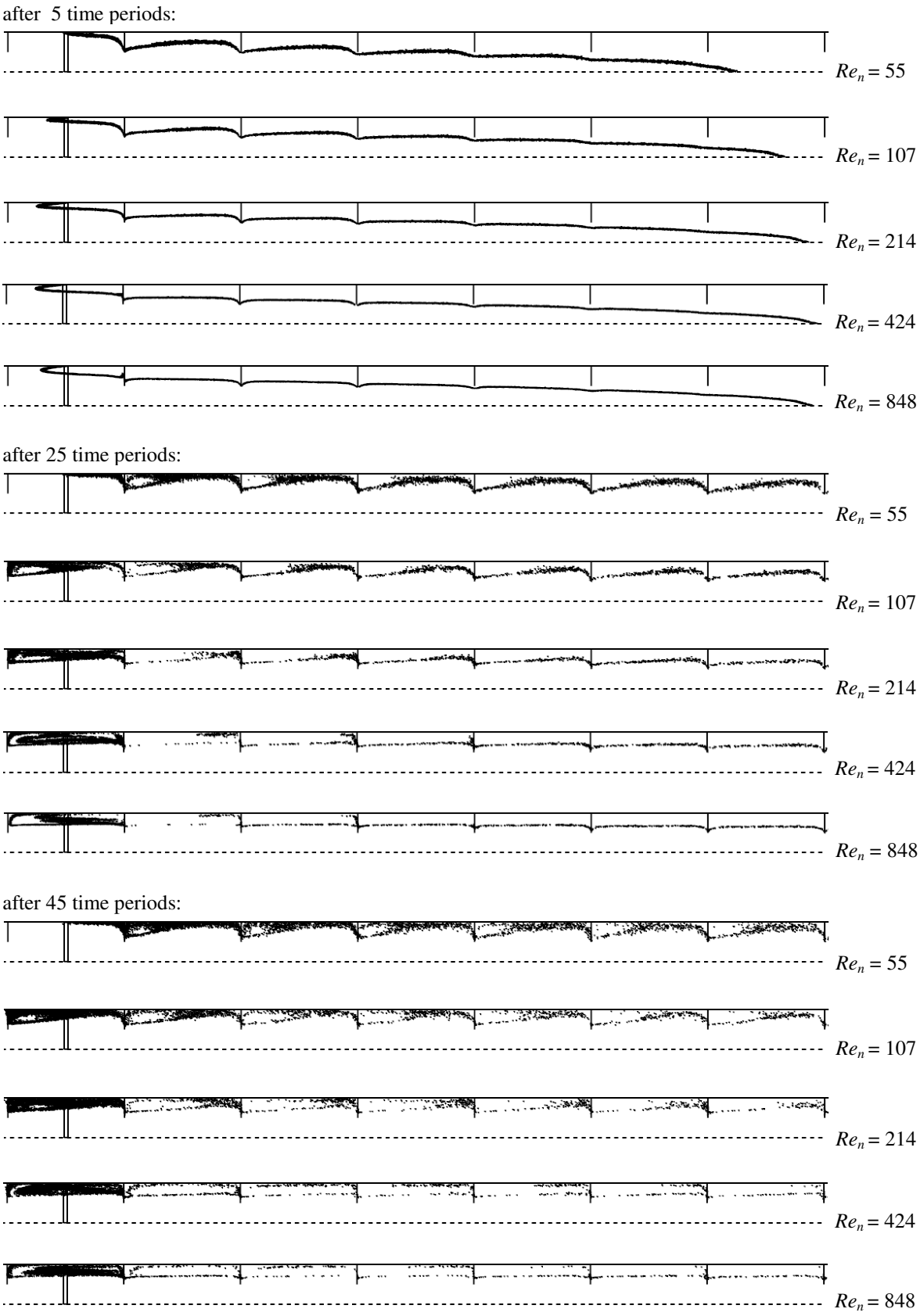

Figure 7.3: Fluid Mechanical Simulation of Inert Particle Tracer Injection for Net Flow Only

7.2 Flow Visualisation - Oscillation with No Net Flow

One of the very first flow visualisation experiments performed as part of this thesis was without the benefit of the fluorescent dye technique but simply with the injection of methylene blue dye into the 24 mm baffled tube with a modest oscillation of 0.3 Hz and 1 mm amplitude. The result was quite striking: after the initial disturbance of the dye injection, a flow structure developed in the inter-baffle cell next to the injection point which created a sharp divide of dye concentration across the middle of the inter-baffle cell. Only gradually then did the dye seep into the other half of the cell by the formation of lobes close to the tube wall and by diffusion across the divide. This type of flow boundary has been termed "manifold" (Figure 7.4). Even after 30 minutes, the manifold is clearly in evidence as a sharp concentration-divide between the two halves of the inter-baffle cell. The manifold is formed by the interaction of axisymmetric vortices travelling in opposite directions and which meet midway between two baffles. The vortices have the same sense of rotation which sweeps elements of fluid from the centre of the tube towards the wall and this creates a separation between the two halves of the inter-baffle cell: because the velocity is primarily radial where the opposing vortices meet, negligible tracer crosses the manifold axially by advection. The manifold moves a small distance up and down with the fluid oscillation, but remains flat except for close to the tube wall where the no-slip condition can generate folds or “lobes” in the manifold due to the oscillations.

The existence and behaviour of these manifolds could be successfully predicted using the fluid mechanical simulation: Figure 7.5 shows a direct comparison between simulation and experiment for Re_o = 75 and Str = 4 in the 54 mm apparatus. Using the fluorescent streakline technique allows the "onion-peel" or “lamella” flow structure that creates the manifolds to be seen, and as a result of uneven dye injection the dye is only present on the left-hand half of the tube despite being well mixed. This is strong evidence that there is minimal toroidal motion of the fluid under the flow conditions that created the manifolds. The manifolds act as a barrier to axial dispersion whilst at the same time the oscillations create relatively good stretch-fold mixing in the regions separated by the manifolds. Where such manifolds are present, the axial diffusion model is a poor physical model for dispersion over short distances in the baffled tube.

Only very delicately controlled oscillatory conditions allow the manifolds to exist. At the same oscillatory Reynolds number to the previous example but with a larger amplitude oscillation (Str = 2), Figure 7.6 (a) shows the resulting experimental streaklines: the axisymmetry of the manifold is broken and although the manifold still exists, axial mixing is much more rapid as the lobes extend into the next inter-baffle cell. The streaklines are shown at four equally spaced times during one complete cycle of the oscillation and are compared with predicted velocity profiles using the fluid mechanical simulation (b) for which the simulation does not predict the asymmetry of the flow. Figure 7.6 (c) shows

simulation predictions of the movement of marker particles under these flow conditions; again, the rate of axial mixing is underpredicted. A feature of the manifolds observed both in experiment and in simulation is that depending upon the exact moment of dye injection, dye injected equidistantly between two baffles will normally move predominantly to either one side or the other of the injection point, i.e. the dye is not distributed evenly each side of the injection point. This explains the apparent asymmetry in readings from concentration measurements made equal distances either side of the injection point at low oscillatory Reynolds numbers noted in §5.2 (Figure 5.13).

Figure 7.7 shows similar results but for a more rapid oscillation: while the simulation still predicts the formation of manifolds, the experimental reality is quite different with asymmetric flow, although the flow around the baffle orifice is similar in form to simulation with large amounts of stretching and folding occurring in successive oscillations.

The same experimental streaklines for the 54 mm apparatus shown in Figure 7.7 are displayed again in Figure 7.8 but this time as a comparison of the observed flow in each of the 24 mm, 54 mm and 150 mm sets of apparatus under similar dynamic conditions at four separate times during a single oscillatory cycle. For each stage in the cycle, the flow shows a similar distribution of vortices and vortex-sizes in the inter-baffle cell. The 54 mm apparatus shows a slightly higher degree of asymmetry in the flow, for which there is no obvious cause other than the possibility of slight baffle eccentricity or of a disturbance to the flow due to the method of dye injection in that particular apparatus.

The flow patterns observed for these conditions and a range of other values of Re_o and *Str* were generally similar enough in the three sets of apparatus to be able to conclude that the flow is not substantially affected by tube diameter in this mixing regime. At much higher Reynolds numbers ($Re_o > 800$), the flow becomes sufficiently chaotic and turbulent in nature that it is not possible to distinguish specific flow patterns, but rather the measurements of other properties such as axial dispersion must be used to draw the conclusion that fluid mechanics are not affected by tube diameter in the range studied. Similarly to the case of net flow only, it has been found that the numerical simulation underpredicts the complexity of the flow even for oscillatory Reynolds numbers as low as 75.

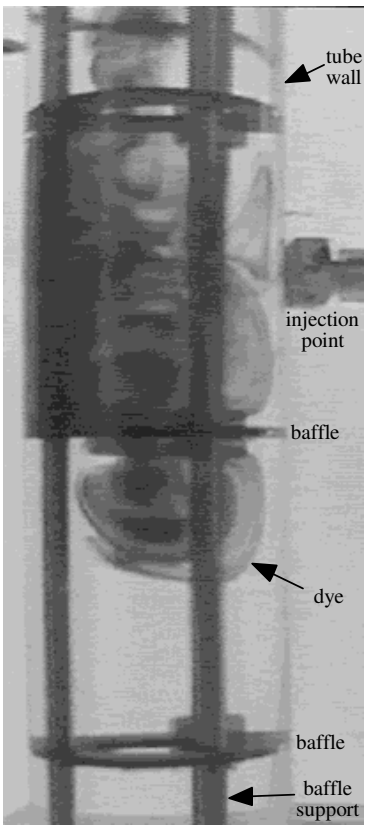

(a) after 20 seconds ("onion-peel effect")

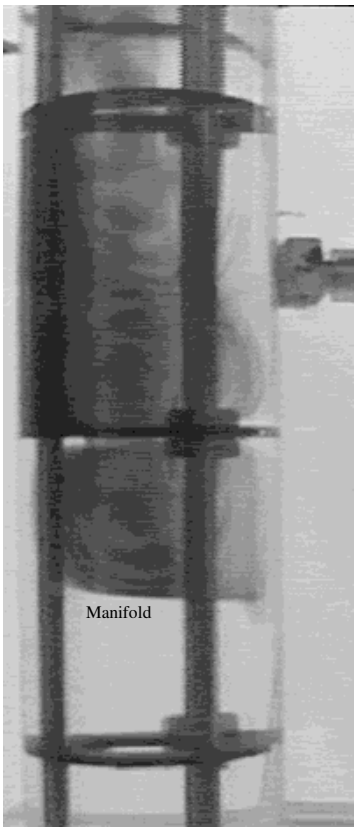

(b) after 40 seconds (manifold develops)

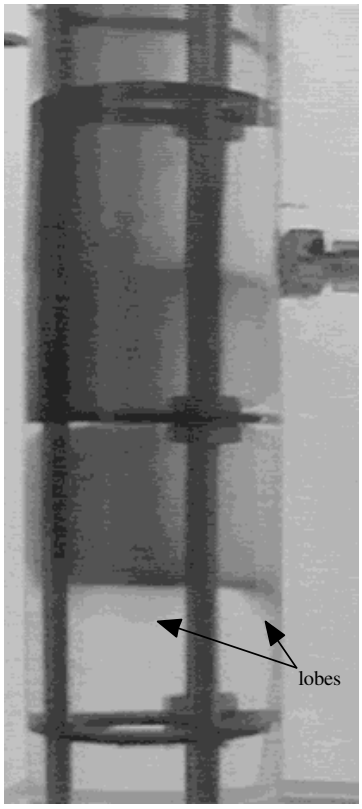

(c) after 90 seconds (lobes forming at tube wall)

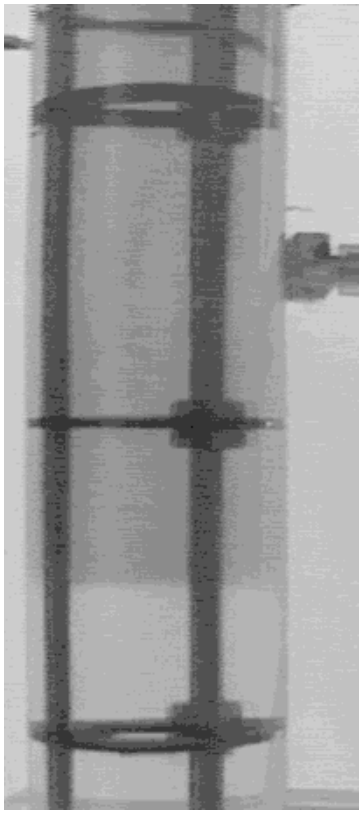

(d) after 1800 seconds (manifold still distinct)

Figure 7.4 (a) – (d): Injection of Methylene Blue Dye into a Baffle Tube Showing the Appearance of Manifolds
Re_n =0, Re_o = 45 & Str = 4 (24 mm apparatus, 0.3 Hz, 1 mm oscillation)

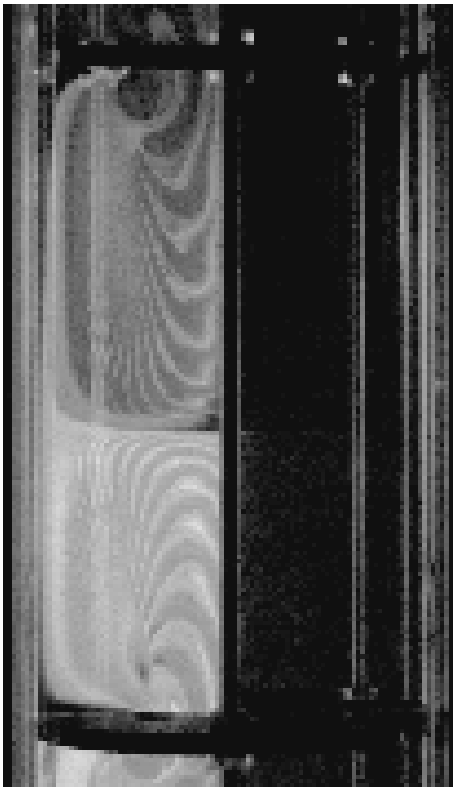

(a) Fluorescent Dye Streaklines

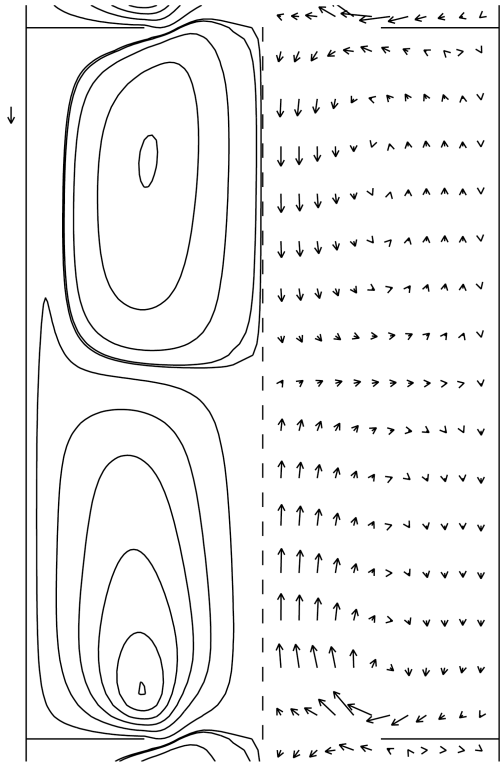

(b) Velocity Profile from Simulation

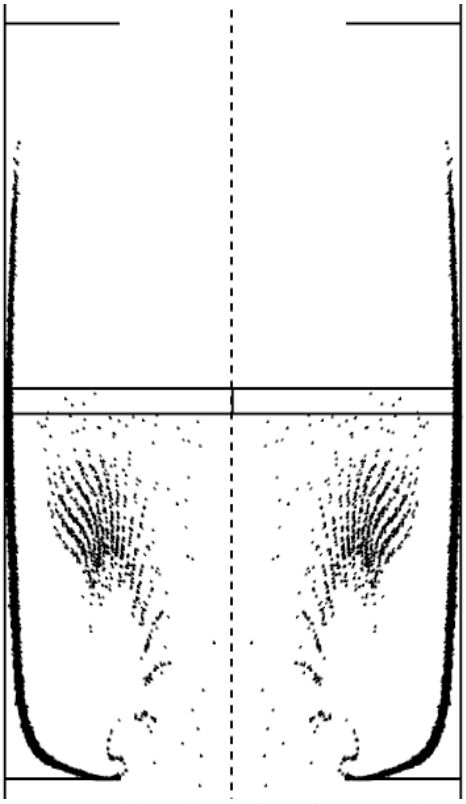

(c) Particles Simulation after 40 Cyles

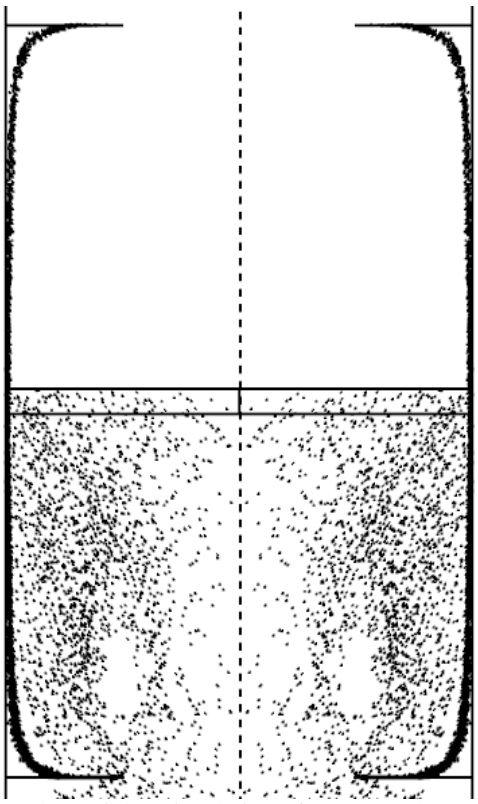

(d) Particles Simulation after 100 Cyles

Figure 7.5 (a) – (d): Manifolds in a Baffle Tube for $Re_n = 0$, $Re_o = 75$ & $Str = 4$
(54 mm apparatus, 0.1 Hz, 2.25 mm oscillation) Dye appears as white in (a)
The Initial Position of Particles is Shown by the Unfilled Rectangle Midway between Baffles

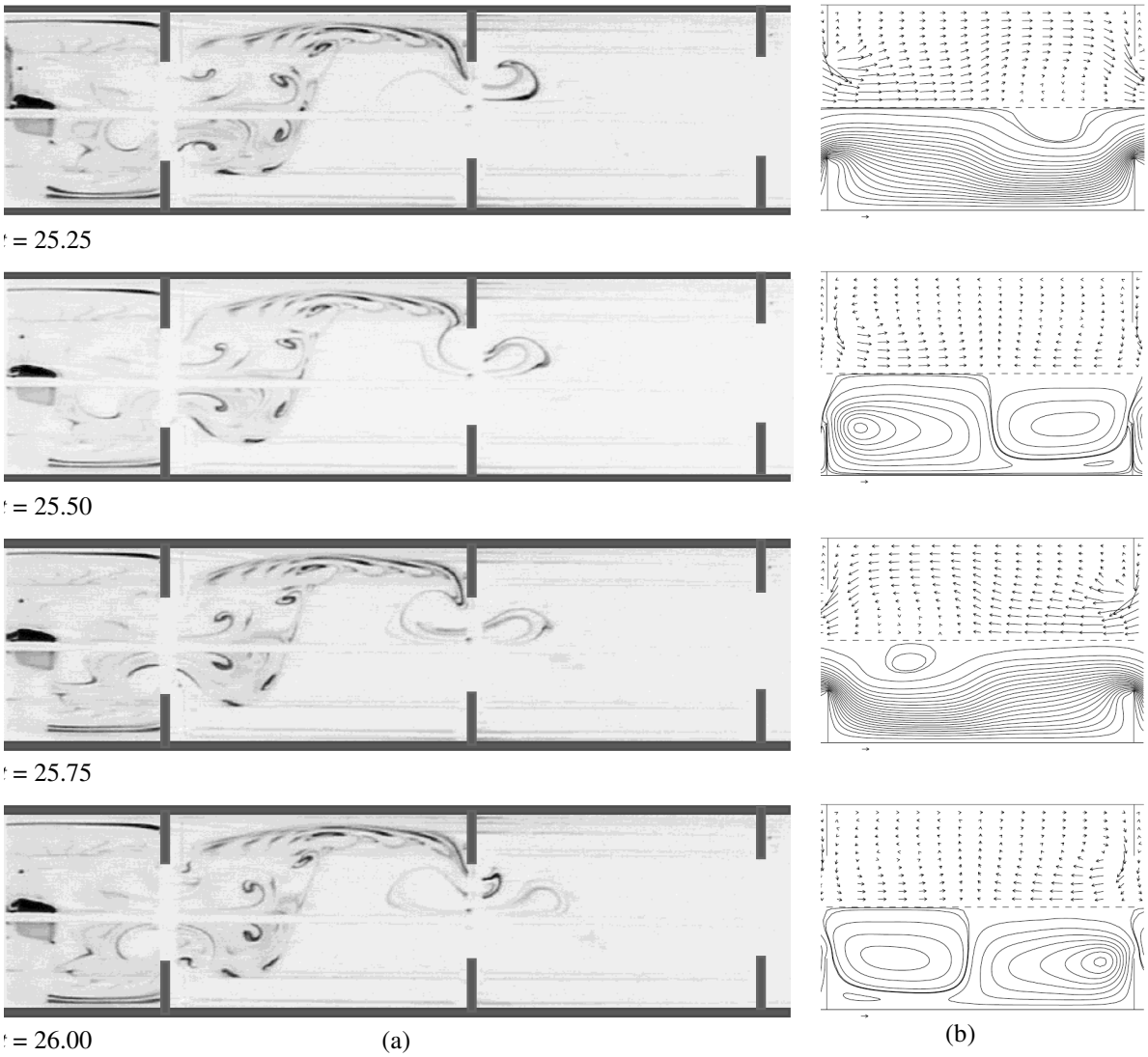

Figure 7.6 (a) & (b): Comparison between Experimental Flow Visualisation & F.M. Simulation
$Re_n = 0$, $Re_o = 75$ & $Str = 2$ at $t = 25.25$, 25.50, 25.75 & 26.00 cycles after dye injection
(54 mm apparatus, 0.1 Hz, 2.25 mm oscillation)

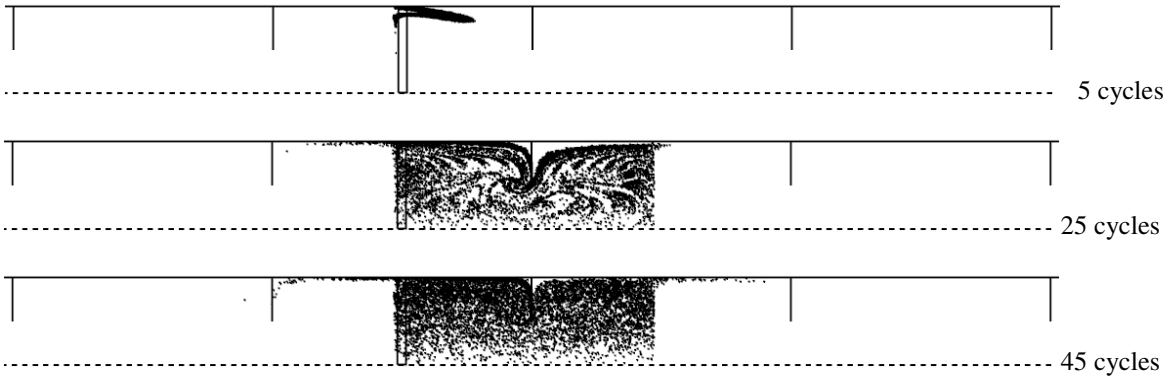

Figure 7.6 (c): Simulation of Inert Particle Tracer Advection for Oscillatory Flow Only
The Initial Position of Particles Midway between Two Baffles is Shown by an Unfilled Rectangle
$Re_n = 0$, $Re_o = 75$, $Str = 2$

t is a dimensionless time unit representing one full oscillatory cycle

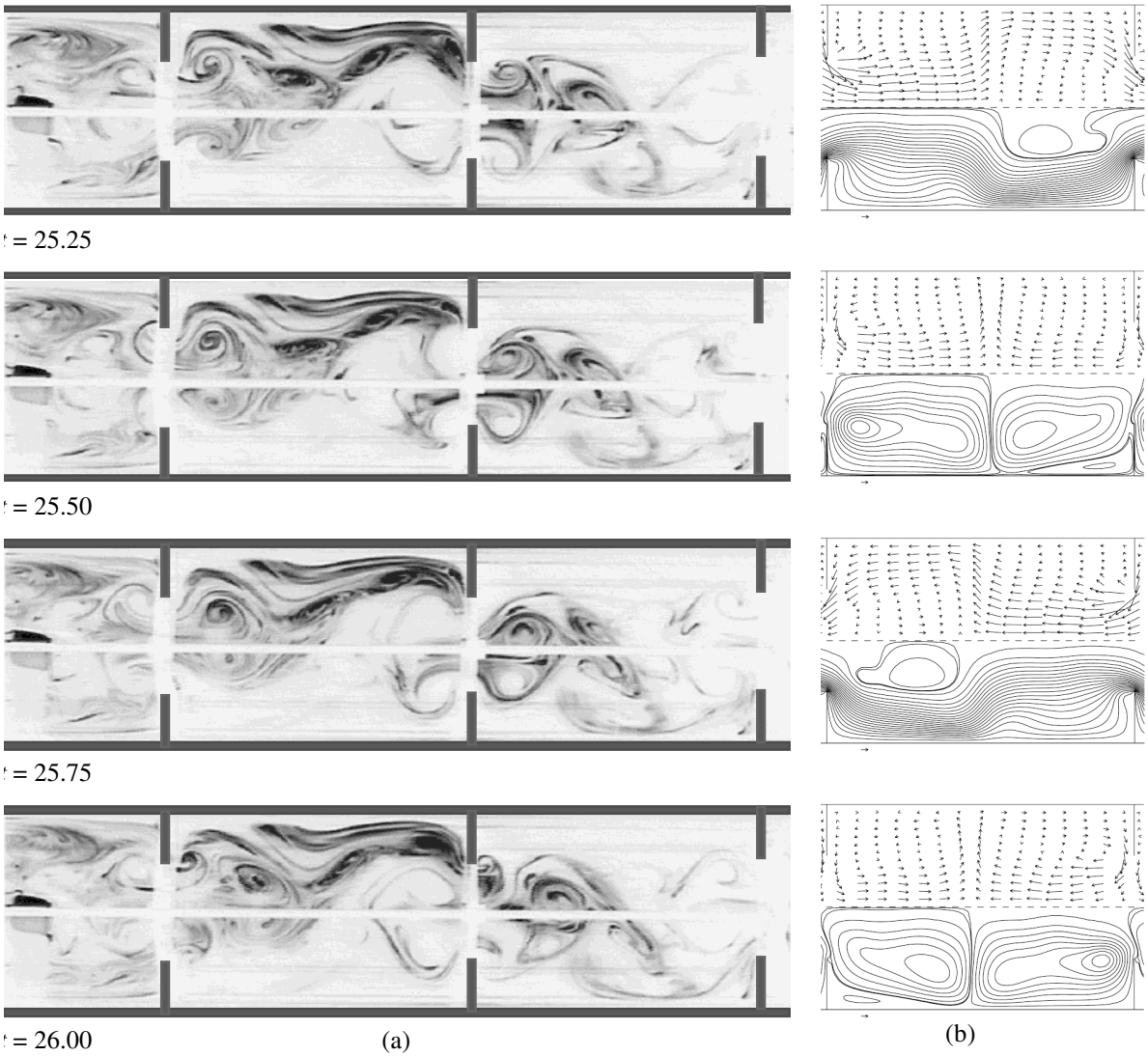

Figure 7.7 (a) & (b): Comparison between Experimental Flow Visualisation & F.M. Simulation
$Re_n = 0$, $Re_o = 150$ & $Str = 2$ at $t = 25.25$, 25.50, 25.75 & 26.00 cycles after dye injection
(54 mm apparatus, 0.2 Hz, 2.25 mm oscillation)

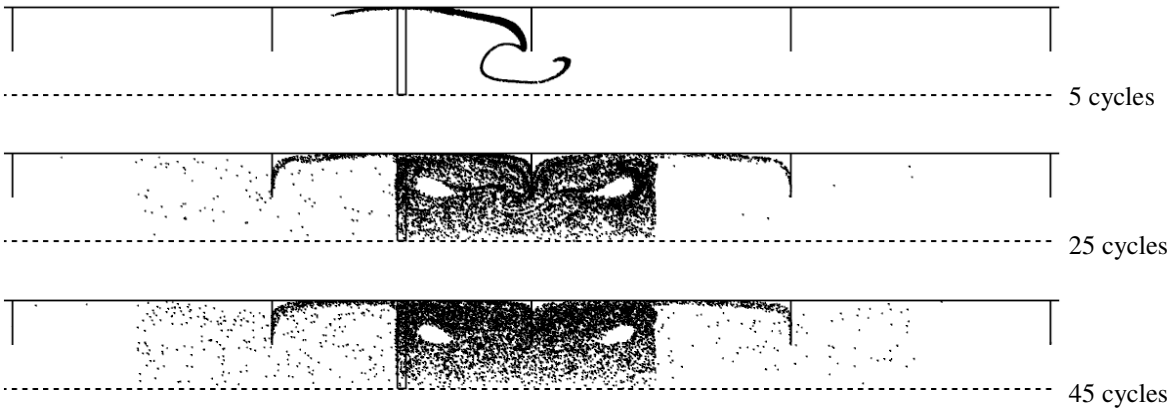

Figure 7.7 (c): Simulation of Inert Particle Tracer Injection for Oscillatory Flow Only
$Re_n = 0$, $Re_o = 150$, $Str = 2$

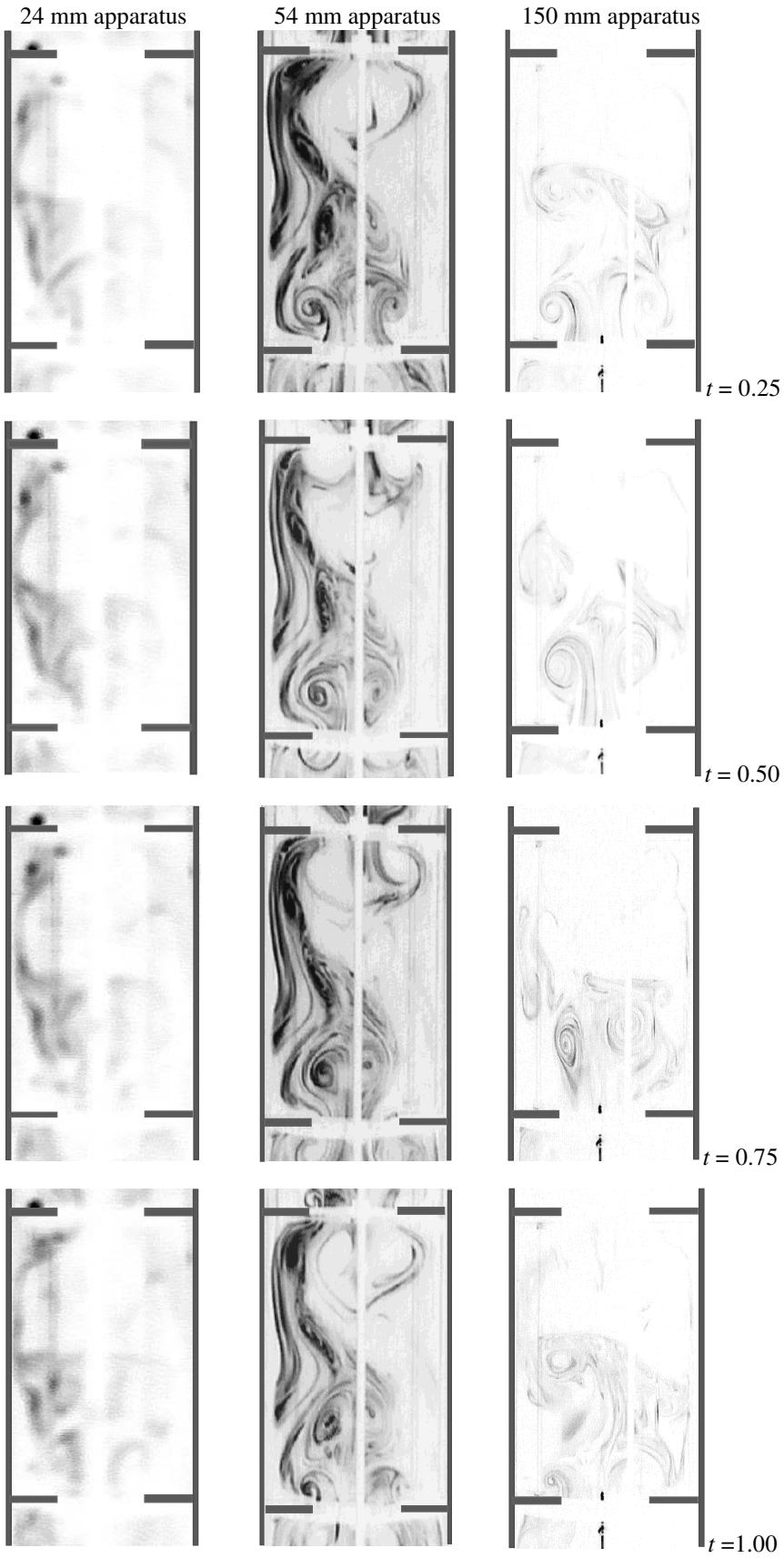

Figure 7.8: Comparison of Fluorescent Dye Streaklines as a Function of Tube Diameter
$Re_n = 0$, $Re_o = 150$, $Str = 2$

7.3 Flow Visualisation - Oscillation with Net Flow

Figure 7.9 shows a net flow corresponding to Re_n = 107 superimposed upon the oscillatory flow conditions depicted in figure 7.8. A direct comparison can be made between the fluorescent streaklines for the 24 mm, 54 mm and 150 mm sets of apparatus at four separate times during a single oscillatory cycle: although the flow is becoming quite complex, with large amounts of stretching and folding of the streaklines, the observed flow patterns are quite similar for each tube diameter. From this and from examination of flow visualisations for a range of other values of Re_o and Str it was possible to surmise that the fluid mechanics are not a function of tube diameter for the range studied.

Figure 7.10 shows observed streaklines for the same net flow and frequency of oscillation but with varying amplitude of oscillation in the 54 mm apparatus. At low amplitude of oscillation (Figure 7.10(a), Str = 4) the oscillations are insufficient for the vortices to disturb fluid behind the baffles, and a "coring" effect is seen where successive small vortices are formed but are swept down the centre of the baffled tube; three distinct sets of vortices can be discerned in each inter-baffle cell. At a higher amplitude of oscillation (Figure 7.10(b), Str = 1) the vortices are much stronger and almost completely sweep-out the region behind the baffle, reaching almost to the tube wall. When the amplitude of oscillation is increased still further (Figure 7.10(c), Str = 0.5) the fluid is ejected so fast through the baffle orifice that there is insufficient time for the formation of large single vortices, and the flow becomes chaotic.

An interesting feature of the superposition of a net flow is that it has the effect of enhancing the symmetry of the flow: whereas in the absence of a net flow asymmetry was seen to develop in oscillatory flow at oscillatory Reynolds numbers lower than 150 and whereas in the absence of oscillations asymmetry was seen to develop for net flows lower than 214, Figure 7.10 shows that for a combined Reynolds number ($Re_n + Re_o$) of over 400, the flow is axisymmetric.

Figure 7.10 (d) shows residual dye remaining behind the baffles once the bulk of the fluorescent dye has been washed through the tube. Although the baffles can provide excellent radial mixing which could contribute to near plug-flow residence time behaviour, they also act as traps for residual dye if the vortex-shedding is not strong enough to flush-out the volume of fluid behind the baffles, leaving a stagnant corner or "dead-zone". In the latter case, the baffles serve to increase rather than decrease the axial dispersion. The possibility of dead-zones is a potential problem for the method of optical sensors used to measure axial dispersion since the sensors are located centrally between the baffles and cannot detect such trapped dye. In this case it is clearly important to scrupulously check the material balance of the dye tracer used for axial dispersion experiments. Moreover, the small amounts of dye residing close to the tube wall are difficult to detect because they are spread thinly around the walls and therefore cannot

attenuate the light beam of the optical sensor to the same degree as if the same quantity of dye were evenly distributed throughout the tube volume.

Because the combination of both net flow and oscillations has a stabilising effect on the axisymmetry of the flow, it is therefore not surprising that the fluid mechanical simulation predictions are much closer to experimental observations where both Re_n and Re_o are present. Figure 7.11 shows simulated velocity profiles and streamlines for the experimental conditions of Figures 7.9 and 7.10; for $Re_o \leq 300$ the simulation maintains excellent agreement with the experimental observation, and even at $Re_o = 600$ the simulation correctly predicts the strong vortex nature of the flow.

Figure 7.12 shows the prediction of the same simulation for the movement of inert fluid marker particles. Again, there is excellent agreement between the particle simulation and the experimental streaklines shown in Figures 7.9 and 7.10 for $Re_o \leq 300$ and is reasonable for $Re_o = 600$ (i.e. the shape, size and location of vortices in the simulation are almost identical to the fluorescent dye streakline experimental results shown in the previous figures for identical dynamic conditions).

Also from Figure 7.12 it is noted that the simulation successfully predicts the onset of backmixing of tracer into the inter-baffle cells upstream of the injection point when the oscillations are increased above a critical value (in this case, $Re_o \geq 300$ & $Str \leq 1$). This corresponds to the measured "*% backmixing*" discussed in Chapter 5.

SUMMARY

The fluorescent dye streakline flow visualisation technique developed for O.F.M. has been shown to be an excellent tool for examining flow structures under a wide range of net flow, oscillatory conditions and tube diameters. Examination of experimental flow visualisations has shown that the fluid flow in O.F.M. is not substantially affected by tube diameter for the range studied. Moreover, comparison between experimental observations and the fluid mechanical simulation shows that the simulation can be validated up to approximately $Re_o = 300$ for O.F.M. if both net flow and oscillations are present. Because the simulation is constrained to be axisymmetric, in the absence of either a net flow or oscillations then the simulation may not adequately predict experimentally-observed asymmetry at Reynolds numbers of significantly less than 300. The effect of net flow and oscillations when combined appears to promote axisymmetry in the flow.

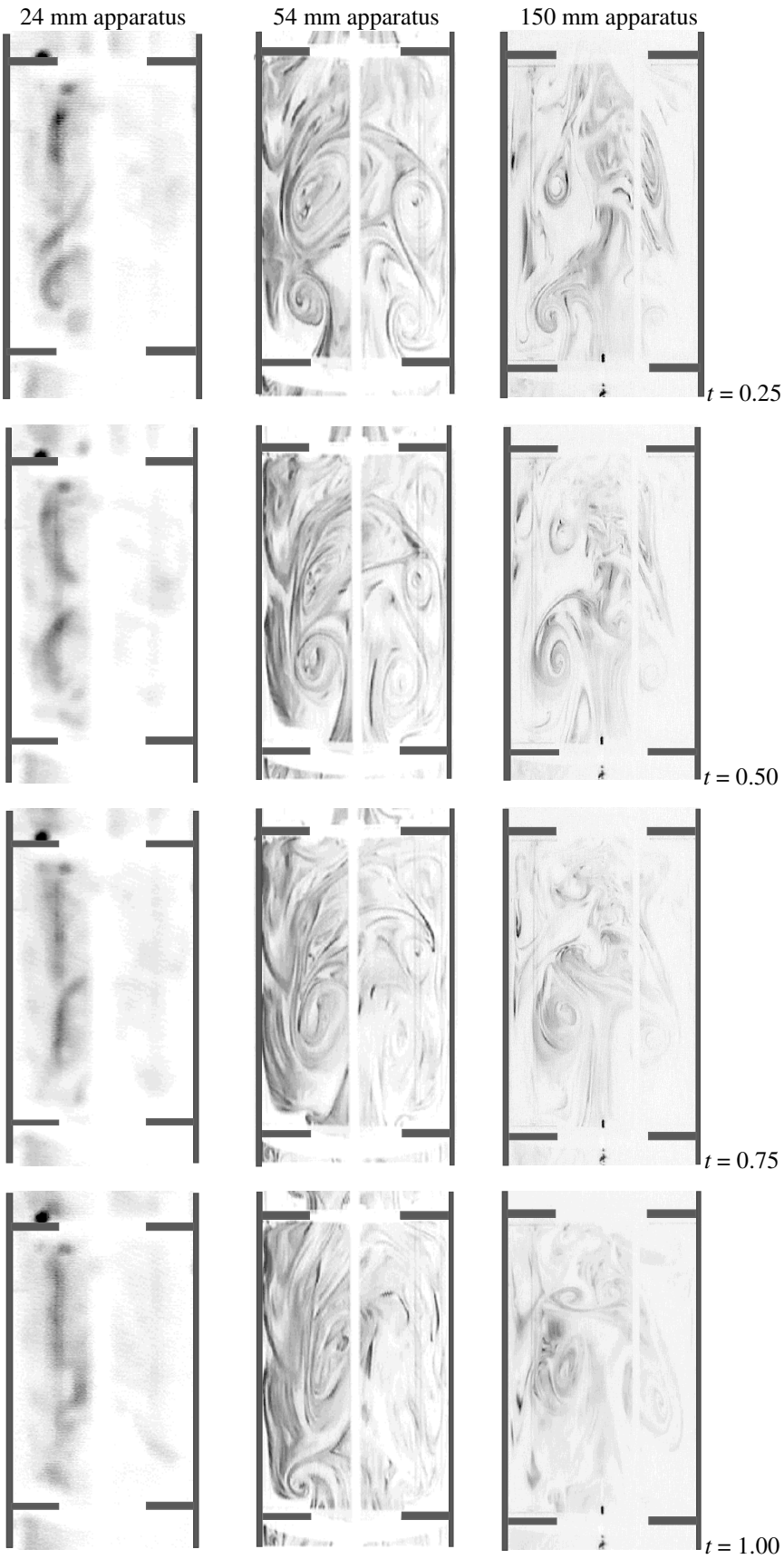

Figure 7.9: Experimental Streaklines in O.F.M. as a Function of Tube Diameter
$Re_n = 107$, $Re_o = 150$, $Str = 2$

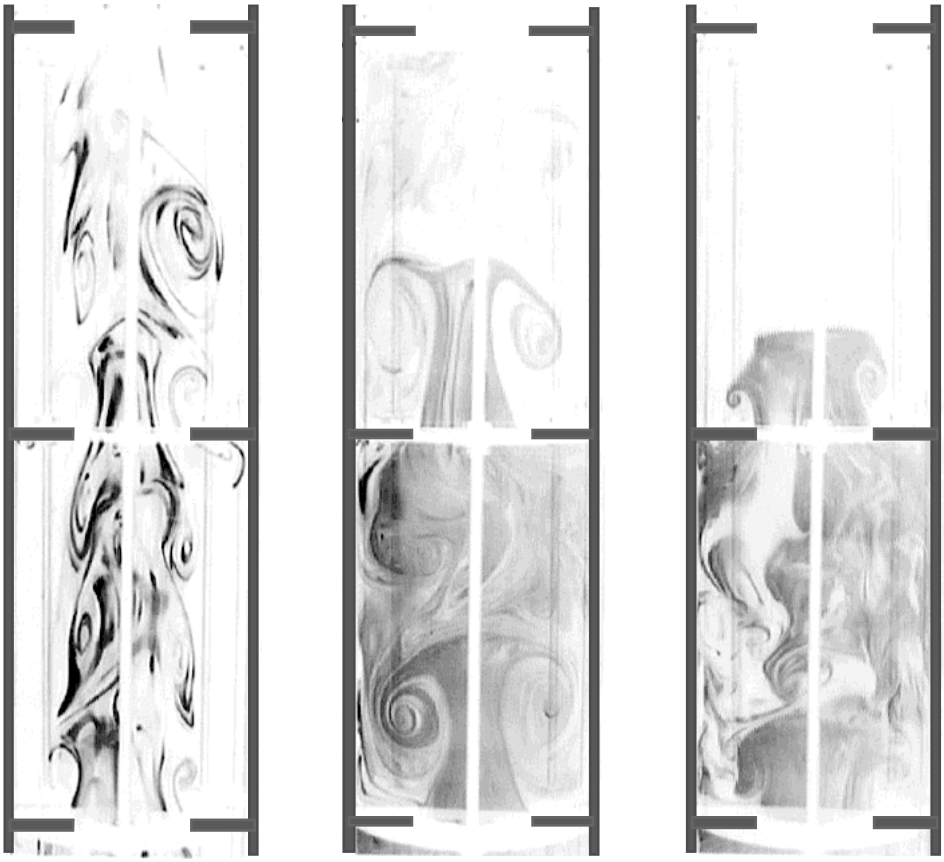

(a) Re_n =107, Re_o =75, Str =4 (b) Re_n =107, Re_o =300, Str =1 (c) Re_n =107, Re_o =600, Str =0.5

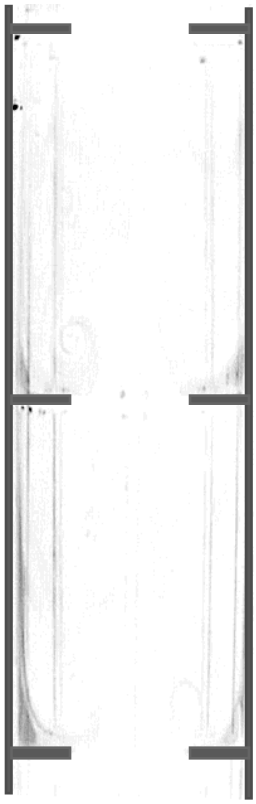

(d) Re_n =107, Re_o =150, Str =2 After 10 minutes Showing Dye Trapped in Stagnant Corners behind Baffles

Figure 7.10 (a) – (d): Fluorescent Streaklines for Various Conditions in the 54mm Apparatus with Re_n =107
Each Diagram Showing 2 Inter-Baffle Cells

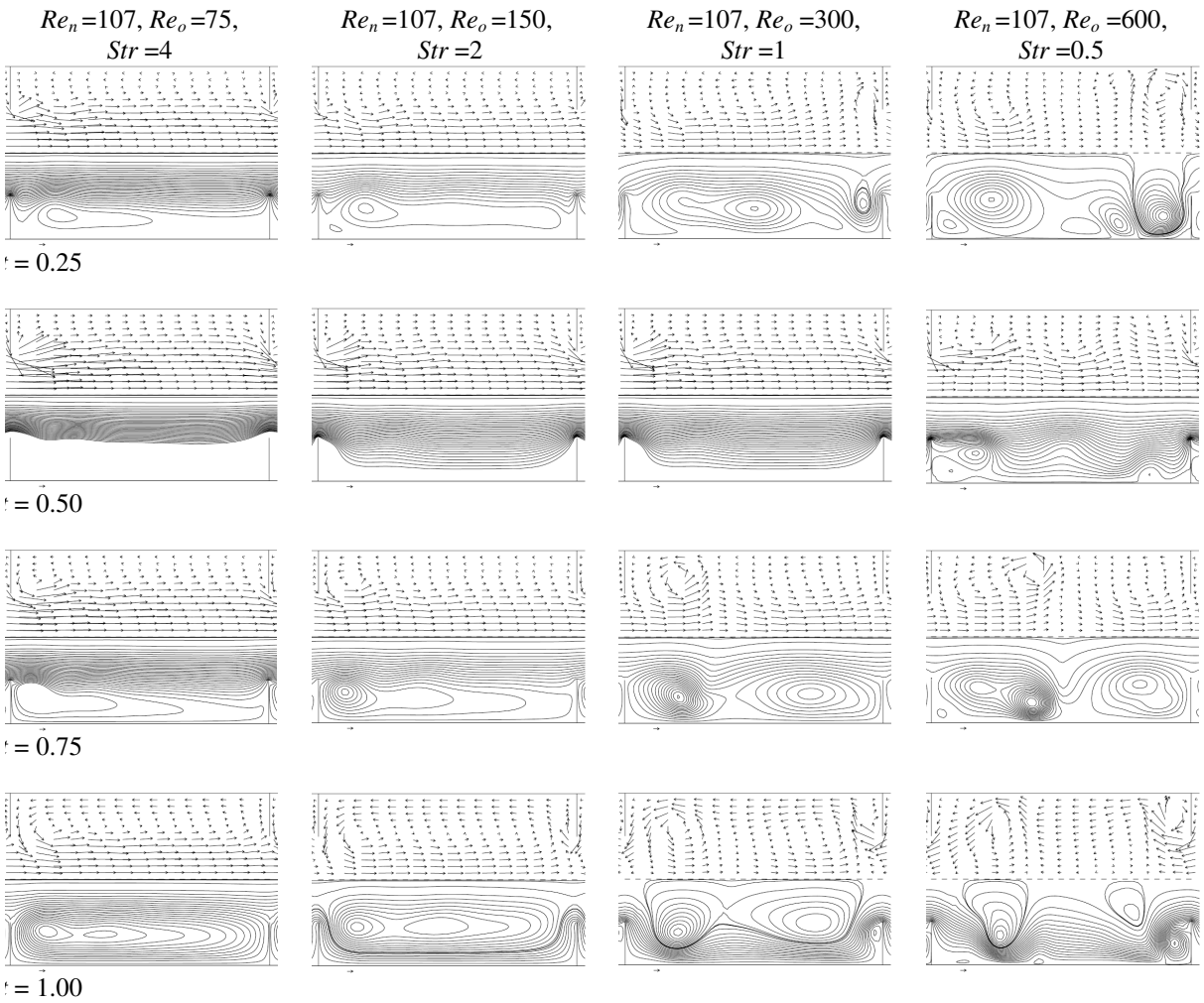

Figure 7.11: Velocity Profiles Predicted by Simulation for Fixed Frequency and Varying Strouhal Number The Flow Conditions Correspond to Those shown in the Previous Two Figures

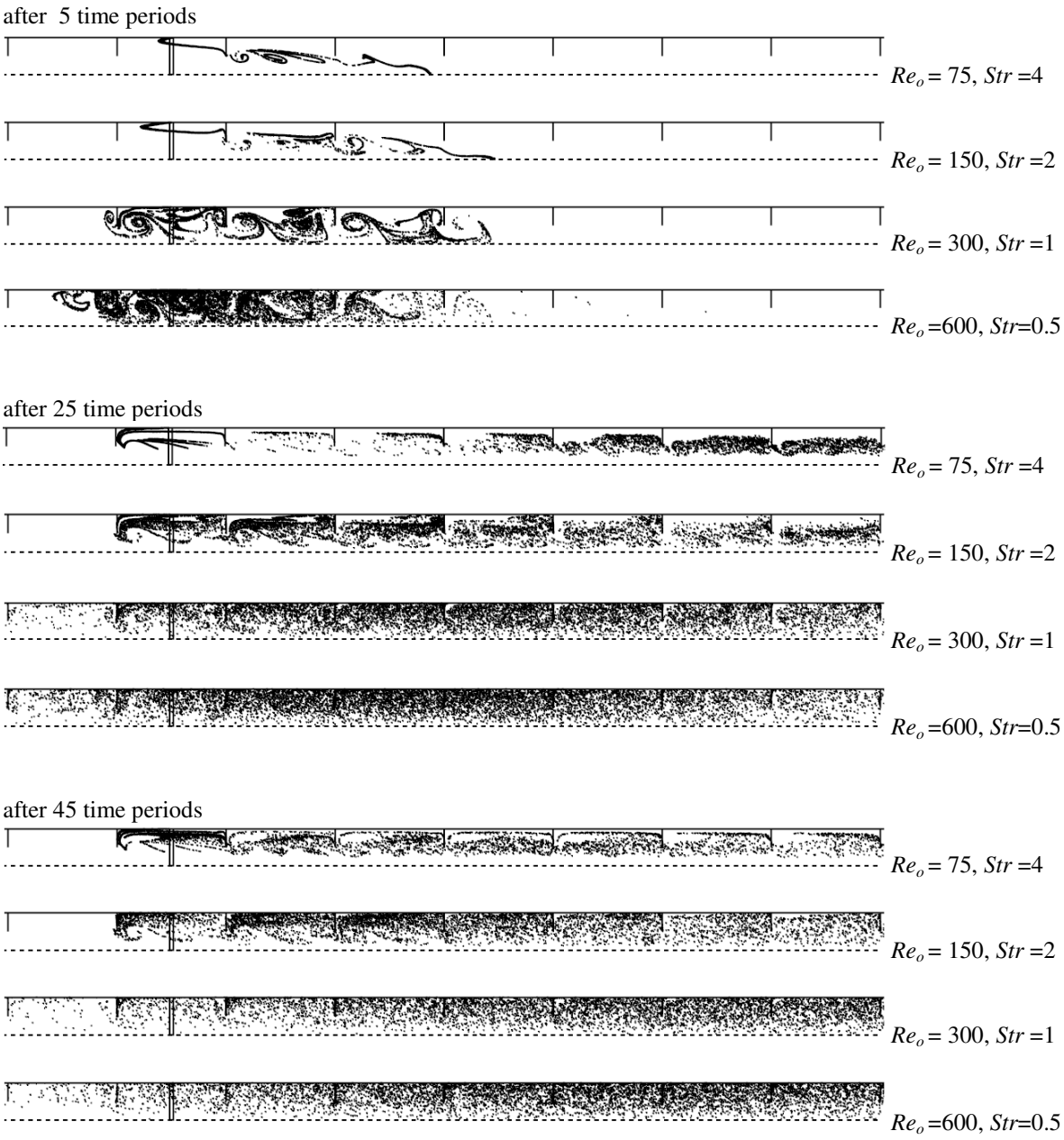

Figure 7.12: Simulation of Inert Particle Tracer Injection for Net Flow (Re_n =107) and Oscillation

8. Multi-Orifice Baffles

The results of the preceding chapters provide strong evidence that for a given geometry of periodically-spaced single orifice baffles, the fluid mechanics and axial dispersion in O.F.M. are not a function of tube diameter for a given Re_n, Re_o and Str. This chapter reports an investigation into the fluid mechanics and axial dispersion of flow in a 150 mm diameter tube containing closely-spaced baffles with multiple orifices and demonstrates their potential usefulness to the scale-up of O.F.M..

The chapter is divided into five sections: §8.1 introduces the rationale behind the design of the multi-orifice baffles; §8.2 outlines the programme of experiments undertaken; §8.3 presents the results of experimental axial dispersion measurements made in the multi-orifice design; §8.4 uses flow visualisations to describe the various flow regimes observed using the multi-orifice baffles, and §8.5 reports on estimates made of the magnitude of radial dispersion when O.F.M. is applied to the multi-orifice design.

8.1 Concept and Design

In setting out to design an industrial scale continuous O.F.M. process with a given residence time, a relatively short length of large-diameter baffled tube could in principle be substituted for a much longer smaller-diameter baffled tube in order to increase the net throughput. If the dynamic conditions were maintained (i.e. Re_n, Re_o and Str are constant) then the change of tube diameter would not affect the mean residence time (Figure 8.1).

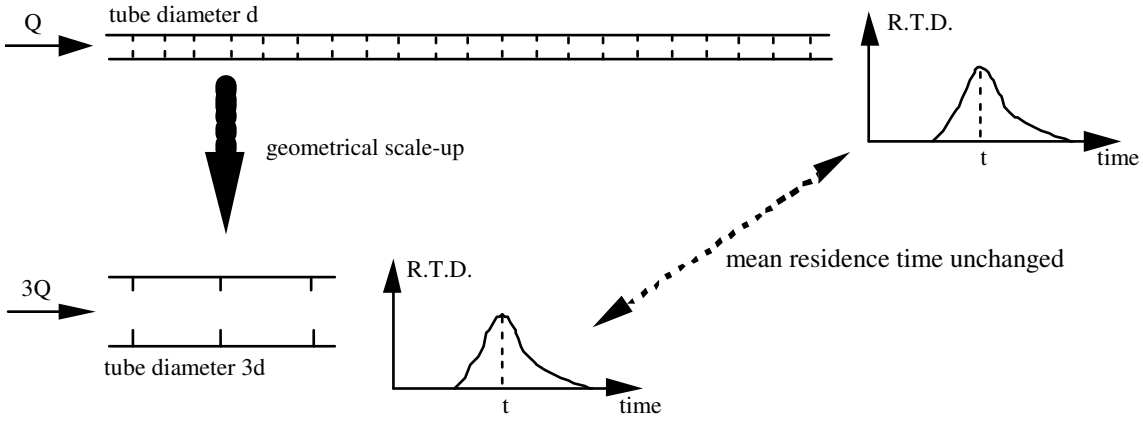

Figure 8.1: Example of Increasing Process Throughput by Increasing Baffled Tube Diameter

In the example given in Figure 8.1, in order to keep Re_n constant as the tube diameter increases by a factor of three the mean net flow velocity reduces inversely proportional to the increase in tube diameter, hence the required length of tube for a given mean residence time must also decrease inversely proportional to tube diameter. Since the

volume of the tube increases by *length* x $(diameter)^2$, the throughput of the process would increase by a factor of three. The absolute magnitude of the axial dispersion coefficient remains constant regardless of tube diameter, therefore if the axial dispersion has been measured for the smaller diameter tube then the residence time distribution for the larger diameter tube can be calculated from, for example, equation (2.17).

Increasing the diameter of the tube is therefore an effective method for scaling-up O.F.M. if residence time and residence time distribution are the only objectives. However, it is most likely that some degree of fluid agitation/mixing and or wall heat transfer will be required for an industrial process and it is then that simple geometrical scaling of O.F.M. becomes problematic. As previously discussed in Chapter 3, in order to maintain dynamic similarity of the flow conditions as the tube diameter increases the peak mean velocity of oscillation is required to decrease inversely-proportional to tube diameter. This means that the likely maximum shear-rates experienced by the fluid will decrease as the inverse-square of the increase in tube diameter (assuming that the typical shear rates will be related to a characteristic velocity divided by a characteristic length scale). This in turn implies that micro mixing of the fluid will become very poor as tube diameter is increased because the oscillations are very slow. Even for the relatively modest tube diameter of 150 mm the required period of oscillation can be of order minutes rather than seconds if the optimum conditions to minimise axial dispersion are sought, meaning very slow fluid mixing and extremely poor wall heat transfer. In the latter case, convective heat transfer would likely dominate any forced heat transfer and would probably change the fluid mechanics of the system. (If however neither rapid mixing nor wall heat transfer were necessary to the process then geometrical scaling could be very attractive since the pressure drops and hence oscillator power requirements would be minimal).

An alternative solution to geometrical scaling-up of O.F.M. was proposed by Ni (1994) who operated several 24 mm diameter tubes in parallel. This method has the advantages of predictable fluid mechanics and good heat-transfer capabilities, although a potentially vast number of individual tubes would be required for a large throughput process and there are potential issues of distributing feed and oscillations evenly to each tube.

An alternative approach to the scale-up of O.F.M. was adopted in this thesis: instead of having many small diameter tubes operating in parallel, the concept of a single large-diameter tube containing closely-spaced baffles each with many orifices was developed (see Figure 8.2). The design therefore mimics the effect of many smaller diameter tubes in parallel and appears similar to a reciprocating plate column (except that the fluid is oscillated and not the baffles). The predicted advantage of the multi-orifice baffles in the 150 mm diameter tube is that the same shear-rates and intensity of mixing can be achieved as in the 24 mm diameter tube while greatly increasing the throughput of the process. In order to achieve the same shear rates, residence time and residence time distribution then the length of the multi-orifice 150 mm diameter tube would be the same

as for the single orifice 24 mm diameter tube, but the net throughput would have increased by a factor of 39 (= 150^2 / 24^2).

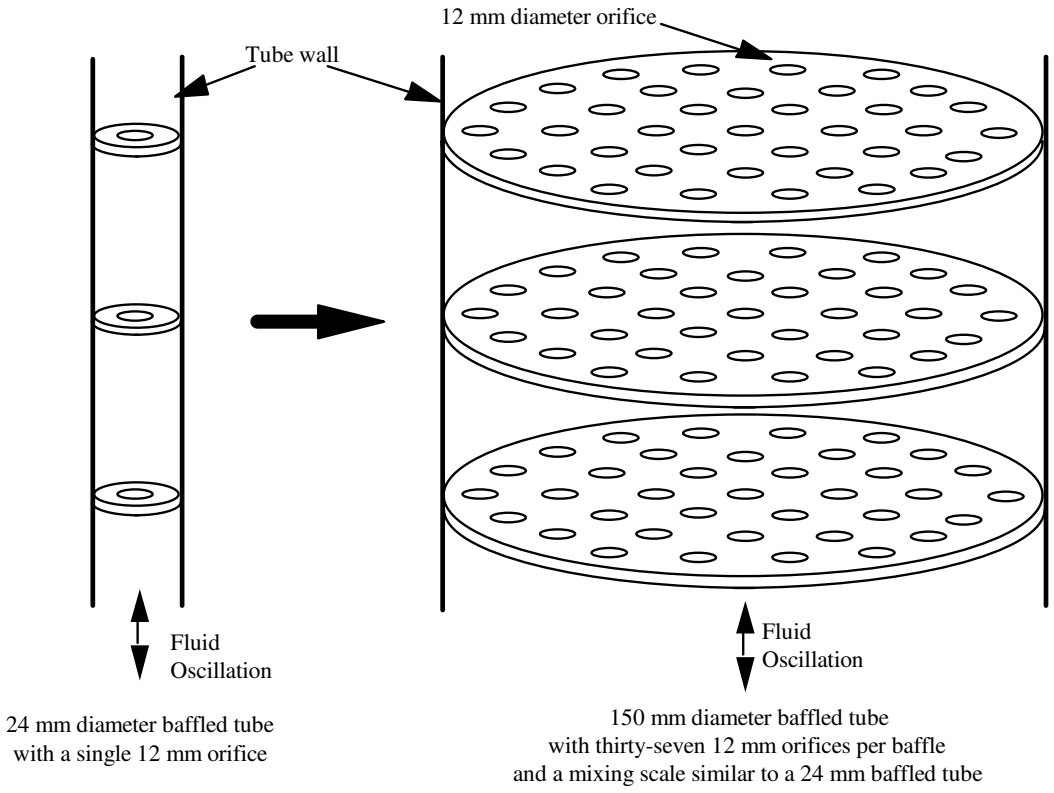

Figure 8.2: Using Multi-Orifice Baffles to Mimic Many Single-Orifice Baffled Tubes in Parallel

This proposal assumes that the fluid mechanics and axial dispersion in the multi-orifice system will behave in a similar manner to the single-orifice design: this cannot be taken for granted since there is no tube wall surrounding each individual baffled orifice and there is also scope for radial dispersion to become an issue. It was therefore proposed to investigate the properties of the flow by a programme of axial dispersion and flow visualisation experiments.

8.2 Experimental Programme

Using the multi-orifice design concept set out in the previous section (Figure 8.2) the 150 mm apparatus was adapted to take a 1m long baffle insert with multi-orifice baffles. Each baffle was constructed from 1 mm thick PVC sheeting using a lathe and drill press and designed to push-fit the existing 150 mm diameter perspex tube. The arrangement of orifices was essentially a two-dimensional hexagonal close-packed array of 37 holes (1 in the middle, surrounded by rings of 6, 12 and 18 orifices respectively), with slight modifications close to the tube wall in order to maximise the distance between each individual orifice and its neighbours. The advantage of using such a layout was that

many of the orifices lay on a straight line, meaning that flow visualisation could easily be carried out on a cross-section through the centre of the tube.

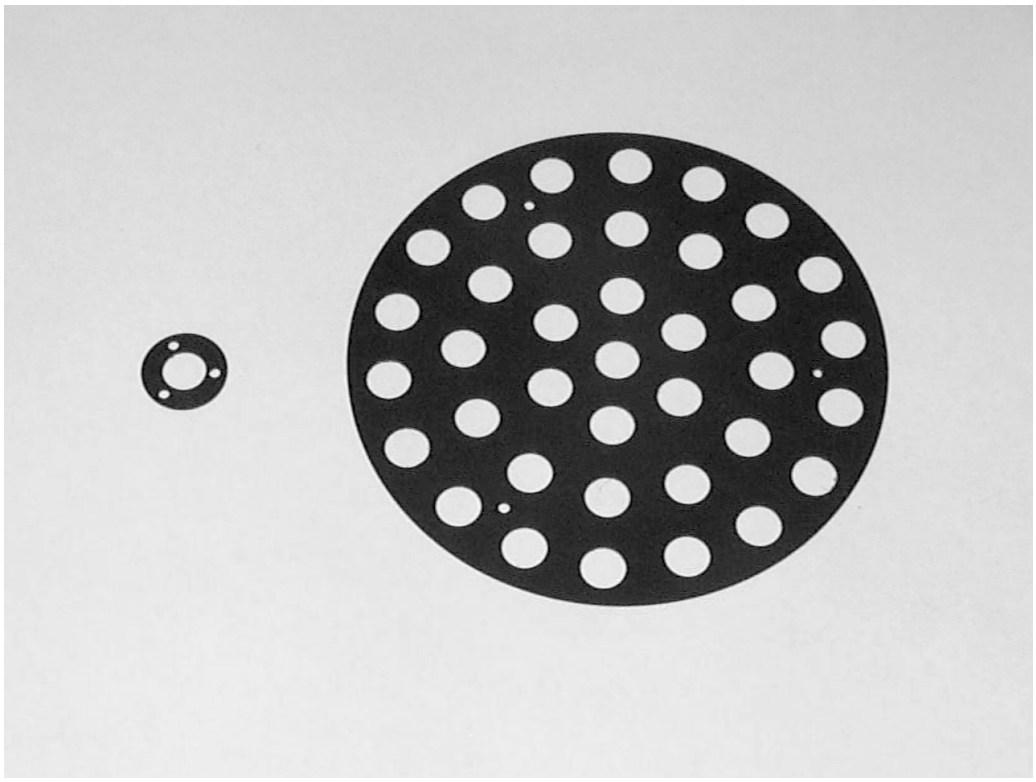

Figure 8.3: Comparison Between a Single-Orifice Baffle for the 24 mm Apparatus and a Multi-Orifice Baffle (37 holes) for the 150 mm Apparatus. Both Have a Thickness of 1 mm.

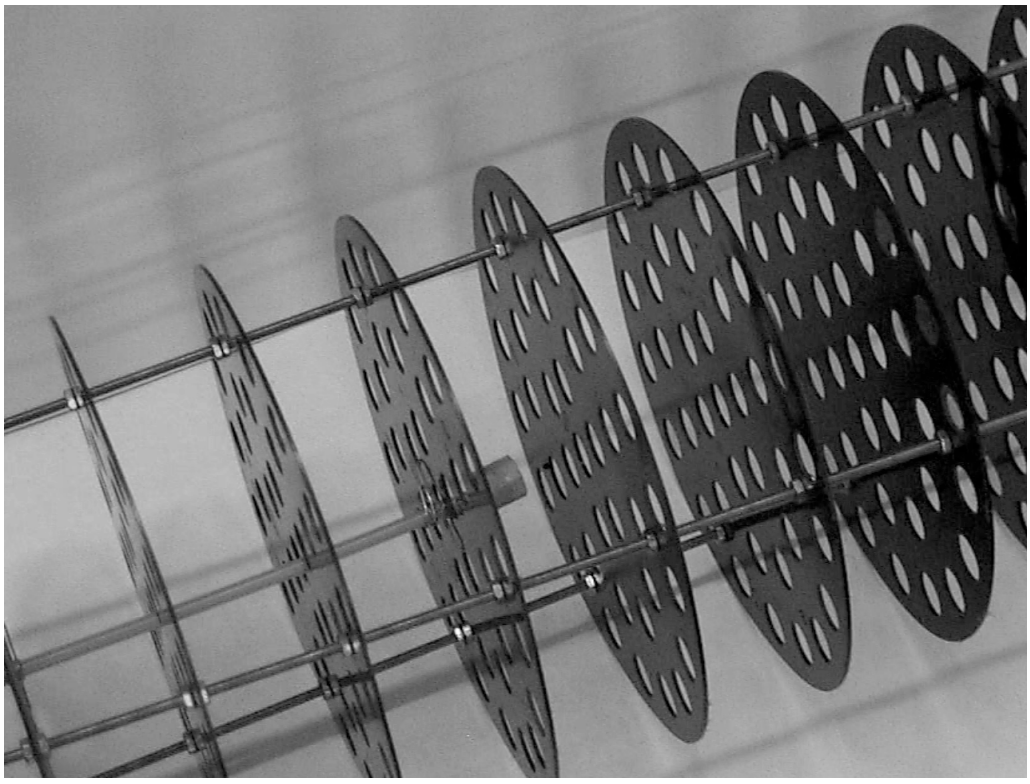

Figure 8.4: Multi-Orifice Baffle Insert for the 150 mm Apparatus (Including Dye Injection Tube)

The idea was to mimic the effect of having thirty-seven individual 24 mm diameter tubes in parallel. This arrangement was not perfectly achieved since the area ratio between the 24 mm and 150 mm diameter tubes was in fact thirty-nine, but the comparison was deemed sufficiently close for the purposes of the investigation. Each orifice therefore had a diameter of 12 mm (the same as the baffle orifice diameter in the 24 mm apparatus).

Figure 8.4 shows a section of the multi-orifice baffle insert: the baffles were supported on M3 A2 stainless steel studding. Separation of the baffles was identical to the single-orifice baffles in the 24 mm apparatus i.e. 36 mm. The choice of a dye injection method was somewhat difficult since there had to be a compromise between the objective of injecting dye at a specified point in the tube and disturbing the flow by the method of injection. It was decided to use a 3mm outside diameter flexible plastic tube to deliver dye to an inter-baffle cell between two of the central orifices and to use a cylinder of porous plastic as a diffusive nozzle. The porous plastic proved most successful in allowing the dye to be injected quite quickly into the tube while exiting evenly in all directions from the cylinder and with negligible momentum so that in the absence of any flow, the dye remained close to the cylinder (Figure 8.5). The presence of the cylinder appeared to affect the flow only in its immediate vicinity and its effect did not extend beyond one baffle spacing in each direction.

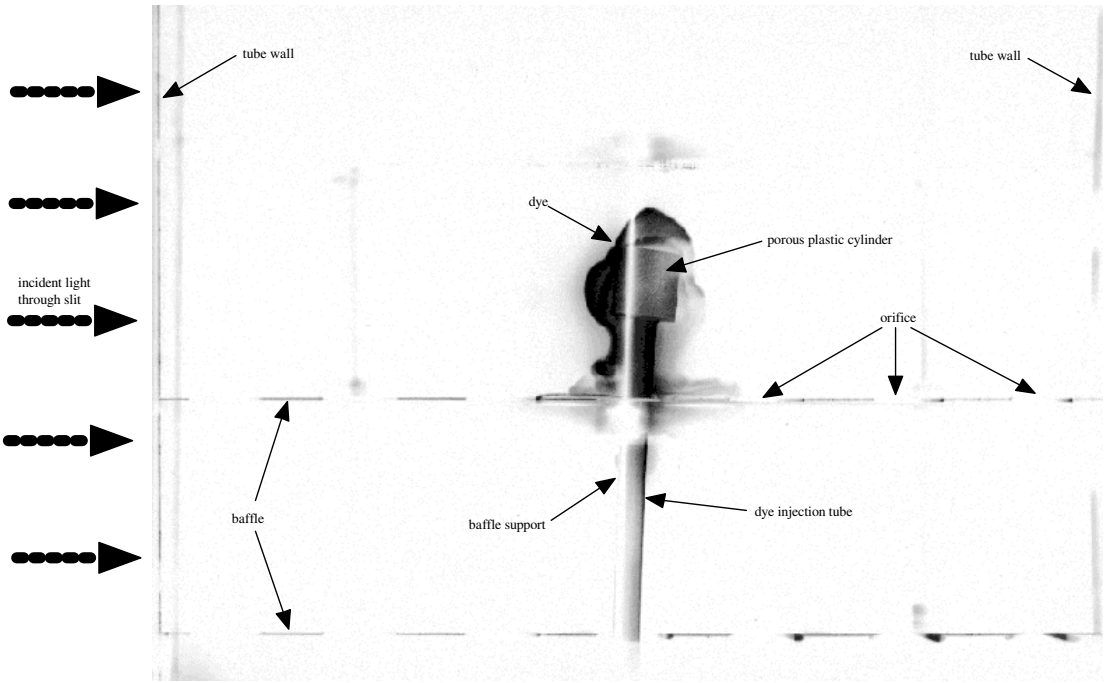

Figure 8.5: Dye Injection Method for the Multi-Orifice Baffles Using a Porous Plastic Cylinder - Dye is Ejected Evenly in All Directions and has Negligible Momentum in the Absence of Flow

An experimental programme was undertaken using the multi-orifice baffled tube. Axial dispersion measurements were made in the same manner as for the single-orifice baffled tubes, with the same optical sensor arrangement (three sensors downstream of the injection point and one upstream, each spaced two inter-baffle cells from one another or

from the dye injection point). Flow visualisation experiments were also performed using the same fluorescent dye streakline method as before, taking care to align the slit light source precisely down the centre-line of a row of orifices (to view a total of seven orifices across the diameter of the 150 mm tube).

8.3 Axial Dispersion Results and Analysis

The concentration-time profiles measured over a range of oscillatory conditions were typical of those obtained for single-orifice O.F.M. However it was found that the diffusion model did not provide a good model fit for downstream sensors 1 to 2 or 1 to 3, but did give a good model fit for sensors 2 to 3. This was thought to be an indication that at the position of sensor 1 (closest to the dye injection point) the dye had insufficient time to disperse radially across the diameter of the tube and was concentrated in the central region of the tube. By the time the dye had reached sensors 2 and 3, it was distributed sufficiently evenly radially across the tube for the axial diffusion model to be valid. In such cases the best-fit value of the axial dispersion coefficient obtained from sensors 2 and 3 was taken as the result and the data from sensor 1 was disregarded.

In calculating the values of Re_n, Re_o and Str it was clear that each term would need to be redefined to account for the change in geometry: the characteristic dimension d (formerly the tube diameter) was replaced by d_e (equivalent diameter) which was the diameter equivalent to the total baffle area divided by the number of orifices. i.e. $d_e = \sqrt{\frac{150^2}{37}} = 24.6$ mm which within experimental error is very close to an effective diameter of 24 mm. (Hence the baffle spacing of 36 mm i.e. one-and-a-half times the effective tube diameter).

Figures 8.6 and 8.7 show the results of axial dispersion measurements. It can be seen that the measured values of axial dispersion for the multi-orifice baffles are very similar to those obtained for the single-orifice baffles. The range of conditions which could be investigated were limited for low Re_o by the validity of the diffusion model in interpreting the results, and for high Re_o by the flexibility of the multi-orifice baffles: for high intensity oscillations the baffles (being only 1 mm thick plastic and full of holes) began to flex considerably, despite the stainless steel studding providing a solid anchor-point. (The upstream-end baffle to which the studding was anchored was constructed of 6 mm thick PVC sheeting for mechanical strength). The use of stainless steel baffles and or a central baffle support would have reduced this problem.

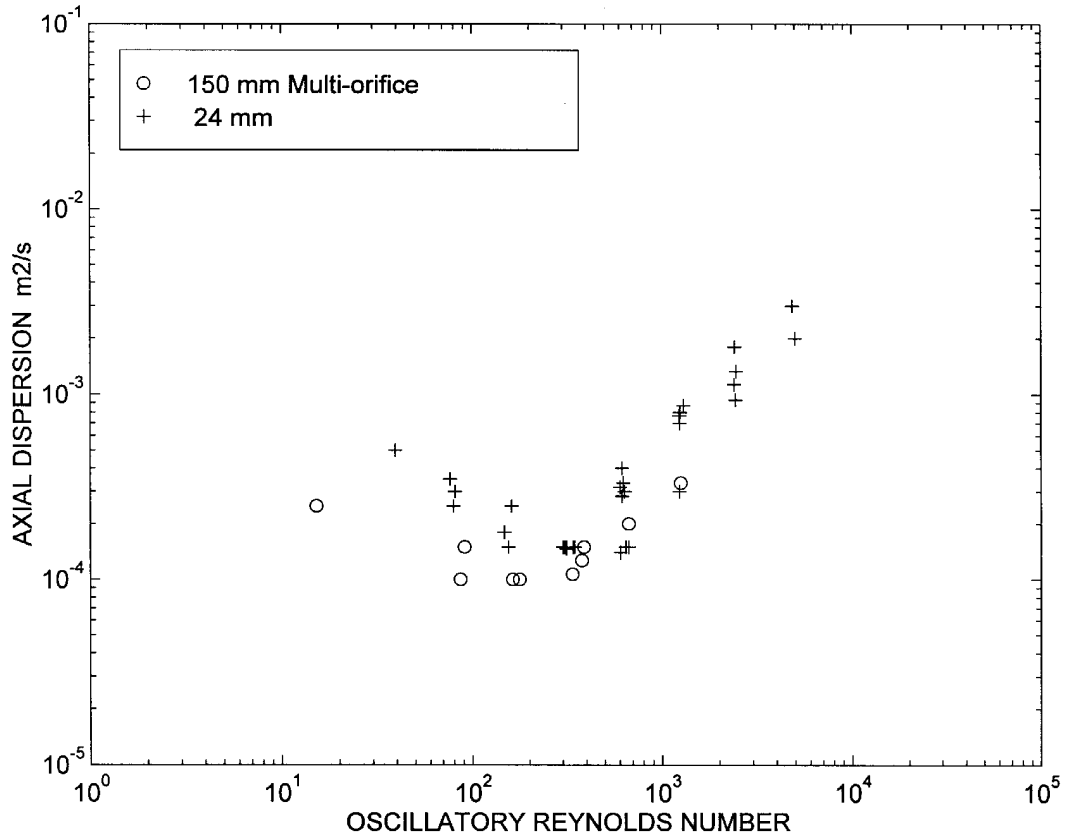

Figure 8.6: Axial Dispersion Measurements for Multi-Orifice Baffles in the 150 mm Apparatus Compared to Single-Orifice Baffles in the 24 mm Apparatus for Oscillations and Net Flow Re_n = 107
(Reynolds Numbers for the Multi-Orifice Baffles are Based upon an Equivalent Tube Diameter)

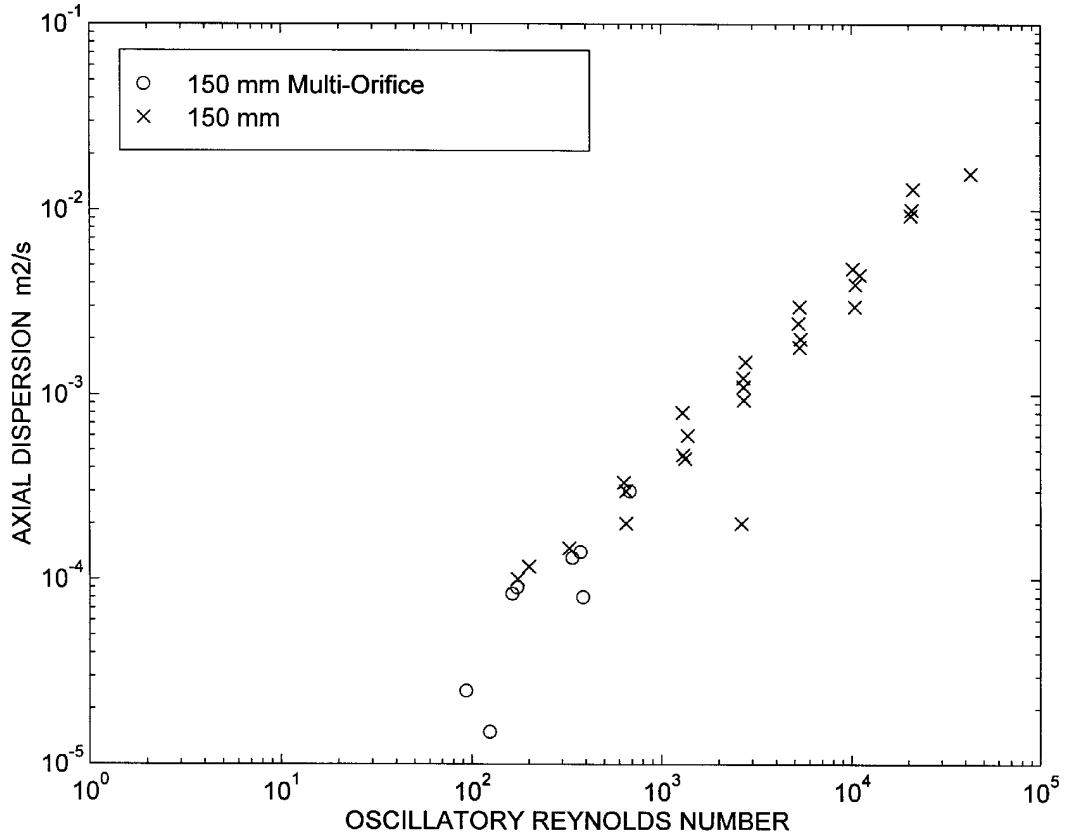

Figure 8.7: Axial Dispersion Measurements for Multi-Orifice Baffles in the 150 mm Apparatus Compared to Single-Orifice Baffles in the 150 mm Apparatus for Oscillatory Flow Only (No Net Flow)

For the net flow & oscillations results (Figure 8.6) it is noted that the multi-orifice baffles appear to give slightly lower values of axial dispersion for $Re_o < 200$. It is speculated that this could be due to the partial elimination of the stagnant corners behind the baffles which provided "dead-zones" of flow when single-orifice baffles were investigated; with the multi-orifice baffles there is no tube wall between orifices therefore the potential for "dead-zones" is greatly reduced. For $Re_o \geq 200$ the differences in measured axial dispersion are insignificant because the vortices are anyway of sufficient strength to eliminate stagnant corners in the case of single-orifice baffles.

The discovery that the use of multi-orifice baffles in place of single-orifice baffles does not substantially affect the measured axial dispersion is a key result of the thesis. It indicates that one can make laboratory-scale measurements of axial dispersion (for example in a 24 mm diameter baffled tube) and then use those results directly to predict with confidence the magnitude of axial dispersion which will occur in a very much larger diameter tube using multi-orifice baffles (of equivalent geometry to the 24 mm tube). This could prove to be a significant advantage compared to the difficulties of, say, predicting the dispersion properties of a scaled-up continuous stirred tank reactor.

8.4 Flow Visualisation

Flow visualisations using the fluorescent dye streakline technique described in §3.2.2 have been used both to understand the types of flow which can occur with multi-orifice baffles and also to make estimates of radial dispersion (see the next section §8.5). What is surprising from the flow visualisations is the extent to which the fluid mechanics of O.F.M. with the multi-orifice baffles is similar to fluid mechanics with the single-orifice baffles. A few interesting cases are presented here. (As before, the images are inverted so that the dye appears as grey or black).

Figure 8.8(a) shows a flow visualisation photograph of a net flow only experiment for Re_n = 55 shortly after dye injection (a net flowrate of 2.34 l/min). Laminar Poiseuille-type flow is observed with very little radial dispersion. Figure 8.8(b) shows the same experiment 10 minutes later by which time the dye has dispersed radially. Dye is trapped in recirculating regions between orifices in a manner similar to the recirculating regions behind baffles in a single-orifice apparatus, although the recirculating regions are more straight-sided than would be expected for single-orifice baffles. The mechanism of radial dispersion is not clear from the photograph but it appears that there is a very slow rotational flow around the circumference of each orifice.

(a) Shortly after Dye Injection (b) 10 minutes after Dye Injection

Figure 8.8: Net Flow Only in the 150 mm Multi-Orifice Apparatus, Re_n = 55 (Laminar)
(a) 1/8s at f2.8 1600ASA film (b) 1/2s at f2.8 1600ASA film

Figure 8.9 shows a net flow only experiment at Re_n = 107 (a flowrate of 4.68 l/min) approximately 15 seconds after dye injection. The flow has become asymmetric and disperses rapidly radially via chaotic shedding of large vortices, so that the dye has just reached the walls of the tube three baffle spacings downstream of the injection point. This implies a maximum radial velocity of approximately 4.4 mm/s, of comparable magnitude to the mean net flow axial velocity which is also 4.4 mm/s. Two deductions can be made from this observation: firstly, flow through the multi-orifice baffles becomes asymmetric at a lower Reynolds number than with the single-orifice baffles; secondly, the baffles produce a relatively homogeneous mixing in which the radial dispersion is of similar magnitude to the axial dispersion.

It is perhaps to be expected that the flow becomes "asymmetric" at a lower Re_n than for single-orifice baffles since there is a reduced ratio of wall perimeter to orifice perimeter. It appears that symmetry is lost for approximately $Re_n > 100$ rather than for $Re_n > 200$ in the case of single-orifice baffles. The observation of radial dispersion suggests a crude method for estimating the magnitude of radial dispersion: since the axial dispersion can easily be measured using the imperfect pulse technique, the relative magnitude of radial dispersion can then be estimated by visual inspection of flow visualisation photographs.

Figure 8.9: Net Flow Only in the 150 mm Multi-Orifice Apparatus, Re_n = 107 (Chaotic)
15 seconds after Dye Injection 1/30s at f2.8 6400ASA film

Figure 8.10: Net Flow Only in the 150 mm Multi-Orifice Apparatus, $Re_n = 480$ (Chaotic/Turbulent)
5 seconds after Dye Injection 1/30s at f2.8 6400ASA film

Figure 8.10 shows the flow observed for a net flowrate of approximately $Re_n = 480$ (21.0 l/min) which appears similar to the mixing intensity observed at $Re_n = 848$ for single-orifice baffles. Under these conditions the dye disperses with apparently very rapid micromixing and axial dispersion is much more rapid than radial dispersion. It is concluded that for multi-orifice baffles the transitions between flow regimes occur at approximately half the net flow Reynolds number that they would in the case of single-orifice baffles. Further evidence to support this belief is given in Figure 8.11 which shows $Re_n = 27$ where the recirculating regions have a characteristic "vase" shape normally associated with $Re_n = 55$ in single-orifice baffled tubes.

Figure 8.11: Net Flow Only in the 150 mm Multi-Orifice Apparatus, $Re_n = 27$ (Laminar)
15 seconds after Dye Injection 1/30s at f2.8 6400ASA film

Figure 8.12 (next page) shows vortex-driven axial and radial mixing for oscillatory flow $Re_o = 75$ and $Str = 2$ superimposed upon a net flow $Re_n = 55$. Radial dispersion is crudely estimated to be half of that in the axial direction. In comparison figure 8.13 shows the same oscillatory conditions but with half the net flowrate ($Re_n = 27$) for which the radial dispersion is minimal compared to axial dispersion: 15 seconds after injection the dye is well mixed axially but poorly mixed radially.

Figure 8.12: O.F.M. in the 150 mm Multi-Orifice Apparatus Re_n = 55, Re_O = 75 and Str = 2 (0.5 Hz, 1 mm Oscillation) 1/30s at f2.8 6400ASA film

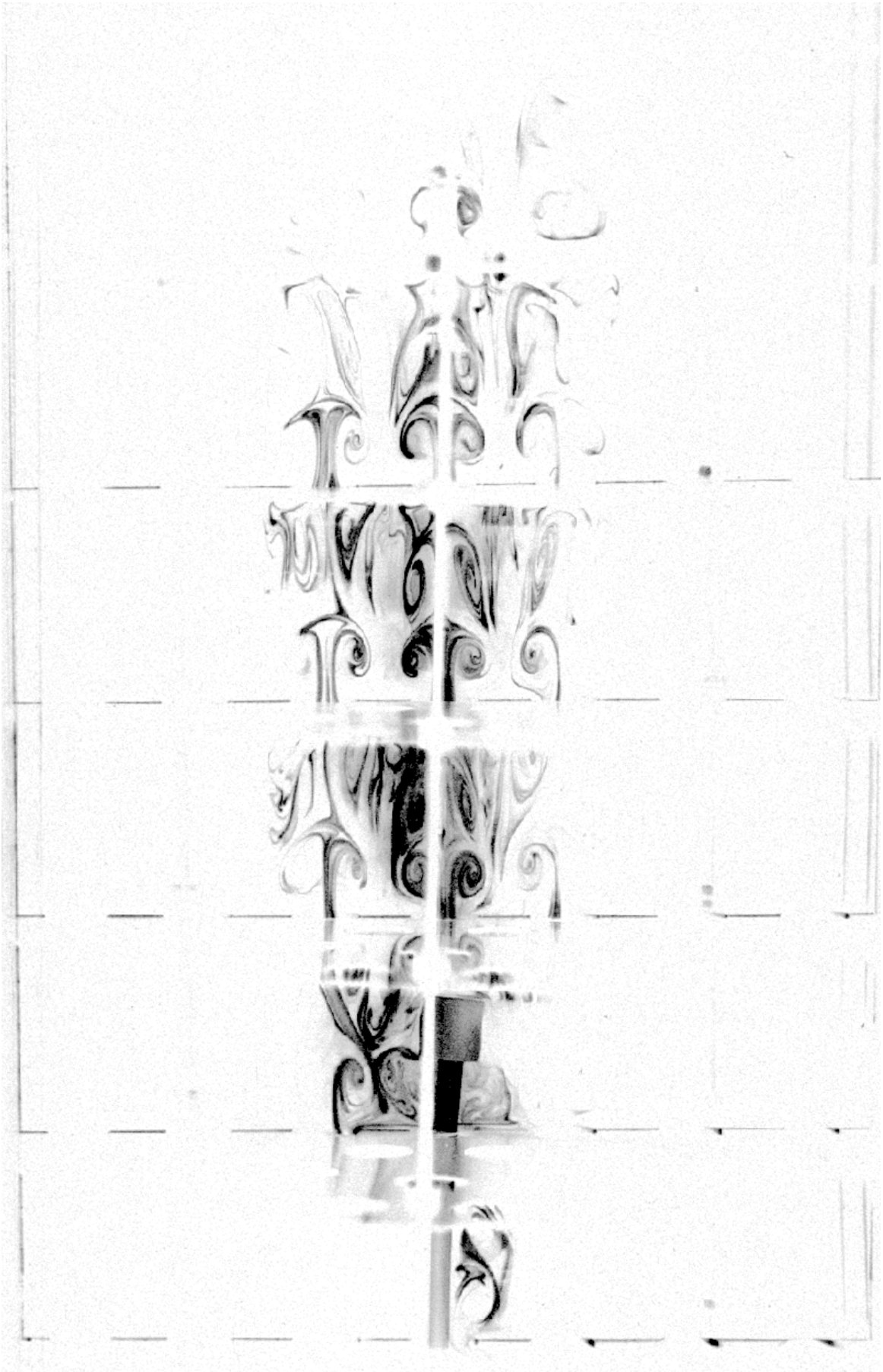

Figure 8.13: O.F.M. in the 150 mm Multi-Orifice Apparatus $Re_n = 27$, $Re_O = 75$ and $Str = 2$ (0.5 Hz, 1 mm Oscillation) 1/30s at f2.8 6400ASA film

In the absence of net flow (oscillation only) an extraordinary flow phenomenon was observed: Figure 8.14 shows the formation of manifolds under the same oscillatory conditions as were shown in Chapter 7 for the single-orifice baffles (Re_o = 75 and Str = 4). As well as the expected horizontal manifolds forming midway between opposing orifices, "vertical manifolds" have formed midway between adjacent inter-baffle cells. The manifolds therefore act as barriers to dispersion in both the axial and radial directions. Figure 8.15 shows a close-up of this unique flow-structure (only half the tube is shown). Interestingly, all of the features of the single-orifice baffle manifolds are retained, including a characteristic asymmetric curve in the horizontal manifold close to the "tube wall" or vertical manifold. It is not clear what dictates the orientation of this lip.

Increasing the oscillation slightly disrupts the manifold and Figure 8.16 shows typical chaotic vortex mixing for Re_o = 150 and Str = 2. Axial dispersion appears to be slightly greater than radial dispersion.

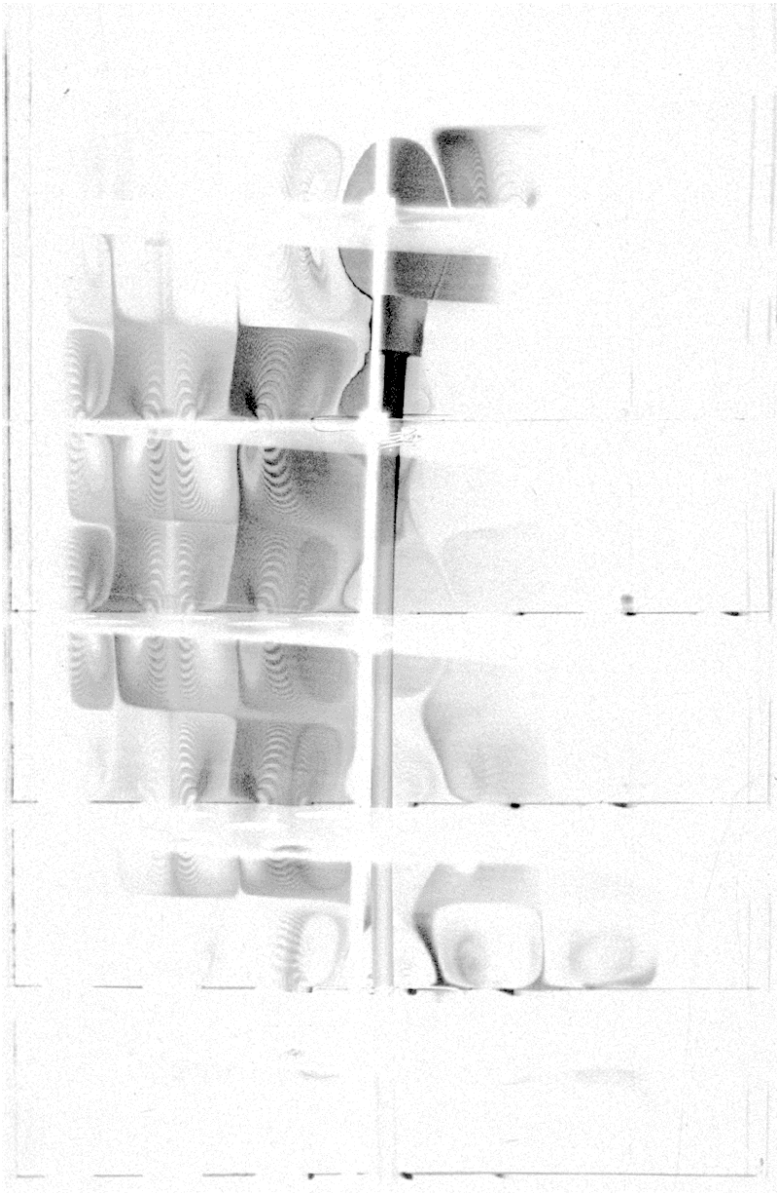

Figure 8.14: O.F.M. in the 150 mm Multi-Orifice Apparatus Re_o = 75 and Str = 4
5 minutes after injection (1 Hz, 0.5 mm Oscillation) 1/30s at f2.8 6400ASA film

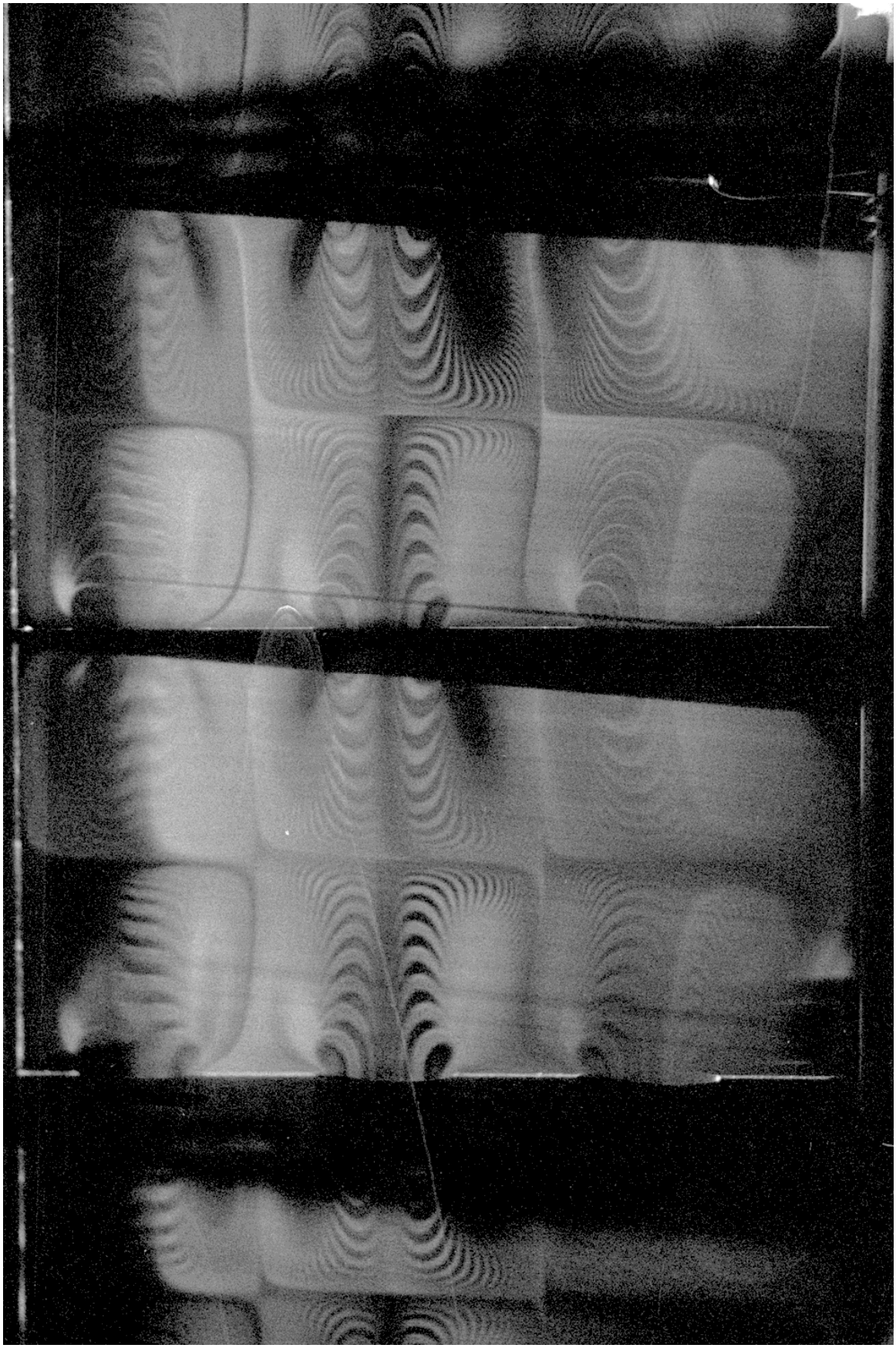

Figure 8.15: O.F.M. in the 150 mm Multi-Orifice Apparatus Re_O = 75 and Str = 4 (Half-Tube Shown)
10 minutes after injection (1 Hz, 0.5 mm Oscillation) 1/30s at f2.8 6400ASA film Non-Inverted Image

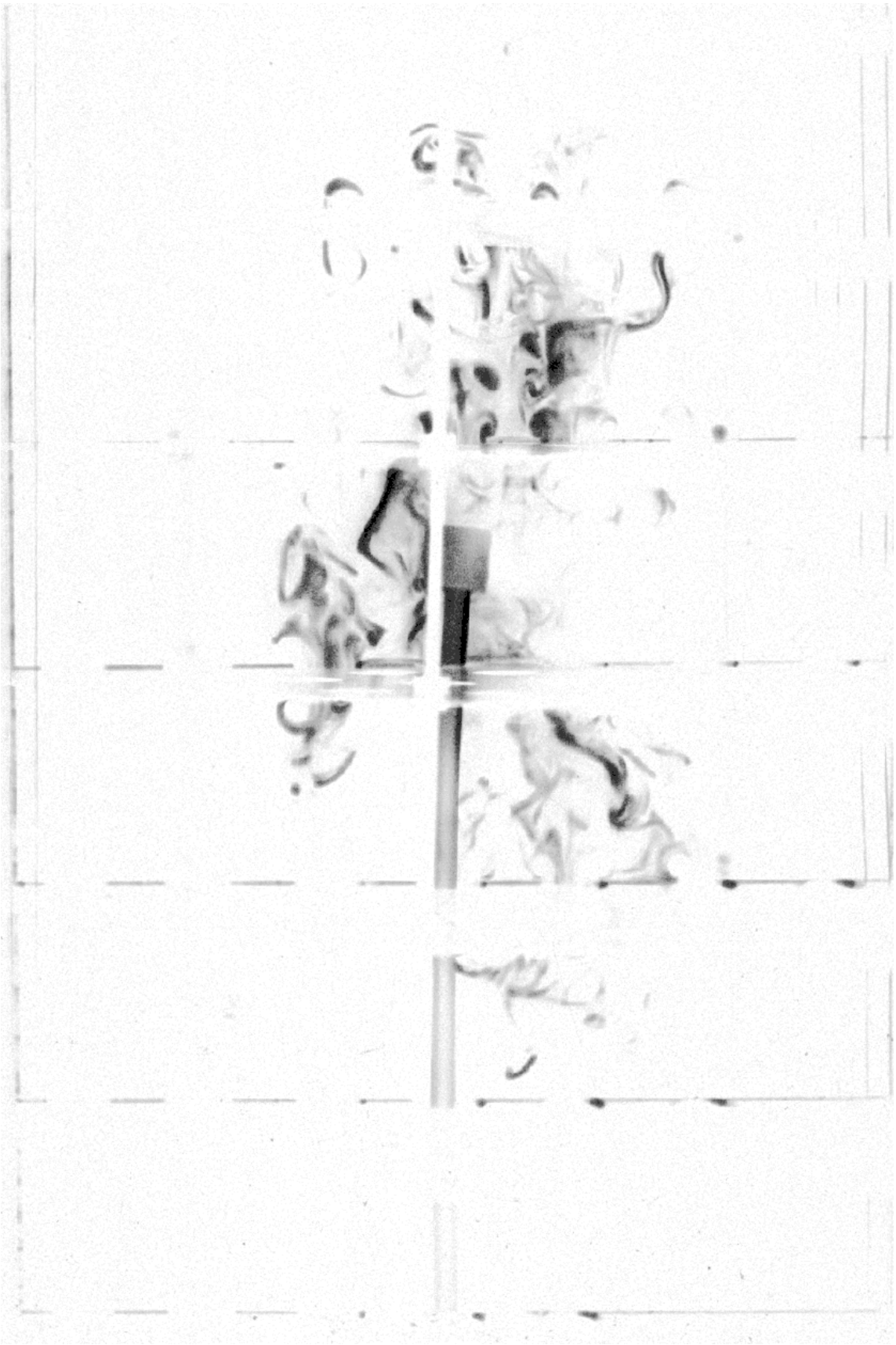

Figure 8.16: O.F.M. in the 150 mm Multi-Orifice Apparatus $Re_O = 150$ and $Str = 2$
12 seconds after injection (1 Hz, 0.5 mm Oscillation) 1/30s at f2.8 6400ASA film

8.5 Estimates of Radial Dispersion

Simple estimates of radial dispersion in the multi-orifice baffle system were made by inspection of the fluorescent dye streakline photographs from each experiment as outlined in the previous section. The relative rates of axial and radial spread of the dye tracer were noted and since the axial dispersion coefficient could be measured accurately (using the imperfect pulse technique), the radial dispersion could be estimated relative to the axial dispersion. This method is very crude and does not take into account the dilution effect as the dye disperses radially outwards, but is adequate for a first-order-of-magnitude assessment of radial dispersion.

For purely oscillatory flow (with no net flow) it was observed that in general the radial dispersion was a similar order of magnitude to the axial dispersion although radial dispersion was always slightly less than axial dispersion. For a typical axial dispersion coefficient of 1 x 10^{-4} m^2/s the radial dispersion was therefore estimated to be around 0.8 to 0.9 x 10^{-4} m^2/s. It is expected that axial dispersion is greater since the oscillations are directly forcing dispersion in the axial direction whereas radial dispersion is a result of indirect vortex formation.

For purely net flow (without oscillation) a range of flow behaviour was observed. For $Re_n < 100$ the flow is laminar without any vortex-shedding, hence radial dispersion is very low (less than 10% of the magnitude of axial dispersion). For $100 \leq Re_n \leq 400$ the flow is comprised of chaotic vortex-shedding and the radial dispersion is close in magnitude to the axial dispersion. For $Re_n > 400$ the flow is sufficiently rapid and turbulent that there is limited time for vortices to develop before they reach the next orifice: for a typical axial dispersion of 6 x 10^{-4} m^2/s at $Re_n = 480$ the radial dispersion is estimated to be around 4 x 10^{-4} m^2/s. Figure 8.17 shows schematically the effect of net flow on radial dispersion.

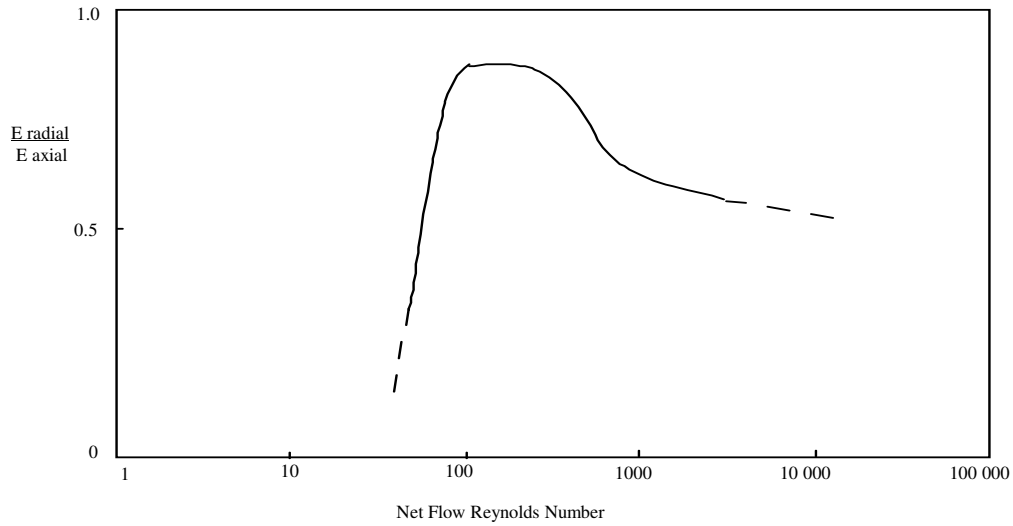

Figure 8.17: The Effect of Net Flow on the Ratio of Radial to Axial Dispersion (Schematic)

For net flow and oscillations together in the multi-orifice system, the flow can be categorised into two distinct regimes: firstly for $Re_n > 100$ and / or $Re_o > 100$ the flow is chaotic and the radial dispersion is of order 80% of the magnitude of the axial dispersion; secondly for $Re_n < 100$ and $Re_o < 100$ a range of radial dispersion is seen depending upon the precise relative values of Re_n, Re_o and Str. For this second regime radial dispersion is always less than axial dispersion and as a rule-of-thumb if Re_n and Re_o are of similar magnitude then increasing the Strouhal number decreases radial dispersion (because smaller amplitude oscillations are less effective at creating large vortices).

SUMMARY:

This chapter has presented a preliminary investigation into the use of multi-orifice baffles as a method of scaling-up O.F.M.. The multi-orifice design appears particularly attractive because of the potential ease of manufacture for large plant but also because of the similarity of the observed fluid mechanics and axial dispersion between single and multi-orifice baffle designs. This means that in principle laboratory scale experiments could be carried out and the results be used with reasonable confidence to predict axial dispersion (and mixing intensity) in a very much larger industrial scale multi-orifice baffle reactor.

9. Discussion

The work presented in this thesis has extended the range and understanding of axial dispersion measurements and fluid mechanics in O.F.M. and has addressed the issue of scale-up. This chapter aims to discuss the work in the wider context of the existing literature and of industrial application. A number of different areas will be addressed.

§9.1 discusses measured axial dispersion in O.F.M. and its relationship to the observed fluid mechanics. §9.2 compares flow visualisations and the measured values of axial dispersion with the results available in the literature. §9.3 examines the potential applicability of either single-orifice or multi-orifice baffles for industrial scale processes. §9.4 and §9.5 address the issues of heat transfer and energy dissipation in large-scale O.F.M.. §9.6 addresses possible engineering considerations for the construction of industrial scale O.F.M..

9.1 Relating Axial Dispersion Measurements to Flow Visualisations

Flow visualisations and axial dispersion measurements have been made across a wide range of conditions for oscillatory flow mixing in baffled tubes (Chapters 5, 6 and 7). Experimental and simulated results have been produced in both cases. The cases of net flow only, oscillations only, and net flow with oscillations have been investigated: the observed flow has ranged from creeping laminar flow to fully turbulent flow and measured axial dispersion has ranged from the order of 10^{-7} to 10^{-1} m^2/s. This section summarises those results and their interrelationship.

NET FLOW ONLY OR OSCILLATIONS ONLY

It appears from experimental flow visualisations that with either oscillations only (without a net flow) or net flow only (without oscillations) the flow is axisymmetric and laminar at low Reynolds number flows, but that at Reynolds numbers of order 80 and above the flow becomes asymmetric (Chapter 7) for the geometry investigated. With increasing Reynolds number the flow becomes increasingly chaotic (with the formation of large-scale vortices by the flow past the baffles) until for Reynolds numbers of approximately 800 and above the flow appears to be fully turbulent. The flow is assumed to be fully turbulent when individual vortices are no longer clearly visible in the flow and the fluorescent dye tracer disperses rapidly and homogeneously (i.e. discrete streaklines are not visible in the flow). These flow regimes for either net flow or oscillatory flow alone are summarised in Figure 9.1. The indicated values of axial dispersion are approximate and vary depending upon whether net flow or oscillation is involved and also the Strouhal number of the oscillation.

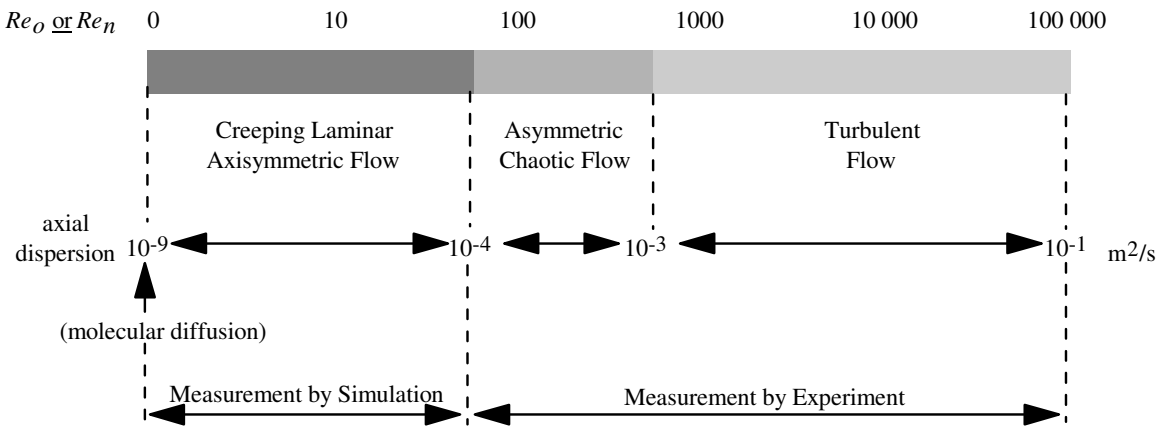

Figure 9.1: Schematic Diagram Showing Flow Regimes and Associated Axial Dispersion as a Function of Reynolds Number for Either Oscillation or Net Flow in Baffled Tubes (but Not Oscillations & Net Flow).

NET FLOW AND OSCILLATIONS

If both net flow and oscillations are present at the same time, the axial dispersion is not a linear function of Reynolds Number (Chapters 5 & 6). Figure 6.9 is reproduced here as an example.

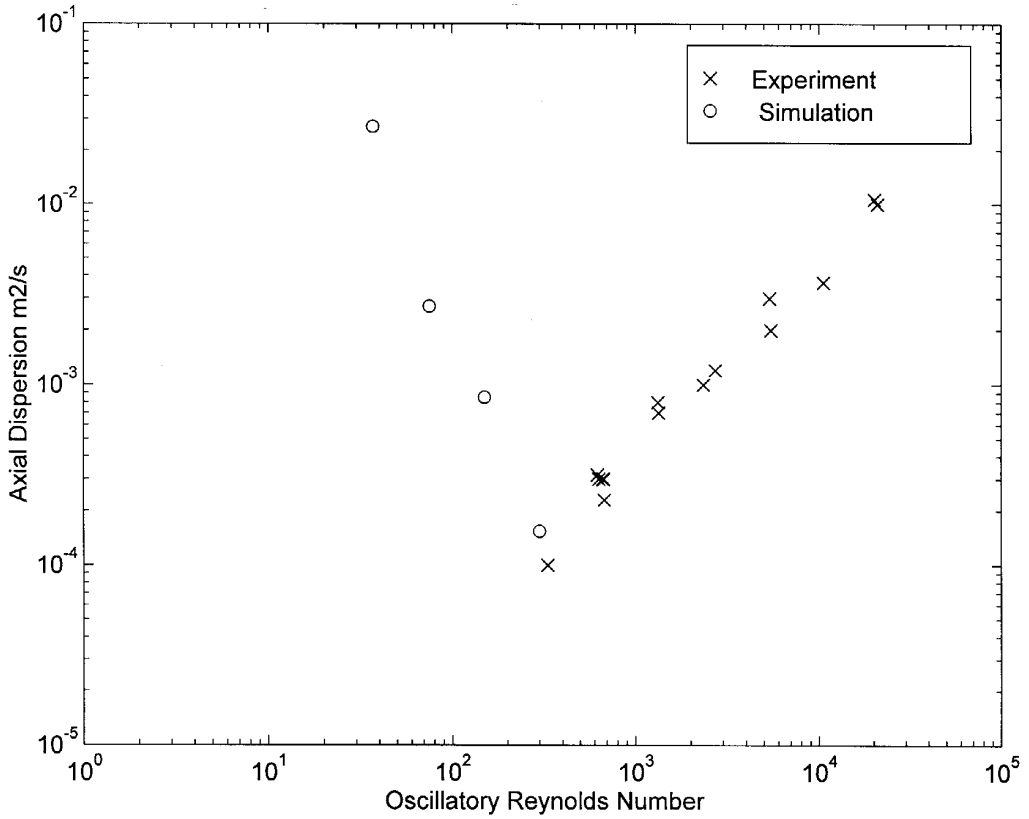

Figure 6.9: Graph Showing Simulated and Experimental Axial Dispersion Results for O.F.M.
$Re_n = 107$, $Str = 1$

At high Reynolds numbers ($Re_o > 800$) the flow is essentially turbulent in nature and flow visualisations show rapid and homogeneous mixing. For these conditions the axial

dispersion increases proportionally to Re_o $e^{(-0.4Str)}$. At lower Reynolds numbers the relationship between axial dispersion and the oscillatory and net flow Reynolds numbers appears to be much more complex. A minimum in axial dispersion is observed at around Re_o = 300 when the vortices formed as a result of the oscillations are powerful enough to give effective radial mixing. Such vortices are seen in Figure 7.10(b) where it is observed (under the conditions Re_o = 300 & Str = 1) that the vortex formed by the combined oscillation and net flow entirely fills the region of fluid behind each baffle and therefore is capable of redistributing fluid from the centre of the tube to the wall and vice-versa. This continual radial redistribution dominates the effect of any radial velocity profile due to the net flow and so axial dispersion is minimised.

Continuing with the example of Figure 6.9, if the oscillations are increased above Re_o = 300 then the vortices become increasingly chaotic and asymmetric (Figure 7.10(c)) and although radial redistribution is still good, the increase in axial dispersion due to vortex formation and interaction outweighs the benefit of improved radial mixing and so overall the axial dispersion increases. If instead the oscillations are decreased below Re_o = 300 then the axial dispersion again increases this time due to the inadequate radial mixing of the vortices. It can be seen in Figure 7.10(d) (for Re_o = 150 & Str = 2) that once the bulk of a pulse of tracer has passed through the tube due to the net flow, a stagnant corner exists behind each baffle where the vortex strength is inadequate for full mixing and that small quantities of the tracer remain trapped in these "dead-zones". At long times after the tracer injection therefore the presence of the stagnant corners becomes a large influence on the magnitude of axial dispersion calculated from the change in variance method applied to the fluid mechanical simulation and gives rise to large values of axial dispersion. It is noted that in the experimental measurements of axial dispersion, for example in Figure 5.3, that no such dramatic increase in axial dispersion was measured for oscillatory Reynolds numbers lower than that which gave the minimum axial dispersion. It is concluded that this is a minor flaw in the imperfect pulse method used to determine dye concentrations: the optical sensors were located centrally between two baffles and would therefore not have detected the presence of the small quantities of trapped tracer adjacent to the baffles. If the oscillations are reduced still further then in the limit (no oscillation) the axial dispersion decreases again to the net flow only result (approximately 2 x 10^{-4} m^2/s at Re_n = 107).

In attempting to measure axial dispersion over relatively short test sections, an interesting feature of dispersion behaviour has been identified. The *% backmixing* identified in §5.4 is a measure of proportion of dye tracer which mixed upstream of the injection point during an experiment. Its interest is two-fold: firstly, it allows the experimenter to determine with ease whether or not the dispersion of the tracer genuinely follows the prediction of the diffusion equation (it was found that at low Reynolds number flows, the measured axial dispersion can be large but in practice no tracer is advected upstream of the injection point; this presents a conundrum since a large axial dispersion would by

definition predict significant upstream advection during an experiment - see Figure 5.17). Secondly, the measurement of *% backmixing* could form the basis of a very useful technique for quickly and easily verifying that the oscillatory conditions in an O.F.M. process are optimum for minimising axial dispersion for a given net flow: it can be seen from Figure 5.16 that if the frequency of oscillations is progressively reduced until just a small amount of a pulse of tracer mixes upstream of the injection point then the axial dispersion will be at a minimum for that particular amplitude of oscillation. If the frequency were to be further reduced then there would be no backmixing and the axial dispersion would increase above the minimum value.

The prediction and measurement of the observed minimum in axial dispersion is of genuine interest for the potential application of O.F.M. to industrial processes. To be able to minimise axial dispersion in such a way as to give good mixing and near plug-flow residence time distributions for non-turbulent flows is a significant process advantage. Moreover, the ability to vary the oscillations means that the conditions can be optimised for residence time distribution in response to changes in throughput. The general observation is made that to achieve the minimum in axial dispersion then the oscillatory Reynolds number is of order of three times greater than the net flow Reynolds number (this is supported by data from Stonestreet 1997). The correlation developed in §5.5 predicts a slightly lower optimum value for the oscillation (equation 5.8) but is an empirical correlation that poorly matches the experimental data around the position of the minimum.

9.2 Comparison of Results with Those in the Literature

The axial dispersion results presented in this thesis are largely consistent with the order of magnitude of measurements by previous researchers although direct comparison is often difficult because of variations in baffle construction or wave form. Table 9.1 compares the experimental axial dispersion from a number of independent studies for similar flow conditions.

Research	Measured Axial Dispersion in m^2/s
Dickens et al 1989	1.7×10^{-4}
Howes 1988	1.5×10^{-4}
Mackley & Ni 1991	1.0×10^{-4}
Mackley & Ni 1993	2.8×10^{-4}
This work	1.3×10^{-4}

Table 9.1: Comparison of Measured Axial Dispersion from Independent Studies for Approximate Conditions: $Re_n = 107$, $Re_o = 370$ and $Str = 2$

Measurements of axial dispersion in O.F.M. by other researchers have been discussed in Chapter 2 but for the first time the results shown in Chapter 5 have measured axial dispersion as a function of tube diameter for geometrically scaled apparatus. For experiments with net flow only, oscillations only, and net flow with oscillations (with Re_n = 107) the dispersion was quantified using an imperfect pulse method with the correct solution to the diffusion model. This work is the first time that the imperfect pulse technique and the diffusion model have been utilised to quantify axial dispersion for oscillations only (in the absence of net flow) in baffled tubes and it is perhaps surprising that previous researchers have not considered the possibility of using the technique in this way.

It is thought that the precision of axial dispersion measurements has been improved in this work by the use of the correct solution to the diffusion equation for the boundary conditions in O.F.M. experiments (Chapter 4). This clarifies discrepancies in the measured axial dispersion noted by Mackely & Ni (1993) whose values appeared to depend upon the length of their test section. In this thesis the measured axial dispersion has been found to be independent of the distance over which it is measured. What is also of note is the discovery that the axial dispersion can be quite accurately measured over relatively short lengths of tube and it is therefore not necessary to have very long test sections in order to make reliable measurements of the residence time distribution. This fact was of particular relevance to the measurement of axial dispersion in the largest apparatus (the 150 mm diameter baffled tube) for which the construction of a long test section would have been time-consuming, costly and unnecessary.

The diffusion model was capable of modelling dispersion for Reynolds numbers of approximately 100 or greater or so long as $Re_o > Re_n$. Experiments were performed up to Re_n = 3000 or Re_o = 30 000 and $0.25 < Str < 16$ and this represents a significant increase in the range of conditions investigated compared to previous studies; it is the versatility of the apparatus constructed that allowed this greater range of conditions to be investigated.

A topic for debate that has often been raised at conferences and discussions on O.F.M. is the question of whether it is more desirable to oscillate the fluid (as is the case in this work) or instead to oscillate the baffles. Figure 9.2 shows directly comparable data taken from the 150 mm apparatus in this work and plotted with data from Rao & Baird (1996) for a 150 mm diameter tube with oscillating baffles of identical spacing and geometry.

The tube used by Rao & Baird (1996) was a 2.4 m tall 150 mm diameter tube containing ten annular baffles with a 76.5% constriction spaced 0.225 m apart. The geometry was therefore almost identical to the 150 mm apparatus except that the baffles were oscillated via a motor drive and yoke instead of the fluid being oscillated. The range of results for the oscillating baffles is limited to Reynolds numbers of 8000 and greater, but they match the axial dispersion results quite well for oscillating fluid. This agreement is consistent

with the supposition that for high oscillatory Reynolds numbers the mixing is homogeneous without strong dependence on the exact tube construction and that the axial dispersion is proportional to frequency of oscillation. This data represents the first time that the effect of oscillating either the fluid or the baffles has been compared experimentally for axial dispersion. Possible advantages of oscillating the baffles rather than the fluid are that the whole mass of fluid need not be oscillated (suggesting a reduced power consumption) and also that the scope for stagnant corners and fouling is likely to be reduced. Disadvantages of the moving baffles are that they entail moving parts within the reactor (that would be undesirable if access is difficult) and would be problematic to install for long tubes containing U-bends.

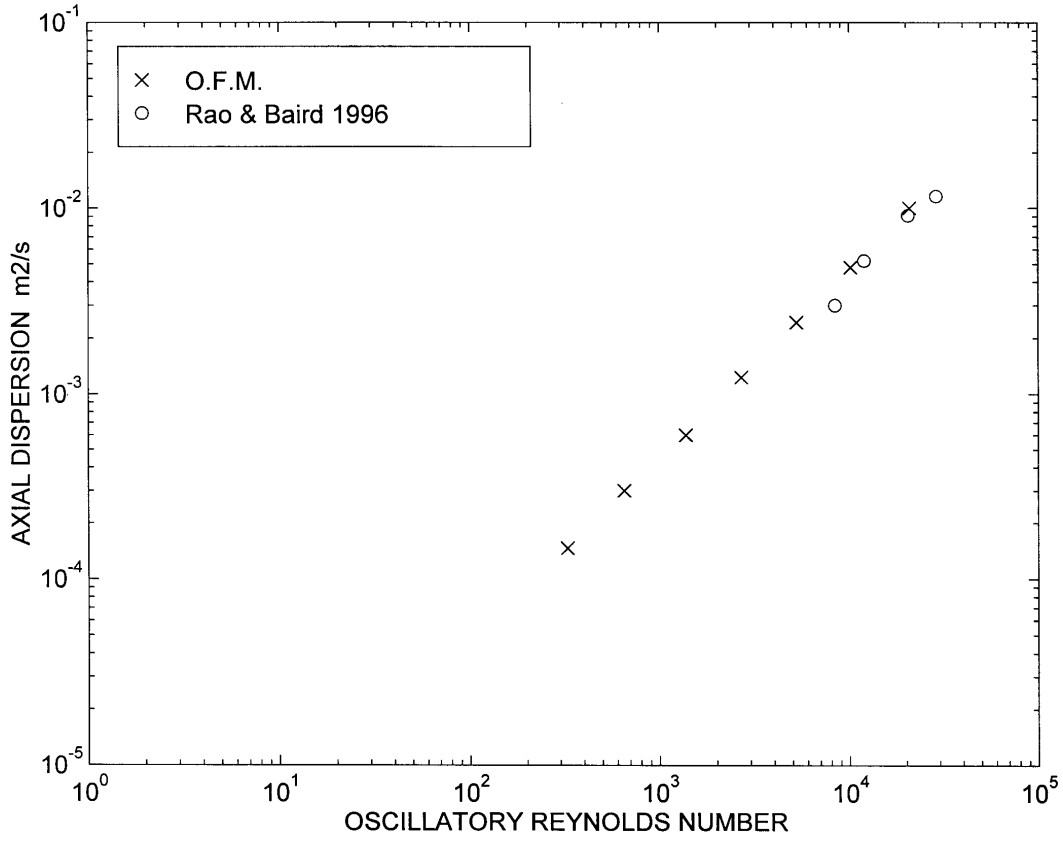

Figure 9.2: Comparison between Oscillating Fluid (O.F.M.) and Oscillating Baffles (Rao & Baird 1996) both in a 150 mm Diameter Tube

The axial dispersion results obtained from fluid mechanical simulation were entirely consistent with previous results of Howes (1988) and Saraiva (1997) where overlap existed. This was not at all surprising since the same code was used, but it served as a useful check that for certain conditions the results were the same as had been achieved by the authors of the simulation code. It became clear in Chapters 6 and 7 that the current fluid mechanical simulation for O.F.M. in baffled tubes was limited in its useful range by its axisymmetric constraint. Howes, Mackley & Roberts (1991) generated flow visualisation simulations in a two-dimensional baffled channel (Figure 9.4) which are intriguingly similar in form to observations of the breaking of axisymmetry for the experimental flow visualisations in this thesis. Although the comparison is only

qualitative, it suggests that the development of a fluid mechanical code which would allow asymmetric flow in baffled tubes would be of considerable interest as a means of further investigating O.F.M..

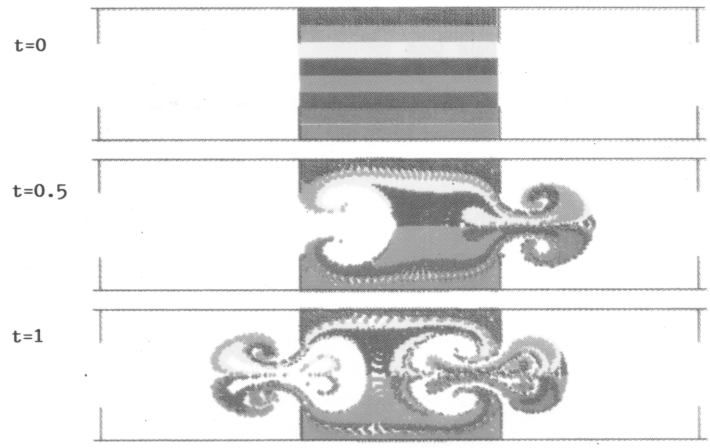

(a) Re_o = 100, Str = 1 (Axisymmetric Flow)

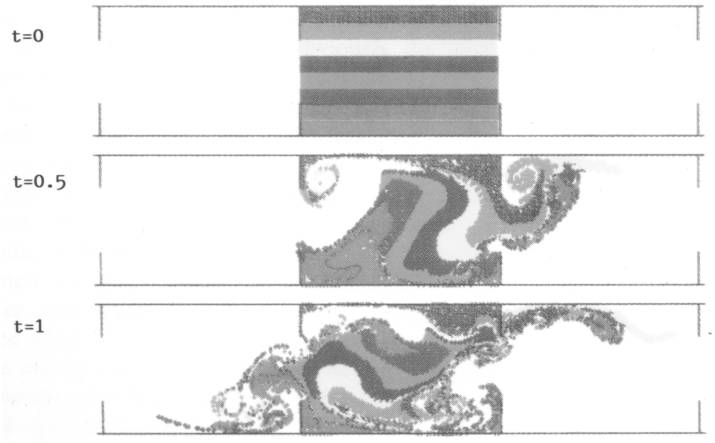

(b) Re_o = 300, Str = 1 (Showing Breaking of Symmetry)

Figure 9.4: Numerical Simulations by Howes et al (1991) for a Baffled Channel during One Oscillation

(reproduced with permission)

9.3 Multi-Orifice Baffles as a Route to Scale-Up

The findings in Chapter 8 have established that the use of multi-orifice baffles is of considerable interest as a means to scaling-up O.F.M.. The case study example given in §8.1 has been modified for the case of multi-orifice baffles and is shown in Figure 9.5.

The multi-orifice baffles appear quite similar in configuration to those typically found in reciprocating plate columns (§2.3.2). This is a useful comparison since it has already been established that for turbulent flows, axial dispersion is the same in O.F.M. as for reciprocating annular baffles (Figure 9.3) of similar geometry. It is therefore not unreasonable to suppose that the results of research on reciprocating plate columns with similar geometry to multi-orifice O.F.M. can be of relevance to O.F.M. for turbulent

flows. For example Kim & Baird (1976b) concluded that $E \propto \frac{c^{1.8}}{H^{1.3}T^{0.3}}$ for orifice diameter c, plate thickness T and separation H. This suggests that reducing the orifice diameter (while keeping the same total percentage baffle constriction) might be the most effective method of minimising axial dispersion by a change in baffle geometry. The dependence upon plate spacing appeared to be a strong function of the particular geometry and so should be approached with caution. Axial dispersion appeared to be only a weak function of baffle thickness. Another finding of Kim & Baird's work was that viscous effects had a negligible effect on the axial dispersion in the essentially turbulent flow regime which they investigated ($Re_o \geq 3000$). This might then require the correlation developed in §5.5 to be revised since a dependence upon Reynolds number was assumed whereas in fact the effects of viscosity and density were not tested.

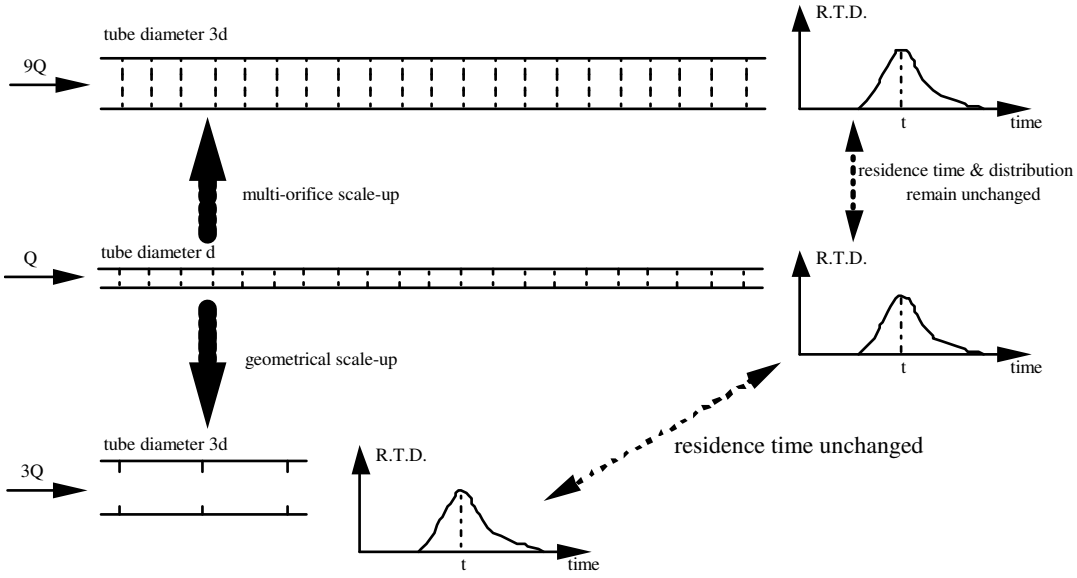

Figure 9.5: Schematic Comparison of Geometrical Scale-Up *vs* Multi-Orifice Scale-Up

A mainstay of the multi-orifice baffles is that the axial dispersion is insensitive to tube diameter. A review paper (Lo et al 1992) on liquid-liquid systems reciprocating plate columns noted that $E \propto d^n$ where d is the column diameter and n is between 0.3 and 0.67 depending upon plate geometry; this suggests that care would need to be taken in transferring the results of single phase liquid flow in multi-orifice O.F.M. to multi-phase flow since the scaling may become non-linear.

9.4 Heat Transfer

Heat transfer in a 12 mm diameter stainless steel baffled tube with O.F.M. was studied experimentally by Mackley & Stonestreet (1995) who showed that the presence of the baffles alone (for a net flow only) could increase the heat transfer coefficient and that the superposition of oscillations could further enhance heat transfer by an order of magnitude. They matched the dependence of heat transfer on the flow conditions with the following approximate correlation:

$$Nu_t = 0.0035 Re_n^{1.3} Pr^{0.33} + 0.3\left[\frac{Re_o^{2.2}}{(Re_n + 800)^{1.25}}\right] \qquad \text{eqn (9.1)}$$

where Nu_t is the tube side Nusselt number and Pr is the Prandtl number. The first term in the correlation was chosen to be similar in form to the Dittus Boelter equation for tube heat transfer in turbulent flow except that Re_n is raised to the power 1.3 to account for the presence of the baffles. The second term accounts for the additional effect of the oscillations. The correlation is compared with standard heat transfer correlations for smooth tubes in Figure 9.6.

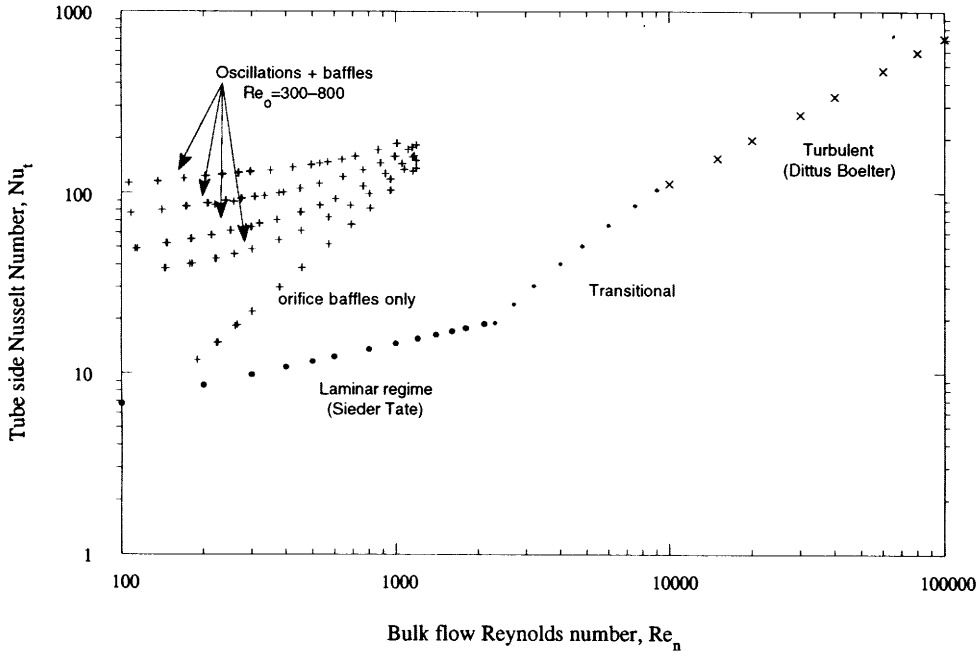

Figure 9.6: Comparison of Oscillatory Flow Heat Transfer Correlation to Standard Heat Transfer Correlations for Smooth Wall Tubes *(Reproduced with Permission from Mackley & Stonestreet 1995)*

It would be reasonable to assume that the same correlation could be used over the given range of conditions in the case of multi-orifice baffles since the fluid mechanics at the wall appear similar to those observed in single orifice baffled tubes if the equivalent tube diameter d_e is substituted such that $Nu_t = \frac{h_i d_e}{k}$. Because the ratio of tube wall area to tube volume decreases inversely proportional to tube diameter, the heat transfer will become less effective at controlling the temperature of fluid inside the tube as the overall

tube diameter increases. For processes where temperature control is critical the maximum tube diameter that can be used for multi-orifice baffles may be limited by the decreasing tube wall area per unit volume of fluid in the tube.

In the case of geometrical scale-up (without the use of multi-orifice baffles) the tube side heat transfer coefficient reduces inversely proportional to tube diameter (under similar dynamic conditions i.e. for a constant Nusselt number). For low Reynolds numbers it is speculated that buoyancy would have an increasingly important effect on the fluid mechanics the larger the diameter of the tube and would eventually dominate the forced oscillations. An indication of this was seen experimentally when taking video pictures of low Reynolds number flows in the 24 mm apparatus using a powerful floodlight: strong convective flow was observed due to heating of the tube wall on the side of the tube nearest the floodlight which caused the flow to become asymmetric.

9.5 Energy Dissipation

Baird & Stonestreet (1995) examined the energy dissipation associated with O.F.M. using the same experimental apparatus as Mackley & Stonestreet (1995). By considering the combination of the inertial and frictional pressure drops in O.F.M. they developed a correlation (equation 9.2) for power density ε_v that gave good agreement with experimental measurements of power density:

Correlation for Power Density: $$\varepsilon_v = 1.5\frac{\rho\omega^3 x_o^2 l}{HS} \qquad (W/m^3) \quad \text{eqn (9.2)}$$

(after Baird & Stonestreet (1995))

where H is the spacing between baffles, S the fractional open area of baffle and l a characteristic mixing length. Their correlation was based upon an eddy enhancement model for the frictional pressure drop and the only adjustable parameter was the mixing length l . They determined the best fit value of l to be 7 mm i.e. of similar magnitude to the orifice diameter in their experiments (although they acknowledged that changing either the baffle geometry or spacing could affect l). Power densities in the range 100 to 10 000 W/m^3 were observed for O.F.M. with $220 \leq Re_o \leq 6750$ and $0.15 \leq Str \leq 0.95$.

The mixing length l could be expected to remain the same for multi-orifice baffles of similar equivalent diameter (since the scale of the fluid mechanics is similar) but for geometrically scaled baffled tubes it is not known how l would vary with tube diameter: for a given Re_o and Str the inertial contribution to equation 9.2 would be expected to remain constant per unit volume but the frictional contribution would probably decrease with increasing tube diameter.

It is recognised that these calculations of power density do not include the additional energy dissipated in the mechanical oscillator due to piston inertia and friction as well as

motor inefficiency: in sizing the oscillator power these factors must also be taken into account.

9.6 Engineering Considerations for Large Scale O.F.M.

For a given process the particular requirements of residence time, residence time distribution (for a continuous process), mixing and temperature control will dictate the most suitable tube diameter and baffle geometry (single or multi-orifice). Because of the ability of O.F.M. to control mixing and axial dispersion independently of net throughput at low Reynolds number flows, the technology is most likely to find application in continuous processes requiring long residence times with a good control of residence time distribution.

The sets of apparatus used in this thesis were simple vertical baffled tubes with a piston or bellows driving the oscillations at the base of the tube and with a free liquid surface at the top of the tube. This configuration makes filling and emptying of the tube easy as well as venting any trapped gases. An industrial process or reaction might need to be pressurised in which case the simplest solution would be a pressurised headspace above the liquid free surface (Figure 9.7a). An alternative of two opposing pistons operating synchronously at each end of the tube has also been used at laboratory scale (for example Howes 1988 who used mechanically linked pistons) although some additional means of venting gas would then be required.

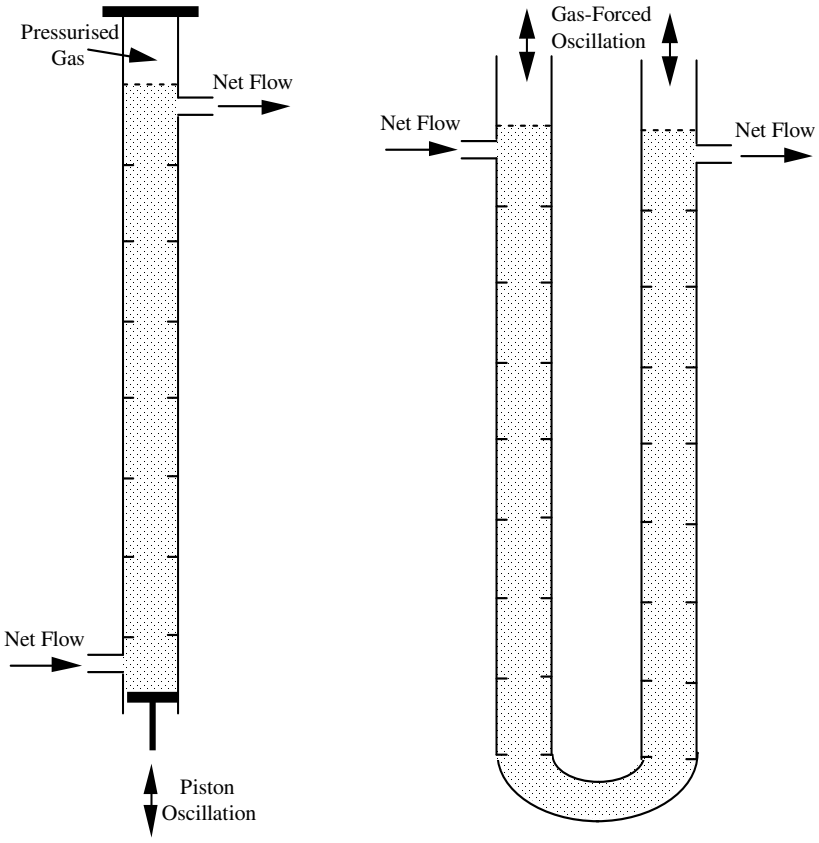

(a) Pressurised O.F.M. Using a Gas Headspace (b) O.F.M. with Gas-Pressure Driven Oscillations

Figure 9.7: Alternative Designs for Industrial O.F.M.

An alternative design option would be to use manometer-style oscillating columns (as used by the nuclear reprocessing industry for liquid-liquid contacting) where the oscillations are driven by gas pressure difference at the top of a U-tube (Figure 9.7b). This design would be suited to low frequency oscillations (Hill et al), but unsuitable if rapid oscillations were required since the forces required to accelerate and decelerate the fluid would be difficult to achieve with gas pressure alone. In the latter case a rigid piston and cylinder oscillator would be preferable.

The use of piston and cylinder arrangements to transmit the oscillations is quite effective and uses standard "off-the-shelf" sealing technology that under normal operating conditions will last many oscillatory cycles, although there is always the potential for leakage if the seals are damaged or worn. The piston seals used in the 150 mm apparatus oscillator remained in good condition after approximately 500 000 cycles without any appreciable leakage. The stainless steel bellows used for the 24 mm apparatus were also successful and did not leak (lasting approximately 1 500 000 cycles without failure), although it is thought that larger scale bellows would be prone to distortion under load and are not generally designed to withstand rapid oscillations without the risk of fatigue.

The use of servo-hydraulics to power oscillations in O.F.M. has been shown to be a versatile method. It has several advantages including "off-the-shelf" components that are cheap and easy to replace, flexible control of frequency and amplitude of oscillation, physical compactness, and spark-free operation in a hazardous area.

A potential issue for O.F.M. in very long tubes with large frictional and inertial pressure drops is the possibility of cavitation. This might be avoided by overall pressurisation of the tube, or alternatively the tube would need to be designed in several sections separated by flow pumps.

10. Conclusions and Suggestions for Further Work

10.1 Conclusions

Three sets of geometrically similar apparatus of different tube diameter were successfully designed and constructed in which to carry out experiments on oscillatory flow mixing in baffled tubes (O.F.M.). The use of hydraulically powered oscillators was found to be reliable and gave experimental flexibility to investigate a wide range of oscillatory flow conditions.

The results presented in this thesis have extended the range and understanding of axial dispersion in O.F.M. and it has been discovered experimentally that axial dispersion is not a function of tube diameter if dynamically similar flow conditions are maintained. This leads to a reliable scale-up criterion for O.F.M. in terms of residence time distribution (Chapter 5). Increasing the tube diameter also drastically reduces the mixing rate in O.F.M. (with the likely maximum shear rate proportional to $diameter^{-2}$) and therefore in instances where to maintain mixing scale is important for a process (for example the mixing of two species in a chemical reaction) then simple geometrical scale-up of O.F.M. may not be appropriate.

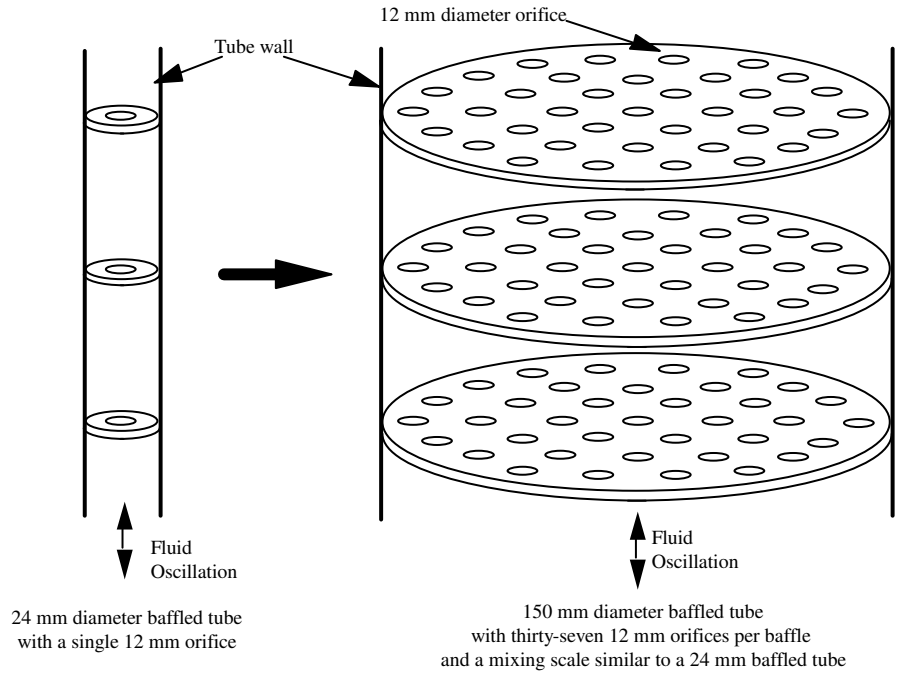

Fig. 8.2 Reproduced: Using Multi-Orifice Baffles to Mimic Many Single-Orifice Baffled Tubes in Parallel

A solution to the problem of changing mixing scale has been found in an initial investigation into the use of large diameter tubes with multi-orifice baffles in place of many smaller diameter tubes with single-orifice baffles (Chapter 8). The multi-orifice design can successfully be modelled as a large number of single-orifice baffled tubes operating in parallel and is shown schematically in Figure 8.2. If for the multi-orifice baffles the baffle spacing, orifice diameter and the effective area surrounding each orifice

is equivalent to the single-orifice baffles then the fluid mechanics, measured axial dispersion and mixing scale are similarly comparable. This means that experiments can be carried out at laboratory scale with O.F.M. in single-orifice baffled tubes and the results can be scaled-up with confidence by large orders of magnitude to a multi-orifice design. (The scale-up factor achieved in this work was an increase in volumetric flowrate of 39 times for the same dynamic conditions. It is speculated that very much larger increases could be achieved without affecting the fluid mechanics, axial dispersion or mixing scale using larger diameter baffles with a commensurately greater number of orifices).

Axial dispersion has been quantified for a wide range of dynamic conditions in O.F.M. using the imperfect pulse technique and the diffusion model. The literature relating to solving the diffusion equation (equation 2.14) has been clarified in Chapter 4 and a reliable method for quantifying axial dispersion measured over short tube lengths in O.F.M. has been developed. The method is quite general and could be applied to any situation involving axial dispersion in a long tube.

A useful fluorescent dye streakline flow visualisation method has been developed and successfully applied to O.F.M. (Chapter 7). The technique has advantages over previous flow visualisation methods applied to O.F.M. and it allows direct comparisons to be made between flow in tubes of different diameter. The technique has been used to show that the fluid mechanics of O.F.M. are not strongly affected by tube diameter. Specific flow regimes ranging from creeping laminar to chaotic and fully turbulent have been identified and used to explain trends in the measured axial dispersion.

An unusual flow phenomenon has been identified for the geometry studied in the absence of net flow and at low oscillatory Reynolds numbers: vortices moving in opposing directions meet midway between two baffles and create strong radial flow from the centre of the tube to the wall and act as barriers to dispersion. These fluid "manifolds" (Chapter 7) are an interesting and unique flow structure: well mixed regions of fluid are separated by the manifolds across which the only mechanism for axial dispersion is molecular diffusion. The manifold flow structure observed in multi-orifice baffles (Figures 8.14 & 8.15) is even more striking in that axial, toroidal and radially oriented manifolds can all exist simultaneously, creating a three-dimensional structure of compartmentalised mixing regions with minimal exchange of fluid into neighbouring compartments. If a batch process required gentle localised stretch-fold mixing with minimal bulk mixing then manifolds would be highly desirable.

The results of both axial dispersion measurements and flow visualisations have been simulated using a computerised fluid mechanical simulation. The simulation was constrained to predict axisymmetric flow and was therefore limited to flows with a Reynolds number of less than approximately 100. Since most experimental results were restricted to Reynolds numbers of greater than 100 by the limitations of the diffusion

model, the fluid mechanical simulation is a useful tool for extending the range of dynamic conditions which can be investigated for axisymmetric flows. Although the fluid mechanical simulation only provided a small overlap with experimental results the observed fluid mechanics and axial dispersion matched well for experiment and simulation, giving confidence in the validity of both techniques.

The experimental results for axial dispersion have been correlated as a function of Re_n, Re_o and Str (Chapter 5, §5.5). This empirical correlation is most successful at high Reynolds numbers (> 800). At intermediate oscillatory Reynolds numbers ($30 < Re_o < 800$) the correlation shows some deviations from the experimental data when a small net flow is introduced although the correct order of magnitude for axial dispersion is predicted. The overall best-fit correlation is only dependent upon $Re_n 0.8$ and $Re_o e^{(-0.4Str)}$ for a water-based system:

$$E = 7.0 \times 10^{-7}\, Re_n^{0.8} + 7.5 \times 10^{-7}\, Re_o\, e^{(-0.4Str)} + \frac{3.0 \times 10^{-12}\, Re_n^{1.6}}{7.0 \times 10^{-7}\, Re_n^{0.8} + 7.5 \times 10^{-7}\, Re_o\, e^{(-0.4Str)}}$$

(m^2/s) eqn (5.6) reproduced

It is concluded that O.F.M. is a technology which in general lends itself readily to scaling-up from laboratory to pilot plant scale, and most probably to industrial scale. Experiments performed on small laboratory apparatus (containing less than one litre of fluid) can with confidence be used to predict mixing behaviour in much larger plant (containing hundreds of litres of fluid.)

10.2 Suggestions for Further Work

A wide-ranging study of axial dispersion in O.F.M. has been presented using results from both experiment and simulation. The limitations of the work are recognised in that the upper limit for simulation results is a Reynolds number of order 100 (above which the simulation cannot predict the flow which becomes asymmetric) while the lower extent of experimental results is also at a similar order of magnitude Reynolds number (below which the diffusion model is unsuccessful at quantifying axial dispersion over short distances). There is therefore a very limited overlap between the two sets of results (from experiment and from simulation). It is suggested that a useful course of work for the future would be to aim to extend the valid range of results for the simulation and / or the experimental model. In the case of the simulation, the code would have to be adapted to include non-axisymmetric flows which might extend the validity of the simulation up to Reynolds numbers of order 800. Turbulent flow modelling would be required to further extend the range of the simulation to higher Reynolds numbers. In the case of the experimental technique for determining axial dispersion, an alternative to the diffusion model would have to be sought in order to extend the useful range of the imperfect pulse technique.

Initial results for dispersion and fluid mechanics using the multi-orifice baffle design (Chapter 8) suggest that this system has potential for excellent ease of scale-up. It is suggested that the design be further investigated for its experimental heat-transfer properties and power dissipation. A fluid mechanical simulation could also be contemplated that would predict flow in an infinite array of regularly spaced orifices per baffle.

An issue which has arisen for the multi-orifice baffles is that of radial mixing from the centre of the tube to the wall. A process involving heat or mass transfer to the wall would be likely to benefit from improved radial mixing and it is speculated that this could be achieved by orienting the orifices in adjacent baffles out-of-line with one another (Figure 10.1). It is suggested that the effectiveness of such a design could be investigated either experimentally or by simulation.

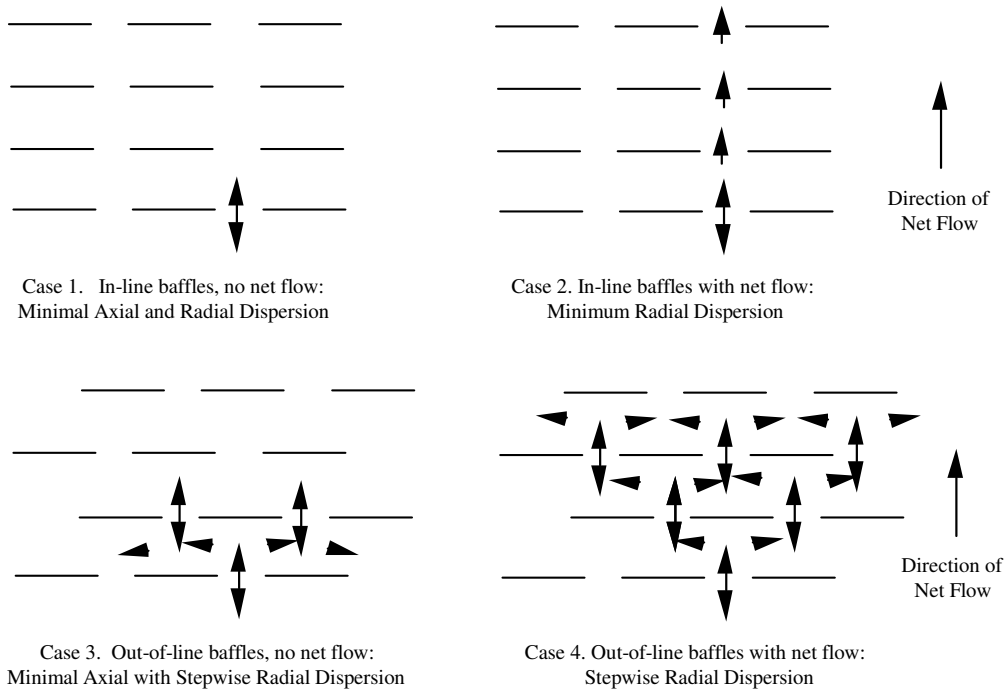

Figure 10.1: Schematic Proposal for Oscillatory Flow with Misaligned Multi-Orifice Baffles

It has been observed that for net flow with minimal oscillations in single-orifice baffled tubes, tracer can become trapped in regions of stagnant flow in the corners between the baffle and the tube wall (Figure 7.10 d). It is suggested that the potential for reducing axial dispersion by creating a "loose-fit" baffle be investigated, i.e. retaining a gap between the baffle and the tube wall.

The correlation for axial dispersion as a function of flow conditions developed in §5.5 provides generally good agreement with experimental data for O.F.M. but does not perfectly match experimental observations where a small net flow (Re_n < 200) is superimposed on an oscillation for Re_o < 800. The current form of the correlation does not allow for the observation that in reality the presence of small net flows can enhance the axisymmetry of the oscillatory flow and therefore reduce the overall axial dispersion

rather than increase it as might have been intuitively expected. It is therefore suggested that an alternative form of correlation be considered which could reflect this behaviour.

References

Aris R. 1956 "On the dispersion of a solute in a fluid flowing through a tube" Proc. Roy. Soc. Lond. A235 pp 67-77

Aris R. 1959(a) "Notes on the diffusion-type model for longitudinal mixing in flow" Chem. Eng. Sci. Vol 9 pp 266-267

Aris R. 1959(b) "The longitudinal diffusion coefficient in flow through a tube with stagnant pockets" Chem. Eng. Sci. Vol 11 pp 194-198

Aris R. 1960 "On the dispersion of a solute in pulsating flow through a tube" Proc. Roy. Soc. Lond. A259 pp 370-376

Baird M.H.I. 1966 "Vibrations and pulsation" British Chem. Eng. Vol 11 No 1 pp 20-25

Baird M.H.I. 1974 "Axial dispersion in a pulsed plate column" Can. J. Chem. Eng. Vol 52 pp 750-757

Baird M.H.I. & Stonestreet P. 1995 "Energy dissipation in oscillatory flow within a baffled tube" Trans IChemE Vol 73 Part A pp 503-511

Baird M.H.I. & Rama Rao N.V. 1996 “Hydrodynamics of reciprocating plate columns” 2nd Conference on Pulsatile Flow, June 3rd, University of Strathclyde, Scotland

Bischoff K.B. 1960 "Notes on the diffusion-type model for longitudinal mixing in flow" Chem. Eng. Sci. Vol 12 pp 69-70

Brunold C.R., Hunns J.C.B., Mackley M.R. & Thompson J.W. 1989 "Experimental observations on flow patterns and energy losses for oscillatory flow in ducts containing sharp edges" Chem. Eng. Sci. Vol 44 No 5 pp 1227-1244

Carberry J.J. & Bretton R.H. 1958 "Axial dispersion of mass in flow through fixed beds" A.I.Ch.E. Journal Vol 4 No 3 pp 367-375

Crittenden B.D., Field R.W. & Pervez M.I. 1995 "Oscillatory flow in packed beds and baffled tubes. A unifiying approach to the interpretation of experimental data" Chem. Eng. Sci. Vol 50 No 23 pp 3839-3845

Danckwerts P.V. 1953 "Continuous flow systems" Chem. Eng. Sci. Vol 2 No 1 pp 1-13

Dickens A.W., Mackley M.R. & Williams H.R. 1989 "Experimental residence time distribution measurements for unsteady flow in baffled tubes" Chem. Eng. Sci. Vol 44 No 7 pp 1471-1479

Gilibaro L.G. 1978 “On the residence time distribution for systems with open boundaries” Chem. Eng. Sci. Vol 33 pp 487-492

Goebel J.C., Booij K. & Fortuin J.M.H. 1986 "Axial dispersion in single-phase flow in pulsed packed columns" Chem. Eng. Sci. Vol 41 No 12 pp 3197-3203

Hayden E.S.S. 1997 "A Quantitative Study of Oscillatory Flows in Plain and Baffled Tubes" Thesis, University of Cambridge

Hewgill M.R., Mackley M.R., Pandit A.B. & Pannu S.S. 1993 "Enhancement of gas-liquid mass transfer using oscillatory flow in a baffled tube" Chem. Eng. Sci. Vol 48 No 4 pp 799-809

Hill H.J., R and DD, BNF Plc Sellafield “Analysis and design of pulsing systems for air pulsed solvent extraction columns” IChemE Symposium Series no 103 pp 87-101

Howes T. 1988 "On the dispersion of unsteady flow in baffled tubes" PhD Thesis, University of Cambridge

Howes T. & Mackley M.R. 1990 "Experimental axial dispersion for oscillatory flow through a baffled tube" Chem. Eng. Sci. Vol 45 No 5 pp 1349-1358

Howes T., Mackley M.R. & Roberts E.P.L. 1991 "The simulation of chaotic mixing and dispersion for periodic flows in baffled channels” Chem. Eng. Sci. Vol 46 No 7 pp 1669-1677

Hwu T., Sobey I.J. & Bellhouse B.J. 1996 "Observation of concentration dispersion in unsteady deflected flows” Chem. Eng. Sci. Vol 51 pp 3373-3390

Keulegan G.H. & Carpenter L.H. 1958 "Forces on cylinders and plates in an oscillatory fluid" Journal of Research (National Bureau of Standards) Vol 60 pp 423-440

Kim S.D. & Baird M.H.I. 1976(a) "Axial dispersion in a reciprocating plate extraction column" Can. J. Chem. Eng. Vol 54 pp 81-89

Kim S.D. & Baird M.H.I. 1976(b) "Effect of hole size on hydrodynamics of a reciprocating perforated plate extraction column" Can. J. Chem. Eng. Vol 54 pp 235-237

Knott G.F. & Mackley M.R. 1980 "On eddy motions near platees and ducts induced by water waves and periodic flows" Proc. Roy. Soc. Lond. A294 pp 599-623

Levenspiel O. & Smith W.K. 1957 "Notes on the diffusion type model for the longitudinal mixing of fluids in flow" Chem. Eng. Sci. Vol 6 pp 227-233

Levenspiel O. 1972 "Chemical Reaction Engineering" John Wiley & Sons 2nd Ed. N.Y.

Lo T.C., Baird M.H.I. & Rama Rao N.V. 1992 "The reciprocating plate column - development and applications" Chem. Eng Comm. Vol 116 pp 67-88

Long J.T. 1967 "Engineering for nuclear fuel reprocessing" Gordon & Breach Science Publishers Inc. N.Y.

Lounes M & Thibault J. 1996 “Axial Dispersion in a Reciprocating Plate Column” Can. J. Chem. Eng. Vol 74 pp 187-194

Mackay M.E., Mackley M.R. & Wang Y. 1991 "Oscillatory flow within tubes containing wall or central baffles" Trans IChemE Vol 69 Part A pp 506-513

Mackley M.R. 1987 "Using oscillatory flow to improve performace" Chemical Engineer, February Edition pp 18-20

Mackley M.R., Tweddle G.M. & Wyatt I.D. 1990 "Experimental heat transfer measurements for pulsatile flow in baffled tubes" Chem. Eng. Sci. Vol 45 No 5 pp 1237-1242

Mackley M.R. 1991 "Process innovation using oscillatory flow within baffled tubes" Trans IChemE Vol 69 pp 197-199

Mackley M.R. & Ni X. 1991 "Mixing and dispersion in a baffled tube for steady laminar and pulsatile flow" Chem. Eng. Sci. Vol 46 No 12 pp 3139-3151

Mackley M.R. & Roberts E.P.L. 1991 "Mixing and flow patterns for unsteady flow in baffled channels" American Soc. Mech. Engineers FED Vol 127 pp57-64

Mackley M.R., Smith K.B. & Wise N.P. 1993 "The mixing and separation of particle suspensions using oscillatory flow in baffled tubes" Trans IChemE Vol 71 Part A pp 649-656

Mackley M.R. & Ni X. 1993 "Experimental fluid dispersion measurements in periodic baffled tube arrays" Chem. Eng. Sci. Vol 48 No 18 pp 3293-3305

Mackley M.R. & Roberts E.P.L. 1995 "The simulation of stretch rates for the quantitative prediction and mapping of mixing within a channel flow" Chem. Eng. Sci. Vol 50 No 23 pp 3727-3746

Mackley M.R. & Stonestreet P. 1995 "Heat transfer and associated energy dissipation for oscillatory flow in baffled tubes" Chem. Eng. Sci. Vol 50 No 14 pp 2211-2224

Mackley M.R., Stonestreet P., Thurston N.C. & Wiseman J.S. 1998 "Evaluation of a Novel Self-Aerating, Oscillating Baffle Column" Can. J. Chem. Eng. Vol 76 pp 5-10

Mak A.N.S., Koning C.A.J., Hamersma P.J. & Fortuin J.M.H. 1991 "Axial dispersion in single-phase flow in a pulsed packed column containing structured packing" Chem. Eng. Sci. Vol 46 No 3 pp 819-826

Mecklenburg J.C. & Hartland S. 1975 "The theory of backmixing" John Wiley & Sons London

Nauman E.B. & Mallikarjun R. 1983 "Generalized boundary conditions for the axial dispersion model" Chem. Engineering Journal Vol 26 pp 231-237

Ni X. & Mackley M.R. 1993 "Chemical Reaction in Batch Pulsatile Flow and Stirred Tank Reactors" Chem. Engineering Journal Vol 52 pp 107-114

Ni X. 1994 "Residence time distribution measurements in a pulsed baffled tube bundle" J. Chem Tech. Biotechnol. Vol 59 pp 213-221

Ni X. 1995 "A study of fluid dispersion on oscillatory flow through a baffled tube" J. Chem Tech. Biotechnol. Vol 64 pp 165-174

Ni X., Gao S., Cumming R.H. & Pritchard D.W. 1995 "A Comparative Study of Mass Transfer in Yeast for a Batch Pulsed Baffled Bioreactor and a Stirred Tank Fermenter" Chem. Eng. Sci. Vol 50 No 13 pp 2127-2136

Ni X. & Gao S. 1996 "Mass transfer characteristics of a pilot pulsed baffled reactor" J. Chem Tech. Biotechnol. Vol 65 pp 65-71

Ni X. & Gough P. 1997 "On the discussion of the dimensionless groups governing oscillatory flow in a baffles tube" Chem. Eng. Sci. Vol 52 No 18 pp 3209-3212

Ni X., Brogan G., Struthers A., Bennett D.C. and Wilson S.F. 1998 "A systematic study of the effect of geometrical parameters on mixing time in oscillatory baffles columns" Trans IChemE Vol 76 Part A pp 635-642

Perry 1984 “Chemical Engineer’s Handbook” 6th Ed. McGraw-Hill

Reeder M., Janz E. and Myers K. 1997 "Experimental Investigation of Viscosity Ratio Effects on the Performance of Static Mixers" AIChemE Annual Meeting, Los Angeles

Saraiva, R.M.D.C.N. 1997 "The Characterisation of Mixing for Oscillatory Flow within Baffled Tubes" PhD Thesis, University of Cambridge

Scott D.M. 1997 (*private communication*)

Simons A.J.F., van Sluys R., Goebel J.C. & Fortuin J.M.H. 1986 "Axial dispersion in pulsed packed columns on both laboratory and industrial scale" Proceedings of I.S.E.C. Muenchen

Sobey I.J. 1985 "Dispersion caused by separation during oscillatory flow through a furrowed channel" Chem. Eng. Sci. Vol 40 No 11 pp 2129-2134

Stevens G.W. & Baird M.H.I. 1990 "A model for axial mixing in reciprocating plate columns" Chem. Eng. Sci. Vol 46 No 2 pp 457-465

Stonestreet P. 1997 (*private communication*)

Taylor G.I. 1953 "Dispersion of soluble matter in solvent flowing slowly through a tube" Proc. Roy. Soc. Lond. A219 pp 186-203

Taylor G.I. 1954 "The dispersion of matter in turbulent flow through a pipe" Proc. Roy. Soc. Lond. A223 pp 446-467

van der Laan 1958 "Notes on the diffusion-type model for the longitudinal mixing in flow" Chem. Eng. Sci. Vol 7 pp 187-191

Wang Y., Howell J.A., Field R.W. & Mackley M.R. 1994 "Oscillatory flow within porous tubes containing wall or central baffles" Trans IChemE Vol 72 Part A pp 686-693

Westerterp K.R., van Swaaij W.P.M. & Beenackers A.A.C.M. 1984 "Chemical Reactor Design and Operation" John Wiley & Sons London

Williams D.H. & Fleming I. 1989 "Spectroscopic methods in organic chemistry" McGraw-Hill 4th Ed London

Appendix 1: Hydraulic Sizing Calculations and Circuit Diagram

The principle of the servo-hydraulic method of powering the oscillations is that high pressure hydraulic oil is delivered to alternating ends of a double-acting hydraulic cylinder. The flow is regulated by a servo-control valve which controls the differential pressure between the two ends of the cylinder (Figure AI.1).

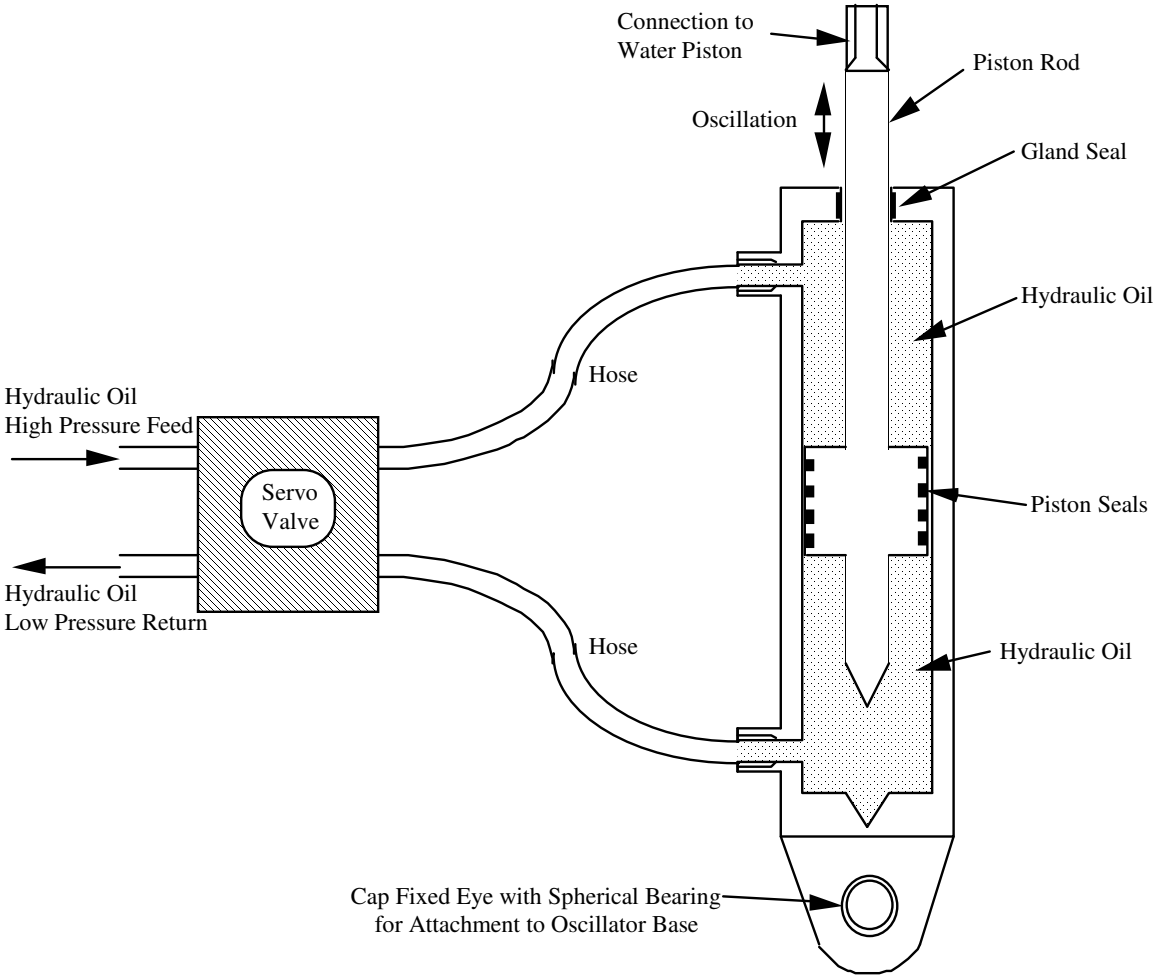

Figure AI.1: Schematic Details of The Hydraulic Cylinder and Servo Valve

The critical specifications of the system are the cross-sectional area of the hydraulic cylinder, the operating pressure of the hydraulic oil and the required flow rate of the oil. At the initial design stage it was decided that the hydraulics for the 150 mm diameter apparatus should be capable of oscillating 250 kg of water (corresponding to a tube length of 14 metres) at 10 Hz and a 3 mm centre-to-peak amplitude. Under these conditions the peak oscillatory velocity is:

$$\text{Peak Oscillatory Velocity} = \omega x_o = 2\pi f x_o = 2\,\pi \text{ x } 10 \text{ x } 0.003 = \underline{0.19 \text{ m/s}}$$

and

$$\text{Peak Oscillatory Acceleration} = \omega^2 x_o = 4\pi^2 f^2 x_o = 4\,\pi^2 \text{ x } 10^2 \text{ x } 0.003 \approx \underline{12 \text{ m/s}^2}$$

The maximum axial force on the piston rod due to the oscillation is therefore

Maximum Force = mass x acceleration = 250 x 12 = <u>3000 N</u>

For a hydraulic cylinder with bore size 40 mm of cross section 1.26 x 10^{-3} m^2 the required working pressure of the oil to give a maximum force of 3000 N would be:

Minimum Pressure of Oil = Maximum Force / Area = 3000 / 1.26 x 10^{-3} ≈ <u>24 bar</u>

The required volumetric flow rate of hydraulic oil was therefore:

Mean Flow Rate of Oil = Area x 4 x fx_o = 1.26 x 10^{-3} x 4 x 10 x 0.003 = 0.15 litres/s

≈ <u>9 litres/min</u>

Maximum Flow Rate of Oil = Area x Peak Velocity = 1.26 x 10^{-3} x 0.19 = 0.24 litres/s

≈ <u>14.4 litres/min</u>

In practice the mean flow rate of oil is more important since peak demand can be accommodated by the use of an accumulator which stores sufficient high pressure oil to meet sinusoidal peak demand. It was judged that a cylinder bore size of 40 mm was a satisfactory compromise between the maximum force available (which could in the future be increased if necessary by adjusting the set pressure of the vane pump to increase the working pressure of the oil) and the required volumetric flow rate of the oil (which increases rapidly if bore size is increased). A cylinder with maximum stroke length 0.125 m was selected (corresponding to a Strouhal number of 0.2).

In order to allow for additional losses in the servo-valve and due to piston seal friction as well as frictional losses in the baffled tube and gravitational force on the mass of fluid, the working pressure was specified as 40 bar at which pressure the vane pump selected was capable of delivering between 9 and 20 litres/min i.e. more than sufficient to meet the specified demand. [Note: since the peak pressure demands in the oscillatory cycle occur when the oil flow rate is at a minimum, the system is over-specified]. These specifications could be accommodated by a 1.5 kW motor but a 3.0 kW motor was installed since the difference in cost was negligible.

Maximum rates of overall energy dissipation measured in O.F.M. by Baird & Stonestreet (1995) for a 12 mm diameter baffled tube were 10 000 W/m^3. If the same energy dissipation rate were generated in the 150 mm apparatus (with a volume of 0.08 m^3) this would require a 1.6 kW motor, allowing for combined energy losses in the motor and vane pump of 50%.

The hydraulic power unit was equipped with a 1 litre volume accumulator as well as a safety relief valve and is shown schematically in Figure AI.2.

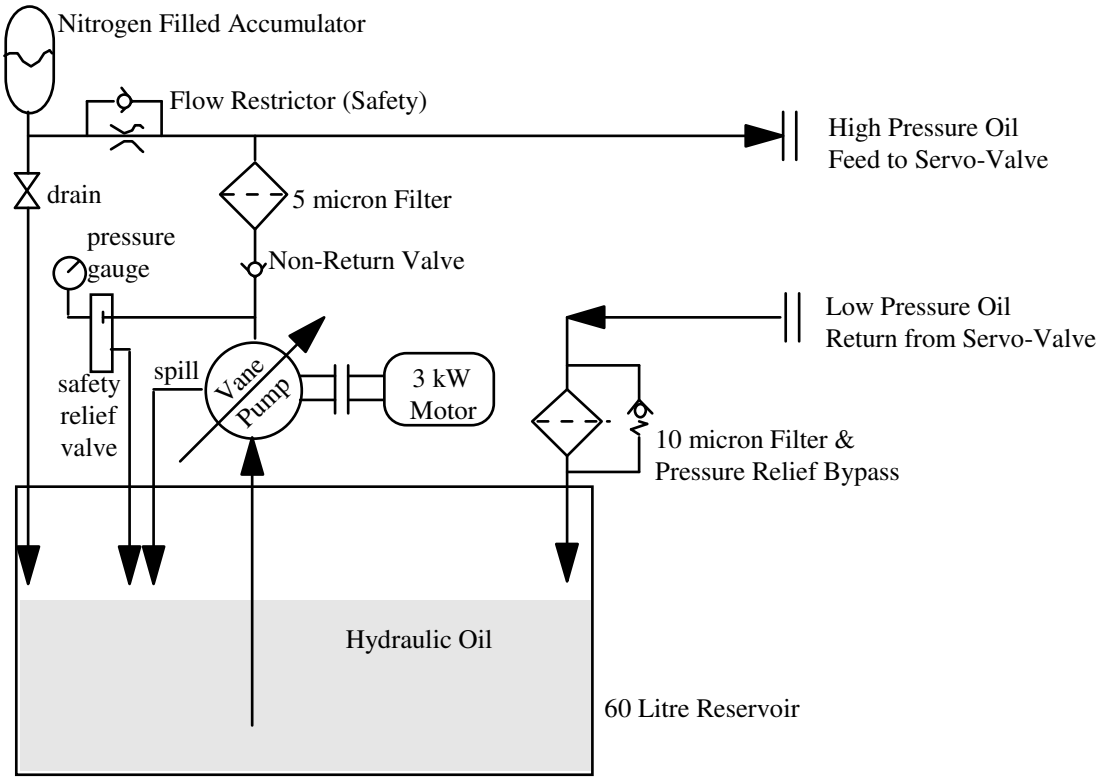

Figure AI.2: Schematic Diagram of the Hydraulic Power Unit

Appendix II: Electronic Servo-Control Circuits

The oscillatory wave form of each apparatus was regulated by a servo-control circuit. In each case the movement of the oscillator was measured by a displacement transducer, the output signal from which was subtracted from the generated input wave form. The degree of feedback control could be manually adjusted to suit the experimental conditions (i.e. strong servo-control for fast low amplitude oscillations or weak servo-control for slow large amplitude oscillations).

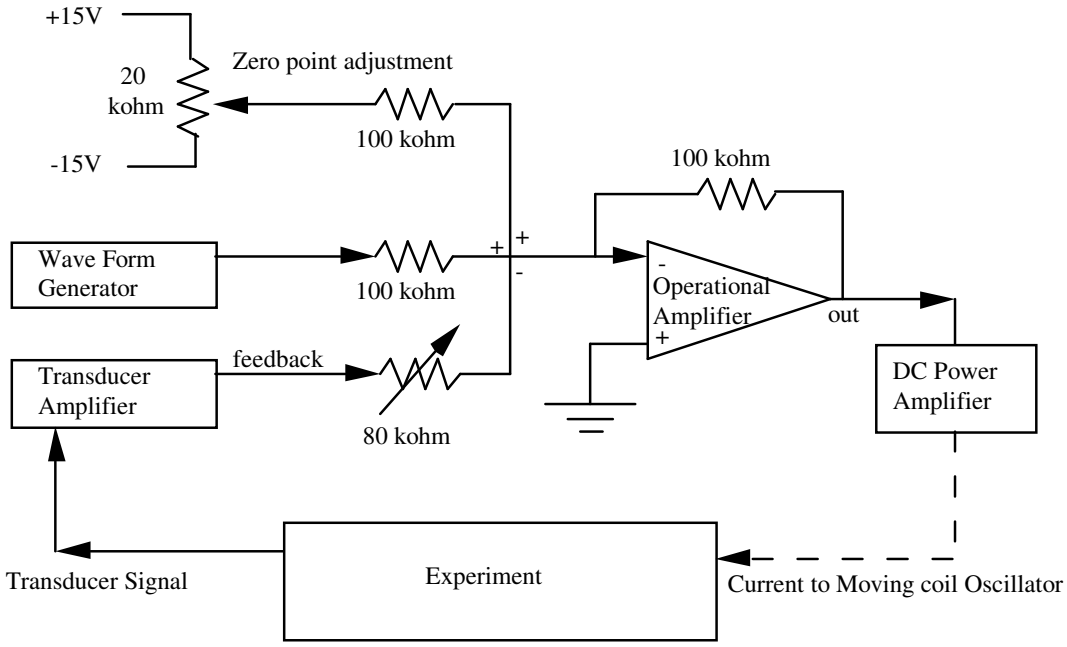

Figure AII.1: Schematic of Servo-control circuit for the 24 mm Apparatus Oscillator

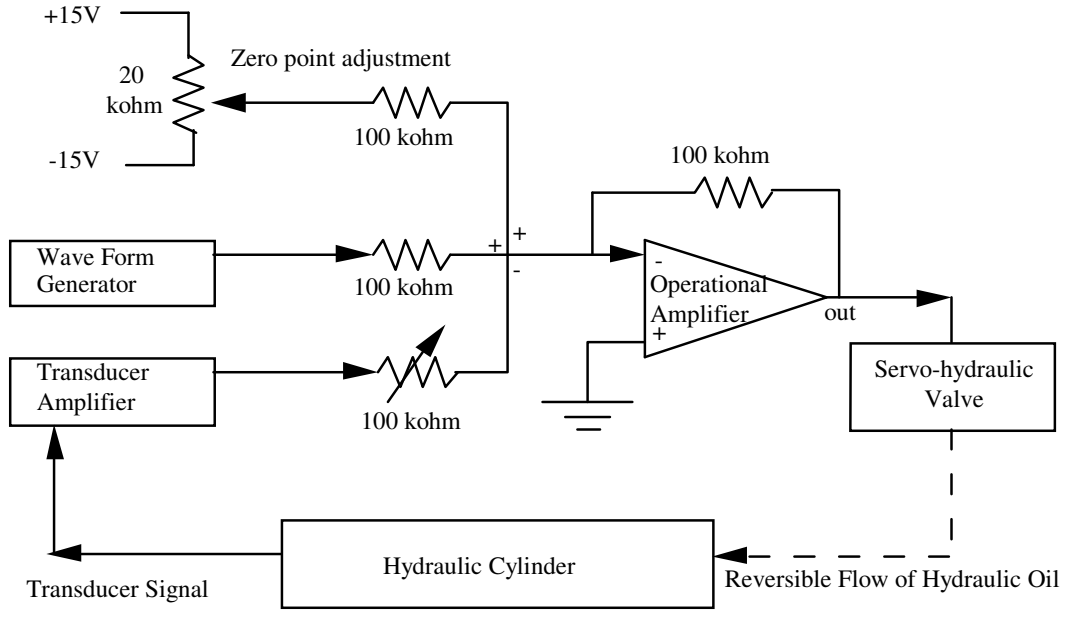

Figure AII.2: Schematic of Servo-hydraulics for 54 mm and 150 mm Apparatus Oscillators

Appendix III: Optical Dye Tracer Technique

It is known empirically in quantitative spectroscopy (for example Williams & Fleming 1989) that the fraction of light absorbed when passing through a dye solution is independent of the intensity of the light source and that the absorption is proportional to the number of absorbing molecules such that:

$$\log_{10}\left(\frac{I_o}{I}\right) = \varepsilon . l . C \qquad \text{eqn (AIII.1)}$$

where I is the measured intensity, I_O is the measured intensity when no dye is present, ε is the extinction coefficient for the dye, l is the path length of the light and C is the average concentration of the absorbing dye.

The dye concentration sensors used experimentally in this thesis comprised a light source and a light detector. The light source was a high power Light Emitting Diode that was affixed to the outside of the clear-walled baffled tube so as to shine a beam of light through the tube. The light was detected on the opposite side of the tube by a photo-diode that allowed a current to pass proportional to the incident light. This current signal was converted to a voltage signal via an operational amplifier (the scaling of the signal was adjusted to suit the sensitivity required for each of the three different sets of apparatus). The voltage signal could be automatically recorded onto P.C. using a standard A/D data capture card. The entire apparatus was shielded with black paper in order to minimise interference by outside light.

Data from the optical sensors was initially recorded at 250 Hz to gain an indication of the amount of noise in the signal. It was found that the standard deviation on a "steady" signal (without changing concentration of dye in the tube) was around 1.5%. Most of the signal noise had a frequency of 50 Hz or its harmonics. The signal was therefore passed through a R-C filter (normally a 10 kΩ resistor and 1 μF capacitor to earth which limited signal noise over 16 Hz) such that the measured standard deviation of a typical signal was reduced to around 0.3%.

Calibration of the sensors was achieved by injecting successive amounts of methylene blue dye into a measured volume of water in the tube and oscillating for 20 minutes (to ensure even distribution) before recording readings from the four optical sensors. The calibration was performed a number of times for each different apparatus at various times during the programme of experiments. In practice it was found that the calibration of the sensors changed very little over time. The results of a typical calibration are shown in Figure AIII.1 (using equation AIII.1 to calculate the optical density). It can be seen that at the low concentrations of dye used in the experiments, the measured optical density is effectively proportional to concentration, confirming equation AIII.1.

The lines are of different gradient: this may be explained by there being different path lengths for each optical sensor depending upon the precise alignment of the L.E.D. and the exact position of the sensor. The gradients were automatically determined in a specially-written Matlab analysis programme that generated a data file containing the measured value of εl for sensor 1 together with a correction factor for sensors 2, 3 and 4 which could be used in the subsequent data analysis (see Appendix IV) to eliminate differences between the sensors. The correction factors were close to unity, typically in the range 0.95 to 1.05.

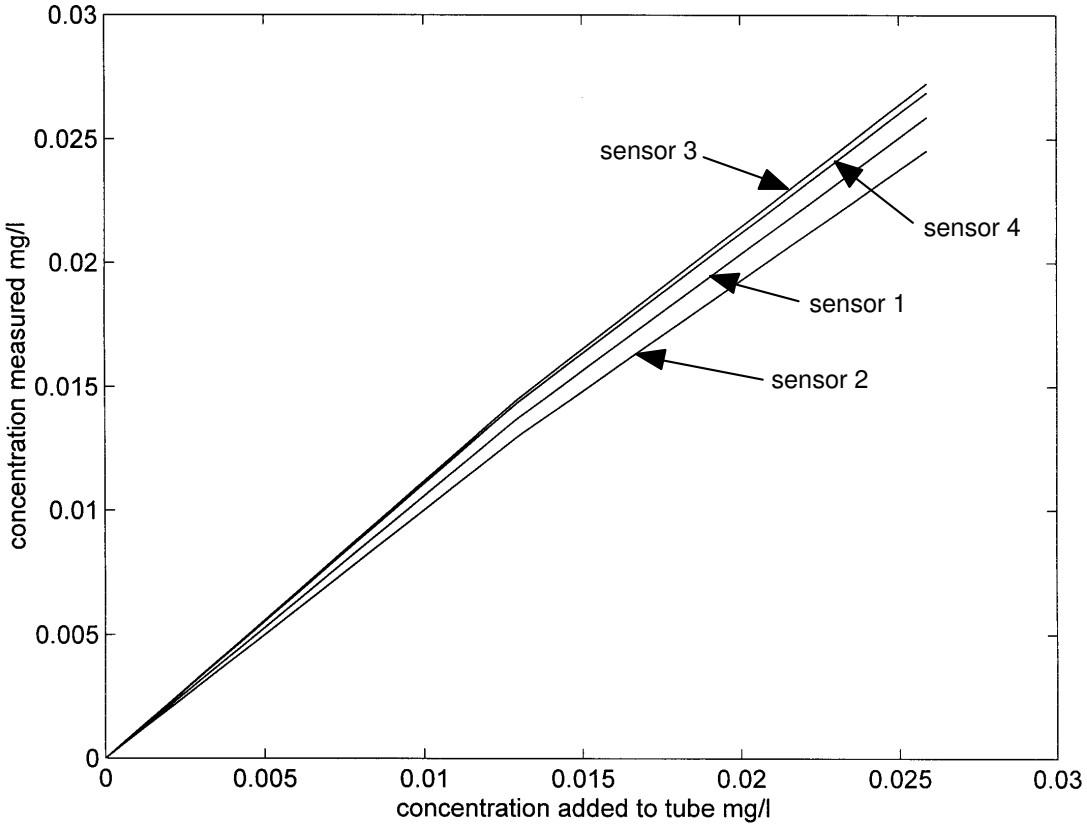

Figure AIII.1: Calibration of Four Experimental Optical Sensors in the 24 mm Apparatus

Appendix 4: Matlab Analysis Programme for Axial Dispersion

The programme `net7` is used to analyse axial dispersion from experiments with net flow; after initially clearing the memory it calls a series of subroutines. Variations on `net7` are given for the cases of no net flow and for net flow without oscillation.

Note that `%` at any point in a line allows annotations to be written in the programme.

```
% ********************************************************************
%    net7 - Programme to read in and process axial dispersion data
% ********************************************************************
clear       %remove all pre-existing variables from the workspace
 variab7a   %read in all the fixed variables (tube diameter, net flow,
            sampling rate, raw data file name, storage file name etc.)
 rdin7      %read in raw data from 12-bit binary file and arrange as a
            16-bit matrix
 start7     %detect the start-point of the experiment (the moment of dye
            injection)
 baselin7   %measure the baseline readings for the 4 optical sensors
            with no dye present
 trimdat7   %top-and-tail the data matrix so that it starts at the
            moment of dye injection
 timaxis7   %deduce the timebase of the data matrix from the sampling
            frequency
 wave7      %determine the oscillation frequency and amplitude, and
            detect irregularities
 reduce7    %reduce the size of the data matrix by averaging over each
            oscillation
 od_conc7   %compute the optical density (hence concentration) for each
            optical sensor
 area7      %calculate the area under each sensor's concentration-time
            profile
 normalz7   %normalise each sensor's concentration-time profile
 graphff    %plot the concentration-time profiles for all 4 optical
            sensors
 moment1    %calculate the first moment of area of each concentration-
            time profile
 moment2    %calculate the second moment of area of each concentration-
            time profile
 optim123   %determine the value of the axial dispersion coefficient E
            which causes the model predicted concentration-time profile
            to most closely match the experimental concentration-time
            profile for each pair of downstream sensors (1 to 2, 2 to 3,
            1 to 3)
Hz_ctpa_Reo_Ren=[cyclefrequency ctpamplitude*1000 reynoldsosc
            reynoldsnet] %display the cycle frequency in Hz, the centre-
            to-peak amplitude in mm, the oscillatory & net flow Reynolds
            numbers
comment = input('input any comment: ');   %record an optional comment
 savit7     %save the analysed data plus key variables and results.
```

Each of the subroutines summoned by `net7` is detailed below; each subroutine is a separate programme, or "M-file". In general, matrices are denoted by upper-case letters (eg. "RAW") and single variables are denoted by lower-case letters (eg. "density").

```
% ********************************************************************
%                              variab7a
% ********************************************************************
%This programme stores all the variables required for a particular expt.

filename=   '\riga\runa320.bin';    %file name of the raw experimental
            data
savname=    'resa320';          %file name under which to save the results
load calba156;                  %optical density info file
numchannels = 6   ;             %data is logged from six channels
samplerate= 400/6;              %sampling frequency Hz (for 6 channels)
flowrate=3840/60/1e6;           %measured net flow from rotameter in m3/s
diffusion=0.0001;               %first guess for the dispersion coeff E
            m2/s
voltsbinary=5/2048;             %conversion factor - displacement
            transducer
metrevolts=0.001/0.1;           %conversion factor - displacement
            transducer
density=1000;                   %density of bulk fluid in kg/m3
viscosity=0.001;                %viscosity of bulk fluid in Pas
diameter = 0.024;               %diameter of the tube in m

%area of tube minus area of studding
area = diameter^2*pi/4-3*0.003^2*pi/4;
velocity=flowrate/area;         %mean net flow velocity of bulk fluid

%location of the four probes in m relative to the dye injection point
 LENGTH=[2*0.036 6*0.036 10*0.036 -2.*0.036];

%Net flow Reynolds
reynoldsnet= density/viscosity*diameter*velocity;



% ********************************************************************
%                              rdin7
% ********************************************************************
%programme to read in experimental data from a 2 byte binary file and
%manipulate it into matrix form:
%     FF is a matrix containing 4 columns of optical sensor data
%     WAVEFORM is a vector containing the displacement transducer data
%     TIMING is a vector containing temperature and start/stop triggers
%the programme also works out the number of data points per channel
%and returns it as the the variable "samplesperchannel"

[fid,message]=fopen(filename,'r','n');
[RAW,count]=fread(fid,inf,'short');

%make sure all the channels have same number of points
r=rem(count,numchannels);
count_r=(count-r);
samplesperchannel=(count_r)/numchannels;

%put the data into column vector (waveform & timing channels)
%and matrix (optical information) form
FF=zeros(samplesperchannel,4);
WAVEFORM=RAW(1:numchannels:(count_r),:)';
FF(:,4)=RAW(2:numchannels:(count_r),:);
FF(:,3)=RAW(3:numchannels:(count_r),:);
FF(:,2)=RAW(4:numchannels:(count_r),:);
FF(:,1)=RAW(5:numchannels:(count_r),:);
TIMING=RAW(6:numchannels:(count_r),:);
clear RAW r count count_r;          %delete the obselete raw data
numchannels=4;                     %the number of columns in matrix FF
```

```
% ********************************************************************
%                              start7
% ********************************************************************
%subroutine start takes a column vector TIMING with start-stop
           information,
%& locates start-stop times by finding the beginning of the +1volt
           signals.
%gives the result as the row numbers "startpoint"   and   "endpoint"

startpoint=0                          ;
for i=2:samplesperchannel             ;
 if startpoint <1                     ;
  if (TIMING(i)) > (TIMING(i-1)+50)   ;
   startpoint = i                     ;
  end
 end
end

endpoint=0                            ;
for i=(startpoint+500):samplesperchannel;
 if endpoint <1                       ;
  if (TIMING(i)) > (TIMING(i-1)+50)   ;
   endpoint=i-1                       ;
  end
 end
end

%if there is no end pulse, the endpoint is requested as an input
if endpoint < startpoint
 endpoint = input('input the number of data points to use')
end

clear TIMING;     %delete the now redundant TIMING channel


% ********************************************************************
%                              baselin7
% ********************************************************************
% This programme takes a matrix of experimental values
% FF=[samplesperchannel,numchannels]
% and extracts the baseline values for each optical
% channel by recording a mean value before the startpoint

%get the mean baseline value for each channel
BASEVALUE=mean(FF(1:(startpoint - 5),1:numchannels));


% ********************************************************************
%                              trimdat7
% ********************************************************************
% This programme takes matrices of experimental values
% FF=[samplesperchannel,numchannels]  and
% WAVEFORM=[samplesperchannel,1]
% and trims the data points before and after the
% previously determined startpoint and endpoint of the experiment.
%
% After trimming, it recalculates the "samplesperchannel"

%remove nose and tail of data, leaving only the timed experimental
           values
FF(endpoint:samplesperchannel,:)=[];
FF(1:(startpoint-1),:)=[];

WAVEFORM(endpoint:samplesperchannel)=[];
WAVEFORM(1:(startpoint-1))=[];
samplesperchannel=endpoint-startpoint;

% ********************************************************************
%                              timaxis7
% ********************************************************************
%generate a time scale vector called TIMEAXIS
 timeunit = 1/samplerate;
 experimentaltime = timeunit*samplesperchannel;
 TIMEAXIS = (timeunit:timeunit:timeunit*samplesperchannel);
```

```
% ********************************************************************
%                              wave7
% ********************************************************************
% this programme uses the column vector WAVEFORM to determine
% the number of oscillations during the experiment ("cycles"),
% the amplitude ("ctpamplitude") and
% the frequency of the oscillation ("cyclefrequency")
% also plot the power spectrum of the oscillation to check for harmonics

%estimate the mean D.C. offset "wavezerovalue"
wavezerovalue=mean(WAVEFORM);

%count the number of times the oscillation falls through the mean D.C.
%offset value ("cycles") and memorise their position ("CYCLES")
cycles=0;
for i=2:samplesperchannel
 if WAVEFORM(i-1)>WAVEFORM(i)
  if WAVEFORM(i-1)>wavezerovalue
   if WAVEFORM(i)<wavezerovalue
    cycles=cycles+1;
    CYCLES(cycles)=i;
   end
  end
 end
end
cycles;
CYCLES;

%obtain a more accurate D.C. offset by taking
%the mean of an exact number of cycles
%and subtract to give a signal centred on zero
newwavezerovalue=mean(WAVEFORM(CYCLES(1):CYCLES(cycles-1)));
WAVEVECTORZERO=WAVEFORM-ones(1,samplesperchannel)*newwavezerovalue;
clear WAVEFORM;

%Fourier analysis and power spectrum
 WAVEFOUR = fft(WAVEVECTORZERO,2048);
 WAVESPECTR = samplerate*(0:1023)/2048;
 x3a = 'Frequency in Hz';
 y3a = 'Fourier Analysis: Centre to Peak Amplitude in m';
 t3a = filename;
 figure(1)
 plot(WAVESPECTR,(abs(WAVEFOUR(1:1024))/1024*voltsbinary*metrevolts))
 xlabel(x3a)
 ylabel(y3a)
 title(t3a)

%calculate the oscillation frequency
cyclefrequency=(cycles-1)*samplerate/(CYCLES(cycles)-CYCLES(1));

%calculate the oscillation amplitude by multiplying
%the square root of 2 by the root mean square of the oscillation data
CYCLEAMPLITUDE=(WAVEVECTORZERO(CYCLES(1):CYCLES(cycles-1)));
CYCLEAMPLITUDE2=CYCLEAMPLITUDE.*CYCLEAMPLITUDE;
CYCLEAMPLITUDERMS=(mean(CYCLEAMPLITUDE2)).^0.5;
cycleamplitude=CYCLEAMPLITUDERMS*(2^0.5);
ctpamplitude=cycleamplitude*voltsbinary*metrevolts;

%calculate the oscillatory Reynolds number
reynoldsosc=cyclefrequency*ctpamplitude*2*pi*diameter*density/viscosity;

% number of points per oscillation
pointsperoscillation=(CYCLES(cycles)-CYCLES(1))/(cycles-1);

clear WAVEVECTORZERO WAVEFOUR WAVESPECTR...
            CYCLEAMPLITUDE CYCLEAMPLITUDE2 CYCLEAMPLITUDERMS ...
            newwavezerovalue wavezerovalue;


% ********************************************************************
%                              reduce7
% ********************************************************************
```

```
% this programme takes experimental data FF and the
% information on the oscillation (cycles & CYCLES)
% and reduces the size of FF by averaging over one cycle.

CYCLESSTART=CYCLES;
CYCLESFINISH=CYCLES-1;
CYCLESFINISH(1)=[];
CYCLESSTART(cycles)=CYCLES(cycles)-1;
CYCLESFINISH(cycles)=CYCLES(cycles);

% enter new values then delete redundant rows of FF data
for i=1:cycles
 FF(i,:)=mean(FF(CYCLESSTART(i):CYCLESFINISH(i),:));
end
clear CYCLESSTART CYCLESFINISH
FF((cycles+1):samplesperchannel,:)=[];    %delete redundant rows
samplesperchannel=cycles;

%generate a new time scale vector called TIMEAXIS
timeunit = 1/cyclefrequency;
experimentaltime = timeunit*samplesperchannel;
TIMEAXIS = (timeunit:timeunit:timeunit*samplesperchannel);

% check that the normalisation worked
AREACHECK=sum(FF)*timeunit


% ********************************************************************
%                              od_conc7
% ********************************************************************
% This programme takes a matrix of experimental values
% FF=[samplesperchannel,numchannels]
% and converts it to concentration values for a given
% set of scaling factors [SCALE]

%calculate the optical density values for each channel
FF=log10(ones(samplesperchannel,1)*BASEVALUE)-log10(FF);
clear BASEVALUE;

% scale the optical density readings into concentration (mg/l)
% using the calibration CORRECTIONVALUE
FF=FF.*(ones(samplesperchannel,1)*CORRECTIONVALUE);
clear CORRECTIONVALUE

%get rid of any negative values
FF=FF.*(FF>0);
```

```
% ********************************************************************
%                              area7
% ********************************************************************
% This programme calculates the area under concentration
% profiles contained in matrix FF
% Also calculates the relative DIFFERENCE in % for
% channels 2 and 3 relative to 1, and the relative
% magnitude of the area under profile 4 (upstream)

%These areas should be the same for the first
%three channels (downstream) but lower for the upstream
%channel (fourth channel)
AREA=sum(FF)*timeunit;

% calculate % error in areas relative to channel 1,
% and also the magnitude of channel 4 relative to 1.
DIFFERENCE(1)=round((AREA(1)-AREA(2))/AREA(1)*1000)/10;
DIFFERENCE(2)=round((AREA(1)-AREA(3))/AREA(1)*1000)/10;
DIFFERENCE(3)=round(AREA(4)/AREA(1)*1000)/10;
DIFFERENCE        %display the results on screen


% ********************************************************************
%                              normalz7
% ********************************************************************
% This programme normalises experimental concentration
% profiles contained in matrix FF using the previously
% calculated areas under the curves AREA
%
% output is FF with area under each concentration-time profile= 1

% calculate adjustment factor for channels 2&3
% factor for channel 4 is the average of that for 2&3
AREAFACTOR=1./(AREA);
AREAFACTOR(4) = (AREAFACTOR(2)+AREAFACTOR(3))/2;
FF=FF.*(ones(samplesperchannel,1)*AREAFACTOR);
clear AREAFACTOR

% check that the normalisation worked
AREACHECK=sum(FF)*timeunit


% ********************************************************************
%                              graphff
% ********************************************************************
%plot the normalised concentration profiles
x1b = 'time after dye injection (seconds)';
y1b = 'normalised dye concentration';
t1b = filename;
figure(2);plot(TIMEAXIS,FF);
xlabel(x1b);ylabel(y1b);title(t1b)


% ********************************************************************
%                              moment1
% ********************************************************************
% calculates the first moment of matrix FF and returns
% the values in vector FIRSTMOMENT

FIRSTMOMENT=(TIMEAXIS*FF)*timeunit;


% ********************************************************************
%                              moment2
% ********************************************************************
% calculates the variance about the mean for all
% columns in results matrix FF.

for i=1:numchannels
 SECONDMOMENT(i)=(TIMEAXIS-[ones(size(TIMEAXIS))...
                  *FIRSTMOMENT(i)]).^2*FF(:,i)*timeunit;
end

% alternative method for calculating the variance
```

```
% VARIANCE=((TIMEAXIS.^2)*FF)*timeunit-FIRSTMOMENT.^2


% ********************************************************************
%                              optim123
% ********************************************************************
% optimize diffusion coefficient for pairs of concentration profiles.
% summons the subroutine optimd7 once the sensors are selected
% the results for each pair are stored in the vector DIFFUSION

i=1;              %probes 2 to 3
upstream=2;
downstream=3;
optimd7

i=2;              %probes 1 to 3
upstream=1;
downstream=3;
optimd7

i=3;              %probes 1 to 2
upstream=1;
downstream=2;
optimd7

DIFFUSION         %display the results for axial dispersion


% ********************************************************************
%                              optimd7
% ********************************************************************
% calculate the distance between two sensors,
% generate a response function by summoning subroutine "resp7b" and
% convolute to give predicted profile CC at the downstream position

clear CC
distance=(LENGTH(downstream)-LENGTH(upstream));

% optimisation loop ---------------------------------
newdiffusion=diffusion;
while newdiffusion>=0
 diffusion=newdiffusion;
 resp7b
 CC=[conv(FF(:,upstream)',R) 0]*timeunit;
 figure(3)
 plot( ...
            TIMEAXIS,FF(:,upstream),'y',...
            TIMEAXIS,FF(:,downstream),'m',...
            TIMEAXIS,CC(1:samplesperchannel),'w')
  x1b = 'time after dye injection (seconds)';
  y1b = 'normalised dye concentration'; t1b = filename;
  xlabel(x1b);ylabel(y1b);title(t1b)
 % demand a new value for the dispersion coefficient
 newdiffusion=input('enter new diffusion or -1 to end: ');
end
% end of optimisation loop ----------------------------

DIFFUSION(i)=diffusion;       %store the result in a vector DIFFUSION


% ********************************************************************
%                              resp7b
% ********************************************************************
%This programme generates the characteristic residence time function for
%an oscillatory flow reactor operating with or without net flow
%using the result after Westerterp et al 1984
%Output matrix is R with a total area of unity.
clear R

R=[0 1*((4*pi*diffusion*TIMEAXIS.^3/distance^2)).^(-0.5).* ...
            exp(-(distance - velocity*TIMEAXIS).^2./ ...
            (4*diffusion*TIMEAXIS))];
```

```
% ********************************************************************
%                              savit7
% ********************************************************************
% this subroutine clears irrelevant data from memory before storing
% useful results and data under the file name "savname"
clear TIMEAXIS CC R AREA ...
            startpoint endpoint upstream downstream ...
            newdiffusion i numpoints numreadings fid ...
            Hz_ctpa_Reo_Ren ans ...
            odscalechannel1 odscalechannel2 ...
            odscalechannel3 odscalechannel4 ...
            x1a x1b x1c y1a y1b y1c t1a t1b t1c ...
            x2a x2b x2c y2a y2b y2c t2a t2b t1c ...
            x3a x3b x3c y3a y3b y3c t3a t3b t3c

eval(['save c:\matlab\keith\riga\' savname ]);

% variables saved to file are:-
%           ' FF WAVEFORM numchannels samplesperchannel '...
%           ' samplerate experimentaltime cycles '...
%           ' DIFFERENCE FIRSTMOMENT SECONDMOMENT '...
%           ' flowrate measuredvolume measuredtime '...
%           ' voltsbinary metrevolts density viscosity '...
%           ' diameter LENGTH area velocity '...
%           ' filename timetaken '...
%           ' cyclefrequency ctpamplitude reynoldsosc pi'
```

When experiments involving no net flow are to be used to calculate axial dispersion coefficients, the programme `nonet7` is used instead of `net7`: the programmes are essentially the same except that in `nonet7` the subroutines `area7`, `normalz7`, `moment1` and `moment2` are not used.

When experiments involving a net flow but no oscillations are to be used to calculate axial dispersion coefficients, the programme `net7` is used except that the subroutines `wave7` and `reduce7` are removed (since they both rely on measurements of the oscillation) and if it is necessary to compress the data file by averaging then the following subroutine `reduce7b` is substituted for `reduce7`:

```
% ********************************************************************
%                                reduce7b
% ********************************************************************
% this subroutine is used in place of reduce7 for experiments without
% oscillations.  It reduces the number of data points in a matrix FF
% but without any averaging.  The reduction factor is determined by the
% variable reducf.  If reducf=4 then FF is reduced by 75%.

reducf=4;
r=rem(samplesperchannel,reducf);

for i=1:((samplesperchannel-r)/reducf)
 FF(i,:)=FF(i*reducf,:);
end
FF((i+1):samplesperchannel,:)=[];  %delete obselete info

samplesperchannel=i;
samplerate=1/timeunit/reducf;
timeunit=1/samplerate;
timaxis7
```

The following subroutine was used in place of `resp7b` when investigating conflicting results in the literature (Chapters 2 and 4):

```
% ********************************************************************
%                                resp7
% ********************************************************************
%This programme generates the a residence time function for
%an oscillatory flow reactor operating with or without net flow
%using the result from Goebel et al 1986
%Output matrix is R with a total area of unity.
clear R

%response with velocity term
R=[0 1*(1/velocity^2*(4*pi*diffusion*TIMEAXIS)).^(-0.5).* ...
      exp(-(distance - velocity*TIMEAXIS).^2./ ...
      (4*diffusion*TIMEAXIS))];

%Note: the values of R give false results - the expression is incorrect.
```

Appendix V: Treatment of Errors

This appendix discusses the magnitude of errors in the estimates of axial dispersion using the imperfect pulse technique and the diffusion model. Errors arise from several sources:

i) Measurement of the Fluid Conditions: estimates of the typical measurement errors (of flow rate, amplitude and frequency of oscillation) for the fluid dynamic conditions are given below for the 24 mm apparatus:

		Maximum Error +/-
Amplitude of Oscillation	2 mm +/- 0.1 mm	5.0 %
Frequency of Oscillation	1 Hz +/- 0.01 Hz	1.0 %
Flow Rate	0.12 l/min +/- 0.003 l/min	2.5 %

Table AV.1: Measurement Errors for the Fluid Conditions in Axial Dispersion Experiments

Although the fluid conditions (*Str*, Re_o & Re_n) could be measured with reasonable confidence, a problem existed in that the amplitude of oscillation (set by monitoring the wave form on an oscilloscope) could only be set to +/- 10% before starting the experiment. The subsequent analysis of the displacement data allowed quite accurate determination of the amplitude of oscillation (+/- 5%), but then in order to compare results at a particular oscillatory amplitude, a significant variation in the amplitude of oscillation had to be accepted, affecting the magnitude of axial dispersion by up to approximately +/- 20%.

ii) Measurement of the Dye Concentration: the concentration of dye is measured by photo-diodes which give a current output. The current output is quite accurate and proportional to the incident light (estimated +/- < 1 %) however it is quite sensitive to temperature variation (+ 0.5% per ˚C). The latter was regulated by maintaining constant temperature conditions as far as possible through the course of an experiment. Unfortunately, because the output from the photo-diodes is converted to an optical density ($\log(I_o/I)$ - see Appendix III) the measured concentration of dye is very sensitive to errors in the output from the photo-diode at low concentrations (when $I \approx I_o$). An additional problem with the method of concentration measurement is that if the dye is not well radially distributed in the tube then the measured optical density can give misleading readings. It is therefore difficult to estimate the possible error in the concentration measurement: if the dye is well mixed radially and there is minimal drift in the output

from the photo-diode then the results are quite accurate (+/- < 1 %); if on the other hand the dye is not well mixed (for example laminar creeping flow with central coring of the flow between the baffles) and the concentrations of dye give a low change in output from the photo-diodes then the errors are potentially large.

It was therefore considered important to adjust the concentration of the injected pulse of dye in order to maximise the overall accuracy of the concentration measurements. A compromise had to be made: if the dye is too dilute then the difference between I and I_o is small and the errors in the calculated optical density are large; if on the other hand the dye is too concentrated then no light passes through the tube and I tends to zero, causing inaccurate estimates of the concentration.

iii) The Diffusion Model Analysis: having obtained concentration-time profiles from dye-tracer experiments the best fit value of axial dispersion E was found by trial and error: the value of the axial dispersion was adjusted until by inspection the best fit was obtained between the experimental concentration-time profile and the diffusion model predicted concentration-time profile. This was considered to be the quickest and most reliable method of determining E: the alternative used by other researchers was a numerical least-squares best fit criterion, but this is affected by stray data points (for example a spike due to a gas bubble passing the optical sensor) and is also sensitive to the larger errors in measured concentration when the concentration approaches zero towards the end of an experiment (see above). Determination of the best fit value of axial dispersion E using the inspection method was found to give a resolution of results for a given experiment of +/- 10%.

SUMMARY:

Where axial dispersion data is presented on a graph for a particular Strouhal number, the measured amplitude of oscillation may in fact vary considerably (+/- 10%) from the nominal Str, with a highly non-linear effect on axial dispersion. This gives an additional estimated error of up to +/- 20 % when comparing results at a specified Strouhal number. Combined with the variation due to amplitude measurement (5%) and the diffusion model analysis (10%) the total error is therefore estimated to be $\sqrt{5^2 + 10^2 + 20^2} \approx 25\%$.

At very low oscillatory or net flow Reynolds numbers, high Strouhal numbers, or where radial distribution of the dye tracer is poor, the overall error in measured axial dispersion may be considerably greater than 25%. The error in the measured Re_o is approximately +/- 5% and about +/- 2.5% for Re_n.

Errors in the estimates of axial dispersion made using the fluid mechanical simulation were estimated to be less than 5% so long as the mean rate of increase of particle variance with time was constant.

Appendix VI: Fluid Mechanical Simulation

The information in this appendix is drawn from Mackley & Roberts (1991) and Saraiva (1997). It is intended as brief overview of the basis of the numerical simulation used to produce flow fields and axial dispersion data; more explicit details of the programme and methodology can be found in Saraiva (1997).

The simulation comprises two parts: firstly a fluid mechanics model that generates a velocity field for oscillatory flow in a baffled tube depending upon the flow conditions (Re_n, Re_o and Str), and secondly a procedure for the advection of passive fluid marker particles in the velocity field and which is used to create flow visualisations and estimates of axial dispersion.

The fluid mechanical model takes the form of a vorticity - stream function finite difference solver for an incompressible Newtonian fluid. It uses two-dimensional cylindrical coordinates (r, z) and is constrained to be axisymmetric in the baffled tube. The programme operates entirely with dimensionless quantities and groups, defined as follows:

$$t = \hat{f}\cdot\hat{t} \qquad r = \frac{\hat{r}}{\hat{R}} \qquad z = \frac{\hat{z}}{\hat{R}} \qquad v_r = \frac{\hat{v}_r}{2\pi\cdot\hat{f}\cdot\hat{x}_o} \qquad v_z = \frac{\hat{v}_z}{2\pi\cdot\hat{f}\cdot\hat{x}_o}$$

$$Str = \frac{\hat{R}}{2\pi\cdot\hat{x}_o} \qquad \mathrm{Re}_o = \frac{2\hat{\rho}\left(2\pi\cdot\hat{f}\cdot\hat{x}_o\right)\cdot\hat{R}}{\hat{\mu}} \qquad \mathrm{Re}_n = \frac{2\hat{\rho}\cdot\hat{U}\cdot\hat{R}}{\hat{\mu}}$$

The carets denote a dimensional quantity: $\hat{R}$ is the tube radius (m), $\hat{t}$ is time (s), $\hat{f}$ is frequency of oscillation (Hz), $\hat{x}_o$ is amplitude of oscillation (m), $\hat{v}_r$ is the velocity in the radial direction (m/s) and $\hat{v}_z$ is the velocity in the axial direction (m/s). The remaining equations in this appendix use the dimensionless forms. The dimensionless stream function ψ and the vorticity ω are defined as:

$$v_z = \frac{1}{r}\frac{\partial\psi}{\partial r} \qquad \text{eqn (AVI.1)}$$

$$v_r = -\frac{1}{r}\frac{\partial\psi}{\partial z} \qquad \text{eqn (AVI.2)}$$

$$\omega = \frac{\partial v_r}{\partial z} - \frac{\partial v_z}{\partial r} \qquad \text{eqn (AVI.3)}$$

These definitions lead to a Poisson relationship between ψ and ω:

$$\frac{\partial^2\psi}{\partial z^2}+\frac{\partial^2\psi}{\partial r^2}-\frac{1}{r}\frac{\partial\psi}{\partial r}=-r\omega \qquad \text{eqn (AVI.4)}$$

Using the Navier-Stokes equations the vorticity transport equation is derived:

$$\frac{\partial\omega}{\partial t}=-\frac{1}{Str}\left(v_z\frac{\partial\omega}{\partial z}+v_r\frac{\partial\omega}{\partial r}-\frac{v_r\omega}{r}\right)+\frac{2}{Re_o Str}\left(\frac{\partial^2\omega}{\partial z^2}+\frac{1}{r}\frac{\partial\omega}{\partial r}+\frac{\partial^2\omega}{\partial r^2}-\frac{\omega}{r^2}\right) \qquad \text{eqn (AVI.5)}$$

In practice, in order to improve resolution of the fluid mechanics model near the wall the above equations were modified using the transformation $s = r^2$. This has the additional benefit that the volume of fluid represented by four adjoining grid points is always equal. A grid of 65x65 points was used to represent the flow in one inter-baffle cell.

In order to compute the changing velocity field the vorticity transport equation (AVI.5) is used to step forward in time using the explicit leapfrog method of Dufort and Frankel. The Poisson equation (AVI.4) is then solved for the stream function using a block iterative method coupled with a multi-grid accelerating scheme. The velocities are then obtained using equations (AVI.1) & (AVI.2).

The boundary conditions for flow in the baffled tube are as follows:

The datum for the stream function is zero at the centreline of the tube ($s = 0$):

$$\psi\big|_{s=0}=0 \qquad \text{eqn (AVI.6)}$$

By symmetry considerations at the centreline the following are true:

$$v_r\big|_{s=0}=0 \qquad \text{eqn (AVI.7)}$$

$$\left.\frac{\partial v_z}{\partial r}\right|_{s=0}=0 \qquad \text{eqn (AVI.8)}$$

$$\omega\big|_{s=0}=0 \qquad \text{eqn (AVI.9)}$$

The stream function at the wall ($s = 1$) is:

$$\psi\big|_{s=1}=0.5\left(\sin(2\pi t)+\frac{Re_n}{Re_o}\right) \qquad \text{eqn (AVI.10)}$$

which allows for both oscillatory and net flow. Since the baffles are impermeable, the value of the stream function along is the same as at the tube wall:

$$\psi\big|_{\text{baffle}}=\psi\big|_{s=1} \qquad \text{eqn (AVI.11)}$$

The no-slip condition at the tube wall determines the wall vorticity:

$$\omega|_{s=1} = -4\frac{\partial^2 \psi}{\partial s^2} \qquad \text{eqn (AVI.12)}$$

and similarly the vorticity at the baffles is:

$$\omega|_{\text{baffle}} = \frac{1}{\sqrt{s}}\frac{\partial^2 \psi}{\partial z^2} \qquad \text{eqn (AVI.13)}$$

The simulation relies upon the periodicity of the system i.e. only the flow field in one inter-baffle cell need be computed and is assumed to be the same for all other inter-baffle cells:

$$(\psi, \omega, v_z, v_r)\big|_{z=L} = (\psi, \omega, v_z, v_r)\big|_{z=0} \qquad \text{eqn (AVI.14)}$$

where L is the distance between two baffles. Initially the fluid starts from rest so the velocities, stream function and vorticity are zero at the start of the simulation:

$$v_z|_{t=0} = 0 \qquad v_r|_{t=0} = 0 \qquad \psi|_{t=0} = 0 \qquad \omega|_{t=0} = 0 \qquad \text{eqn (AVI.15)}$$

In the case of net flow only, the following dimensionless variables are redefined:

$$t = \frac{\hat{U}\cdot\hat{t}}{\hat{R}} \qquad v_r = \frac{\hat{v_r}}{\hat{U}} \qquad v_z = \frac{\hat{v_z}}{\hat{U}}$$

Under these conditions the vorticity transport equation (equation AVI.5) then becomes:

$$\frac{\partial \omega}{\partial t} = v_z\frac{\partial \omega}{\partial z} + v_r\frac{\partial \omega}{\partial r} - \frac{v_r\omega}{r} + \frac{2}{Re_n}\left(\frac{\partial^2 \omega}{\partial z^2} + \frac{1}{r}\frac{\partial \omega}{\partial r} + \frac{\partial^2 \omega}{\partial r^2} - \frac{\omega}{r^2}\right) \qquad \text{eqn (AVI.16)}$$

The advection of passive fluid marker particles was computed by

$$\frac{\partial z}{\partial t} = \frac{1}{Str}v_z(z, r, t) \qquad \text{eqn (AVI.17)}$$

$$\frac{\partial r}{\partial t} = \frac{1}{Str}v_r(z, r, t) \qquad \text{eqn (AVI.18)}$$

i.e. the particles moved with the fluid velocity. A 4$^{\text{th}}$-order Runge-Kutta method was used for the integration of equations (AVI.17) & (AVI.18) where the fluid velocities were found by interpolation both in space and time from the discretised numerical velocity field. An additional term was superimposed on equations AVI.17 & 18 to model the effect of molecular diffusion in the form of a random walk model: the magnitude of this simulated molecular diffusion was dependant upon $\sqrt{\frac{\rho D}{\mu}}$.

Note: the nomenclature in this appendix has been kept consistent with Saraiva (1997), however some of the symbols used for dimensionless quantities are also used to denote dimensional quantities elsewhere in this thesis. In order to avoid confusion, the dimensionless symbols used in this self-contained appendix are not included in the nomenclature at the end of the thesis.

Nomenclature:

A	cross-sectional area of the tube (m^2)
A_1, A_2, A_3	constants
c	orifice diameter (m)
C	concentration of a dye tracer (mg/l)
C_1	concentration measured at position 1 (mg/l)
$C_1^{'}$	normalised concentrations at position 1
$C_2^{'}$	normalised concentrations at position 2
d	tube internal diameter (m)
d_e	equivalent tube diameter (m)
d_p	packing diameter in a packed bed (m)
D	molecular diffusion coefficient (m^2/s)
E	axial dispersion coefficient (m^2/s)
f	frequency of oscillation (Hz)
F	equivalent backmixing coefficient
h_t	heat transfer coefficient (W/m^2K)
H	distance between baffles (m)
I	intensity of transmitted light (cd)
I_o	intensity of transmitted light with no dye present (cd)
k	thermal conductivity (W/mK)
l	path length of transmitted light (m)
L	length of tube between optical sensors (m)
m	constant
n	volume of unit concentration tracer injected (m^3) ; constant
N	number of equivalent perfectly stirred tanks
q	constant
Q	measured net volumetric flow rate (m^3/s)
r	constant
t	time (s) ; dimensionless time equivalent to one oscillatory cycle (Chap 7)
t'	time at which an equivalent perfect pulse of tracer is injected (s)
T	baffle thickness (m)
u'	mean interstitial fluid velocity in a packed bed (m/s)
U	mean net axial velocity through tube (m/s)
V	measured volume of fluid between sensors 1 and 2 (m^3)
x	distance along the tube (m)
x_o	oscillatory amplitude (centre to peak) (m)

Greek Symbols:

δ	Dirac delta function
Δt	short time interval (s)
ε	extinction coefficient of methylene blue dye (m^2/kg)
ε_v	power density (W/m^3)
μ	viscosity of fluid (Ns/m^2)
ω	angular velocity of oscillation (rad/s)
ρ	density of fluid (kg/m^3)
σ^2	variance of particle or concentration distribution (units of m^2 in eqn 6.1, otherwise dimensionless)

Dimensionless Groups:

$Str = \frac{d}{4\pi x_o}$	Strouhal number
$Re_o = \frac{\rho \omega x_o d}{\mu}$	Oscillatory Reynolds number
$Re_n = \frac{\rho U d}{\mu}$	Net flow Reynolds number
$Pe = \frac{UL}{E}$	Peclet number
$Sc = \frac{\mu}{\rho \mathrm{E}}$	Schmidt number
$Nu_t = \frac{h_t d}{k}$	Tube side Nusselt Number
$\theta = \frac{tU}{L}$	dimensionless time